Assessment of Non-Destructive Testing Technologies for Quality Control/Quality Assurance of Asphalt Mixtures

Final Report
February 2015

ASPHALT MATERIALS &
PAVEMENTS PROGRAM

IOWA STATE UNIVERSITY

Institute for Transportation

About InTrans

The mission of the Institute for Transportation (InTrans) at Iowa State University is to develop and implement innovative methods, materials, and technologies for improving transportation efficiency, safety, reliability, and sustainability while improving the learning environment of students, faculty, and staff in transportation-related fields.

About AMPP

The Asphalt Materials and Pavements Program (AMPP) at InTrans specializes in improving asphalt materials and pavements through research and technology transfer and in developing students' technical skills in asphalt.

Disclaimer Notice

The contents of this report reflect the views of the authors, who are responsible for the facts and the accuracy of the information presented herein. The opinions, findings and conclusions expressed in this publication are those of the authors and not necessarily those of the sponsors.

The sponsors assume no liability for the contents or use of the information contained in this document. This report does not constitute a standard, specification, or regulation.

The sponsors do not endorse products or manufacturers. Trademarks or manufacturers' names appear in this report only because they are considered essential to the objective of the document.

ISU Non-Discrimination Statement

Iowa State University does not discriminate on the basis of race, color, age, ethnicity, religion, national origin, pregnancy, sexual orientation, gender identity, genetic information, sex, marital status, disability, or status as a U.S. veteran. Inquiries regarding non-discrimination policies may be directed to Office of Equal Opportunity, Title IX/ADA Coordinator, and Affirmative Action Officer, 3350 Beardshear Hall, Ames, Iowa 50011, 515-294-7612, email eooffice@iastate.edu.

Iowa DOT Statements

Federal and state laws prohibit employment and/or public accommodation discrimination on the basis of age, color, creed, disability, gender identity, national origin, pregnancy, race, religion, sex, sexual orientation or veteran's status. If you believe you have been discriminated against, please contact the Iowa Civil Rights Commission at 800-457-4416 or the Iowa Department of Transportation affirmative action officer. If you need accommodations because of a disability to access the Iowa Department of Transportation's services, contact the agency's affirmative action officer at 800-262-0003.

The preparation of this report was financed in part through funds provided by the Iowa Department of Transportation through its "Second Revised Agreement for the Management of Research Conducted by Iowa State University for the Iowa Department of Transportation" and its amendments.

The opinions, findings, and conclusions expressed in this publication are those of the authors and not necessarily those of the Iowa Department of Transportation or the U.S. Department of Transportation.

Technical Report Documentation Page

1. Report No. IHRB Project TR-653	2. Government Accession No.	3. Recipient's Catalog No.	
4. Title and Subtitle Assessment of Nondestructive Testing Technologies for Quality Control/Quality Assurance of Asphalt Mixtures		**5. Report Date** March 2015	
		6. Performing Organization Code	
7. Author(s) Shibin Lin, Jeramy C. Ashlock, Hanjun Kim, Jeremy Nash, Hosin (David) Lee, and R. Christopher Williams		**8. Performing Organization Report No.** InTrans Project 13-446	
9. Performing Organization Name and Address Institute for Transportation Iowa State University 2711 South Loop Drive, Suite 4700 Ames, IA 50010-8664		**10. Work Unit No. (TRAIS)**	
		11. Contract or Grant No.	
12. Sponsoring Organization Name and Address Iowa Highway Research Board Iowa Department of Transportation 800 Lincoln Way Ames, IA 50010	Federal Highway Administration 1200 New Jersey Avenue SE Washington, DC 20590	**13. Type of Report and Period Covered** Final Report	
		14. Sponsoring Agency Code IHRB and SPR Project TR-653	

15. Supplementary Notes

Visit www.intrans.iastate.edu for color pdfs of this and other research reports.

16. Abstract

Asphalt pavements suffer various failures due to insufficient quality within their design lives. The American Association of State Highway and Transportation Officials (AASHTO) *Mechanistic-Empirical Pavement Design Guide (MEPDG)* has been proposed to improve pavement quality through quantitative performance prediction. Evaluation of the actual performance (quality) of pavements requires in situ nondestructive testing (NDT) techniques that can accurately measure the most critical, objective, and sensitive properties of pavement systems. The purpose of this study is to assess existing as well as promising new NDT technologies for quality control/quality assurance (QC/QA) of asphalt mixtures. Specifically, this study examined field measurements of density via the PaveTracker electromagnetic gage, shear-wave velocity via surface-wave testing methods, and dynamic stiffness via the Humboldt GeoGauge for five representative paving projects covering a range of mixes and traffic loads. The in situ tests were compared against laboratory measurements of core density and dynamic modulus. The in situ PaveTracker density had a low correlation with laboratory density and was not sensitive to variations in temperature or asphalt mix type. The in situ shear-wave velocity measured by surface-wave methods was most sensitive to variations in temperature and asphalt mix type. The in situ density and in situ shear-wave velocity were combined to calculate an in situ dynamic modulus, which is a performance-based quality measurement. The in situ GeoGauge stiffness measured on hot asphalt mixtures several hours after paving had a high correlation with the in situ dynamic modulus and the laboratory density, whereas the stiffness measurement of asphalt mixtures cooled with dry ice or at ambient temperature one or more days after paving had a very low correlation with the other measurements. To transform the in situ moduli from surface-wave testing into quantitative quality measurements, a QC/QA procedure was developed to first correct the in situ moduli measured at different field temperatures to the moduli at a common reference temperature based on master curves from laboratory dynamic modulus tests. The corrected in situ moduli can then be compared against the design moduli for an assessment of the actual pavement performance. A preliminary study of micro-electromechanical systems- (MEMS)-based sensors for QC/QA and health monitoring of asphalt pavements was also performed.

17. Key Words asphalt mixture—nondestructive testing—quality assurance—quality control		18. Distribution Statement No restrictions.	
19. Security Classification (of this report) Unclassified.	**20. Security Classification (of this page)** Unclassified.	**21. No. of Pages** 181	**22. Price** NA

Form DOT F 1700.7 (8-72)   **Reproduction of completed page authorized**

ASSESSMENT OF NONDESTRUCTIVE TESTING TECHNOLOGIES FOR QUALITY CONTROL/QUALITY ASSURANCE OF ASPHALT MIXTURES

Final Report
March 2015

Principal Investigator
Jeramy C. Ashlock, Assistant Professor
Civil, Construction, and Environmental Engineering, Iowa State University

Co-Principal Investigators
R. Christopher Williams, Director
Asphalt Materials and Pavements Program, Institute for Transportation, Iowa State University

Hosin (David) Lee, Professor
Civil and Environmental Engineering, University of Iowa

Research Assistant
Shibin Lin, Iowa State University

Authors
Shibin Lin, Jeramy C. Ashlock, Hanjun Kim, Jeremy Nash,
Hosin (David) Lee, and R. Christopher Williams

A report from
Institute for Transportation
Iowa State University
2711 South Loop Drive, Suite 4700
Ames, IA 50010-8664
Phone: 515-294-8103 / Fax: 515-294-0467
www.intrans.iastate.edu

TABLE OF CONTENTS

LIST OF FIGURES

LIST OF TABLES

ACKNOWLEDGMENTS

EXECUTIVE SUMMARY

Quality control/quality assurance (QC/QA) is of critical importance for asphalt pavements to achieve their design lives and to minimize failures. The purpose of this study is to assess several in situ nondestructive testing (NDT) technologies for QC/QA of asphalt mixtures. The NDT technologies examined include the electromagnetic PaveTracker gage for measuring density, surface-wave testing methods for measuring shear-wave velocity profiles, and the Humboldt GeoGauge for measuring stiffness.

Five representative paving projects in Iowa were selected for NDT: (1) newly constructed pavement sections for a separate research project at the Boone Central Iowa Expo site featuring low-volume roads with hot mix and warm mix asphalts, with various base and pavement treatments, construction techniques, and equipment; (2) US 69; (3) US 169 (both US 69 and US 169 are medium-volume roads with hot mix asphalt resurfacing; (4) IA 93, which is a low-volume road with three different resurfacing methods: cold-in-place recycling, thin overlay, and full-depth-reclamation; and (5) US 6, which is a high-volume road with both hot mix and warm mix asphalts containing steel slag.

For each project, six or more test locations were randomly selected for measurement by the three NDT methods, followed by coring for laboratory testing. Surface-wave tests were carried out along straight lines centered on the testing locations and running parallel to the paving direction. Immediately before or after surface-wave tests, in situ density and stiffness were also measured at the test locations using the PaveTracker and GeoGauge, respectively. Because asphalt stiffness and shear-wave velocity are very sensitive to temperature, the asphalt surface layer temperature was recorded at the same time as the NDT measurements. "Hot" tests were performed up to a few hours after paving, and "cold" tests were performed after cooling the pavement surface with dry ice. Additional ambient-temperature tests were also performed on several projects one or more days after paving to examine the influence of temperature on the NDT measurements. This can be important for properly interpreting the results of in situ tests, which will inevitably be performed over a range of seasonal ambient temperatures.

Immediately after completing the NDT measurements, field cores were taken at the testing locations. Laboratory dynamic modulus tests were performed on the field cores over a range of frequencies and temperatures using the indirect tension (IDT) method. A master curve was constructed for each pavement section to correct the in situ moduli measured at different field temperatures to the moduli at a common reference temperature. A quality measurement was then developed by comparing the corrected in situ moduli to their design values.

Conclusions from the results of this study can be summarized as follows:

- The in situ PaveTracker density has a low correlation with laboratory density, and it is not sensitive to variations in temperature or pavement type. Therefore, QC/QA based solely on in situ density measurement by this device is not recommended.
- The GeoGauge stiffness measured on hot asphalt mixtures several hours after paving has a

high correlation with in situ dynamic modulus and laboratory density, whereas the stiffness measured on cold and ambient-temperature asphalt mixtures has a very low correlation with the other measurements. Therefore, the GeoGauge stiffness measured on hot asphalt mixtures is recommended for QC.

- Among all methods examined, the shear-wave velocity from surface-wave testing is the most sensitive to variations of temperature and pavement type. Therefore, shear-wave velocity is an objective property to measure asphalt pavement quality.
- The in situ density and shear-wave velocity measurements can be combined to calculate the in situ dynamic modulus, which is directly related to pavement performance. To account for temperature effects and provide a uniform quality comparison, the in situ modulus measured at a given field temperature should be corrected to the modulus at a common reference temperature.
- The laboratory moduli measured with the IDT method are in good agreement with those measured with the axial method (AASHTO T 342-11). The moduli of samples measured over a range of frequencies and temperatures was used to construct master curves, with one of the reference temperatures chosen to be the same as one of the field-test temperatures.
- To construct a master curve for the field temperature given laboratory modulus measurements at other temperatures, linear interpolation of logarithmic moduli from the measured master curves was found to yield the best agreement with the curve measured at the actual field temperature.
- The measured and interpolated master curves from laboratory tests on cores by the IDT method can be employed to correct the in situ moduli measured at different field temperatures to the moduli at a common reference temperature.
- A modulus-based QC/QA procedure was developed that is accurate, objective, and sufficiently sensitive to quantitatively measure the quality of asphalt mixtures.
- A preliminary study on MEMS-based sensors identified a battery-free, wireless, radio-frequency identification (RFID) passively powered sensor technology that shows promise for further development of embedded strain gauges for QC/QA and health monitoring. Among three different sensor configurations tested, one was found to survive the paving process and was successfully interrogated through 2 in. of asphalt pavement, giving temperature measurements immediately after paving as well as one week later.

CHAPTER 1 – INTRODUCTION

1.1 Problem Statement

Asphalt pavements suffer various failures after construction, and they commonly require rehabilitation to achieve their design lives. The empirical design of asphalt pavements has been identified as one of the major reasons for their undesirable performance. The mechanistic-empirical pavement design guide (MEPDG) was developed to enable quantitative performance prediction for the design of new and rehabilitated pavement structures. In addition to traffic and climate data, the mechanistic-empirical (M-E) design procedure requires measurement of fundamental pavement material properties rather than the use of empirical relationships. Quality control and quality assurance (QC/QA) procedures based on measured fundamental properties are thus necessary for enabling quantitative evaluations of pavement condition and performance.

Significant time and financial resources are routinely spent on QC/QA testing of asphalt pavement construction projects. A substantial amount of research has been performed on several nondestructive testing (NDT) technologies for flexible pavements, with the goals of improving the speed and accuracy of QC/QA methods and enabling practice to evolve beyond destructive testing. Some examples of these NDT technologies are nuclear gauges, electromagnetic gauges, permeability-based approaches, seismic testing techniques, and intelligent compaction based on measurement of machine variables during the construction process. However, the destructive and relatively time-consuming process of coring for laboratory measurement of bulk specific gravity (G_{mb}) continues to be the most widely used QC/QA method in the US. This may be due to the burdens of licensing and regulation requirements for nuclear gauge testing, and the need for improved accuracy and precision before the other NDT QC/QA technologies can be accepted into practice. The time required for coring and density measurement can result in multiple days of inadequate mix being placed by the contractor before the in-place density is known via QA testing. As a result, contractors may suffer losses from reduced pay factors, and projects may be delayed while substandard pavement sections are removed and replaced.

Asphalt pavements in Iowa are cored for determination of the in-place density for QC by the contractor and QA by the Iowa DOT. Core density is typically evaluated in the laboratory by measuring the G_{mb} according to AASHTO T 166 (AASHTO 2007). Although it is considered the standard by which other methods are measured, the procedure is time consuming and costly. The process of coring slows construction progress, whereas placement of inadequate pavement before test results are obtained can cause project delays as mentioned above. Additionally, the destructive coring process creates holes in the new pavement that are sometimes improperly repaired, leaving it more susceptible to premature failure.

In search of more efficient and nondestructive QC/QA tools to replace coring procedures, nuclear density gauges have found some utility because they offer rapid assessment of in-place asphalt mixture density during construction. However, nuclear gauges have a number of drawbacks, because they require a state radioactive materials license, a radiation safety officer, dosimeter badges for operators, regular recalibration, and certification records for the operators, calibrations, and badges.

Development of nonnuclear density measurement technologies that can be verified in terms of accuracy and repeatability potentially offer significant savings of time, money, and natural resources. However, density measurements of asphalt pavements are not sensitive to temperature variations that can significantly affect performance (e.g., modulus).

To obtain a more performance-based measure of pavement quality, significant progress has been made in several previous studies on in situ measurement of dynamic modulus of asphalt pavements by seismic testing methods. However, more robust and less delicate seismic testing systems still need to be developed for seismic testing methods to provide consistent, reliable and objective results. Additionally, a straightforward and practical QC/QA procedure is needed to convert the in situ dynamic modulus measurements to more quantitative measures of pavement quality. Both of these research needs are addressed in the present study.

1.2 Objectives

The goal of this research is to assess the performance of a range of selected NDT technologies for QC/QA of asphalt pavement construction and rehabilitation, and to make recommendations on their implementation or further development for Iowa DOT paving projects. The field NDT technologies to be examined include the Humboldt GeoGauge, Troxler PaveTracker (PT) electromagnetic (EM) gauge, and seismic surface-wave methods (SWMs). Laboratory measurements of density and dynamic modulus of core samples will be used as common benchmarks by which the accuracy, precision, and repeatability of the NDT technologies will be assessed. Statistical analyses will also be performed to identify the significant factors affecting the measurements of the individual field technologies.

The secondary research objective is to perform a preliminary feasibility study on QC/QA and subsequent health monitoring of asphalt pavements using embedded microelectromechanical systems (MEMS) sensors. Based on the survivability of the sensors and results of the preliminary study, recommendations will be made for further research or implementation of MEMS sensors for QC/QA and health monitoring on a larger scale.

1.3 Report Organization

This report includes seven chapters. Chapter 1 contains an overview of the research problem, objectives, and report organization. Chapter 2 provides a literature review of QC/QA, NDT techniques, and laboratory testing methods. Chapter 3 includes nondestructive measurements of density, shear-wave velocity, and stiffness of asphalt pavements using the PT, surface-wave testing equipment, and GeoGauge, respectively. Chapter 4 presents laboratory measurements of density and dynamic modulus of asphalt cores. Chapter 5 introduces a QC/QA procedure based on the in situ and laboratory results. Chapter 6 presents a preliminary study on the use of embedded MEMS-based sensors for QC/QA of asphalt pavements. Finally, Chapter 7 describes the conclusions and recommendations. Raw data and analysis results for the field nondestructive tests are presented in Appendix A, while the same for laboratory tests are detailed in Appendix B.

CHAPTER 2 – LITERATURE REVIEW

2.1 Quality Control/Quality Assurance of Asphalt Mixtures

Traditional QC/QA procedures are based on properties of asphalt mixtures (density, air voids, and permeability) measured either using in situ methods at the surface of an asphalt layer (e.g., Larsen and Henault 2006, Williams 2008, Mason and Williams 2009, Williams et al. 2013), or taking cores for laboratory measurement (e.g., Williams 2001, Buchanan and White 2005, Williams et al. 2013). Although these traditional QC/QA procedures play an important role in ensuring high-quality pavements, they employ only the volumetric properties, thickness, and roughness (i.e., present serviceability index) but not actual mechanical properties such as modulus. However, the mechanical properties are more sensitive than volumetric properties to quality variation, and are also required for the performance-based MEPDG. A pavement structure can be modeled as an elastic and/or viscoelastic multilayered system, the quality and remaining life of which can be evaluated based on prediction of the strains and stresses at the interfaces of different layers (Celaya et al. 2006). The modulus of an asphalt layer is also of critical importance for estimating fatigue cracking (Finn et al. 1977).

The use of modulus for QC/QA has been promoted by Li and Nazarian (1995), Nazarian et al. (2005), Celaya and Nazarian (2006), Celaya et al. (2006), Jiang (2007), Barnes and Trottier (2010a and 2010b), and Icenogle and Kabir (2013). A variety of testing equipment for in situ modulus measurement has been developed by Nazarian (1984), Stokoe et al. (1994), Park et al. (2001), Ryden (2004), and Lin and Ashlock (2011 and 2014). Overall, good correlations have been found between the in situ modulus and laboratory modulus (e.g., Saeed and Hall 2003, Bai 2004). Additionally, QC/QA based on measured moduli has been demonstrated to be more objective for characterization of asphalt layers by accounting for effects of temperature and loading frequency (Abdallah et al. 2005, Nazarian et al. 2005, Celaya et al. 2006). The advancement of QC/QA from methods based on volumetric and geometrical properties to those based on mechanical properties has been driven by the evolution of design procedures from empirical to M-E (Bai 2004).

Celaya et al. (2006) developed a QC/QA procedure based on seismic NDT measurements consisting of three steps: (1) a target modulus is determined by laboratory testing of asphalt mixtures prior to construction, (2) an in situ modulus is measured using surface-wave methods, and (3) a quality measurement is obtained by comparing the in situ modulus to the target modulus. Four major features of a quality measurement device were identified in the procedure: (1) measurement of fundamental material properties, (2) high measurement accuracy, (2) high sensitivity of the device to the properties of interest, and (4) high precision of the device.

2.2 Nondestructive Measurement of Modulus

To identify the quality of placed asphalt, specimens are usually cored in the field and tested in the laboratory. To replace the expensive, destructive, and time-consuming coring process, researchers have studied a variety of NDT methods, such as surface-wave methods and falling weight deflectometer (FWD) tests, which have also been used for determination of asphalt

modulus (e.g., Tertre et al. 2010, Icenogle and Kabir 2013). It is difficult, however, to accurately determine the modulus of pavement layers from FWD tests because of the large spacing between the receivers, lack of high-frequency content in the impact load, and low sampling rates. On the other hand, SWM test equipment can generate surface waves with smaller receiver spacing to cover a wide range of wavelengths to reach the depths of interest, with much greater high-frequency content in the loading than FWD tests (greater than 10 kHz vs. 1 kHz; Icenogle and Kabir 2013).

Surface wave testing of pavements can be traced back to the continuous surface wave (CSW) method developed by Van der Poel (1951) and further advanced by Heukelom and Foster (1960), Jones (1955, 1958, 1962), and Vidale (1964) (Figure 2.1).
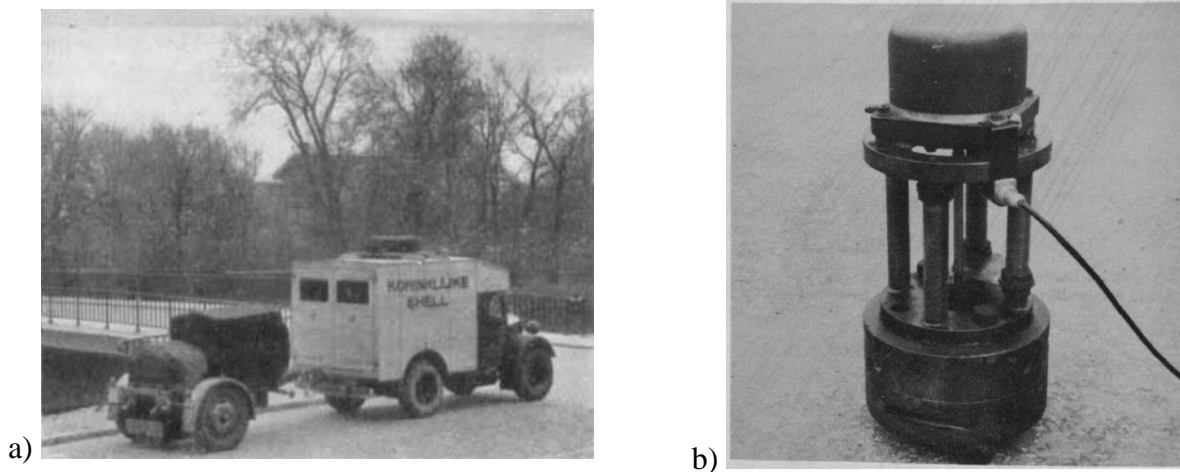

a)   b)

Figure 2.1. Continuous surface wave testing equipment developed by (a) Van der Poel (1951) and (b) Heukelom and Foster (1960)

After the popularization of the fast Fourier transform (FFT) in the 1960s, the CSW testing procedure evolved into the widely used spectral analysis of surface waves (SASW) method developed by Heisey et al. (1982), Nazarian (1984), Rix (1988), and Stokoe et al. (1994) (Figure 2.2).
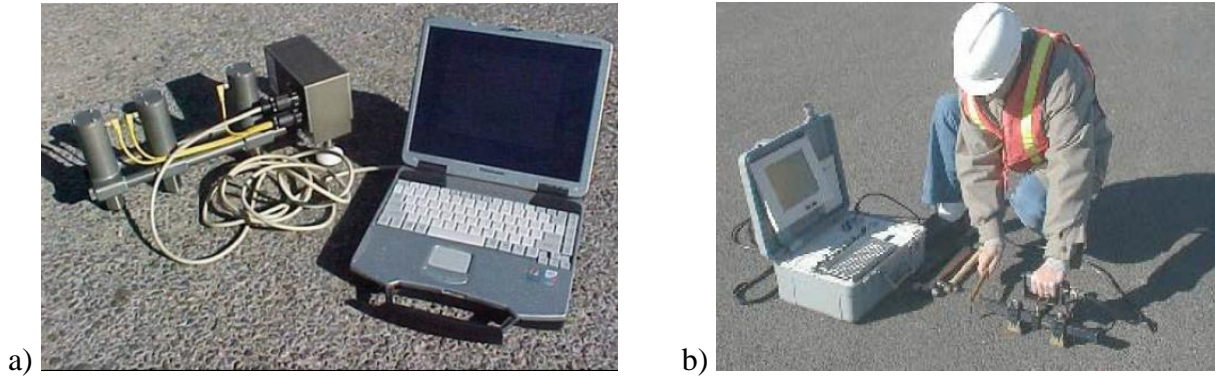
Figure 2.2. SASW testing equipment developed by (a) Nazarian et al. (1995), (b) Olson (2008)

Following the success and wide usage of the multichannel analysis of surface waves (MASW) method in near-surface stiffness profiling of soils (e.g., Park et al. 1999), the method was also applied to pavements using arrays of geophones by Park et al. (2001) and later using arrays of accelerometers by Tertre et al. (2010) and Lin and Ashlock (2014) (Figure 2.3). The evolution of the surface-wave methods is summarized in Figure 2.4.
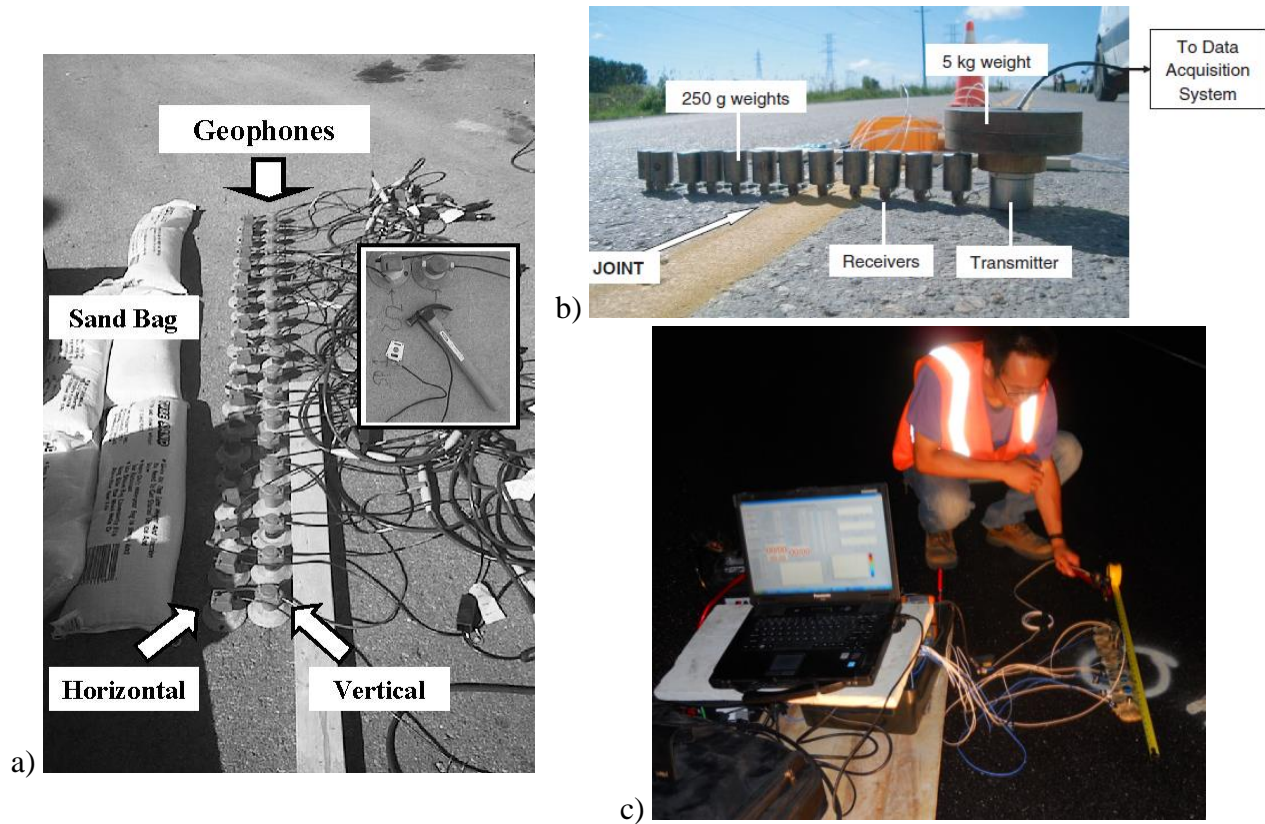
Figure 2.3. MASW testing equipment developed by (a) Park et al. (2001), (b) Tertre et al. (2010), and (c) Lin and Ashlock (2014)
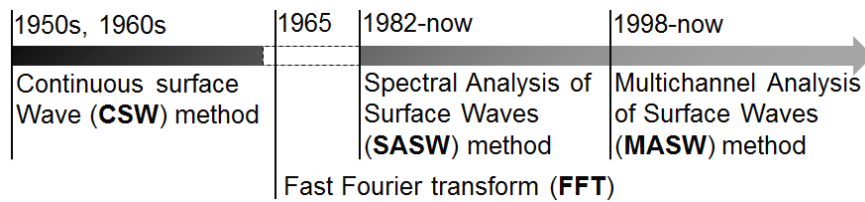

Figure 2.4. Evolution of surface-wave methods

To reduce the cost and inconvenience of coupling multiple receivers to pavement in MASW testing (Figure 2.5a), the multichannel simulation with one receiver (MSOR) method was developed and applied to pavement stiffness profiling by Ryden et al. (2001, 2002a, 2002b, 2006), Park et al. (2002), Olson and Miller (2010), and Lin and Ashlock (2011). In one form of MSOR testing, synthetic multichannel records are created by applying multiple impacts at a fixed source location while a single receiver is incrementally moved out over a range of offsets. More commonly, the source and receiver are reversed according to the reciprocity theorem of mechanics, such that the receiver is fixed while the impact location is moved out (Figure 2.5b).
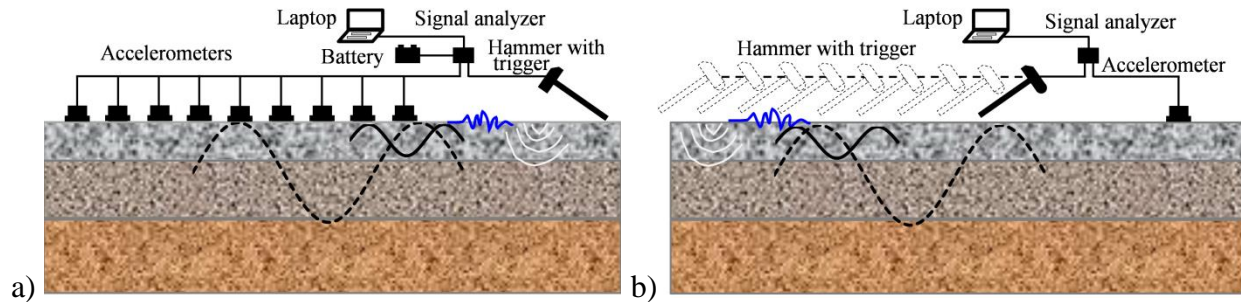
Figure 2.5. Schematic of setup for (a) MASW tests, (b) MSOR tests (after Ryden et al. 2002b)

The data from SASW and MASW tests are processed to obtain the shear-wave phase-velocity spectra in the form of dispersion images or dispersion curves. Low frequencies correspond to material properties at greater depths, and high frequencies correspond to shallower depths. To measure the properties of the pavement layer, the measurement depth can be reduced by decreasing the receiver spacing, increasing the high-frequency content of the impact, and increasing the sample rate. For the small strains involved in surface-wave testing, the asphalt behaves visco-elastically, and the Young's modulus (or stiffness, E) can be obtained from shear wave velocity (V_S) as

$$E = 2(1 + \nu)\rho V_S^2 \tag{1-1}$$

where ρ is mass density and ν is Poisson's ratio.

Because of the decreasing velocity (stiffness) with depth for typical pavement structures consisting of pavement, base, subbase, and subgrade layers, the phase-velocity spectra from surface-wave tests on pavements primarily show an increase in phase velocity with frequency. However, wave propagation in pavement layers is very complex.

As detailed in Ryden et al. (2006), the phase-velocity spectrum of a layered pavement system actually consists of several branches that can be approximated as multiple modes of anti-symmetric and symmetric Lamb waves for a free plate corresponding to the material properties of the pavement layer. The correspondence to Lamb waves is approximate, because the pavement layer is not truly free but interacts with the underlying base and subgrade layers to create partial branches of leaky quasi-Lamb waves in the low-frequency regime. At high frequencies (typically above 10 kHz), however, the experimental phase velocities approach those of the fundamental anti-symmetric (A0) and symmetric (S0) modes of dispersive Lamb waves, which themselves asymptotically approach the pavement layer's Rayleigh-wave velocity (Figure 2.6).
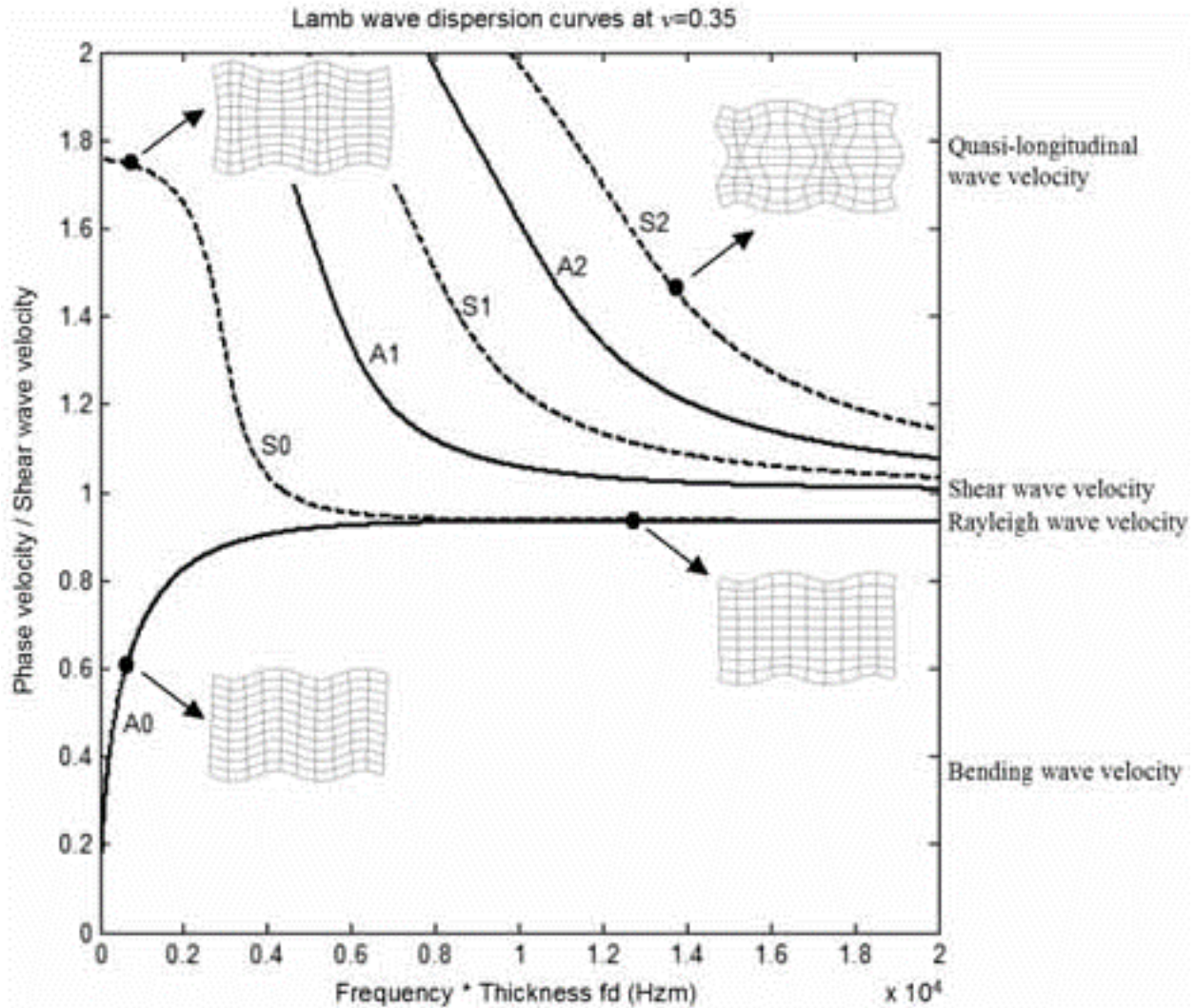
Figure 2.6. Anti-symmetric and symmetric modes of a free plate (Ryden and Park 2004)

To obtain accurate properties of the base and subgrade layers, inversion of the phase-velocity dispersion data would require matching of the low-frequency branches generated by interaction of leaky quasi-Lamb waves in these layers. Alternatively, if only the properties (*E*-modulus and thickness) of the stiff top pavement layer are desired, inversion can be avoided by using a simplified analysis in which experimental phase velocities are matched to the fundamental A0 mode of Lamb waves in a free plate (as well as segments of the S0 mode, if detected), as described by Ryden et al. (2004, 2006). As shown in Figure 2.6, the A0 mode approaches the Rayleigh-wave velocity at high frequencies. If the experimental dispersion data can be measured to sufficiently high frequencies, the Rayleigh-wave velocity of the pavement layer can simply be read as the horizontal asymptote.

In this study, a more general approach is taken in which a numerical model of the pavement, base, subbase, and soil layers is used in a multilayer inversion procedure to solve for the thickness and phase velocity of each layer. Because the solution is not unique, optimization

8

methods are used to minimize the misfit between the experimental dispersion curves and theoretical dispersion curves of randomly generated multilayer models (Lin 2014).

Whether employing a multilayer inversion or the free-plate Lamb wave approximation, resolution of the pavement-layer properties first requires accurate experimental measurement of the phase-velocity spectrum at high frequencies. A high-resolution testing setup and delicate operation are required because of the high wave speeds, short wavelengths, and small motions involved. To reliably measure high-frequency dispersion characteristics, the MSOR method requires a repeatable impact source that can generate waves with consistent timing and triggering (Park et al. 2002), with minimal deviation from the intended impact locations. This is because all sensors in an MASW test measure the same seismic waves from a single triggered impact, whereas generation of the equivalent data by MSOR requires a separate triggered impact for each sensor. Based on the results of several tests performed in this study, the MASW method can provide more reliable measurement of high-frequency components owing to the fixed receiver locations and less-stringent requirement on impact repeatability. The primary drawbacks of MASW testing for pavements are the costs of multiple accelerometers and a multichannel signal analyzer, as well as the time required to couple and decouple multiple accelerometers.

For more than a decade, the portable seismic pavement analyzer (PSPA) has been the state-of-the-practice equipment for surface-wave testing for engineers and DOT agencies (Nazarian et al. 1995, Celaya et al. 2006, Icenogle and Kabir 2013). Portable seismic pavement analyzer users, however, have experienced occasional difficulties in measuring high-quality data because of deterioration of the rubber feet and unsmooth asphalt surfaces (e.g., Icenogle and Kabir 2013). Moreover, the PSPA produces significant uncertainty in the shear-wave velocity of asphalt pavement layers by averaging a wide range of discrete dispersion data at short wavelengths (<6 in.) and high frequencies (>10 kHz) (Figure 2.7). To overcome those challenges, the study by Lin and Ashlock (2014) demonstrated that the custom-built MASW equipment and data acquisition (DAQ) program developed in this study can improve the robustness of the equipment and the certainty of dispersion data with great efficiency at relatively low cost.
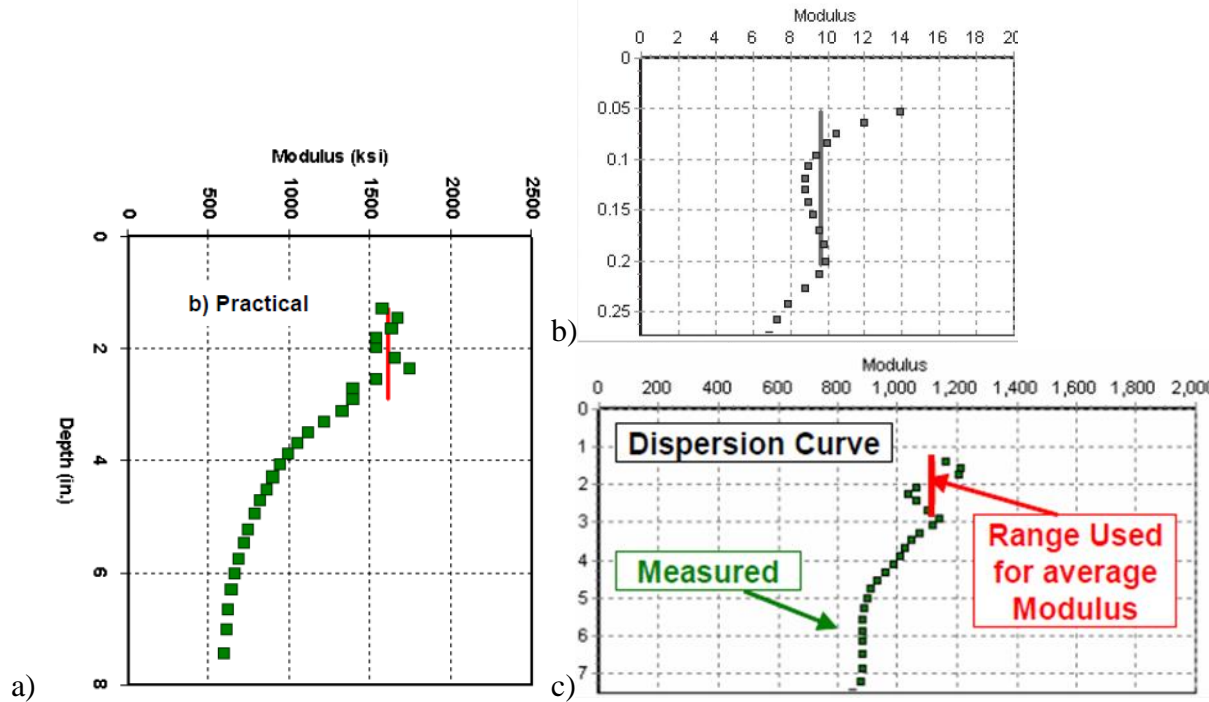
Figure 2.7. Examples of uncertainty in near-surface (high-frequency) experimental dispersion data measured with PSPA: (a) and (b) from Celaya and Nazarian (2006), (c) from Celaya et al. (2006)

2.3 Nondestructive Measurement of Stiffness

The Humboldt GeoGauge is a portable device that provides a simple, rapid means of obtaining a measure of stiffness and modulus of prepared soil and aggregate. The recommended operating temperature of the device is between 0 and 38°C. Humboldt specifications state that the GeoGauge measures the mechanical impedance of a material at the material surface by imparting very small displacements to the ground ($<1.27 \times 10^{-6}$ m or <0.00005 in.) at 25 steady-state frequencies between 100 and 196 Hz. The GeoGauge measures the stiffness by dividing the force imparted to the material by the resulting surface deflection for each frequency. A single stiffness value is determined by computing the average stiffness over the 25 frequencies.

The GeoGauge weighs approximately 10 kg (22 lb), is 28 cm (11 in.) in diameter and 25.4 cm (10 in.) tall, and rests on the ground surface via a ring-shaped aluminum foot, as shown in Figure 2.8. The annular foot has an outside diameter of 144 mm (4.50 in.), an inside diameter of 89 mm (3.50 in.), and annular ring thickness of 13 mm (0.5 in.). The foot rests directly on the ground surface without penetrating it and supports the weight of the GeoGauge via rubber isolators. Attached to the foot is the electromechanical shaker that vibrates the foot in the vertical direction. Velocity sensors are attached to the shaker and footing to measure the force and displacement of the foot at each harmonic frequency, from which an equivalent homogeneous half-space material stiffness is computed.

10

Figure 2.8. Humboldt GeoGauge (Humboldt Manufacturing)

When the shaker vibrates, a force (F) is applied and the material deflects a certain amount (δ). The shaker generates a force of approximately 9 N (2 lb). The magnitude of the vertical displacement induced at the soil-ring interface is typically less than 1.27×10^{-6} m (0.00005 in.), measured using velocity sensors (Alshibli et al. 2005). The deflection is proportional to the outside radius of the ring foot (R), the Young's modulus (E), and Poisson's ratio (v) of the material being tested. The stiffness is the ratio of the force to displacement:

$$K = F/\delta \tag{1.2}$$

The static stiffness, K, of a rigid annular ring on a linear-elastic, homogeneous, and isotropic half-space has the following functional form (Egorov 1965):

$$K = \frac{ER}{(1-v^2)\omega(n)} \tag{1.3}$$

where $\omega(n)$ is a function of the ratio of the inside to outside diameter of the annular ring. For the ring geometry of the GeoGauge, the parameter $\omega(n)$ is equal to 0.565. Therefore, the static stiffness of the GeoGauge has the following function form:

$$K = \frac{1.77ER}{(1-v^2)} \tag{1.4}$$

These equations assume that the underlying soil is linear elastic, homogeneous, and isotropic. Although these assumptions are frequently invoked in soil mechanics and pavement design, they do not accurately reflect the layered nature of pavement and soil profiles. Therefore, any

11

computation of such an "equivalent homogeneous" elastic modulus from the GeoGauge measured stiffness must be carefully evaluated in view of the foregoing assumptions (Lenke et al. 2003).

The equations above are programmed internally in the GeoGauge, which outputs the stiffness on the screen. However, this value is actually an average of the measured stiffness at 25 frequencies; in the field it is not possible to examine the variation of the data with frequency. After each use, however, the internal data at each frequency can be downloaded to a computer using infrared-to-serial cable and serial-to-usb adapter, as shown in Figure 2.9.
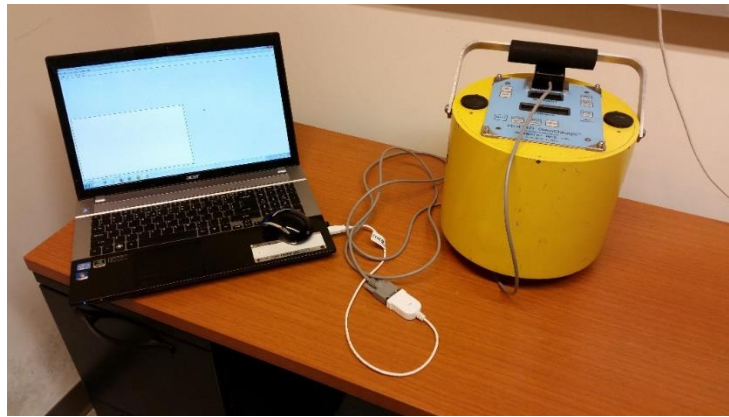
Figure 2.9. GeoGauge connected to a computer for transfer of data.

Many states across the county are beginning to examine stiffness and its use in quality control of subgrade/base layers of roads. Use of the Humboldt GeoGauge for measuring the stiffness of subgrade and base layers as a new nondestructive QC/QA tool has been increasing. In previous studies, typical stiffness values of subgrade/base layers under Portland cement concrete (PCC) pavements in Iowa measured using the GeoGauge were between 2 and 8 MN/m, except for some sections containing fly ash and special granular materials, which had stiffnesses up to 15 MN/m (White and Harrington 2005). Mohammad et al. (2003) measured stiffness of crushed limestone and foamed asphalt bases in Louisiana for continuously reinforced concrete (CRC) pavements and obtained average stiffnesses of 18.0 MN/m and 22.8 MN/m, respectively. Chen et al. (2000) measured the stiffness of different base materials throughout Texas and developed a quality criterion based on the GeoGauge stiffness (Table 2.1). It was reported that the quality of the base correlated better with its stiffness than its density. Also reported was a poor correlation between density and stiffness measurements.

Table 2.1. Base quality designation in terms of GeoGauge stiffness (Chen et al. 2000)

Base Quality	Stiffness (MPa)	Stiffness (MN/m)
Weak	<87	<10
Good	156–208	18–24
Excellent	>260	>30

Lee et al. (2011) used the GeoGauge to measure the stiffness of a cold-in-place recycling (CIP) layer and reported that the stiffness steadily increased over the curing time despite the occurrence of rainfall. The stiffness of the CIP layer did not decrease immediately after rainfall, but did decrease one or two days after rainfall. After the decrease, the stiffness increased gradually over time. Despite the occurrence of continuous rainfall, the stiffness remained above the initial stiffness value measured immediately after construction. Overall, the stiffness of the CIP layer increased over time, with all test sections reaching 20 MN/m before an overlay, with one section reaching 30 MN/m. The stiffness of this CIP layer increased from about 24 MN/m to 30 MN/m in the first three days after construction, then remained constant for 30 days before application of an overlay. The stiffness exhibited a daily fluctuation during the curing period. In some cases, the in situ stiffness remained constant, and in other cases it steadily increased during the curing period before an overlay, despite some rainfall. The initial stiffness of one CIP section immediately after construction, during a late season when pavement temperature was relatively low, was relatively high at about 25 MN/m, but it did not increase throughout the curing period. After the stiffness was measured with the GeoGauge, the density was then measured by a nuclear gauge at five times during the curing period (Lee et al. 2011). Figure 2.10 shows the resulting low correlation between the nuclear gauge density and GeoGauge stiffness.
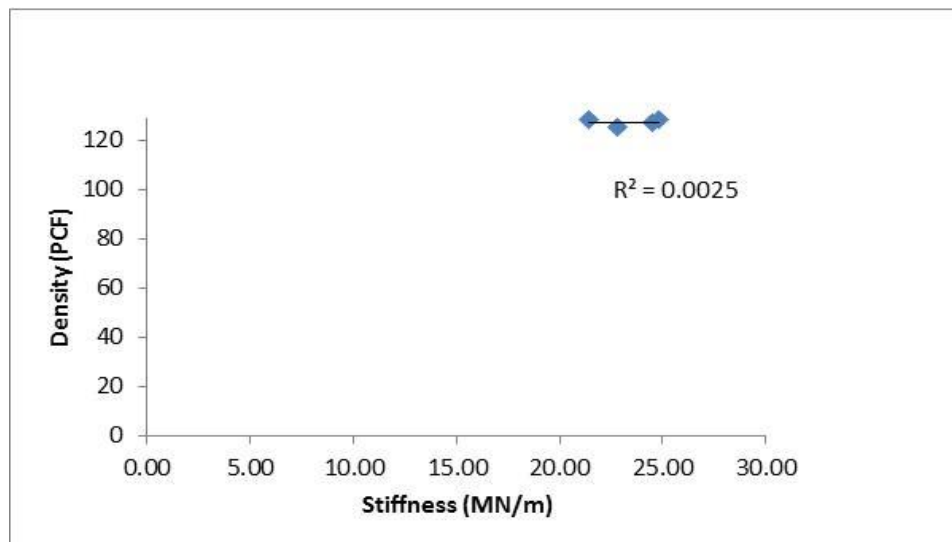
Figure 2.10. Low correlation between nuclear gauge density and GeoGauge stiffness measurements from study by Lee et al. (2011).

The GeoGauge was originally designed for measuring the stiffness of subgrade and base layers. While the Humboldt Manufacturing Company claims that the GeoGauge may be applicable for monitoring the compaction of asphalt to prevent over-compaction, use of the GeoGauge to measure stiffness of asphalt pavements has yet to be demonstrated. The feasibility of using the GeoGauge for this purpose is examined in this report.

The main objective of using the GeoGauge in this study is to explore the possibility of using the device as part of the QC/QA process for new asphalt pavement construction. First, stiffness, temperature, and field density (using the PT device) were measured for the selected new asphalt

pavement sections. Through analysis of data from several sites with different pavement types, along with other in situ and laboratory testing methods, the feasibility of using GeoGauge stiffness measurements for QC/QA of asphalt pavements was assessed.

2.4 Laboratory Testing Technologies

Various laboratory testing techniques have been developed to measure resilient and dynamic moduli of asphalt specimens. Resilient modulus has been widely used in the past (e.g., Celaya et al. 2006, Bai 2004); however, dynamic modulus is a better mechanical parameter for characterizing the actual behavior of asphalt concrete and is adopted for design in the MEPDG (Bai 2004). Dynamic modulus has four advantages over resilient modulus (Bai 2004): (1) the shear modulus G^* that can be calculated from dynamic modulus E^* and Poisson's ratio is adopted by the new asphalt binder specifications, thus relationships between the shear moduli of asphalt binder and mixes can be developed; (2) creep compliance and stress relaxation can be estimated from dynamic modulus (Pagen 1963); (3) permanent deformation and low-temperature cracking can be modeled using dynamic modulus; and (4) dynamic modulus tests exhibit less variation than resilient modulus tests.

Aimed at capturing the viscoelastic behavior of asphalt mixtures, both axial and indirect tension (IDT) testing methods have been developed to measure dynamic moduli over a range of temperatures and loading frequencies (e.g., Dougan et al. 2003, Kim et al. 2004). The measured moduli are then combined to construct a master curve representing properties of the asphalt mixture material at a reference temperature and over a range of loading frequencies. The axial method requires 6 in. high specimens, which precludes testing field cores from asphalt pavement courses or overlays that do not meet this thickness. Therefore, axial dynamic modulus specimens must typically be compacted in the laboratory using mixes from the field, whereas IDT dynamic modulus tests can be performed on cores of field-compacted mixes having a diameter of 4 or 6 in. and a height of only 1.5 or 2 in. Compared to field-cored specimens of as-built pavements, laboratory-compacted specimens will possess different asphalt structures and therefore different moduli, which are typically greater than the field values (Bai 2004). Because of these advantages, the IDT dynamic modulus testing method was used on 101.6 mm (4 in.) and 152.4 mm (6 in.) diameter field cores for this study.

The IDT test equipment used in this study is shown in Figure 2.11.
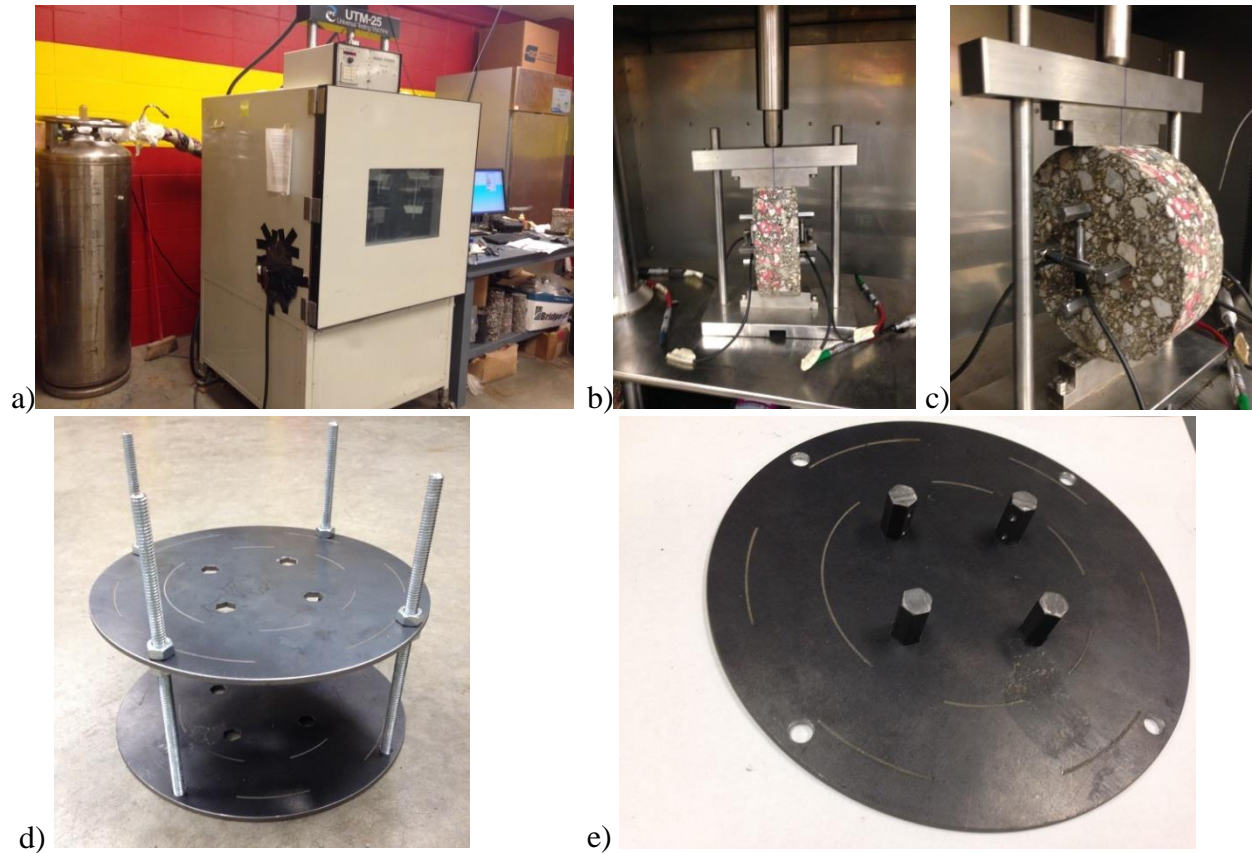
Figure 2.11. Indirect tension test setup: (a) full view, (b) 4 in. core with two LVDTs on each side in the chamber, (c) horizontal and vertical LVDTs mounted on one side of a 4 in. core, (d) custom-built alignment jig for installation of LVDT targets, (e) bottom plate of jig with four LVDT targets.

Test procedures were performed in accordance with the proposed AASHTO standard (AASHTO 2014). The testing system was retuned for specimens from each project in order to minimize loading error and be able to reach target strain ranges recommended by the proposed AASHTO standard. The modulus can be calculated by

$$\left| E^* \right| = \frac{2P_0}{\pi a d} \frac{\beta_2 \gamma_1 + \beta_1 \gamma_2}{U \beta_2 - V \gamma_2}$$

(1.5)

where P_0 is the amplitude of the centered sinusoidal load, U is the amplitude of the corrected and centered horizontal displacement, V is the amplitude of the corrected and centered vertical displacement, a is the loading strip width, d is the specimen thickness, and β_1, β_2, γ_1, and γ_2 are coefficients given in Table 2.2, which depend on the specimen geometry and linear variable differential transformer (LVDT) gauge length.

Table 2.2. Coefficients for dynamic modulus calculation

Specimen Diameter d (mm)	Loading Strip a (mm)	Gauge Length (mm)	β_1	β_2	γ_1	γ_2
101.6	12.3	65	0.0296	-0.0075	0.0050	0.0174
152.4	18.54	65	0.0262	-0.0078	0.0063	0.0206

CHAPTER 3 – NONDESTRUCTIVE TESTING OF ASPHALT PAVEMENTS

This chapter presents nondestructive testing of five newly constructed asphalt pavement projects in Iowa. The five projects include hot-mix asphalt (HMA) and warm-mix asphalt (WMA) pavements at the Central Iowa Expo in Boone; HMA pavements on US 69; HMA pavements on US 169; three sections of IA 93 featuring thin overlay (OL), cold-in-place (CIP) recycling, and full-depth reclamation (FDR); and HMA and WMA pavements on US 6. Detailed information on the pavement sections and tests is presented in the following sections.

3.1 Asphalt Test Sections

Five representative asphalt paving projects were selected to cover a range of pavement types including high-volume versus low-volume, HMA versus WMA, and newly-constructed versus resurfacing projects. Details of each paving project and designations for the testing locations and cores are given in Table 3.1.

Table 3.1. Description of paving projects in this study

Project/ Pavement Type	# of Testing Locations	Location (core) Designators
1. Boone HMA base	19	HB1-1, HB1-3, HB1-5, HB1-7, HB2-1, HB2-2, HB2-5, HB2-7, HB5-1, HB5-3, HB5-6, HB5-7, HB6-3, HB6-4, HB6-5, HB6-7, HB7-2, HB7-4, HB7-7
2. Boone WMA base	16	WB3-2, WB3-4, WB3-5, WB3-7, WB4-1, WB4-2, WB4-3, WB4-7, WB8-4, WB8-5, WB8-7, WB8-8, WB9-2, WB9-3, WB9-6, WB9-7
3. Boone HMA surface	7	HS1-1, HS1-2, HS1-3, HS1-4, HS2-1, HS2-2, HS2-3
4. Boone WMA surface	9	WS3-1, WS3-2, WS3-3, WS3-4, WS4-1, WS4-2, WS4-3, WS4-4, WS4-5
5. US 69 HMA	9	US 69-1, US 69-2, US 69-3, US 69-4, US 69-5, US 69-6, US 69-7, US 69-8, US 69-9
6. US 169 HMA	6	US 169-1, US 169-2, US 169-3, US 169-4, US 169-5, US 169-6
7. IA 93 FDR	2	IA 93 FDR-1, IA 93 FDR-2
8. IA 93 CIP	2	IA 93 CIP-1, IA 93 CIP-2
9. IA 93 OL	2	IA 93 OL-1, IA 93 OL-2
10. US 6 HMA	6	US 6 H20-2, US 6 H20-3, US 6 H25-1, US 6 H25-2, US 6 H30-2, US 6 H30-3
11. US 6 WMA	4	US 6 W15-1, US 6 W15-2, US 6 W30-2, US 6 W30-3

For each project site, at least six testing locations were randomly selected in the paving lane (Figure 3.1).
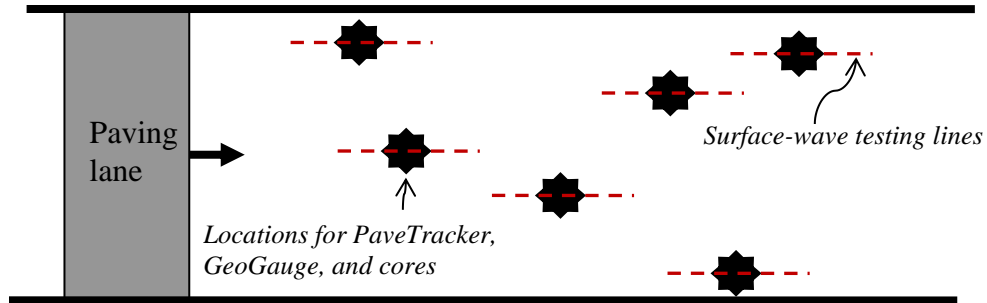
Figure 3.1 Schematic of six randomly selected NDT testing locations per project site

Surface-wave testing was carried out along straight lines parallel to the paving direction and centered on the testing locations. Immediately before or after the surface-wave tests, the in situ density and stiffness were measured at the testing locations using the PT and GeoGauge, respectively. For each testing location, five PT readings were recorded with the device rotated 90° between readings (the first and fifth readings had the same orientation), and the values were averaged. Similarly, three GeoGauge readings were recorded with the device rotated 120° between readings. To provide uniform contact and fill any gaps under the GeoGauge foot, a thin layer (approximately 1/4 in.) of fine, moist sand was first spread on the pavement surface as recommended in the device manual, then the GeoGauge was placed on the sand and gently rotated slightly about its vertical axis. Photos of the various field and NDT testing procedures are shown in Figure 3.2.
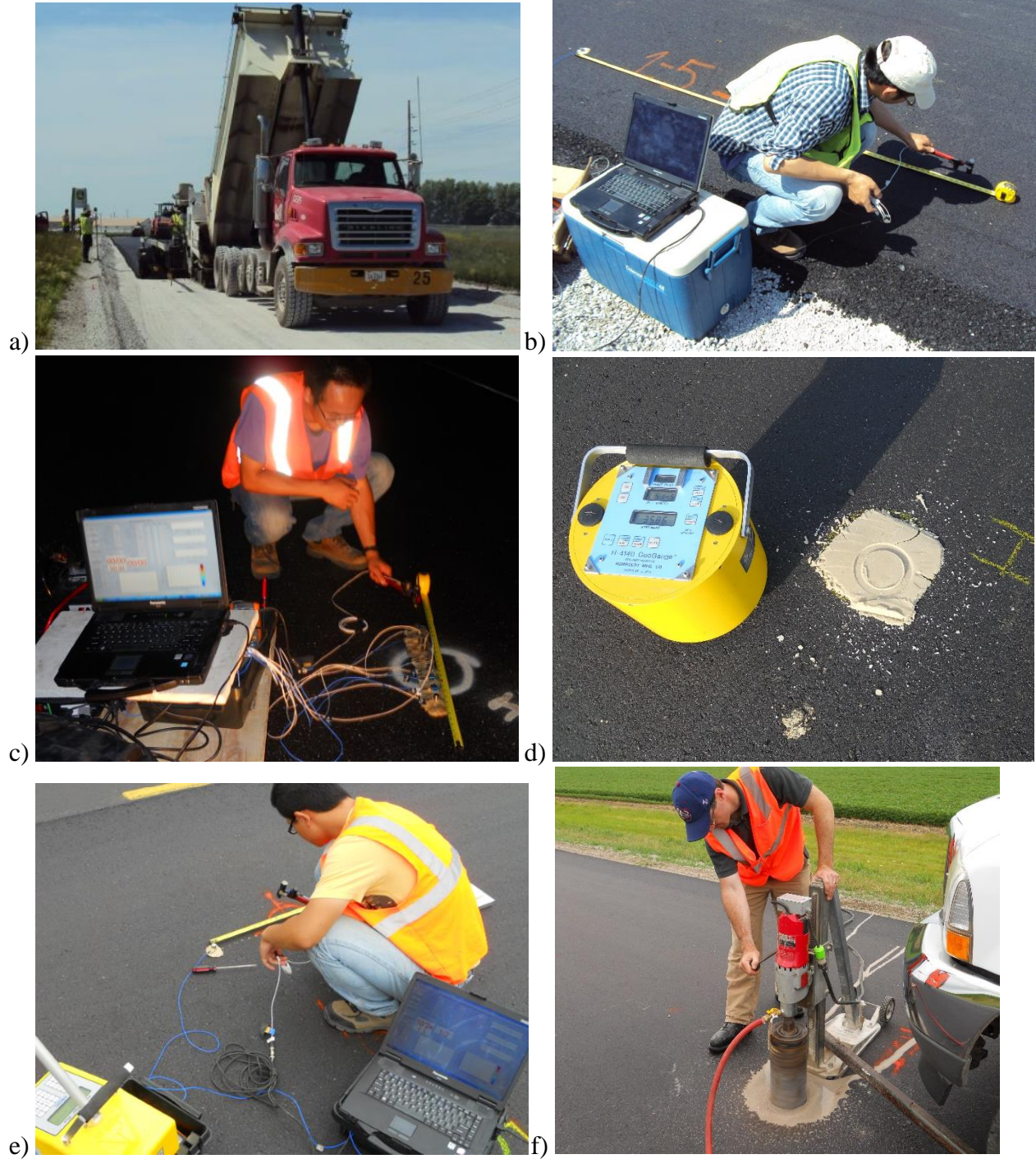
Figure 3.2. (a) Pavement construction at Central Iowa Expo site, (b) MSOR surface-wave testing at Central Iowa Expo site, (c) MASW surface wave testing on US 6, (d) GeoGauge testing on IA 93, (e) MSOR surface-wave testing on US 69, (f) coring on US 69
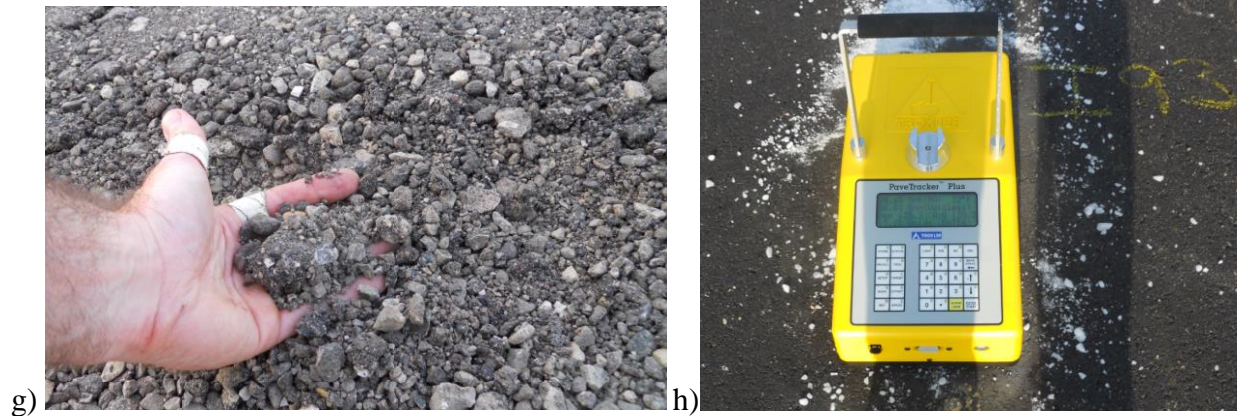
Figure 3.2 (continued). (g) FDR section on IA 93, (h) PaveTracker testing on IA 93

Field temperatures at each test location were recorded by inserting a thermocouple probe into holes created by pushing a screwdriver into newly placed hot asphalt pavements, or by holding the probe against the surface of cured asphalt pavements. "Hot" tests were performed up to a few hours after paving, and "cold" tests were performed after cooling the pavement surface with dry ice. Additional ambient-temperature tests were performed on selected projects one or more days after paving.

3.2 Surface-Wave Testing Results

The surface wave testing equipment and DAQ program developed in this study were first used for MSOR testing at the Central Iowa Expo site in Boone County. Several different types of pavements, base courses, and stabilization technologies were constructed at this site for the Iowa DOT research project "Boone County Expo Research Phase I—Granular Road Compaction and Stabilization." The MSOR testing was carried out for 19 HMA and 16 WMA locations on the base courses, and 7 HMA and 9 WMA locations on the surface courses, as detailed in Table 3.1. For the first eight testing locations, MSOR data were recorded using impact stations spaced from 0.1 to 2.4 m from the receiver in 0.1 m increments. After examining the data for the first eight locations, the testing spread was subsequently decreased to 0.05 to 1.2 m with smaller 0.05 m increments, to obtain better resolution for the asphalt layer, which is of interest for this study.

3.2.1 Boone HMA and WMA Tests on Base and Surface Courses

The field data and corresponding experimental dispersion trends of hot and ambient-temperature surface-wave tests for Boone HMA base course location HB1-1 are shown in Figure 3.3. Data for all other Boone base and surface courses are detailed in Figures A.1 to A.8 in Appendix A. The experimental dispersion images were obtained by the MASW phase-velocity scanning method of Park et al. (1999) with enhancements by Lin (2014). The experimental dispersion image is a color map for which the maximum amplitude at each frequency gives the surface-wave phase velocity at that frequency. The peaks are "picked" algorithmically to give an experimental dispersion curve, which can then be used in the inversion procedure to determine the material properties (modulus and thickness) of the pavement-system layers.
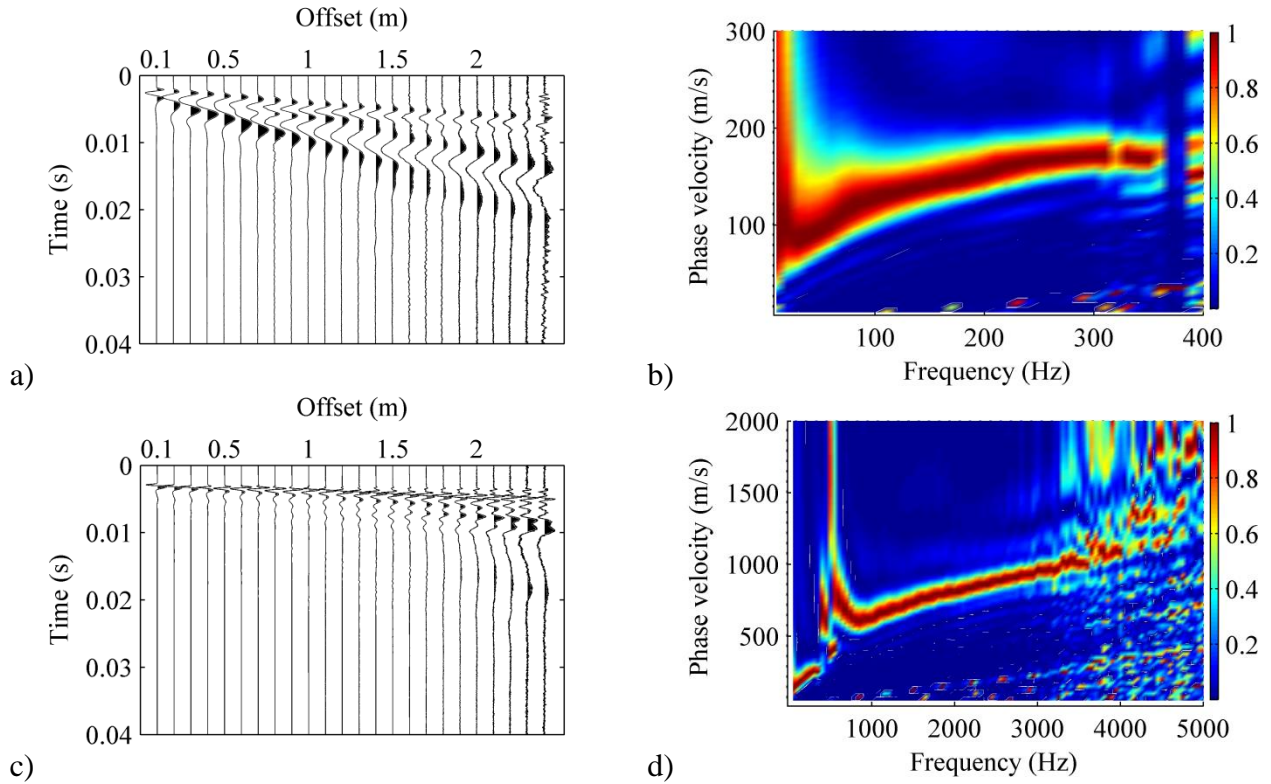
Figure 3.3. MSOR surface-wave test results for Boone HMA base course location HB1-1: (a) normalized time-domain data for hot test, (b) experimental dispersion image for hot test, (c) normalized time-domain data for ambient-temperature test, (d) experimental dispersion image for ambient-temperature test

The experimental dispersion trends from all hot and ambient-temperature tests performed at the Boone site are compared in Figure 3.4.
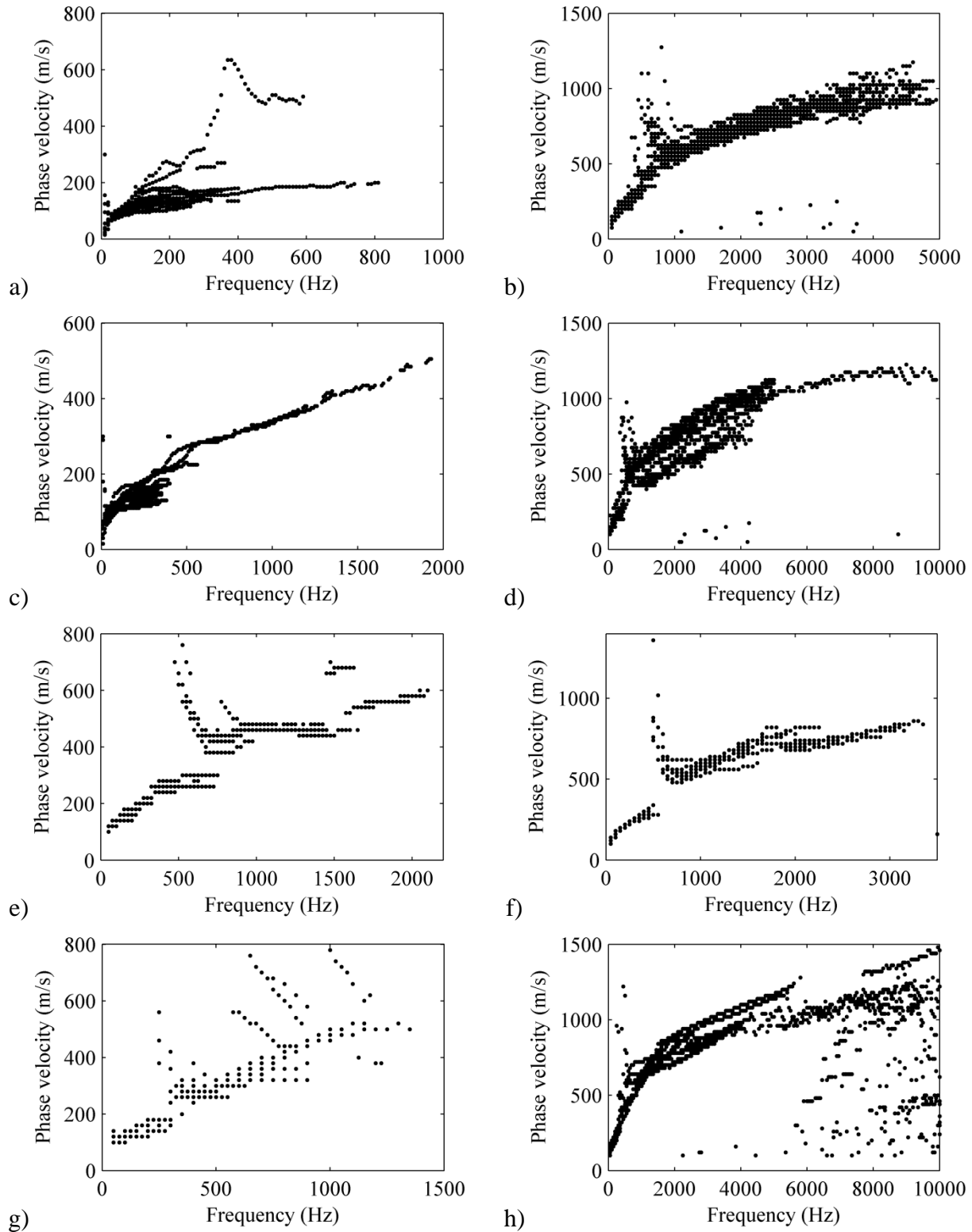
Figure 3.4. Dispersion trends of Boone HMA base courses: (a) several hours after paving, (b) several days after paving; Boone WMA bases: (c) several hours after paving, (d) one day after paving, Boone HMA surface: (e) several hours after paving, (f) one day after paving; Boone WMA surface: (g) several hours after paving, (h) several days after paving

23

The left column of the figure shows four groups of dispersion trends from the hot tests at 19 HMA base course locations (Figure 3.4a), 16 WMA base course locations (Figure 3.4c), 7 HMA surface course locations (Figure 3.4e), and 9 WMA surface course locations (Figure 3.4g). The right column shows the corresponding results from the ambient-temperature tests, performed one or more days after construction.

It can be seen in Figure 3.4a and b that the maximum measureable frequency and phase velocity in the dispersion curves of the HMA base courses increased from 400 Hz and 200 m/s in the hot tests to 5,000 Hz and 1,200 m/s in the ambient-temperature test, as the average testing temperature decreased from 73.4°C to 28.7°C (Table A.14 in Appendix A). This phenomenon is a result of (1) the curing and associated hardening of the viscoelastic asphalt mixture, causing its stiffness to increase and damping to decrease, and (2) to a lesser extent, the dependence of the asphalt mixture's modulus on temperature. Similar trends can be seen for the WMA base course as the average temperature decreases from 61.8 to 33.4°C (Figure 3.4c and d, Table A.15). The differences for the HMA and WMA surface courses were not as considerable as those of the base courses (Figure 3.4e to h) because these tests had smaller temperature decreases, from 46.1°C to 45.2°C for HMA and 52.5°C to 49.1°C for WMA (Tables A.16 and A.17). From these temperatures, it is evident that more time had elapsed between paving and testing for the hot surface courses compared to the hot base courses.

The Genetic and Simulated Annealing (GSA) inversion program (Lin 2014) was used to back-calculate the shear-wave velocities of the pavement profile using assumed layer thicknesses from the design plans and an assumed Poisson's ratio of 0.3. Six testing locations from the Boone HMA base courses were randomly selected and their experimental dispersion curves were input into the inversion program. The program searches over randomly perturbed layered profile parameters (within specified ranges) and performs a nonlinear optimization to match theoretical dispersion curves to the experimental dispersion curves. The output is the final inverted shear-wave velocity profile whose theoretical dispersion curve best fits the experimental one. The solution is nonunique, however, because the Monte-Carlo-based GSA program will result in different final inverted profiles that are close to the true profile.

For selected Boone tests on ambient-temperature base courses, the target experimental dispersion curves and theoretical dispersion curves of the final inverted profiles are shown in Figures A.9 and A.10 of Appendix A. The shear-wave velocities (V_{s1}) of the first layers, which correspond to the asphalt pavement layer, are given in Table 3.2 and Table 3.3. Also reported in these tables are the corresponding Young's moduli and test temperatures. The HMA tests had an average temperature of 28.4°C and an average modulus of 10,053 MPa, whereas the WMA tests had a higher average temperature of 33.2°C and lower average modulus of 9,428 MPa.

Table 3.2. Inversion results for ambient-temperature Boone HMA base courses

Location	Field Temperature (°C)	V_{s1} (m/s)	E_1 (MPa)
HB1-1	24.7	1,412	11,877
HB1-7	26.4	1,381	11,461
HB2-1	31.8	1,237	9,156
HB5-1	30.1	1,310	10,342
HB6-3	29.4	1,100	7,265
HB7-4	27.7	1,307	10,218
Average	28.4	1,291	10,053
Coefficient of variation (COV)	9.1%	8.7%	16.6%

Table 3.3. Inversion results for ambient-temperature Boone WMA base courses

Location	Field Temperature (°C)	V_{s1} (m/s)	E_1 (MPa)
WB3-2	25.9	1,441	12,339
WB3-5	28.9	1,454	12,500
WB4-1	27.7	1,435	12,362
WB8-4	38.9	903	4,883
WB8-8	35.5	1,301	10,346
WB9-2	42.1	833	3,898
Average	33.2	1,228	9,428
COV	20.0%	23.2%	41.3%

3.2.2 US 69 HMA Tests

Multichannel simulation with one receiver surface-wave tests were carried out at nine testing locations on the HMA surface course after resurfacing of US 69. To improve measurement of the high-frequency components, the testing spread was decreased to the range 0.03–0.72 m, with 0.03 m increments. Data from all tests performed on US 69 are detailed in Figures A.11 and A.12 of Appendix A. Field data and corresponding dispersion trends at location US 69-9 are shown in Figure 3.5 for a hot test and a cold test after applying dry ice.
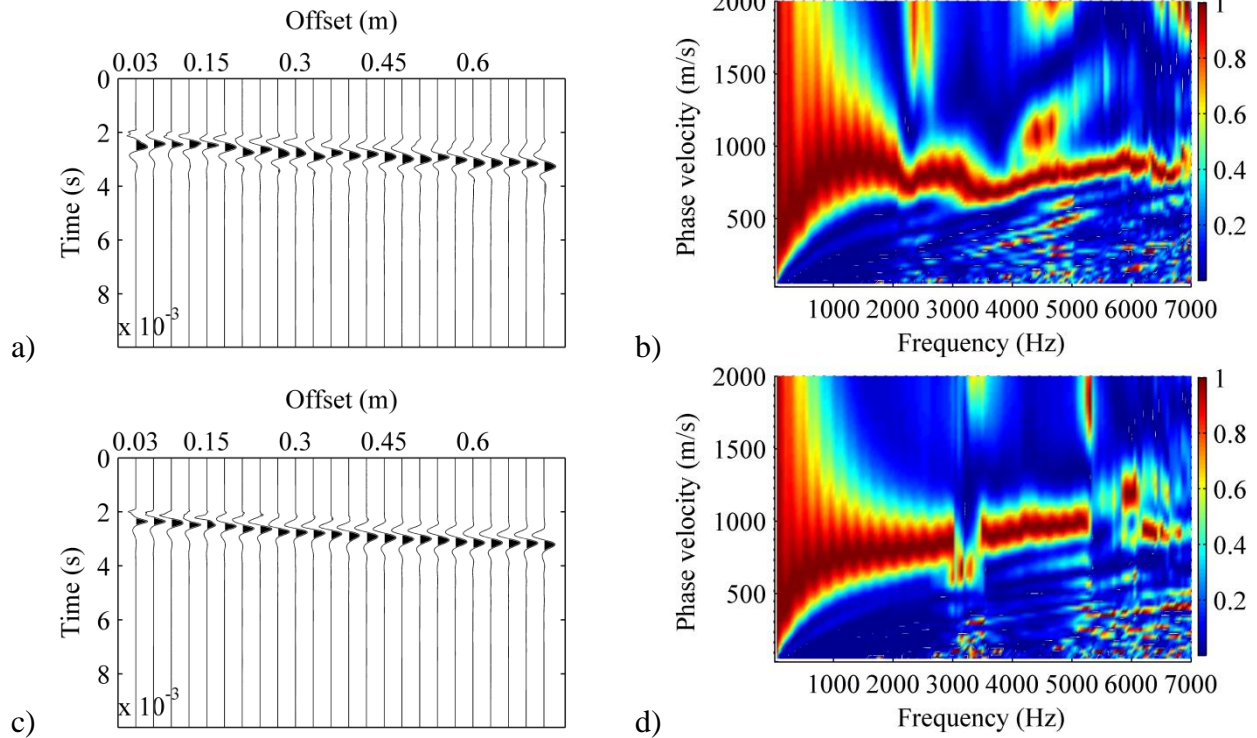
Figure 3.5. MSOR surface-wave test results at location US 69-9: (a) normalized time-domain data for hot test, (b) experimental dispersion trend for hot test, (c) normalized time-domain data for cold test, (d) experimental dispersion trend for cold test

Although the cold test shows a more regular dispersion trend similar to the A0 mode in Figure 2.6, it is measured up to only 5.5 kHz, which in this particular case is less than the maximum frequency of nearly 7 kHz obtained in the hot test. However, upon comparing all hot and cold tests, the scatter decreased and the maximum measurable frequency increased from about 5 kHz in the hot tests to about 7 kHz in the cold tests (Figure 3.6), as average testing temperature decreased from 60.5°C to 17.9°C (see Tables A.5 and A.6 in Appendix A).
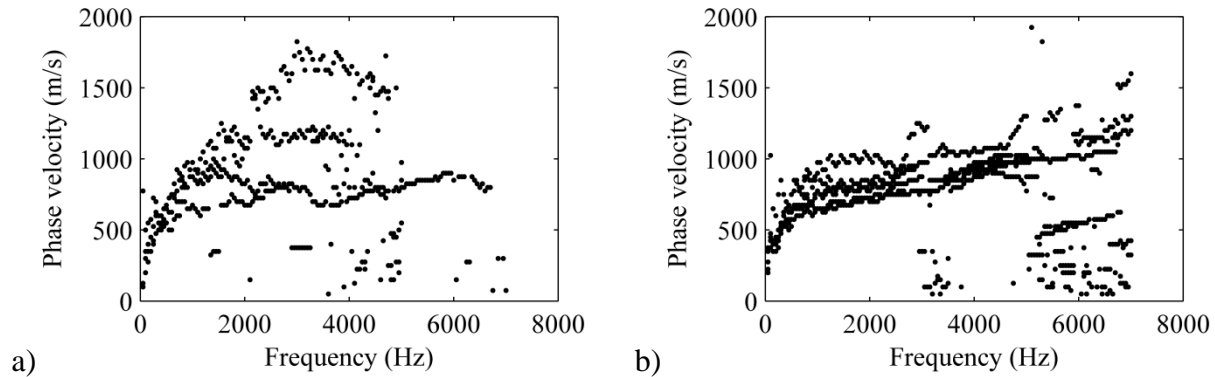
Figure 3.6. Dispersion trends for US 69 HMA surface course: (a) four hot tests at locations 1–3 and 9, (b) six cold tests at locations 4–9 several hours after paving and using dry ice

In these tests, the variation of phase velocity was more complex than in typical tests, because of the existing underlying asphalt pavement and PCC layers. The phase velocity and stiffness of these underlying layers were much higher than the newly paved HMA surface in the hot tests, which may be the main reason for the high phase velocities between 2 and 5 kHz in Figure 3.6a. After cooling the newly paved HMA layer using dry ice, it became stiffer and the associated dispersion data in Figure 3.6b appeared more regular. The low-velocity data points below 500 m/s are considered to be noise due to physical sources, measurement error, and the MASW phase-velocity scanning algorithm.

The GSA inversion program was employed to back-calculate the pavement profile in terms of shear-wave velocity with known thicknesses and an assumed Poisson's ratio of 0.3. Six experimental dispersion curves from the cold tests were selected for inversion, and their corresponding cores were taken for laboratory measurements of density and dynamic modulus. The inverted theoretical dispersion curves are compared against their experimental counterparts in Figure A.13 of Appendix A. The shear-wave velocity of the inverted first asphalt layer (V_{s1}) is listed in Table 3.4, along with the test temperature and Young's modulus. The cold HMA tests had an average temperature of 17.9°C and an average modulus of 7,581 MPa.

Table 3.4. Inversion results for cold tests on US 69 surface course

Location	Field Temperature (°C)	V_{s1} (m/s)	E_1 (MPa)
US 69-4	16	1,056	6,664
US 69-5	18.5	1,055	6,628
US 69-6	16.8	1,122	7,457
US 69-7	18	1,246	9,241
US 69-8	19.3	958	5,483
US 69-9	18.5	1,298	10,013
Average	17.9	1,123	7,581
COV	6.9%	11.4%	22.7%

3.2.3 US 169 HMA Tests

Multichannel simulation with one receiver surface-wave testing was carried out at six locations on the US 169 HMA surface course. Two different types of tests were performed: (1) cold tests after application of dry ice several hours after paving, and (2) ambient-temperature tests four days after paving. Tests on hot asphalt shortly after paving were not performed because of their limited usefulness as demonstrated in the previous two sections. The testing spread was 0.03–0.72 m in 0.03 m increments. Field data and corresponding dispersion trends for the cold and ambient-temperature tests at location US 169-4 are shown in Figure 3.7. The maximum useful frequency increased from about 7 kHz in the cold test (Figure 3.7b) to approximately 10 kHz in the ambient test (Figure 3.7d), and the stiffness also increased during the 4-day span, as evidenced by higher phase-velocities in Figure 3.7d.
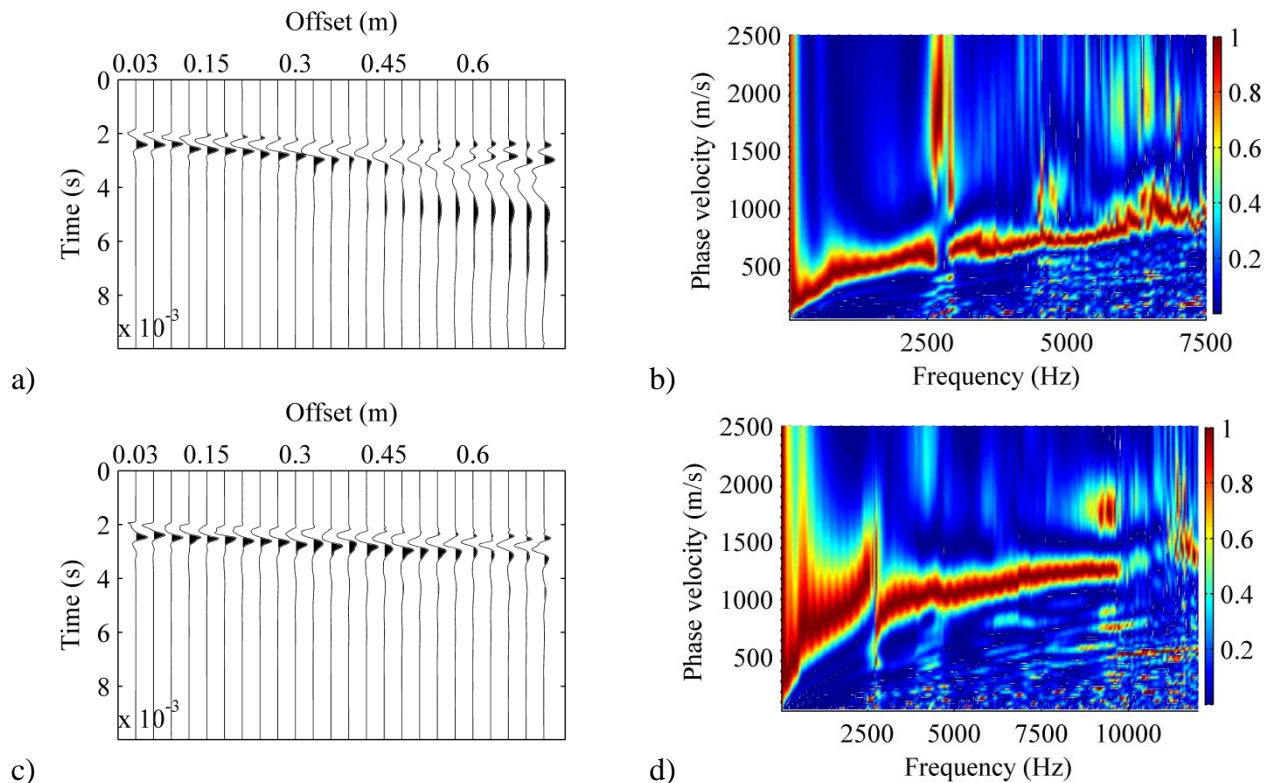
Figure 3.7. MSOR surface-wave test results for location US 169-4: (a) normalized time-domain data for cold test after dry ice, (b) experimental dispersion trend for cold test after dry ice, (c) normalized time-domain data for ambient-temperature test four days after paving, (d) experimental dispersion trend for ambient-temperature test four days after paving

Data from all other surface-wave tests on US 169 are detailed in Figures A.14 and A.15 of Appendix A. Comparison of the dispersion trends between the cold and ambient-temperature tests is presented in Figure 3.8. Because superposition of dispersion images like those of Figure 3.7b would not result in a clear picture because of the different frequency and velocity ranges of different tests, the maximum points from the dispersion images were instead picked to

28

obtain the dispersion curves, which were then plotted together to give Figure 3.8. This way of visualizing the data from all tests makes the dispersion trends more difficult to see compared to the clear trends in the dispersion images of individual tests such as those in Figure 3.7 or the clear trends in the picked dispersion curves (see Figure A.10 for examples). By referring back to the individual dispersion images in Figures A.14 and A.15, however, one can identify the noise from the primary dispersion trends in Figure 3.8, which are approximated by the red dashed lines.

a)   b)
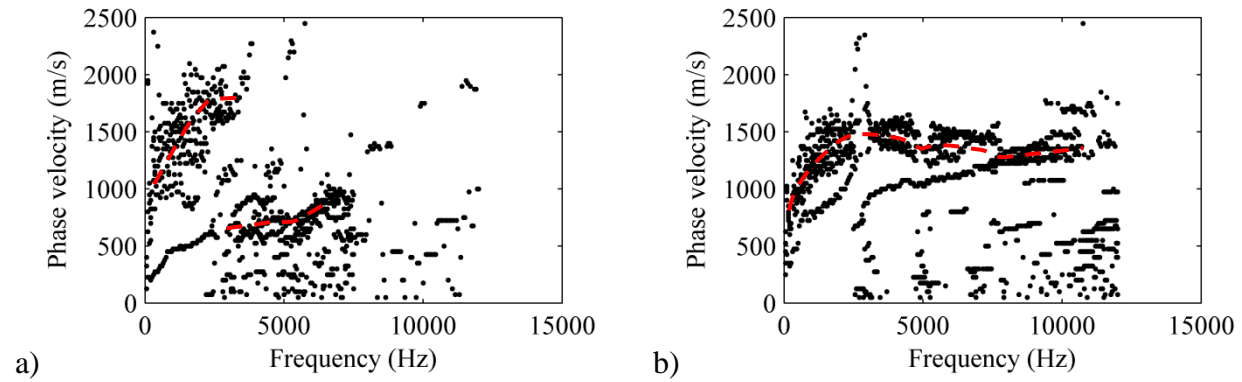
Figure 3.8. Dispersion trends for US 169 HMA surface course tests: (a) cold tests several hours after paving and applying dry ice, (b) ambient-temperature tests four days after paving

From these trends, the maximum measurable frequency of the dispersion data increased from about 7 kHz in the cold tests with dry ice to about 11 kHz in the ambient-temperature tests four days after paving, whereas the average testing temperature increased slightly from 26.6°C to 29.2°C (Table 3.5).

Table 3.5. Field temperatures of US 169 testing locations

Location	Temperature (°C) Several Hours After Paving and Applying Dry Ice	Ambient Temperature (°C) Four Days After Paving
US 169-1	20	27.4
US 169-2	27.9	28.6
US 169-3	33	28.6
US 169-4	29.6	29.1
US 169-5	23.5	30.6
US 169-6	25.4	31.1
Average	26.6	29.2

Similar to the tests on US 69, the variation of phase velocity is complex because of the much stiffer PCC pavement underlying the newly paved HMA. This could be the main reason for the

spike in phase velocity near 2,500 Hz in Figure 3.8b for the ambient-temperature tests after four days. Above 2,500 Hz in Figure 3.8a, the phase velocities of four of the dispersion curves (from locations 2, 3, 5, and 6) also decrease significantly from around 1,700 m/s to 600 m/s. The decreased velocities are in a range close to those of the dispersion curves from locations 1 and 4, where the four dispersion curves from both cold and ambient-temperature conditions (see Figures A.14 and A.15) indicate a normal pavement structure having decreasing stiffness with depth.

One possible reason for the exception at locations 1 and 4 is that the underlying layer might consist of patched asphalt pavements or PCC with severe cracking and thus behave much softer than the existing PCC and new asphalt layers. Above 2,500 Hz in Figure 3.8b, the phase velocities of all dispersion curves with the exception of location 4 have a decreasing velocity trend as frequency increases (see also Figure A.15). This indicates that although the asphalt pavement layer naturally cooled down after four days, causing the newly paved HMA layer to stiffen, it was still softer than the underlying PCC layer. To accurately measure the HMA layer's velocity in this soft-stiff-soft pavement structure, a testing system with a much higher frequency capability is needed to detect high-frequency dispersion characteristics. One solution is to use an MASW rather than MSOR testing approach (Lin and Ashlock 2014), as was done for the US 6 tests in this study.

3.2.4 IA 93 FDR, CIP, and OL Tests

Multichannel simulation with one receiver surface-wave tests were carried out at two surface course locations on each of three IA 93 sections with different pavement types. Chronologically, these were CIP, thin OL, and FDR sections. Multichannel simulation with one receiver data were recorded with receiver stations from 0.03 to 0.72 m in 0.03 m increments for the CIP and OL sections, and from 0.05 to 1.2 m in 0.05 m increments for the FDR section. Field data and corresponding dispersion trends of hot and cold surface wave tests at the IA 93 OL-1 location are shown in Figure 3.9. Data for all tests on IA 93 are detailed in Figures A.16 through A.20 of Appendix A.
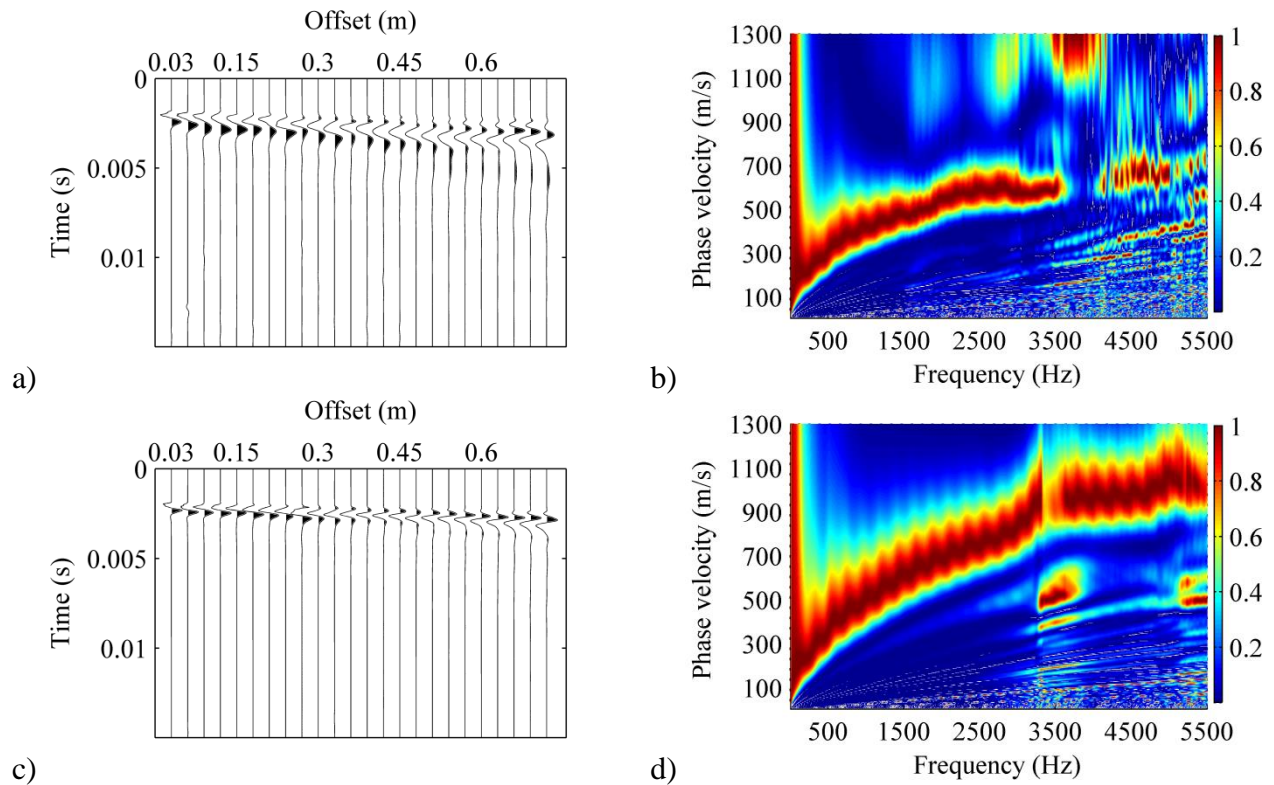
Figure 3.9. MSOR surface-wave tests on IA 93-OL1: (a) normalized time-domain data for hot test, (b) experimental dispersion trend for hot test, (c) normalized time-domain data for cold test, (d) experimental dispersion trend for cold test

Comparison of the dispersion trends from hot and cold tests is shown in Figure 3.10. The left column shows three groups of dispersion images from hot tests at two locations each on the CIP, OL, and FDR sections. The right column shows the corresponding results from cold tests performed at the CIP and OL locations. Cold tests could not be performed at the FDR section because of insufficient dry ice and safety concerns as testing stretched into the night.

a)

b)

c)

d)

e)
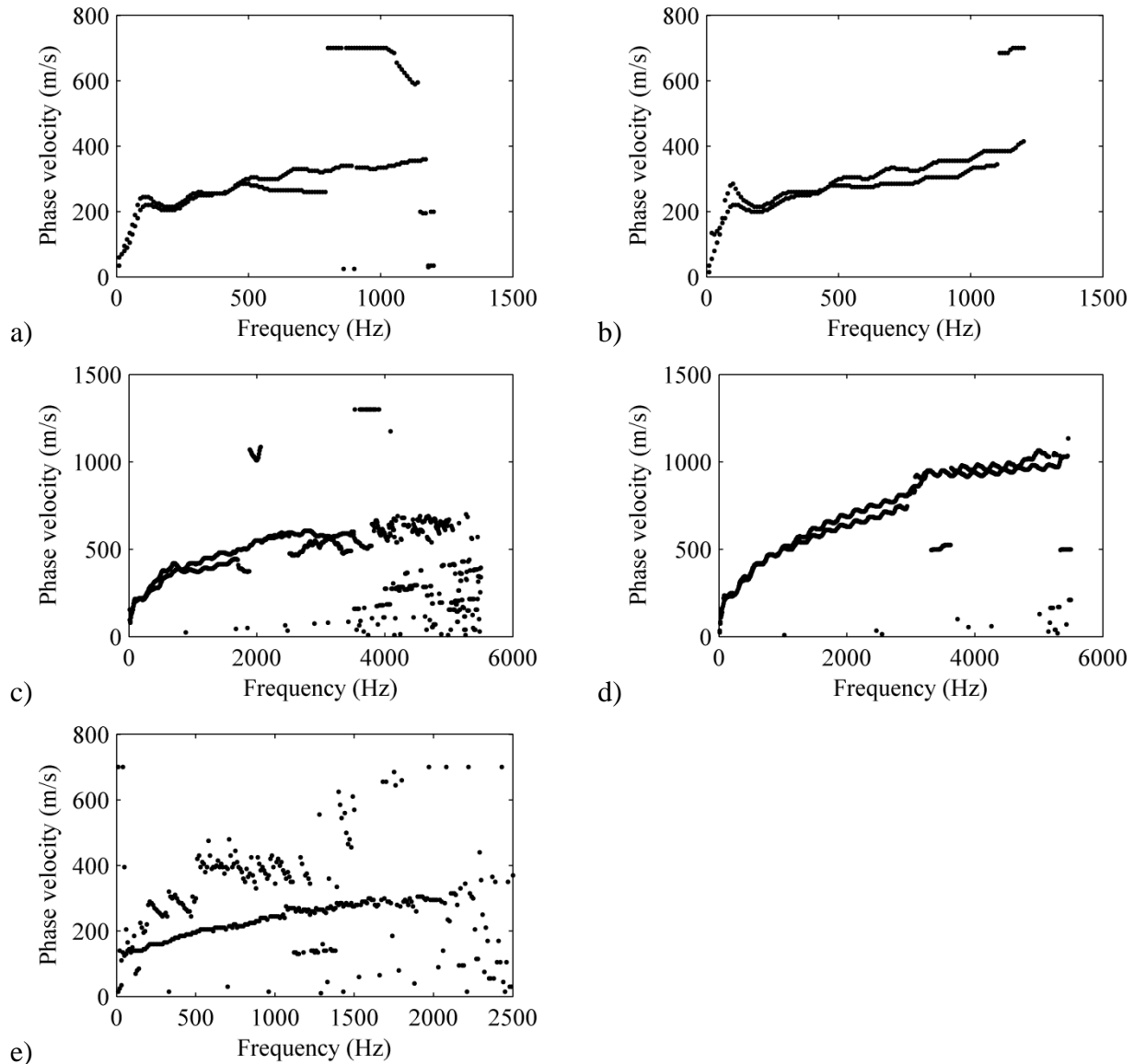
Figure 3.10. Dispersion trends of IA 93 sections: CIP section (a) several hours after paving, (b) several hours after paving and using dry ice; OL section: (c) several hours after paving, (d) several hours after paving and using dry ice; FDR section: (e) several hours after paving

Figure 3.10a and b show that the maximum useful frequency and phase velocity for the CIP section increased slightly in the cold tests, especially at location 2, as the average testing temperature decreased from 42.7°C to 18.2°C (see Tables A.8 and A.9 in Appendix A). For the OL section, the maximum phase velocity increases significantly from approximately 600 m/s to 1,000 m/s with a temperature decrease from 44.9°C to 12.9°C as shown in Figure 3.10c and d, although the maximum useful frequency increases only slightly. Figure 3.10e shows dispersion curves from two FDR locations; location 1 has a noisy dispersion image (Figure A.16), whereas location 2 has a clear dispersion image up to about 2,100 Hz. The reclaimed pavement at this location was similar to a macadam or very well-packed and lightly cemented gravel road that

32

crumbled by hand or when cored (see Figure 3.2g). Because of the surface roughness and granular nature of this pavement, surface-wave testing would be better accomplished with a landstreamer of closely spaced geophones instead of small accelerometers.

The GSA inversion program was employed to back-calculate the pavement profiles in terms of shear-wave velocity with known thickness and an assumed Poisson's ratio of 0.3. The inverted theoretical dispersion curves are compared to the experimental dispersion curves in Figure A.21. The shear-wave velocity of the inverted first layer (V_{s1}) is listed in Table 3.6 along with the field temperature and Young's modulus using the assumed Poisson's ratio of 0.3. The OL section has the highest modulus of 9,615 MPa, whereas the CIP and FDR courses have similar average moduli of 1,134 MPa and 858 MPa, respectively.

Table 3.6. Inversion results of dispersion curves from cold IA 93 tests

Location	Field Temperature (°C)	V_{s1} (m/s)	E_1 (MPa)
I93-CIP1	18.8	554	1,540
I93-CIP2	17.5	385	727
Average	18.2	469	1,134
COV	5.1%	25.5%	50.7%
I93-FDR1	33.8	488	1,229
I93-FDR2	29.4	299	488
Average	31.6	394	858
COV	9.8%	33.9%	61.1%
I93-OL1	13.5	1,409	10,718
I93-OL2	12.3	1,190	8,512
Average	12.9	1,299	9,615
COV	6.6%	11.9%	16.2%

3.2.5 US 6 HMA and WMA Tests

To enhance measurement precision in the high-frequency regime, which gives information on the asphalt pavement surface layer, the equipment and DAQ program were extended to enable MASW testing using an array of 9 accelerometers on US 6. Multichannel analysis of surface waves tests were then performed at six HMA and four WMA testing locations on the surface course. Hot tests and ambient-temperature tests were performed several hours and several days after paving, respectively. Multichannel analysis of surface waves data were recorded with receiver stations from 0.5 to 0.45 m in 0.05 m increments.

Field data and corresponding dispersion trends of hot and cold surface-wave tests at location US 6 W30-2 are shown in Figure 3.11. Data from all other field tests are detailed in Figures A.22 to A.25 in Appendix A.
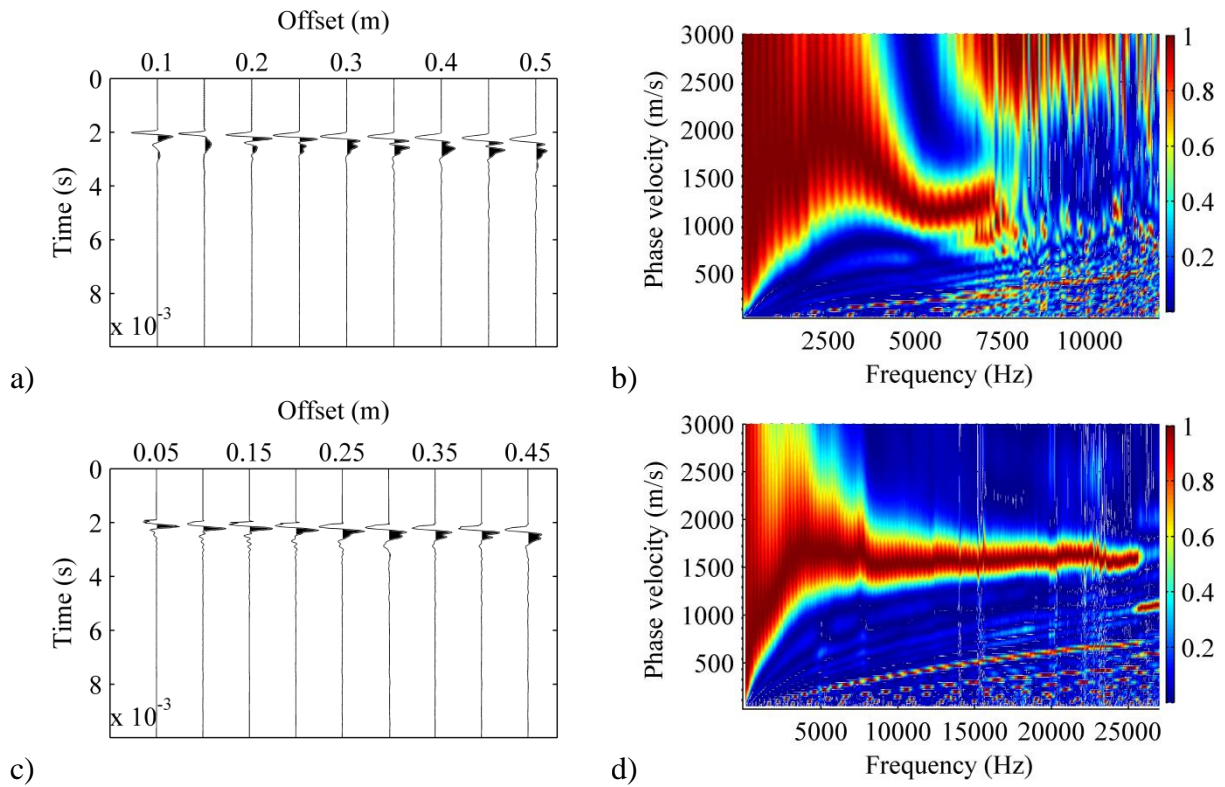
Figure 3.11. MASW surface-wave tests on US 6 W30-2: (a) normalized time-domain data for hot test, (b) experimental dispersion trend for hot test, (c) normalized time-domain data for ambient-temperature test, (d) experimental dispersion trend for ambient-temperature test

Comparison of dispersion trends from all hot and cold tests is presented in Figure 3.12.
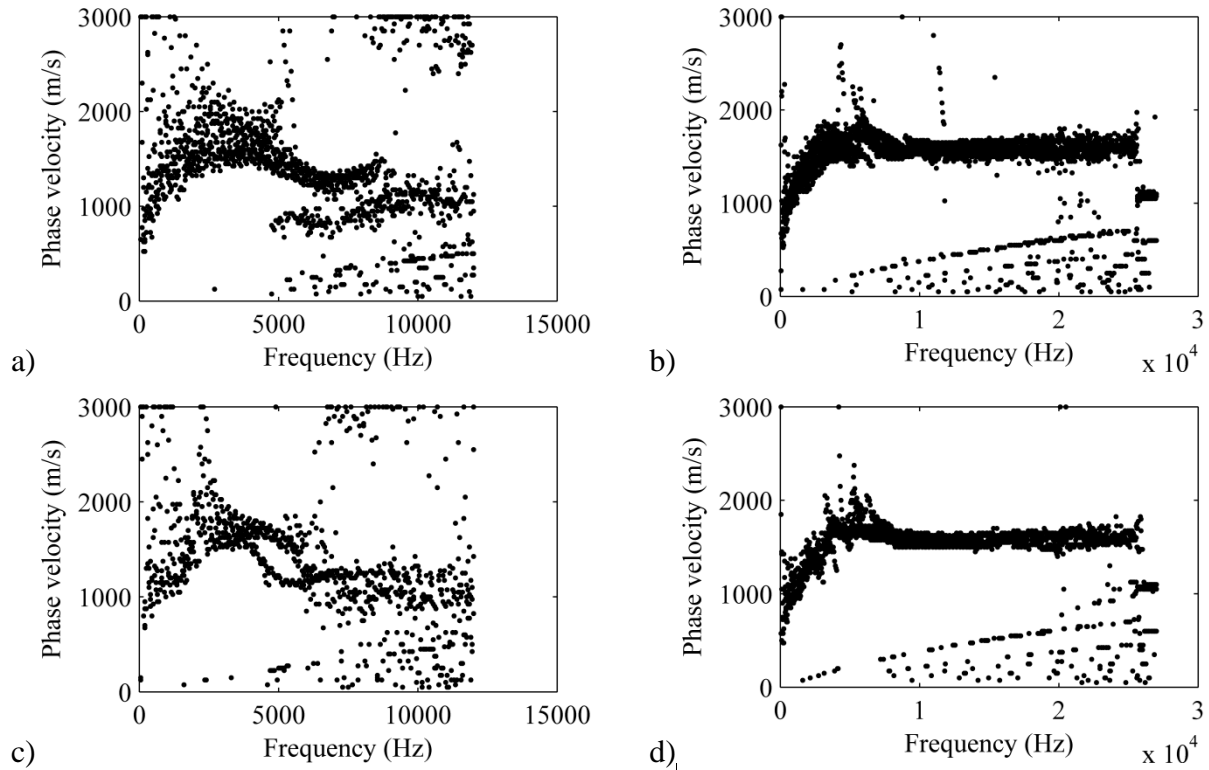
Figure 3.12. Dispersion trends of US 6 HMA surface course: (a) several hours after paving, (b) several days after paving; and US 6 WMA surface course: (c) several hours after paving, (d) several days after paving

The comparison shows that the maximum useable frequency in the dispersion curves increases significantly from about 9 kHz in the hot test to about 25 kHz in the cold test, as the average testing temperature decreased from 43.4°C to 26.6°C (Tables A.10 and A.11) for the HMA section and from 44.0°C to 22.4°C (Tables A.12 and A.13) for the WMA section.

More importantly, the tests on US 6 revealed that the MASW testing approach enabled measurement of dispersion data to significantly higher frequencies than the MSOR approach. This is due to several factors, including much less stringent requirements on impact repeatability and trigger accuracy in MASW testing, as discussed in Lin and Ashlock (2014). The tests are also much more consistent, as evidenced by a significantly lower coefficient of variation (COV) for shear-wave velocity and modulus of the asphalt layer relative to the MSOR tests detailed in the previous sections (Table 3.7 and Table 3.8).

Table 3.7. Inversion results for ambient-temperature tests on US 6 HMA surface course

Location	Field Temperature (°C)	V_{s1} (m/s)	E_1 (MPa)
US 6 H20-2	26.2	1,766	20,114
US 6 H20-3	25.7	1,648	16,557
US 6 H25-1	24.7	1,691	17,836
US 6 H25-2	25.9	1,755	19,313
US 6 H30-2	30.6	1,712	18,814
US 6 H30-3	26.4	1,648	17,343
Average	26.6	1,703	18,330
COV	7.7%	3%	7.2%

Table 3.8. Inversion results for ambient-temperature tests on US 6 WMA surface course

Location	Field Temperature (°C)	V_{s1} (m/s)	E_1 (MPa)
US 6 W15-1	22.2	1,755	19,710
US 6 W15-2	23.0	1,648	17,381
US 6 W30-2	22.0	1,691	18,137
US 6 W30-3	22.2	1,733	18,733
Average	22.4	1,707	18,490
COV	2.0%	2.8%	5.3%

Similar to the other pavements with overlays, the variation of phase velocity is more complex than a typical profile with decreasing stiffness with depth because of the existing PCC pavement layer. The PCC layer is much stiffer than the newly paved HMA surface course, which is likely the main factor for the high phase velocities near a frequency of 2.5 kHz in Figure 3.12a and Figure 3.12b. Above 2.5 kHz in Figure 3.12a, the phase velocities from both HMA and WMA sections decrease significantly, consistent with a pavement structure having a softer HMA layer over a stiffer PCC layer. Above 5 kHz in Figure 3.12b, the phase velocities of dispersion curves first decrease and then level off above 10 kHz. This indicates that although the newly paved HMA surface course naturally cooled down and stiffened several days after paving, it remained softer than the underlying PCC layer.

With its improved high-frequency measurement capabilities, the MASW testing system enabled the constant phase velocity of the quasi-Rayleigh waves in the first layer to be measured (see mode A0 in Figure 2.6). Therefore, the shear-wave velocity of the first layer, obtained by the inversion procedure in Table 3.7 and Table 3.8 can be obtained directly without the need for inversion, by simply multiplying the phase velocity of the dispersion curve's constant high-frequency asymptote by a factor related to Poisson's ratio (see Lin 2014).

Hot mix asphalt normally has a higher modulus than WMA; however, the HMA tests in Table 3.7 had a lower average modulus than the WMA tests in Table 3.8 because of a higher testing temperature. Therefore, a correction method is developed in Chapter 4 based on laboratory dynamic modulus measurements on the field cores to account for the effect of temperature on modulus.

3.2.6 Comparison of Results from Different Pavement Types

A comparison of the average moduli from in situ SWM testing on eight of the different pavement types with temperatures in the range of 12.9 to 33.2°C is shown in Figure 3.13.
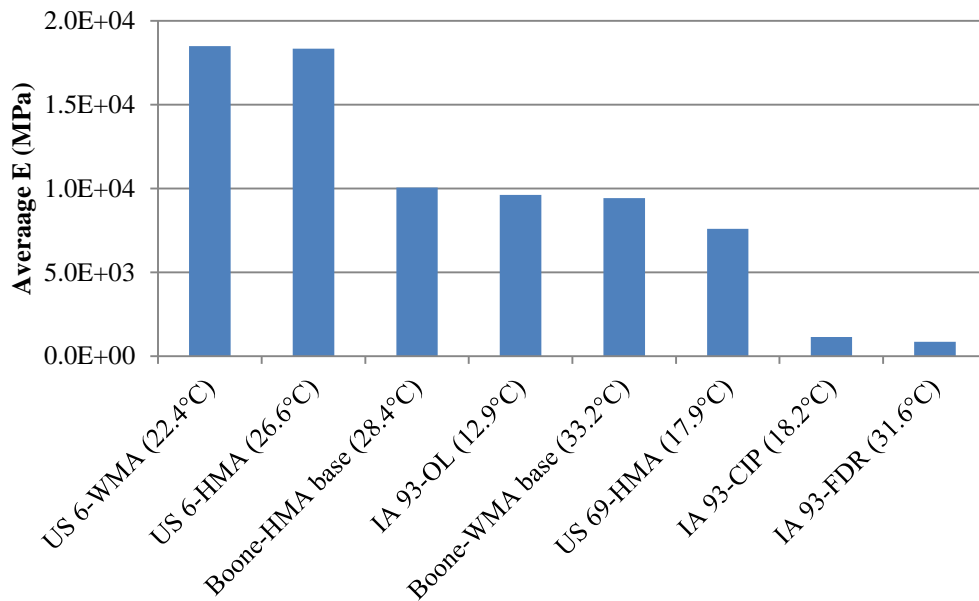
Figure 3.13. Comparison of average dynamic moduli from cold and ambient-temperature surface-wave tests on eight pavement types

For all cases, the moduli were determined from the results of a multilayer inversion using the experimental dispersion curves, as discussed in the previous sections. The HMA and WMA pavements from US 6 have the highest moduli of approximately 18,000 MPa. The Boone Central Iowa Expo, IA 93-OL, and US 69 pavements have intermediate moduli that are approximately half of those from US 6. The IA 93-CIP and IA 93-FDR pavements have the lowest moduli, which are approximately 5 percent of those from US 6. A procedure to correct modulus based on measured master curves is introduced in the next chapter. It will be shown (in Table 4.4) that when all in situ moduli at different temperatures are corrected to a common reference temperature, the comparison of the corrected moduli from different sections is more convincing and reasonable.

3.3 GeoGauge Testing Results

To evaluate the feasibility of using the Humboldt GeoGauge for measuring the stiffness of asphalt pavements, GeoGauge field tests were performed immediately before or after the surface wave tests at the project locations detailed in Table 3.1. To examine the effect of temperature on the stiffness measurements, GeoGauge tests were performed under hot, cold, and ambient-temperature conditions. As described in Section 3.2, hot tests were performed on uncured asphalt within a few hours of paving, whereas cold tests were performed within a few minutes of the hot tests, after first cooling the pavement surface with dry ice. Ambient-temperature tests were performed one or more days after paving, by which time the pavement had cooled, partially cured, and stiffened.

The GeoGauge manufacturer specifies a stiffness measurement range from 3 to 70 MN/m. The manufacturer advertises that the device can be used for stiffness measurement of subgrade, subbase, and base layers of pavement structures because the stiffness of such materials typically falls within the specified measurement range. The product brochure also claims that the device can be used for "monitoring the compaction of asphalt and cold in-place recycling to peak properties to prevent wasted effort and damaging over-compaction." However, the GeoGauge might not be universally applicable to asphalt layers, as their stiffness may exceed 70 MN/m. To examine the usefulness of the GeoGauge for QC/QA of asphalt mixtures in this study, the field stiffness measurements on newly placed asphalt pavements will be assessed against the other NDT methods and laboratory measurements of core density and modulus.

GeoGauge stiffness measurements from hot and cold/ambient tests on six of the project sections are plotted against their corresponding temperatures in Figure 3.14.
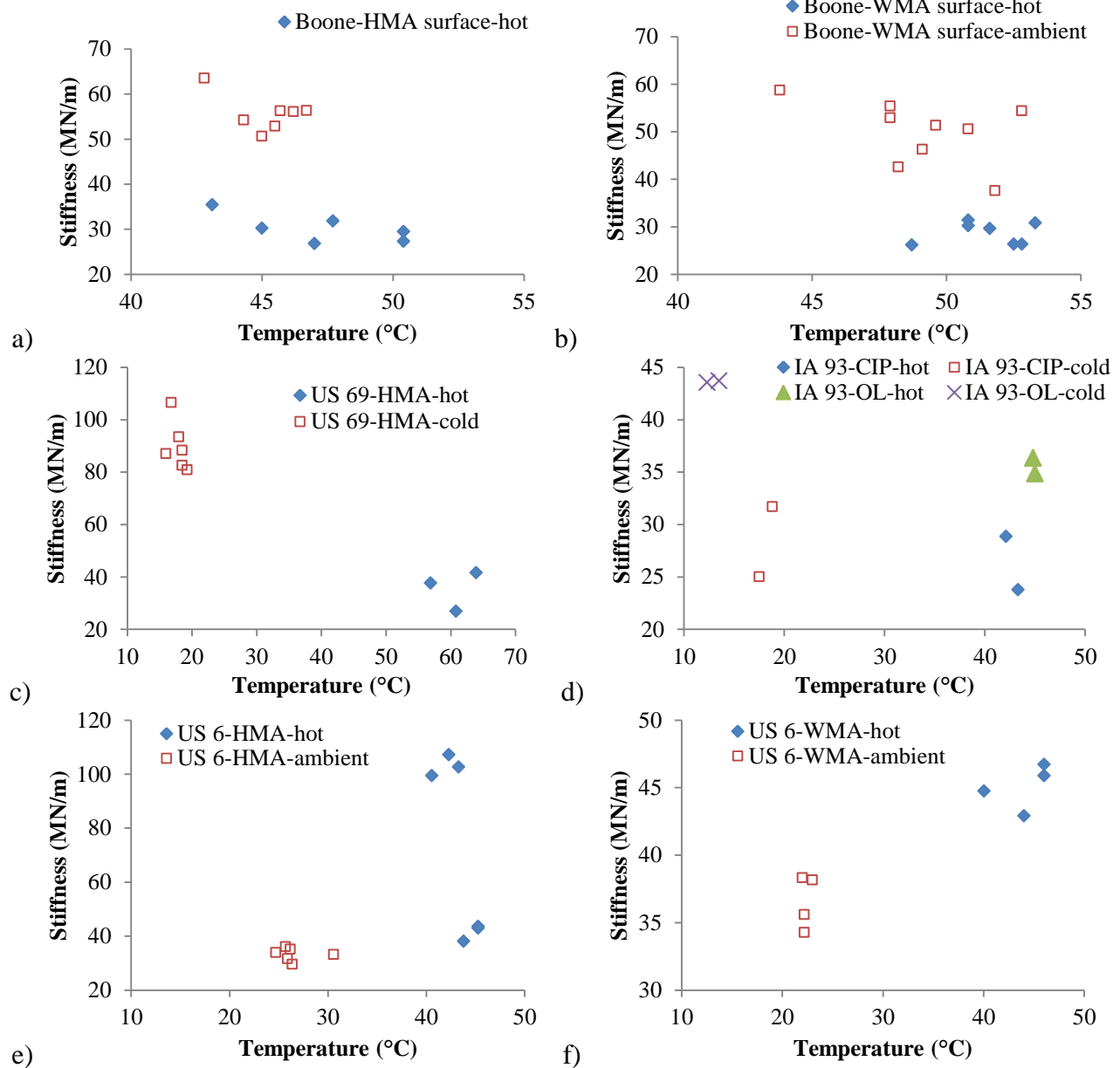
Figure 3.14. GeoGauge stiffness measurements: (a) Boone HMA surface course, (b) Boone WMA surface course, (c) US 69 HMA section, (d) IA 93 CIP and OL sections, (e) US 6 HMA section, and (f) US 6 WMA section

All individual and average measured temperatures and stiffnesses are detailed in Tables A.1 through A.13 of Appendix A. On US 169, only cold tests with dry ice were performed (Table A.7).

Most of the measured values were within the specified stiffness range of the device, although the stiffnesses from US 69 and US 6 exceeded the maximum recommended value of 70 MN/m. This indicates that the stiffness of most pavements is within the measurement range of GeoGauge. Moreover, the stiffnesses generally decreased with increasing temperature, except for the case of

US 6, which featured high-volume HMA and WMA asphalt mixes containing steel slag. These results indicate that the GeoGauge may be capable of monitoring stiffness variations due to temperature for most asphalt types.

The average stiffness values from the nine sections shown in Figure 3.14 are compared in Figure 3.15.

a)

b)
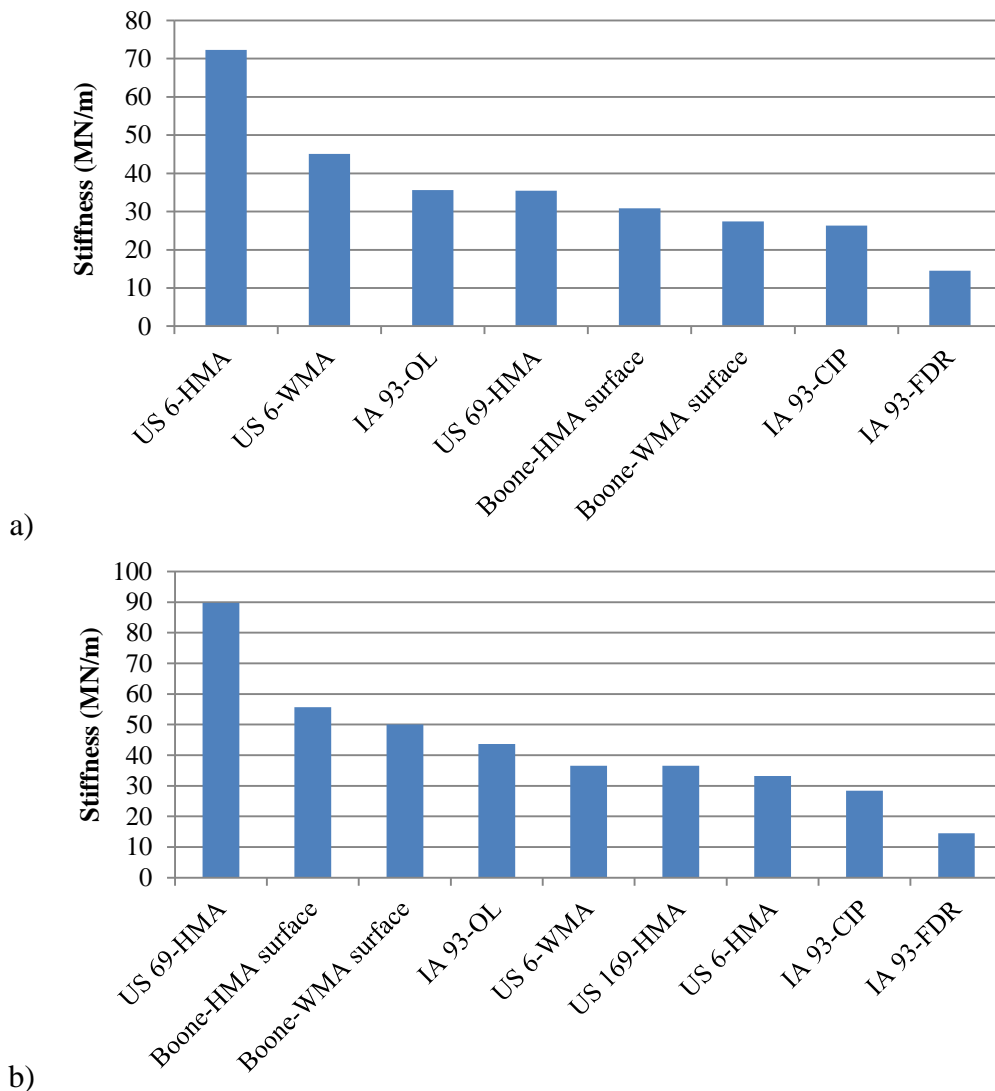
Figure 3.15. Comparison of average GeoGauge stiffness from nine sections: (a) hot tests and (b) cold and ambient-temperature tests

The hot measurements in Figure 3.15a show that (1) HMA and WMA from US 6 have the highest stiffnesses, (2) IA 93-OL, US 69, Boone Central Iowa Expo, and IA 93-CIP have intermediate stiffnesses, and (3) IA 93-FDR has the lowest stiffness. These relative GeoGauge stiffness rankings generally correlate well with the SWM modulus rankings from cold and ambient-temperature tests in Figure 3.13. However, the corresponding stiffness rankings for the

cold and ambient-temperature GeoGauge tests shown in Figure 3.15b do not agree with the SWM modulus rankings in Figure 3.13.

3.4 PaveTracker Testing Results

To evaluate the performance of the Troxler PT electromagnetic gauge relative to the SWM and GeoGauge NDT tests for QC/QA of asphalt pavements, field PT density measurements were taken immediately before or after the other two types of nondestructive tests at the project locations detailed in Table 3.1. For the Boone base and surface courses, hot tests were performed several hours after paving and ambient-temperature tests were performed the following day. For the US 69 and US 169 projects, hot tests were performed several hours after paving, then cold tests were performed after applying dry ice. By the time tests were performed on the US 6 project, it was concluded that cold and ambient-temperature PT tests were of limited value. Therefore, only hot tests were performed on US 6. Data from all PT tests are detailed in Tables A.14 through A.22 of Appendix A.

The measured densities from hot and ambient-temperature tests on the Boone asphalt layers are shown in parts (a) and (c) of Figure 3.16, including 19 HMA and 16 WMA base course locations and 7 HMA and 9 WMA surface course locations.

a)
b)
c)
d)
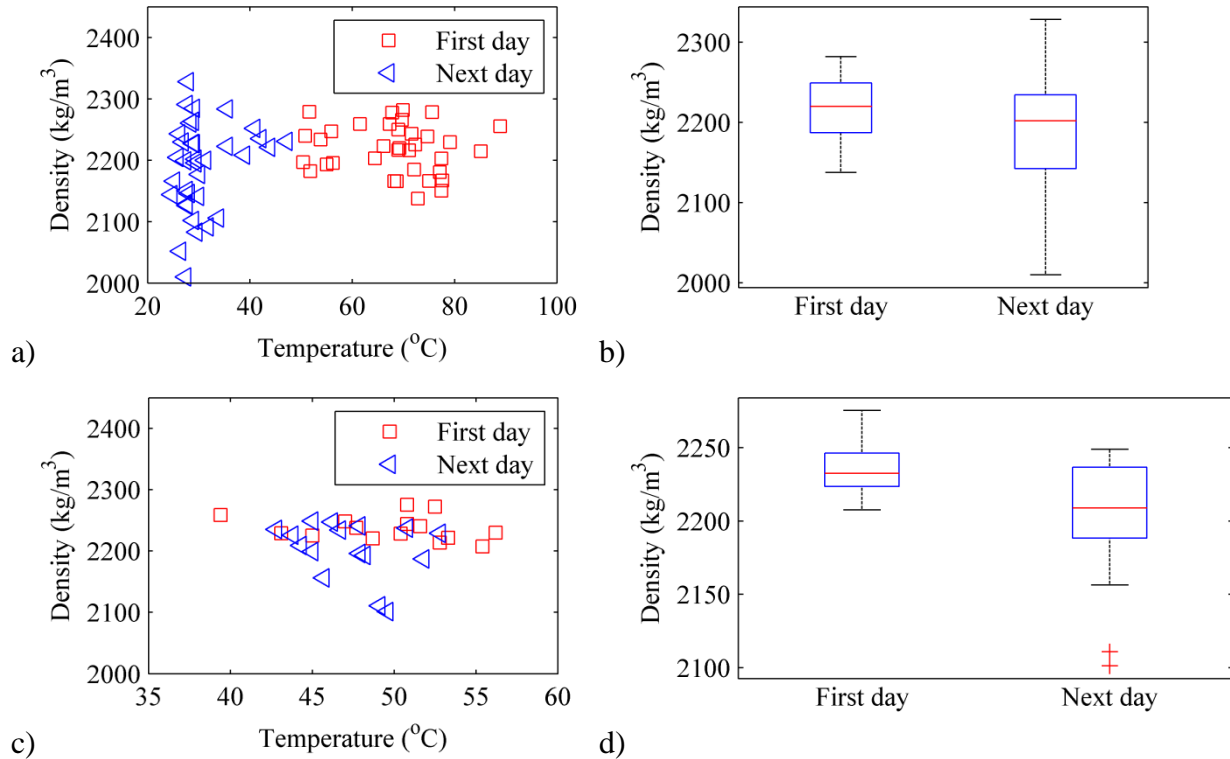
Figure 3.16. PT density measurements from Boone HMA and WMA: (a) base-course densities, (b) boxplot of base-course densities, (c) surface-course densities, (d) boxplot of surface-course densities

Statistical boxplots of the base- and surface-course densities are shown in parts (b) and (d) of Figure 3.16. In the boxplots, the central red line is the median, the box edges are at the 25th and 75th percentiles, the whiskers extend to most extreme data not considered by the algorithm to be outliers, and any outliers are shown as + marks. The boxplots in Figure 3.16b and Figure 3.16d indicate that the hot measurements on the first day have a slightly higher density but a much smaller standard deviation and, therefore, higher certainty than the next-day ambient measurements. A direct comparison and regression of the hot versus cold/ambient densities from all 51 locations demonstrates a poor correlation between the two (Figure 3.17).

$y = 0.9588x + 61.276$
$R^2 = 0.2708$
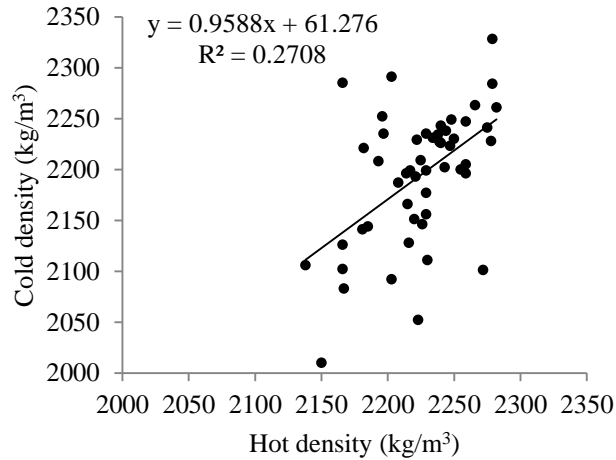
Figure 3.17. Correlation between in situ PT densities measured on hot versus cold/ambient-temperature asphalt pavements

Since they exhibit a small variation, only the hot PT densities were measured on US 6 as discussed above. The average PT densities from all 11 pavement sections are shown in Figure 3.18. Compared to SWM and GeoGauge measurements, the PT densities show less variation with pavement type. The US 6 pavements have the highest densities, as expected, followed closely by IA 93-FDR, while all others have close densities within a range of four percent.
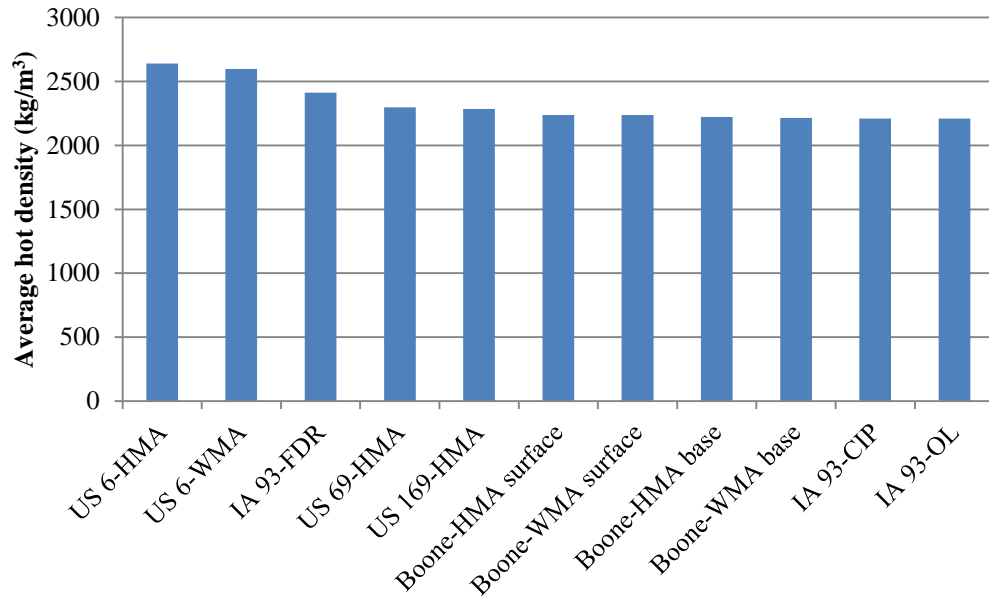
Figure 3.18. Comparison of average PT densities from 11 testing sections

3.5 Chapter Summary

The SWM, GeoGauge, and PT NDT technologies were used to quantitatively assess in situ measures of pavement quality across a variety of asphalt pavement types. Because of the strong dependence of asphalt modulus on temperature, all nondestructive tests were accompanied by pavement temperature measurements. Recognizing that the pavement properties (especially stiffness/modulus) will also evolve as a newly placed pavement cools and cures, tests were conducted on hot uncured pavements soon after paving, on cold pavements soon after paving and applying dry ice, and at ambient temperatures one or more days after paving. The shear-wave velocity measured by surface-wave methods was found to be most sensitive to pavement type and temperature, followed by the GeoGauge stiffness, and finally the PT density. In the next chapter, the in situ measured density and modulus will be further evaluated against more accurate laboratory measurements on field cores taken from the center of each testing location.

CHAPTER 4 – LABORATORY TESTING OF ASPHALT CORES

This chapter presents laboratory measurement of densities and moduli of asphalt cores extracted from each testing location after completing the NDT measurements. The field cores were from a variety of asphalt pavements, including different courses (surface and base), a variety of materials (HMA, WMA, HMA and WMA with slag), and different construction types (new paving, resurfacing, OL, CIP, and FDR). Detailed information on the cores is presented in the following section.

4.1 Asphalt Pavement Field Cores

Laboratory density tests were performed on all cores listed in Table 3.1. Most surface cores had sufficiently smooth surfaces that did not require trimming prior to density tests, whereas most base cores had rough bottoms that were trimmed smooth before testing. A subset of these cores, detailed in Table 4.1, was also selected for dynamic modulus testing.

Table 4.1. Cores selected for laboratory dynamic modulus tests

Project/Pavement Type	# Cores/ Diameter	Location (core) Designators
1. Boone HMA base	6/4 in.	HB1-1, HB1-7, HB2-1, HB5-1,HB6-3, HB7-4
2. Boone WMA base	6/4 in.	WB3-2, WB3-5, WB4-1, WB8-4, WB8-8, WB9-2
3. Boone HMA surface	0	–
4. Boone WMA surface	0	–
5. US 69 HMA	6/6 in.	US 69-4, US 69-5, US 69-6, US 69-7, US 69-8, US 69-9
6. US 169 HMA	6/6 in.	US 169-1, US 169-2, US 169-3, US 169-4, US 169-5, US 169-6
7. IA 93 FDR	2/6 in.	IA 93 FDR-1, IA 93 FDR-2
8. IA 93 CIP	2/6 in.	IA 93 CIP-1, IA 93 CIP-2
9. IA 93 OL	2/6 in.	IA 93 OL-1, IA 93 OL-2
10. US 6 HMA	6/4 in.	US 6 H20-2, US 6 H20-3, US 6 H25-1, US 6 H25-2, US 6 H30-2, US 6 H30-3
11. US 6 WMA	4/4 in.	US 6 W15-1, US 6 W15-2, US 6 W30-2, US 6 W30-3

For modulus tests on the Boone HMA and WMA base courses, six cores from each pavement type were randomly selected with the constraint that at least one core would be tested for each section. After completing the density tests, the cores selected for dynamic modulus testing were

trimmed to have a thickness of about 2 in. with parallel top and bottom surfaces. Photos of the cores selected for modulus testing are shown in Figure 4.1.
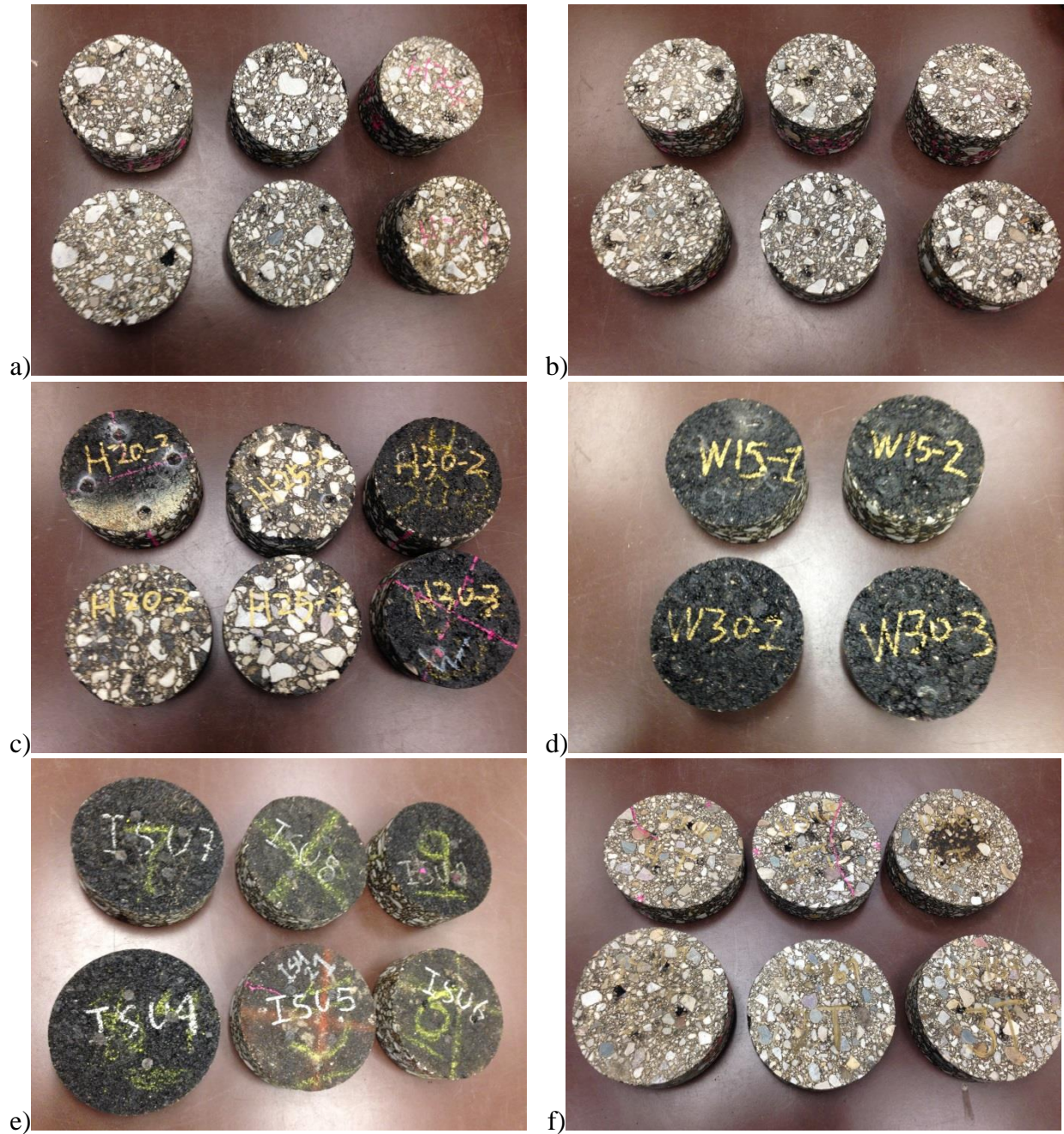
Figure 4.1. Field cores selected for dynamic modulus testing: (a) Boone HMA, (b) Boone WMA, (c) US 6 HMA, (d) US 6 WMA, (e) US 69, (f) US 169
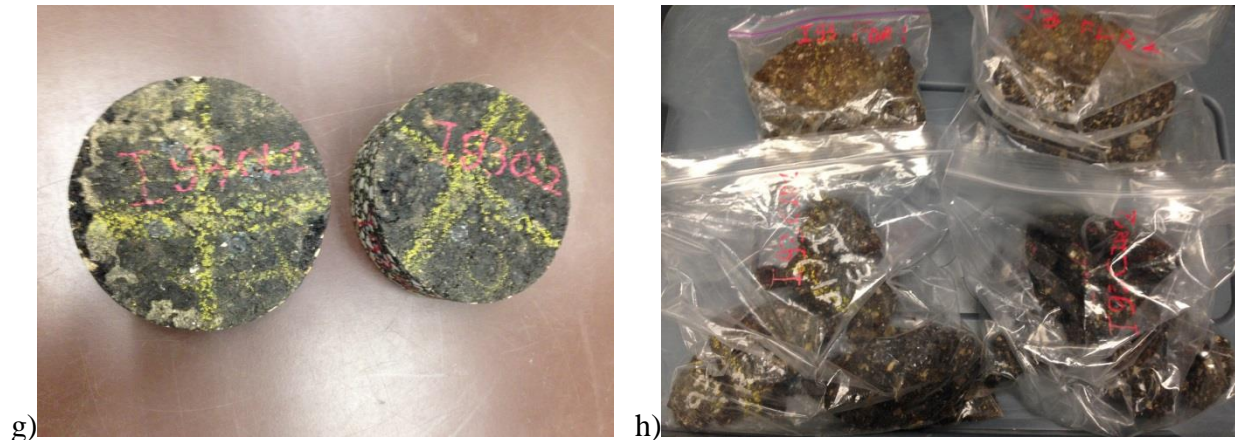
Figure 4.1 (continued). Field cores selected for dynamic modulus testing: (g) IA 93-OL, (h) IA FDR and CIP

4.2 Density Measurement by CoreLok and Saturated Surface Dry

Both CoreLok and saturated surface dry (SSD) methods were employed to measure the density of 19 cores from the Boone HMA base courses, 16 cores from the Boone WMA base courses, and 9 HMA cores from US 69. Results from these tests are detailed in Tables B.1, B.2, and B.5 of Appendix B. Boxplots of the CoreLok and SSD values, as well as direct comparisons and regressions between the two, are shown in Figure 4.2.

In the boxplots, the central red line is the median, the box edges are at the 25th and 75th percentiles, the whiskers extend to most extreme data not considered by the algorithm to be outliers, and any outliers are shown as + marks. The results in Figure 4.2 demonstrate that the CoreLok and SSD methods provide density measurements that are in very good agreement. Specifically, the CoreLok and SSD data shown in parts (b), (d), and (f) of Figure 4.2 are highly correlated, with R^2 ranging from 0.896 to 0.980.
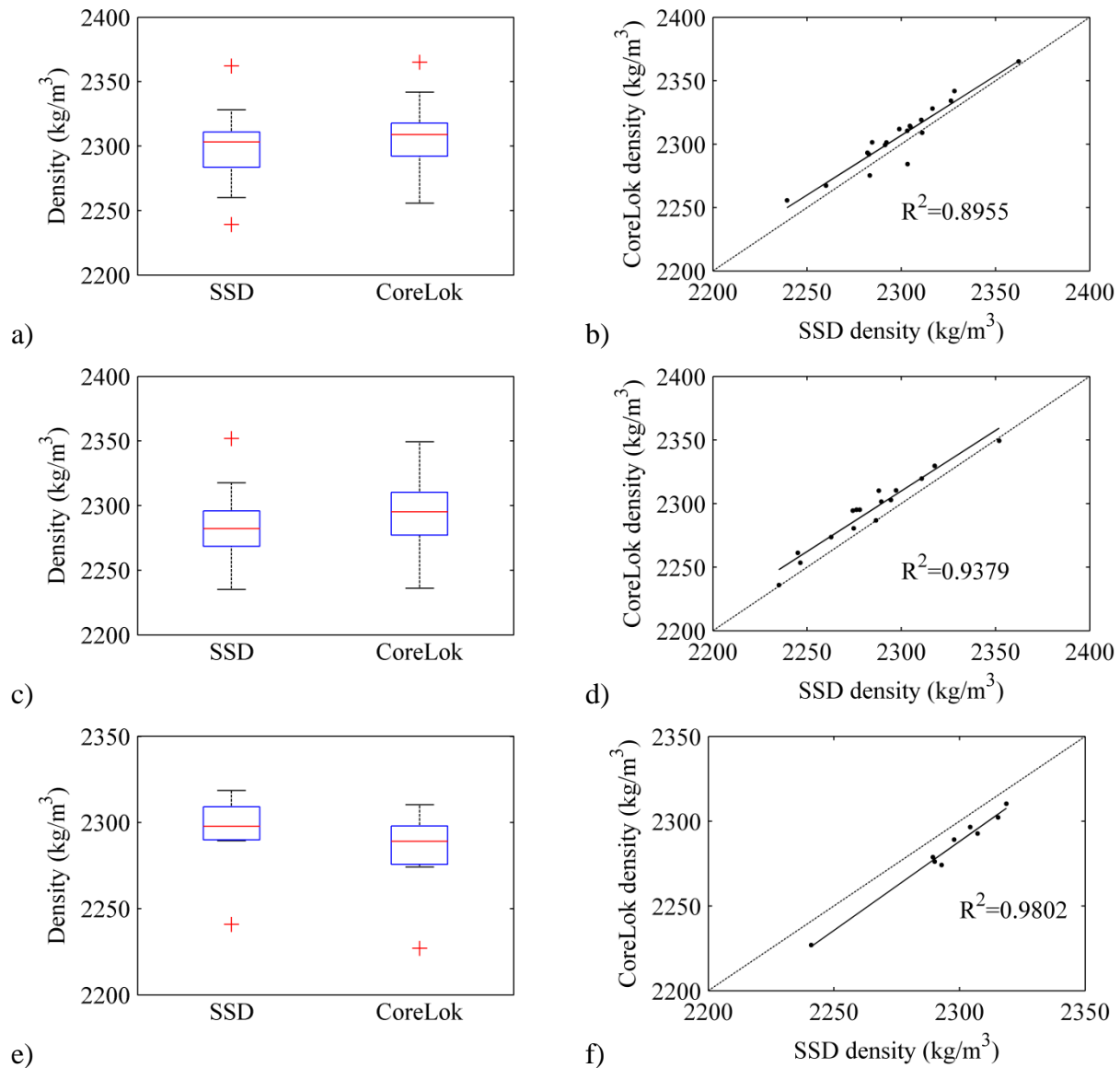
Figure 4.2. Comparison of SSD and CoreLok densities for 19 Boone HMA base course cores: (a) boxplot and (b) correlation; 16 Boone WMA base course cores: (c) boxplot and (d) correlation; 9 US 69 surface course cores: (e) boxplot and (f) correlation

A statistical analysis of the density difference between CoreLok and SSD for the above 44 cores is shown in Figure 4.3. The average density difference is about 0.05%, and the maximum difference is less than 1%. Based on this excellent agreement, the CoreLok method alone was used for density measurement of all remaining field cores (Tables B3, B.4, and B.6−B.9). CoreLok was selected over SSD because CoreLok could be used on loose core specimens that fell apart after field coring, particularly the FDR and CIP specimens from IA 93 shown in Figure 4.1h.
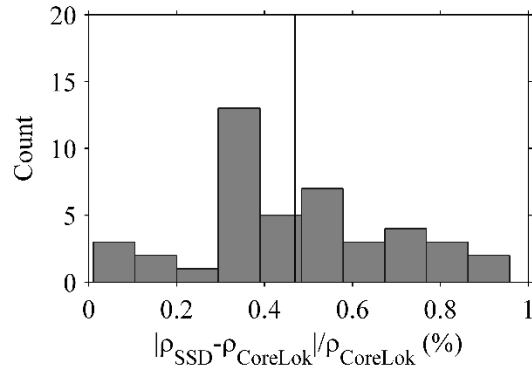
Figure 4.3. Density difference between CoreLok and SSD densities

A comparison of the average CoreLok densities of all 11 sections is shown in Figure 4.4.
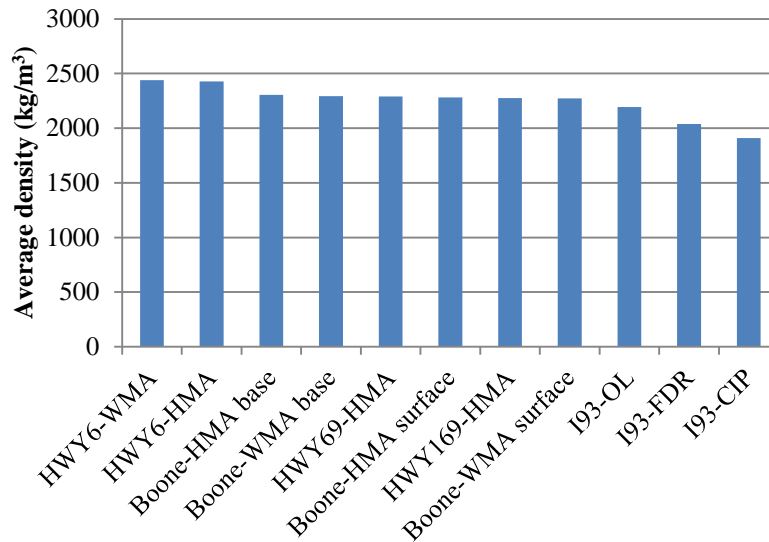
Figure 4.4. Comparison of average CoreLok densities from 11 sections

This figure shows that US 6 HMA and WMA cores have the highest densities, whereas the Boone, US 169, and US 69 pavements all have similar densities that are about 94% of the average US 6 density. The IA 93-OL, IA 93-FDR, and IA 93-CIP cores have the lowest densities, which are approximately 90%, 83%, and 78% of the US 6 density, respectively.

To assess the accuracy of the PT densities, the hot PT test values are compared to the CoreLok values in Table 4.2, and the project sites are ranked separately for PT and CoreLok in order of decreasing density.

50

Table 4.2. Rank of average densities from 11 sections by PT versus CoreLok tests

	Field PT Density Tests		Laboratory CoreLok Density Tests	
Rank	Project/Pavement Type	Avg. PT Hot Density (kg/m³)	Project / Pavement Type (PT→CoreLok rank)	Avg. CoreLok Density (kg/m³)
1	US 6-HMA	2,639.0	US 6-WMA (2→1)	2,440.6
2	US 6-WMA	2,596.3	US 6-HMA (1→2)	2,427.6
3	IA 93-FDR	2,411.0	Boone-HMA base (8→3)	2,306.2
4	US 69-HMA	2,295.3	Boone-WMA base (9→4)	2,293.8
5	US 169-HMA	2,283.5	US 69-HMA (4→5)	2,283.0
6	Boone-HMA surface	2,236.7	Boone-HMA surface (6→6)	2,280.0
7	Boone-WMA surface	2,236.2	US 169-HMA (5→7)	2,276.2
8	Boone-HMA base	2,222.6	Boone-WMA surface (7→8)	2,270.8
9	Boone-WMA base	2,213.7	IA 93-OL (11→9)	2,194.5
10	IA 93-CIP	2,208.5	IA 93-FDR (3→10)	2,037.0
11	IA 93-OL	2,208.5	IA 93-CIP (10→11)	1,909.9

The density of IA 93-FDR drops considerably from rank #3 in PT testing to #10 in CoreLok testing, whereas the densities of Boone HMA and WMA base cores jump from #8 and #9 in PT testing to #3 and #4 in CoreLok testing. Variations of the ranks of all the other densities are small: a decrease of only 1 rank for US 6-HMA, US 69-HMA, Boone-WMA surface, and IA 93-CIP; a 2-rank decrease for US 169-HMA; 1-rank increase for US 6-WMA; 2-rank increase for IA 93-OL; and no change for Boone-HMA surface.

The correlation of the average densities between PT hot testing and CoreLok testing is very small, with an R^2 of 0.234 (Figure 4.5).
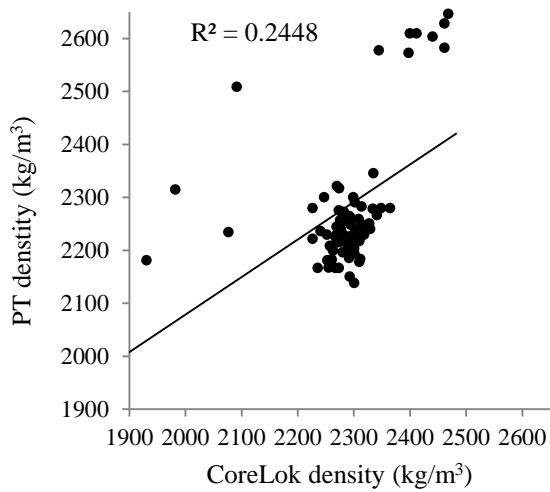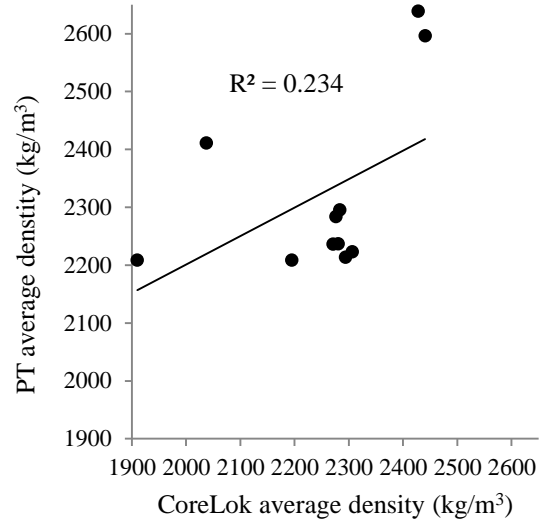
Figure 4.5. Correlation between in situ PT and laboratory CoreLok densities from 11 sections: (a) all cores, (b) average densities for each project

4.3 Dynamic Modulus by Indirect Tensile Test Method

To assess the accuracy of the modulus values obtained from the in situ nondestructive surface-wave tests, the dynamic moduli of the field cores identified in Table 4.1 were measured by the IDT test method (Kim 2002, AASHTO 2014). The IDT testing setup used in this study is shown in Figure 4.6.
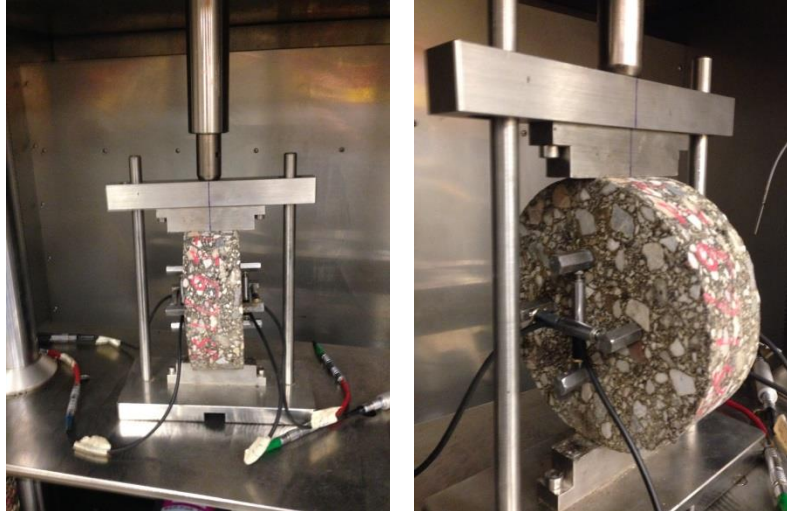
Figure 4.6. IDT dynamic modulus testing setup used in this study

4.3.1 Calibration Specimens

To verify the accuracy of the IDT method compared to the traditional axial dynamic modulus test method (AASHTO 2011a), the moduli of seven cylindrical calibration specimens with 6 in. height and 4 in. diameter were first measured by the axial testing method (see Table 4.3 and Figure 4.7). Each specimen was then sliced into three 2 in. thick specimens for modulus measurement using the IDT method. Axial tests included nine frequencies (25, 20, 10, 5, 2, 1, 0.5, 0.2, and 0.1 Hz) and three temperatures (4, 21, and 37°C). The IDT tests included six frequencies (25, 10, 5, 1, 0.5, 0.1 Hz) and three temperatures (4, 21, and 37°C).

Table 4.3. CoreLok density and air voids of the seven calibration specimens

Sample No.	Density (kg/m^3)	Air Voids (%)
1	2,229	7.2
2	2,236	6.9
3	2,236	6.9
4	2,238	6.8
5	2,241	6.7
6	2,243	6.6
7	2,243	6.6
Avg. (COV)	2,238 (0.22%)	6.8 (3.1%)

Figure 4.7. Photos of the seven calibration specimens for axial vs. IDT dynamic modulus tests

All dynamic modulus test results on the calibration specimens are detailed in Tables B.10 and B.11 of Appendix B. A very high correlation was found between the axial and IDT average moduli at the common testing frequencies and temperatures, as shown in Figure 4.8.
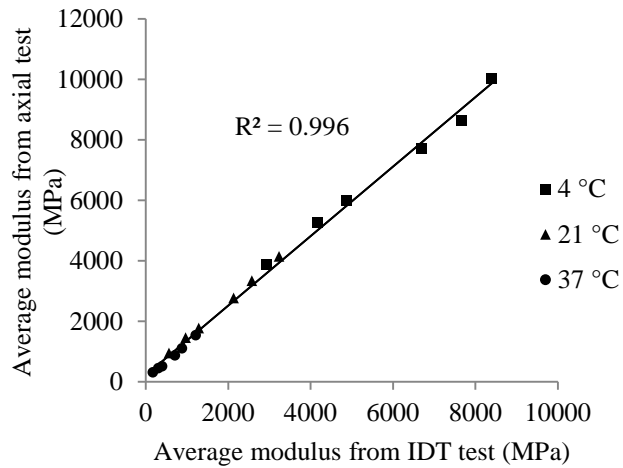
Figure 4.8. Correlation of dynamic modulus between axial and IDT methods

The master curves for the axial and IDT tests obtained using the AASHTO method (AASHTO 2011b) are shown in Figure 4.9. The master curve for the IDT method has slightly smaller moduli than the curve for the axial method, and the modulus difference between two tests decreases as frequency increases.
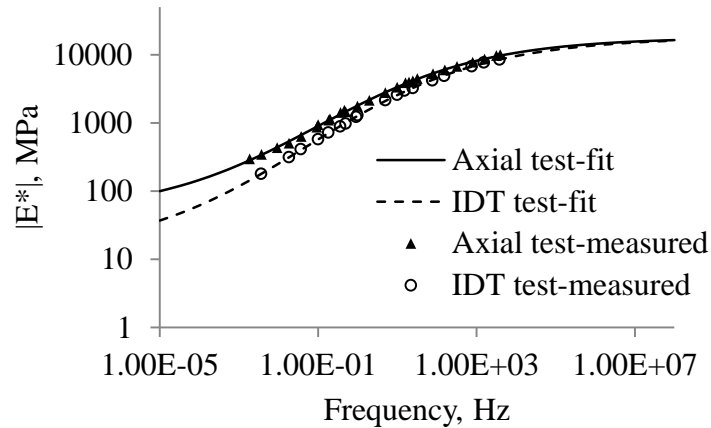
Figure 4.9. Dynamic modulus master curves of seven calibration samples using axial and IDT methods

4.3.2 Field Cores

The moduli of field cores from seven of the pavement test sections were measured using the IDT procedure at six frequencies (25, 10, 5, 1, 0.5, 0.1 Hz) and three temperatures (4, 21, and 37 or 32°C). The decreased temperature of 32°C was used for some samples that had permanent deformations above the limit recommended by the proposed standard (AASHTO 2014). Before performing IDT dynamic modulus tests on samples from each section, tuning was carried out to minimize the loading error and reach the target strain range recommended by the proposed standard.

All experimental data from the seven sections are detailed in Tables B.12 to B.18 of Appendix B. The average moduli of the cores from each section were used to construct the master curves with a reference temperature of 21°C (Figure 4.10).

The overall rank of the master curves in decreasing order of modulus is as follows: US 6-HMA, US 6-WMA, Boone HMA base, Boone WMA base, US 69, IA 93-OL, and US 169. Comparison between the rank of the dynamic modulus master curves in Figure 4.10 and the in situ moduli from SWM testing in Figure 3.13 demonstrates some differences: US 6 WMA and IA 93 OL have higher ranks in Figure 3.13 than in Figure 4.10 because the field temperature also played an important role in the ranks in Figure 3.13. Therefore, it is necessary to account for the effect of field temperature on the SWM in situ modulus if the SWM method is to be used for QC/QA of asphalt pavements.
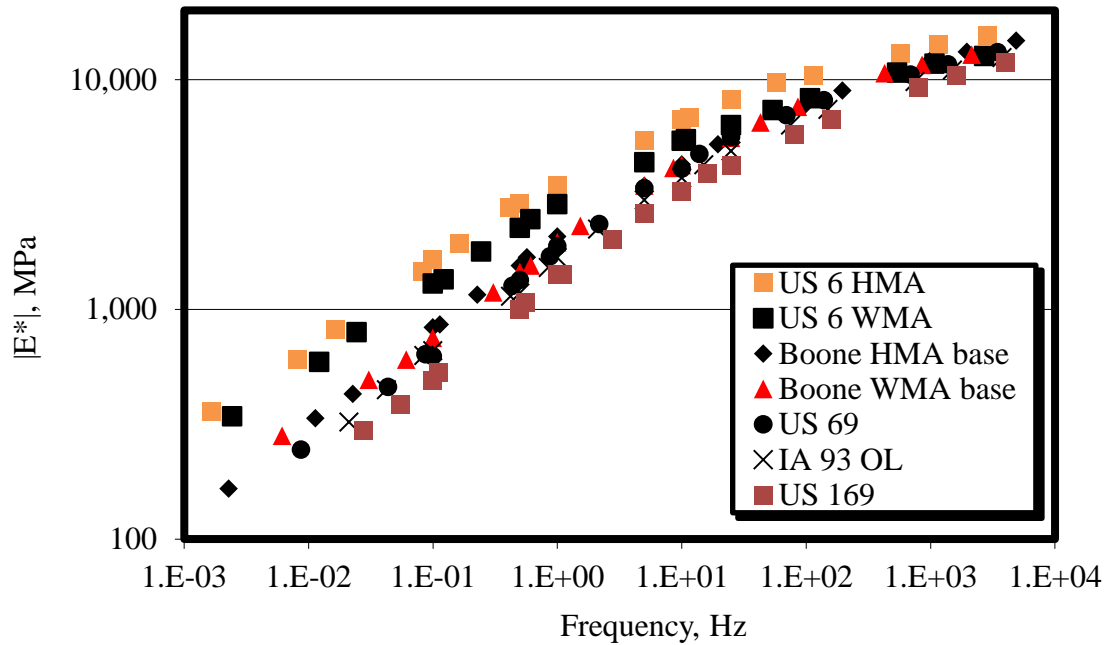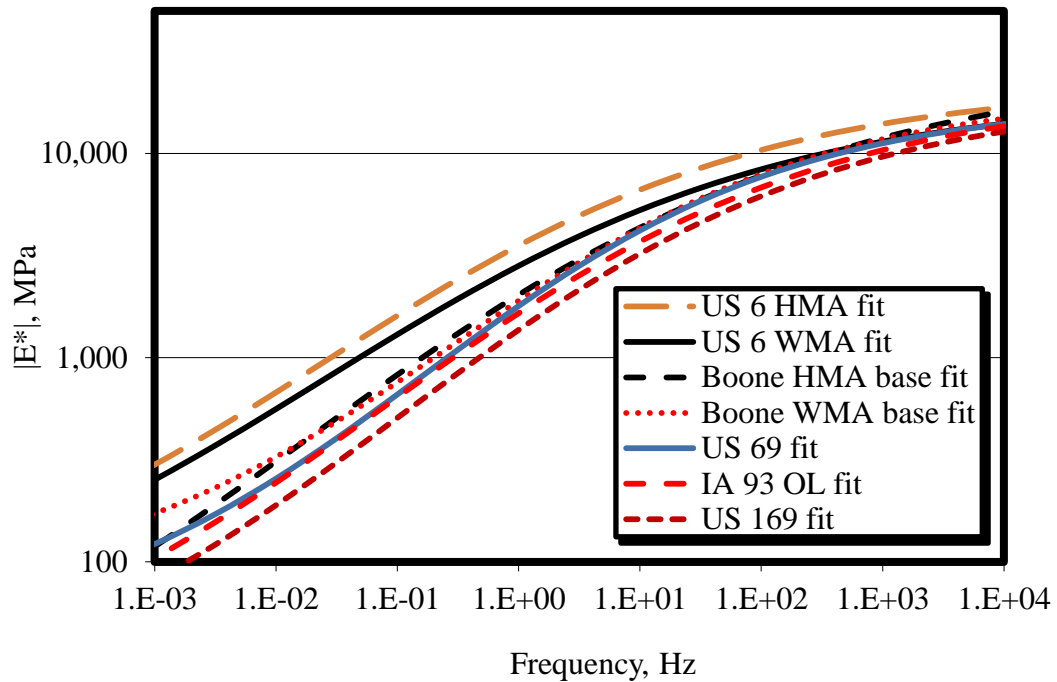
Figure 4.10. Dynamic modulus master curves from field cores: (a) experimental master curves, (b) fitted master curves

4.3.3 Field Modulus Correction Procedure

A procedure is proposed herein to correct an in situ modulus measured at a given field temperature to a modulus at a reference temperature (e.g., 21°C) based on master curves from laboratory dynamic modulus testing. First, three master curves are obtained from laboratory

dynamic modulus tests performed at three reference temperatures. For example, the three master curves from US 69 cores tested at 4, 21, and 32°C are shown in Figure 4.11a. A master curve corresponding to the field-test temperature can then be interpolated based on the three measured master curves.
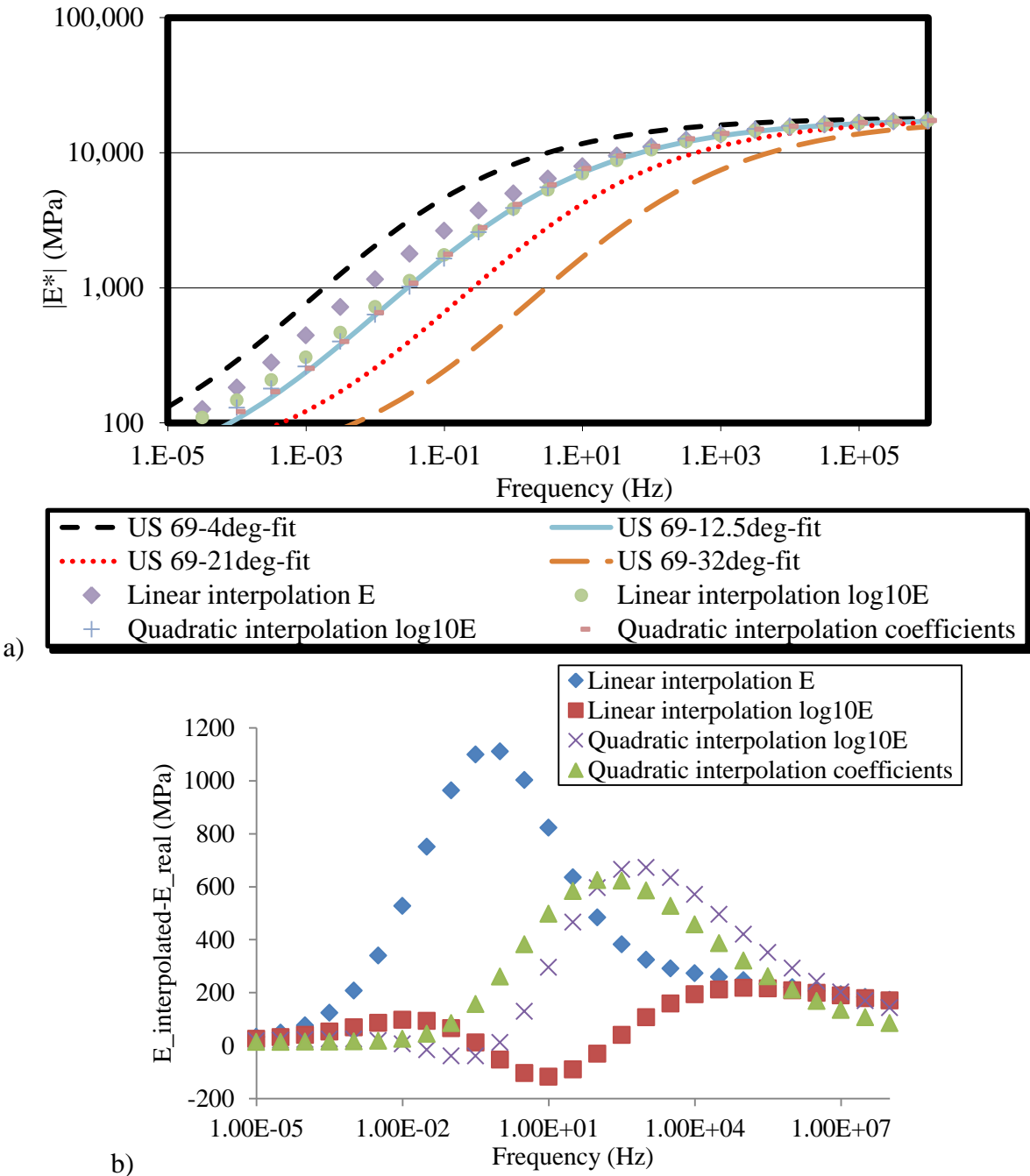
Figure 4.11. Interpolation of master curves at a reference temperature of 12.5°C: (a) four measured and four interpolated master curves, and (b) discrepancy between interpolated and measured master curves versus frequency

Four methods were examined for interpolating the master curves to obtain the unknown master curve at the field-test temperature. These methods included linear interpolation of modulus (E), linear interpolation of log10(E), quadratic interpolation of log10(E), and quadratic interpolation of the master-curve fitting coefficients. To identify the most accurate interpolation method, an actual laboratory master curve at 12.5°C was measured to compare against the interpolated

curves for a field test on US 69 having a temperature of 12.5°C (Figure 4.11a). The discrepancy between the measured and interpolated master curves, shown in Figure 4.11b, indicates that the linear interpolation of log10(E) results in the best agreement over the entire frequency range. Therefore, a linear interpolation of log10(E) can be employed to interpolate between three measured master curves at three reference temperatures to obtain a master curve at a given field temperature.

The interpolated field-temperature master curve can then be used to find the reduced frequency of the in situ measured modulus, as illustrated in Figure 4.12.
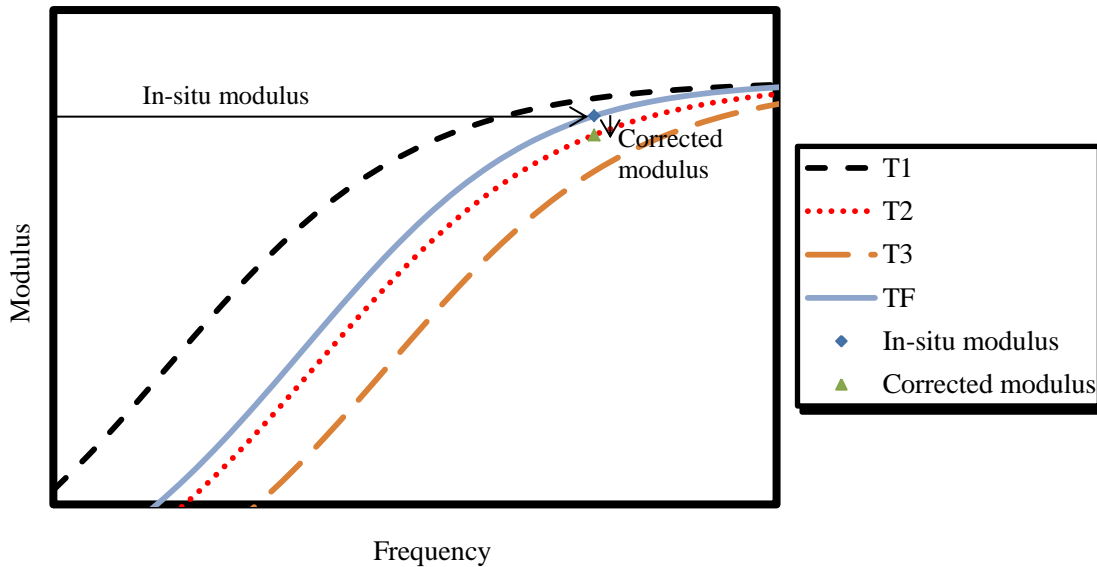
Figure 4.12. Procedure for correcting an in situ modulus at a measured field temperature TF to a corrected modulus at a desired reference temperature T2

Finally, the corrected modulus at the reduced frequency can be found for any of the three master curves at the three reference temperatures. Using this procedure, the in situ moduli measured under various field temperatures can all be corrected to a common master curve for a selected reference temperature. This procedure enables more meaningful comparisons between in situ moduli and those from different field test sites or laboratory tests. This procedure was employed to correct the in situ moduli from seven field pavement sections to the moduli at a common reference temperature of 21°C. The results are shown in Figure 4.13 and Table 4.4. After correcting the field moduli to the common reference temperature, the rank of the corrected field moduli in Table 4.4 agrees with that of the laboratory dynamic modulus master curves in Figure 4.10.

a)

b)

c)

d)

e)

f)
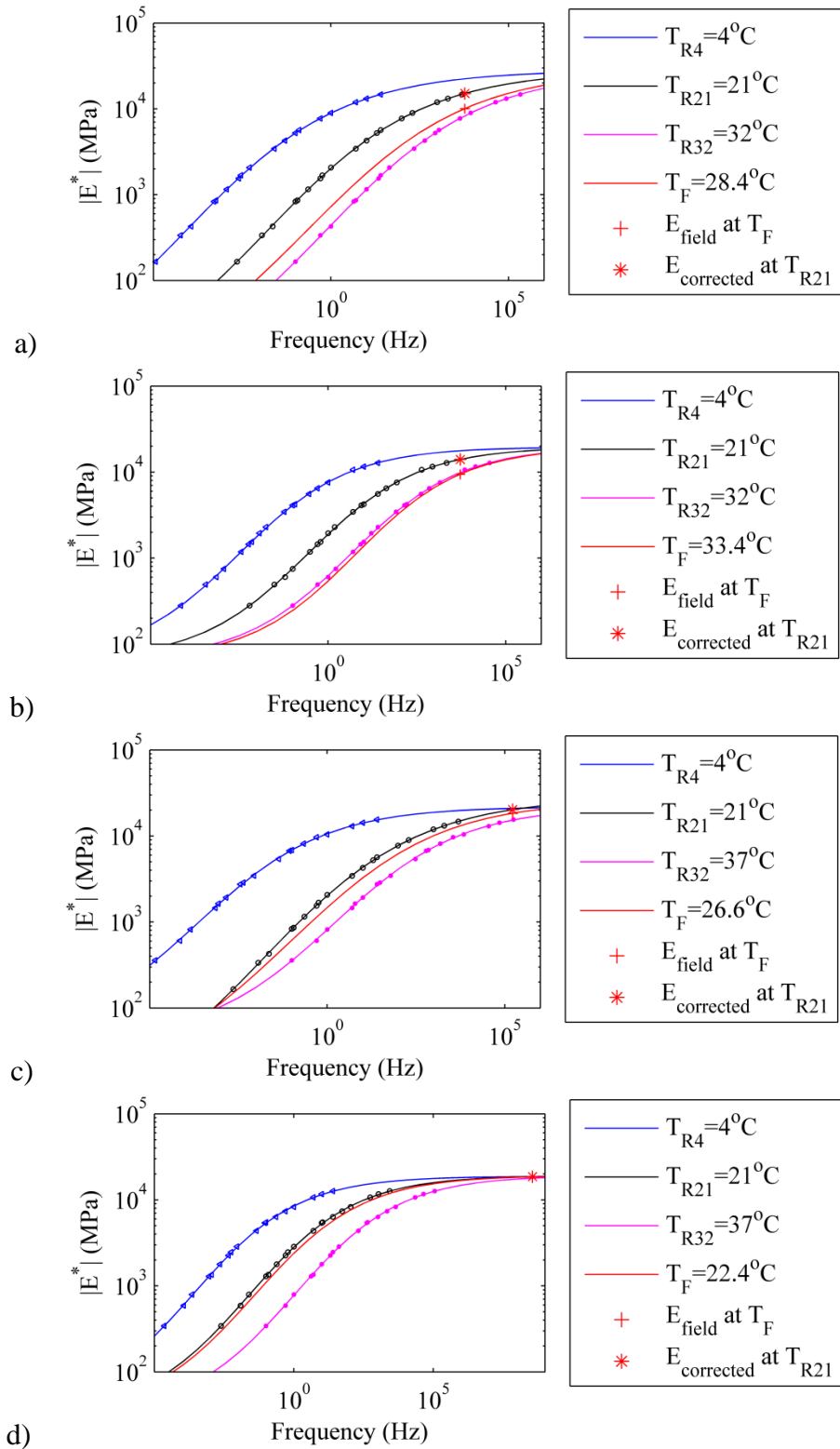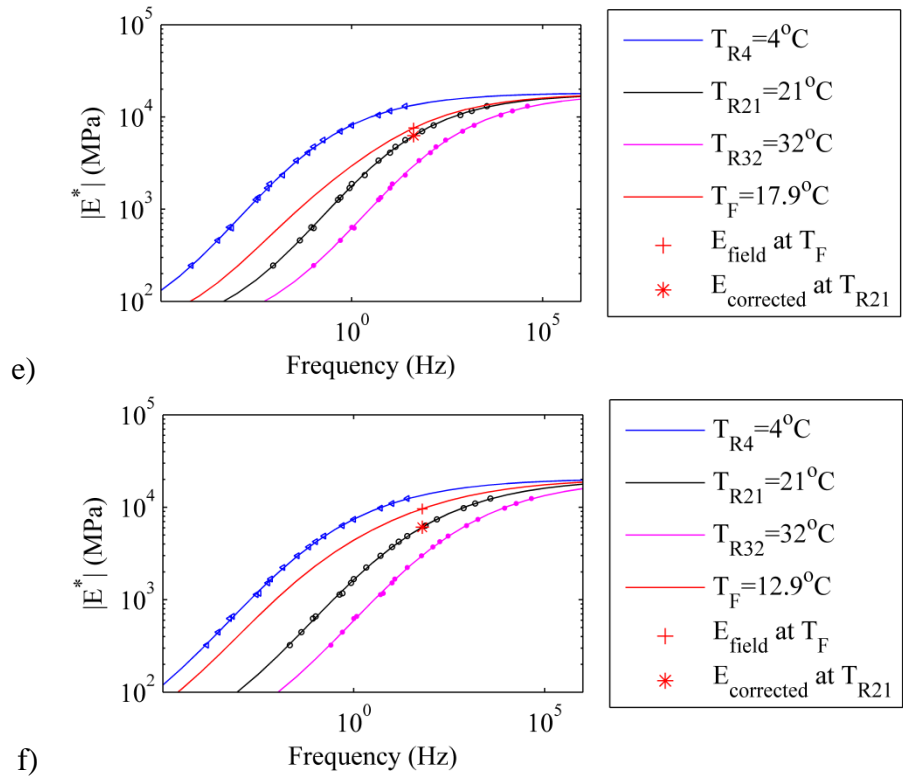
Figure 4.13. Correction of in situ moduli to a reference temperature of 21°C: (a) Boone HMA base, (b) Boone WMA base, (c) US 6 HMA, (d) US 6 WMA, (e) US 69, (f) IA 93 OL

Table 4.4. Ranking of field moduli and corrected field moduli

Rank	Project/ Pavement Type	Avg. Field Temp. (°C)	Avg. Field Modulus (MPa)	Project/Pavement Type (rank)	Corrected Field Modulus (MPa)
1	US 6 WMA	22.4	18,490	US 6 HMA (2→1)	20,229
2	US 6 HMA	26.6	18,330	US 6 WMA (1→2)	18,586
3	Boone HMA base	28.4	10,053	Boone HMA Base (3→3)	15,087
4	IA 93 OL	12.9	9,615	Boone WMA Base (5→4)	14,013
5	Boone WMA base	33.2	9,428	US 69 (6→5)	6,269
6	US 69	17.9	7,581	IA 93 OL (4→6)	6,078

61

4.4 Chapter Summary

The density and modulus of field cores were measured in laboratory tests and compared against the in situ measurements. A low correlation was found between the laboratory density and the in situ PT density. A high correlation was found between the dynamic modulus measured using the axial and IDT test methods. A procedure was developed, based on laboratory dynamic modulus master curves, to correct the field moduli measured at various temperatures to the moduli at a common reference temperature. Upon correcting the field moduli to a common reference temperature of 21°C, the resulting rank of the corrected moduli showed an excellent agreement with the rank of the master curves.

CHAPTER 5 – QUALITY CONTROL AND QUALITY ASSURANCE ANALYSES

This chapter presents a procedure for quality control and quality assurance of asphalt pavements based on quantitative mechanics properties (modulus and stiffness) from rapid in situ NDT measurements. The in situ modulus primarily depends on shear-wave velocity, which can be measured by surface-wave testing equipment, and density, which can be measured by electromagnetic gauges such as the PT. A master curve database is needed to correct the in situ moduli measured at various field temperatures to the moduli at a common reference temperature, which can then be used for quality control. The dimensionless ratio of achieved field modulus over design modulus can be used for quality assurance. An alternative quality control method using GeoGauge stiffness measured on hot asphalt pavements is also presented in this chapter.

5.1 Primary Factors Affecting Quality

Density has been widely employed as a quantitative scale of quality, measured either in situ by field equipment (e.g., Larsen and Henault 2006, Williams 2008, Mason and Williams 2009, Williams et al. 2013) or on cores in the laboratory by SSD or CoreLok methods (e.g., Williams 2001, Buchanan and White 2005, Williams et al. 2013). Pavement quality is assumed to increase as density increases (or air void decreases). However, as discussed in Chapter 3, the density is not very sensitive for distinguishing quality differences among different pavement types. Moreover, the density does not capture the temperature dependence of asphalt pavement mechanistic properties such as modulus.

In contrast, shear-wave velocity is very sensitive to pavement type and variations in temperature. Therefore modulus, which is a combination of density and shear-wave velocity, i.e.,

$$E = 2(1+\nu)\rho V_s^2$$

(5.1)

is a sensitive and objective quality measurement. In Equation 5.1, ρ is density, V_s is shear-wave velocity, and ν is Poisson's ratio. Moreover, modulus is directly used to estimate the fatigue damage of asphalt layers (Ayres and Witczak 1998) due to the tensile strain at the bottom of the layers (Finn et al. 1977).

5.2 Correlation between Density and Shear-wave Velocity

The field and laboratory data from Chapters 3 and 4 are used in this section to study the main factors affecting an accurate estimation of asphalt pavement modulus. The correlation between shear-wave velocity and in situ PT density is very low, with an R^2 of 0.233 (Figure 5.1a), whereas the correlation between shear-wave velocity and laboratory CoreLok density is very high, with an R^2 of 0.889 (Figure 5.1b).
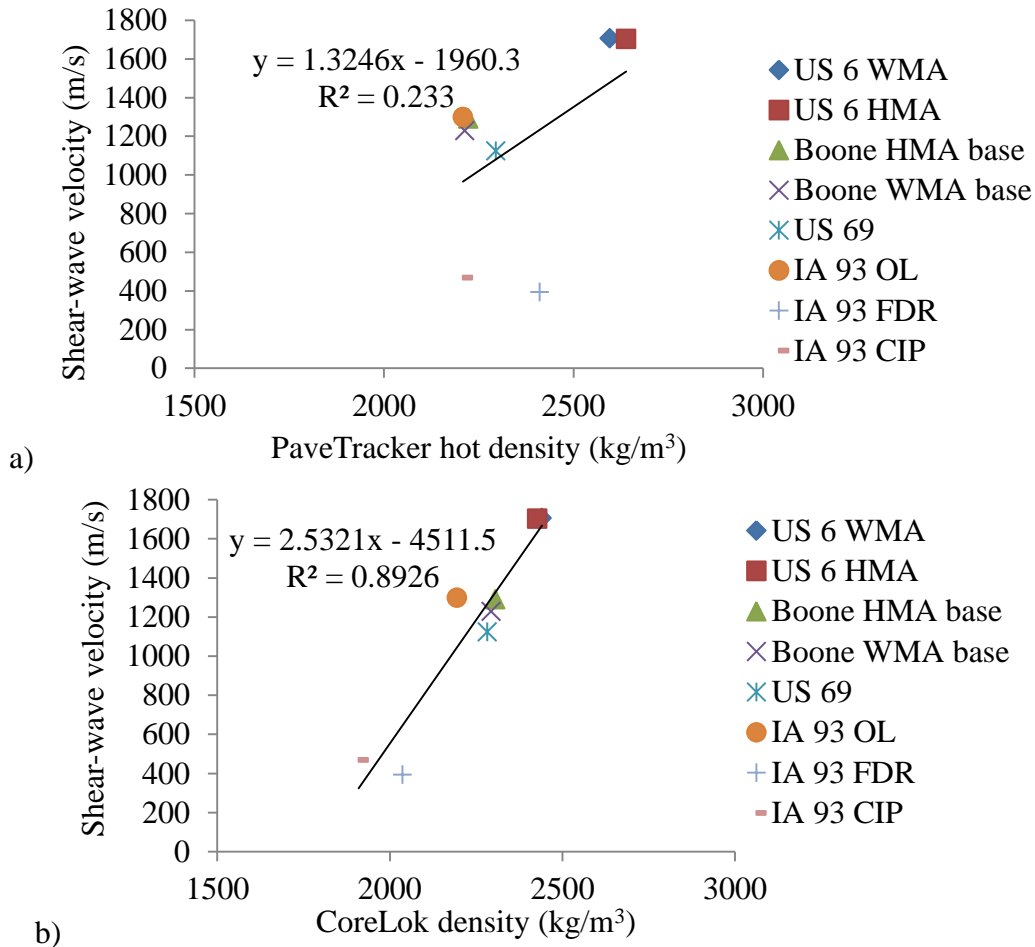
Figure 5.1 Correlation between in situ shear-wave velocity and density: (a) PT density and (b) CoreLok density

If the CoreLok density is believed to be objective and accurate, then the low correlation between PT density and CoreLok density in Figure 4.5 indicates that the accuracy of the PT measurement is low, whereas the high correlation between shear-wave velocity and CoreLok density indicates that the accuracy of the surface-wave measurement is relatively high.

Although the state of practice for in situ density measurement (e.g., PT) was found in this study to have a relatively low accuracy (Figure 4.5), the density still must be measured to calculate the in situ modulus by Equation 5.1. Furthermore, for the modulus to be a viable QC measure, the density should be obtained by rapid NDT techniques rather than slower laboratory methods.

To examine the consequence of using the in situ density to calculate the in situ modulus, the shear-wave velocity from SWM tests was used with the PT density and again with the laboratory CoreLok density in Equation 5.1. The resulting correlation between the in situ modulus with PT density (E_{PT}) and the modulus with CoreLok density (E_{CL}) is very good, with an R^2 of 0.9937 (Figure 5.2). This is because the V_s has an exponent of 2 in Equation 5.1 and therefore exhibits a significantly greater influence on modulus than does density, which varies over a limited range.
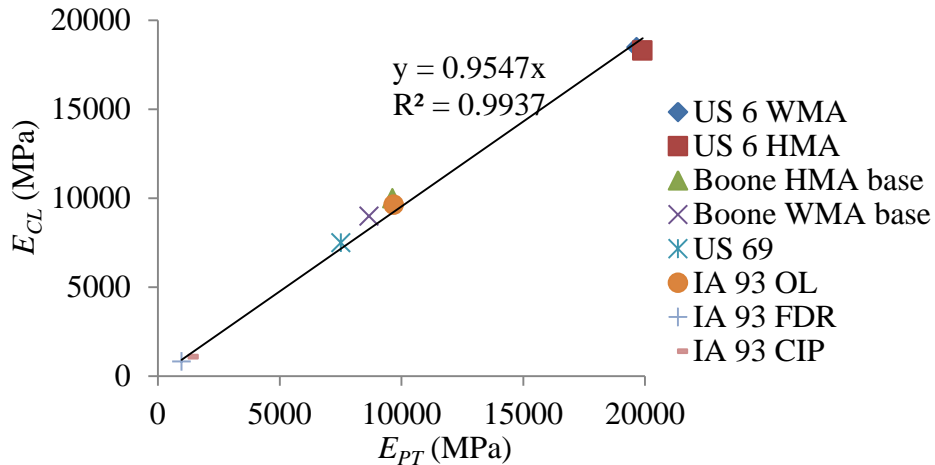
Figure 5.2 Correlation between in situ modulus calculated with PT density (E_{PT}) vs. CoreLok density (E_{CL})

As shown in Figure 5.3, the relative difference between E_{PT} and E_{CL} is small; below 10% for the denser pavements, and no more than 20% for the lower density CIP and FDR pavement sections. Thus, the in situ modulus E_{PT} calculated from rapid NDT PT and SWM tests appears to be an acceptable measure for QC/QA of asphalt pavements.
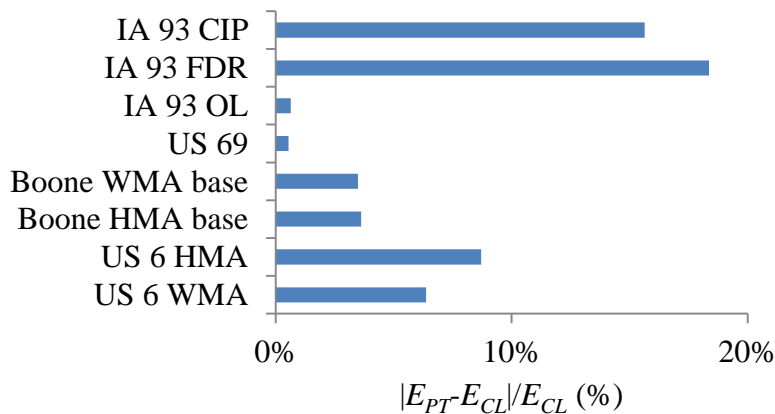
Figure 5.3 Relative differences between E_{PT} and E_{CL}

5.3 Correlation between Density and Stiffness

The field and laboratory data from Chapters 3 and 4 is employed in this section to study the feasibility of QC based on stiffness measured with the GeoGauge. The correlations between SWM modulus from cold and ambient-temperature tests and GeoGauge stiffness from hot and cold/ambient tests are shown in Figure 5.4. The correlation between SWM cold/ambient modulus and GeoGauge hot stiffness is high with $R^2=0.705$ (Figure 5.4a). However, despite the measurements being taken at the same temperature conditions, the correlation between SWM cold/ambient modulus and GeoGauge cold/ambient stiffness is very low with $R^2=0.018$ (Figure 5.4b). This is likely a result of the stiffness increasing beyond the recommended measurement

range of the device as the pavement cools and cures. If the SWM cold/ambient modulus is assumed to be objective and accurate, the results in Figure 5.4 indicate that the GeoGauge is more suitable for measuring the stiffness of hot asphalt pavements several hours after paving, but not suitable for cold or ambient-temperature conditions.
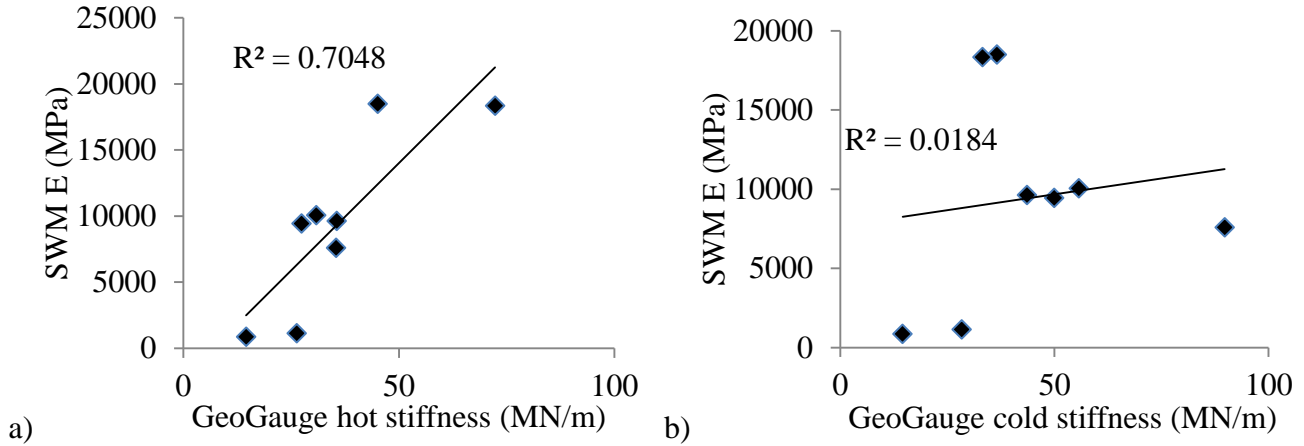
Figure 5.4 Correlation between GeoGauge stiffness and SWM cold/ambient modulus: (a) hot GeoGauge tests and (b) cold/ambient GeoGauge tests

Correlations between stiffness and in situ or laboratory density are shown in Figure 5.5. The correlation between CoreLok density and GeoGauge hot stiffness has the highest R2 of 0.518 as shown in part (c), followed by an R2 of 0.468 between PT density and GeoGauge hot stiffness in part (a). Again, the correlations with GeoGauge cold/ambient stiffness are very low, with R2 of 0.105 and 0.128 for PT (part b) and CoreLok (part d), respectively. If the CoreLok density is assumed to be objective and accurate, the high correlation in Figure 5.5c and low correlation in Figure 5.5d also indicate that the GeoGauge is more suitable to measuring stiffness of hot asphalt layers several hours after paving rather than that of cold/ambient asphalt layers several days after paving.

The GeoGauge hot stiffness can therefore be recommended as a quantitative property for quality control, because of the relatively good correlation between GeoGauge hot stiffness and SWM modulus (or CoreLok density). However, it should be noted that the GeoGauge cold/ambient stiffness measured in this study did not show a good agreement with the other in situ or laboratory measurements. As mentioned above, this is likely due to the stiffness increasing beyond the measurement range of the device as the pavement cools and cures.
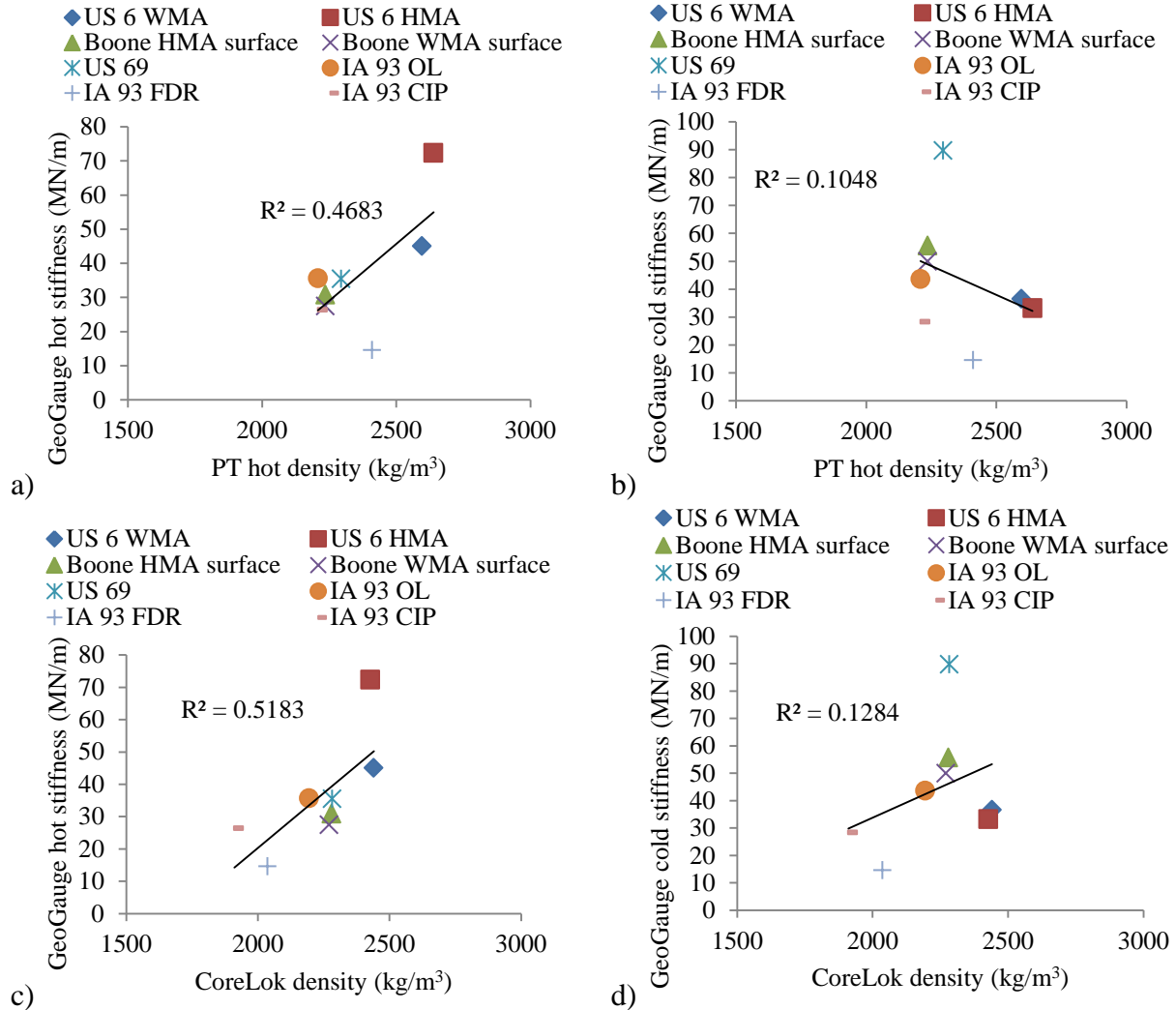
Figure 5.5 Correlation between GeoGauge stiffness and density: (a) hot GeoGauge and hot PT tests, (b) cold/ambient GeoGauge and hot PT tests, (c) hot GeoGauge and CoreLok tests, (d) cold/ambient GeoGauge and CoreLok tests

5.4 Calculation of Achieved Modulus Based on In Situ Modulus and Master Curves

As demonstrated in the previous sections, asphalt pavement modulus is very sensitive to temperature, and thus a poor-quality pavement tested at a lower temperature might exhibit a higher modulus than a good-quality pavement at a higher temperature. To account for the effects of temperature on modulus, the in situ moduli measured at different field temperatures (e.g., using a combination of SWM and EM tests) should be corrected to moduli at a common reference temperature, such as 21°C. The correction procedure was detailed in Chapter 4 and shown schematically in Figure 4.12.

For general implementation, however, it may not be convenient to measure the required master curves in the laboratory on each new project. Alternatively, a database of master curves can be

generated and a set of three master curves at three reference temperatures (e.g., T_1=4°C, T_2=21°C, T_3=37°C) can be selected according to the asphalt pavement type. The master curve equation is

$$\log\left(E^*\right) = \delta + \frac{\alpha}{1 + e^{\beta - \gamma \log f_r}}$$

(5.2)

where δ is the minimal modulus, $\delta+\alpha$ is the maximum modulus, β and γ are the shape coefficients, and f_r is the reduced frequency. After the three master curves are selected for the appropriate asphalt mix used on the project, linear interpolation of log10(E) can employed as described in Section 4.3.3 to obtain master curves at the field temperatures (T_F) of each NDT test point. The reduced frequency of the in situ modulus can then be found on the interpolated master curves, and the corrected modulus having the same reduced frequency on the 21°C reference master curve can be found. The achieved modulus (E_a) at other frequencies of interest (e.g., design frequencies from 10 to 30 Hz) can then be found on the 21°C master curve.

5.5 Quality Control Procedure

After collecting the field NDT data, a quicker QC procedure is needed to convert the in situ measurements (e.g., density and shear-wave velocity) to a quality measurement such as the achieved modulus, which can be compared against a quantitative design value such as the design modulus. One possible method is to use the modulus difference (field modulus minus corrected field modulus at 21°C in Table 4.4), which is highly correlated to the temperature difference (field temperature minus the reference temperature of 21°C), as shown in Figure 5.6.
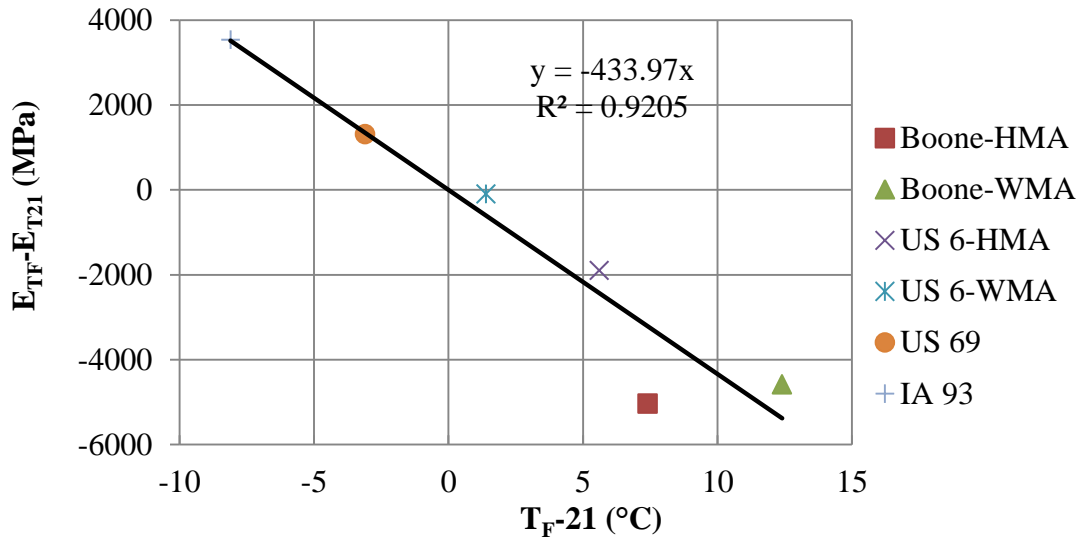
Figure 5.6 Correlation between modulus difference and temperature difference of field and reference values across six sites

For example, a fitting function was calculated for the data in this study to correct in situ modulus:

$$E_{C21} = E_I + 433.97(T_I - 21) \tag{5.3}$$

where modulus is in MPa, temperature is in °C, E_I is the in situ modulus, T_I is the in situ temperature, and E_{C21} is the corrected modulus at 21°C.

A quick QC procedure can thus be summarized in four steps: (1) measure in situ moduli and temperatures of several randomly selected locations in one construction section; (2) correct the average in situ modulus to account for temperature effects using Equation 5.3; (3) find the design modulus of the constructed pavement section from a master-curve database based on the pavement type and the reference temperature; and (4) calculate a dimensionless index as the ratio of corrected modulus over design modulus (E_a/E_{d21C}) to quantify the achieved quality.

5.6 Quality Assurance Procedure

After the pavement has been constructed as guided by the QC procedure, a more accurate QA procedure is needed to convert in situ measurements to a quality measurement that can be compared against a quantitative design value. The procedure described schematically in Figure 5.7 and consisting of the following eight steps is proposed:

1. Determine a design modulus of the asphalt mix for a given project.
2. Measure field density and shear-wave velocity using NDT techniques.
3. Calculate in situ modulus using Equation 5.1 with the measured density and shear-wave

velocity.

4. Construct a set of three master curves at three reference temperatures according to the asphalt pavement type from a master-curve database, then employ linear interpolation of $\log 10(E)$ to obtain a master curve corresponding to the measured field temperature.
5. Determine the reduced frequency of the in situ modulus on the interpolated master curve.
6. Use the reduced frequency to find the corrected modulus on the T2 reference-temperature master curve (e.g., 21°C).
7. Use the T2 reference-temperature master curve to find the achieved modulus (Ea) at the design frequency.
8. Calculate a dimensionless index as the ratio of achieved modulus over design modulus (Ea/Ed) to quantify the achieved quality.
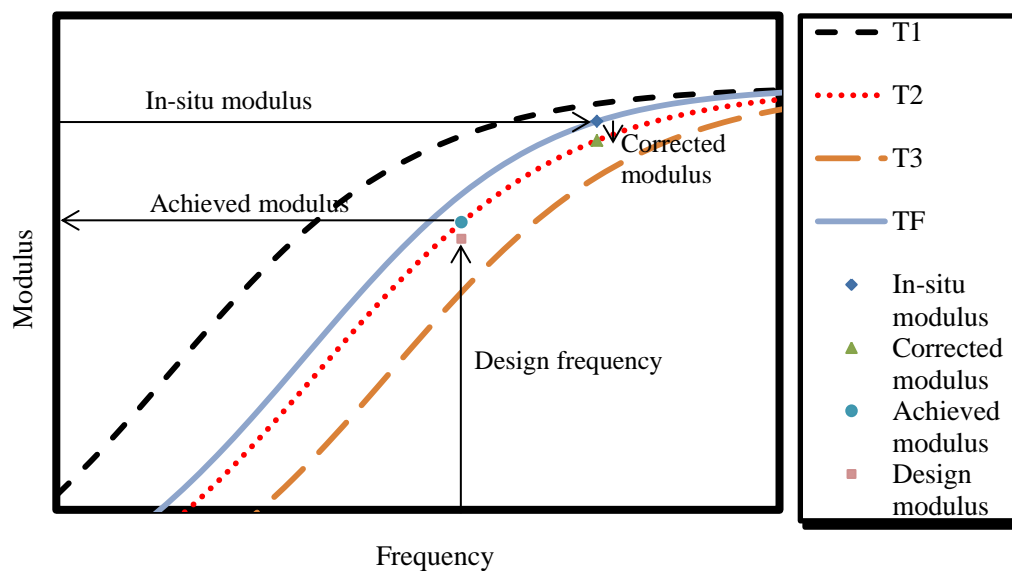
Figure 5.7 Quality assurance procedure based on NDT measurements

5.7 Chapter Summary

The in situ shear-wave velocity is very sensitive to pavement type and temperature, whereas the density is much less sensitive. Although modulus is a combination of shear-wave velocity and density, its value primarily depends on shear-wave velocity. Therefore, an in situ modulus calculated from SWM shear-wave velocity combined with EM gauge density is still accurate enough for QC/QA, even though the accuracy of the in situ density may be limited. A QC/QA procedure was developed employing the in situ modulus from SWM and EM gauge tests and a master-curve database. An alternative QC method has been developed based on GeoGauge stiffness measurements of hot asphalt pavements up to several hours after paving.

CHAPTER 6 – PRELIMINARY STUDY ON EMBEDDED MEMS SENSORS FOR QC/QA

The secondary research objective was to perform a preliminary feasibility study on QC/QA and subsequent health monitoring of asphalt pavements using embedded MEMS sensors, and, based on the survivability of the sensors and results of the study, recommend further research or implementation of MEMS sensors for QC/QA and health monitoring on a larger scale.

A previous feasibility study sponsored by the Iowa Highway Research Board was recently completed on embedded MEMS for monitoring highway structures (Ceylan et al. 2011). The study focused primarily on detection of the degree of hydration of concrete structures by measuring the moisture content. The study recommended five areas for future consideration, one of which was a MEMS-based pavement strain monitoring system, which would be useful for QC/QA and subsequent health-monitoring of asphalt pavements. Development of one such MEMS device for biaxial strain measurement was reported in Yun et al. (2001) and Obadat et al. (2003). However, the device was delicate and would not survive the paving process. Similarly sized sensors have recently been developed for measuring strain in harsh environments by Azevedo et al. (2007), but they are currently cost prohibitive until mass production of such MEMS sensors is realized (Yun et al. 2001).

Two primary challenges for using MEMS-based sensors for QC/QA and health monitoring of asphalt pavements are (1) power for the electronics, and (2) sufficiently rugged construction and electronics that can survive the temperatures and pressures under paving machines. Although off-the-shelf battery-powered MEMS sensors are available, the batteries would eventually die and render the embedded sensors useless. Embedded MEMS-sensors powered by electrical wires running to the edge of the pavement would likely not be rugged or practical enough for widespread implementation. Two alternatives that appear promising are energy-harvesting devices and sensors passively powered by radio-frequency identification (RFID) technology.

A product search was conducted for this study, but no economically feasible MEMS-based strain measuring devices were identified that could survive the paving process. However, a promising battery-free, wireless, RFID passively-powered MEMS-based sensor technology from Phase IV engineering was identified (Figure 6.1).

Figure 6.1. MEMS-based passively powered RFID temperature and wet/dry sensor

These MEMS-based sensors are installed in a disk package that is approximately 3 in. in diameter and 3/8 in. thick. They measure temperature and also indicate a binary wet/dry moisture state. The sensors are powered and interrogated from up to several feet away by a 902–928 MHz antenna. To assess the survivability of the devices, Phase IV provided one off-the-shelf sensor as well as four ruggedized versions, which had an additional epoxy layer and fiberglass cover.

Five sensors were embedded between a 3 in. thick intermediate course and a 2 in. surface course of HMA on IA 17 just north of Stanhope, Iowa, on June 18, 2014. One standard unit (Figure 6.1) was installed along with four of the ruggedized versions. Two of the ruggedized units were installed directly on the tack coat, and the other two were first glued to a steel plate, which was intended to improve the signal strength (Figure 6.2).

Figure 6.2. MEMS-based sensors embedded in IA 17 pavement: (a) 5 sensors laid on tack coat on intermediate course, (b) location of sensors in paving lane, (c) interrogation of sensors with RF antenna, (d) orange paint showing positions of first 3 embedded sensors

Immediately after paving, the three sensors not attached to the steel plate were successfully read through the 2 in. surface course. However, the unprotected sensor stopped responding within a few minutes. Temperatures recorded from the two surviving sensors were approximately 70°C, and they steadily dropped by 5°C after 1 hour (Figure 6.3).
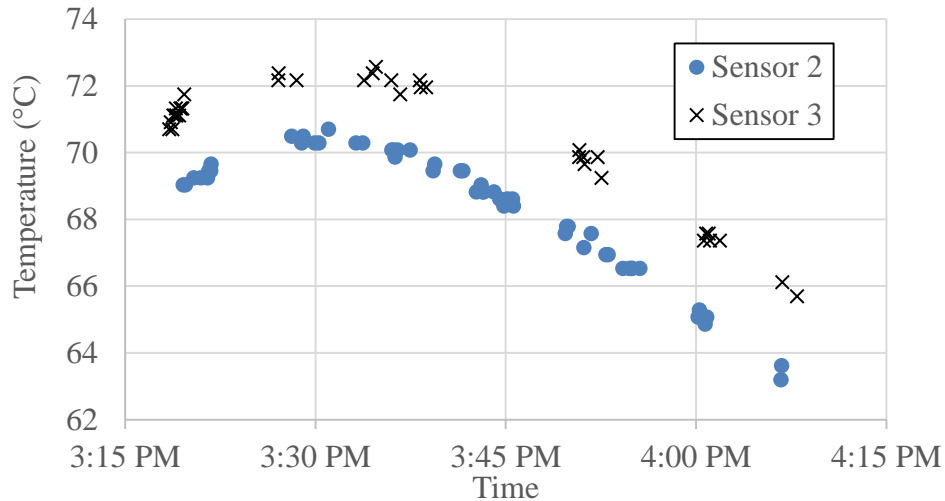
Figure 6.3. Temperature data from surviving sensors immediately after paving

The two units attached to the steel plate did not survive the paving process, most likely due to the steel plate conducting heat from the new asphalt around to the underside of the sensors; whereas the other units were somewhat insulated by being placed on the intermediate course. The two surviving sensors were interrogated approximately one week later on July 2, 2014, and only one responded, giving temperatures of 20°C.

This MEMS technology shows promise for embedded sensing in asphalt pavements, although the sensors may require further ruggedization. If the longevity of the devices can be demonstrated, the battery-free passively powered circuit design means that the sensors could outlast other battery-powered sensors. However, Phase IV Engineering does not currently offer commercial strain sensors using the passive RFID technology. Based on the successful survival and readability of the sensors under the new asphalt pavement, development of strain-gauge sensors based on the technology is recommended for further research. One challenge, however, is that strain-gauge sensors will require more power than the temperature/moisture sensors used in this preliminary study.

By their nature, the NDT methods described in Chapter 3 could also enable health monitoring of new and existing pavements through comparison of periodic measurements against benchmark readings taken at some previous point in the pavement's life cycle. Health monitoring can be achieved by performing periodic NDT of pavement modulus using surface-wave methods, or by tracking stiffness using the GeoGauge. For new pavements, the initial benchmark readings can be taken immediately after construction. For existing pavements, the benchmark readings may be taken at any point in the pavement's life cycle. Comparison of the benchmark readings with subsequent measurements will allow performance metrics such as stiffness or density to be monitored over time.

With further research, threshold criteria in terms of the NDT modulus or stiffness may be developed to indicate when the pavement's health reaches a critical state. Multiple measurements

covering a pavement section of interest can be plotted as color maps for different points in time to highlight areas of deterioration, which may not be visually evident at the surface.

Surface-wave methods can offer a significant advantage relative to the other technologies for health monitoring applications, because surface waves provide measurements from wave propagation through the pavement over distances of 2 to 5 m (6.6 to 16.4 ft), whereas nuclear gauges, EM gauges and the GeoGauge only give measurements at selected points. Surface-wave methods may therefore measure pavement integrity over larger volumes, translating into significant time savings for profiling large sections of pavement. Wave propagation methods have also been shown to indicate damage such as subsurface cracking, which causes reflection and scattering of the waves, reducing the energy reaching the sensors.

As outlined above, there are two options for studying health monitoring of asphalt pavements by tracking changes in pavement behavior over time: (1) development and preliminary testing of embedded MEMS sensors for stress and strain, and (2) periodic measurement of modulus or stiffness by surface-wave or GeoGauge tests.

CHAPTER 7 – CONCLUSIONS AND RECOMMENDATIONS

An accurate and objective quality measurement procedure was developed in this study based on dynamic modulus obtained by a combination of shear-wave velocity and density measured with two efficient and economical NDT methods (i.e., surface-wave tests and electromagnetic density gauges). The shear-wave velocity can be obtained by inversion of MSOR dispersion data, or by simply multiplying the constant phase velocity of the horizontal portion of MASW dispersion data in the high-frequency range by a factor related to Poisson's ratio.

The in situ density can be measured by devices such as the Troxler PT. The researchers found that the PT density had a low correlation with laboratory density. However, the modulus calculated using the PT density was highly correlated and close to the modulus calculated with the CoreLok density, because the modulus is much more sensitive to shear-wave velocity than density. The in situ density is not sensitive to temperature variation, whereas the shear-wave velocity is very sensitive. To account for effect of temperature on modulus, the in situ moduli measured at different field temperatures should be corrected to a common reference temperature for quality comparisons. Procedures were developed in Chapter 4 for this purpose.

The GeoGauge stiffness measured on hot asphalt mixtures several hours after paving has a good correlation with the in situ dynamic modulus and the laboratory density, whereas the GeoGauge stiffness of cold and ambient-temperature asphalt mixtures has a very low correlation with the other measurements. Therefore, the GeoGauge stiffness measured on hot asphalt pavements is recommended for QC.

The in situ moduli, temperatures, densities, and stiffnesses of five representative asphalt pavement projects were measured, and field cores were tested for density and dynamic modulus in the laboratory. Prior to measuring the dynamic moduli of the field cores, the indirect tension dynamic modulus method was first validated against the axial method. Dynamic modulus of the field cores was then measured over a range of frequencies and temperatures with the IDT method and used to construct master curves for correcting the in situ moduli at various temperatures to a common reference temperature. To obtain a master curve at a given field temperature from measured master curves at different reference temperatures, linear interpolation of $\log10(E)$ was found to have the smallest discrepancy with the actual master curve across the whole frequency range. After correcting the in situ modulus, a quick QC procedure was developed by comparing the corrected modulus to the design modulus, and a more accurate quality assurance procedure was developed by comparing the achieved modulus with the design modulus at a given design frequency.

A comprehensive master-curve database covering a variety of pavements with different mixes and traffic volumes is needed to correct the in situ modulus values for temperature, and to determine design modulus values. To generate such a comprehensive master-curve database, laboratory modulus measurements of field cores from various asphalt pavement projects should be made.

A preliminary study on MEMS-based sensors for QC/QA and health monitoring of asphalt mixtures was performed. One out of three configurations of a ruggedized battery-free wireless RFID-powered temperature/moisture sensor was found to survive the paving process, and one out of two of the surviving sensors was successfully read through a 2 in. thick asphalt pavement course after a period of one week. It is recommended that the technology be further studied for application to embedded RFID-powered strain gauges. The use of NDT tests performed periodically was also discussed and is recommended for health monitoring of asphalt pavements.

REFERENCES

AASHTO. 2007. Standard method of test for bulk specific gravity of compacted hot mix asphalt HMA using saturated surface-dry specimens. AASHTO Designation: T 166, Washington, D.C.

AASHTO. 2011a. Determining dynamic modulus of hot mix asphalt (HMA). AASHTO Designation: T 342-11, Washington, D.C.

AASHTO. 2011b. Developing dynamic modulus master curves for hot mix asphalt (HMA). AASHTO Designation: PP 62-10, Washington, D.C.

AASHTO. 2014. Proposed standard test method for determining the dynamic modulus for hot-mix asphalt (HMA) using the indirect tension testing method. AASHTO TP XX-XX, Washington, DC.

Abdallah, I., A. Meshkani, D. Yuan, and S. Nazarian. 2005. *Design Modulus Values Using Seismic Moduli*. Report. Austin, TX: Texas Department of Transportation.

Alshibli, K. A., M. Abu-Farsakh, and E. Seyman. 2005. Laboratory evaluation of the GeoGauge and light falling weight deflectometer as construction control tools. *Journal of Materials in Civil Engineering* 17:560–9.

Ayres, M., and M. W. Witczak. 1998. AYMA: mechanistic probabilistic system to evaluate flexible pavement performance. *Transportation Research Record: Journal of the Transportation Research Board* 1629(1):137–48.

Azevedo, R. G., D. G. Jones, A. V. Jog, B. Jamshidi, D. R. Myers, L. Chen, X. Fu, M. Mehregany, M. B. J. Wijesundara, and A. P. Pisano. 2007. A SiC MEMS resonant strain sensor for harsh environment applications. *IEEE Sensors Journal* 7 (4): 568–76.

Bai, X. 2004. Assessment of relationship between dynamic and seismic moduli of asphalt concrete mixtures. Master thesis, University of Texas at El Paso.

Barnes, C. L., and J. F. Trottier. 2010a. Evaluating in-service asphalt concrete damage using surface waves. *International Journal of Pavement Engineering* 11:449–58.

Barnes, C. L., and J. F. Trottier. 2010b. Evaluating laboratory-induced asphalt concrete moisture damage using surface waves. *International Journal of Pavement Engineering* 11:489–97.

Buchanan, M., and T. White. 2005. Hot mix asphalt mix design evaluation using the Corelok vacuum-sealing device. *Journal of Materials in Civil Engineering* 17:137–42.

Celaya, M., and S. Nazarian. 2006. Seismic testing to determine quality of hot-mix asphalt. *Transportation Research Record: Journal of the Transportation Research Board* 1946:113–22.

Celaya, M., S. Nazarian, M. Zea, and V. Tandon. 2006. *Use of NDT Equipment for Construction Quality Control of Hot Mix Asphalt Pavements*. Report. Phoenix, AZ: Arizona Department of Transportation.

Ceylan, H., K. Gopalakrishnan, P. Taylor, P. Shrotriya, S. Kim, M. Prokudin, S. Wang, A. F. Buss, and J. Zhang. 2011. *A Feasibility Study on Embedded Micro-Electromechanical Sensors and Systems (MEMS) for Monitoring Highway Structures*. Final Report. IHRB Project TR-575, National Concrete Pavement Technology Center and Iowa Highway Research Board.

Chen, D. H., W. Wu, R. He, J. Bilyeu, and M. Arrelano. 2000. *Evaluation of In-Situ Resilient Modulus Testing Techniques*. Report. Austin, TX: Texas Department of Transportation.

Dougan, C. E., J. E. Stephens, J. Mahoney, and G. Hansen. 2003. *E*-Dynamic Modulus Test Protocol—Problems and Solutions*. Report. Storrs, CT: Connecticut Department of Transportation.

Egorov, K. E. 1965. Calculation of bed for foundation with ring footing. *Proceedings of the Sixth International Conference on Soil Mechanics and Foundation Engineering* 2:41–5.

Finn, F., C. Saraf, R. Kulkarni, K. Nair, W. Smith, and A. Abdullah. 1977. The use of distress prediction subsystems for the design of pavement structures. Paper presented at the 4th International Conference on the Structural Design of Asphalt Pavements, Ann Arbor, MI.

Heisey, J. S., K. H. Stokoe II, and A. H. Meyer. 1982. Moduli of pavement systems from spectral analysis of surface waves. *Transportation Research Record*, Issue 852, Washington DC, pp. 22–31.

Heukelom, W., and C. R. Foster. 1960. Dynamic testing of pavements. *Journal of the Soil Mechanics and Foundations Division* 86:2368–72.

Humboldt Mfg. Co. 2014. H-4140 *GeoGauge Compaction Uniformity via In-Place Stiffness Measurement*. Product Brochure. Humboldt Mfg. Co., 3801 North 25 Ave., Schiller Park, IL 60176, www.humboldtmfg.com.

Icenogle, P., and M. S. Kabir. 2013. *Evaluation of Non-Destructive Technologies for Construction Quality Control of HMA and PCC Pavements in Louisiana*. Report. Baton Rouge, LA: Louisiana Department of Transportation.

Jiang, Z. 2007. Innovative nondestructive testing (NDT) for condition assessment of longitudinal joints in asphalt pavements. Master thesis, University of Waterloo, Waterloo, Ontario, Canada.

Jones, R. 1955. A vibration method for measuring the thickness of concrete road slabs in situ. *Magazine of Concrete Research* 7:97–102.

Jones, R. 1958. In-situ measurement of the dynamic properties of soil by vibration methods. *Géotechnique* 8:1–21.

Jones, R. 1962. Surface wave technique for measuring the elastic properties and thickness of roads: Theoretical development. *British Journal of Applied Physics* 13:21–9.

Kim, J. S. 2002. Complex modulus from indirect tension testing. Master thesis, University of Florida.

Kim, Y. R., Y. Seo, M. King, and M. Momen. 2004. Dynamic modulus testing of asphalt concrete in indirect tension mode. *Transportation Research Record: Journal of the Transportation Research Board* 1891:163–73.

Larsen, D. A., and J. W. Henault. 2006. *Quantifying Segregation in HMA Pavements Using Non-Nuclear Density Devices: Data Collection Report for Connecticut*. Report. Newington, CT: Connecticut Department of Transportation.

Lee, H., A. Woods, and Y. Kim. 2011. *Examination of Curing Criteria for Cold In-Place Recycling: Phase 3 Calibration of Moisture Loss Indices and Development of Stiffness Gain Model*. Report. Ames, IA: Iowa Department of Transportation.

Lenke, L. R., R. G. McKeen, and M. P. Grush. 2003. Laboratory evaluation of GeoGauge for compaction control. *Transportation Research Record: Journal of the Transportation Research Board* 1849:20–30.

Li, Y., and S. Nazarian. 1995. Evaluation of aging of hot-mix asphalt using wave propagation techniques. Paper presented at Engineering Properties of Asphalt Mixtures and the Relationship to Their Performance, American Society for Testing and Materials, Philadelphia. ASTM STP 1265, Gerald A. Huber and Dale S. Decker (eds.).

Lin, S. 2014. Advancements in active surface wave methods: Modeling, testing, and inversion. PhD dissertation, Iowa State University.

Lin, S., and J. C. Ashlock. 2011. A study on issues relating to testing of soils and pavements by surface wave methods. Paper presented at the 38th Annual Review of Progress in Quantitative Nondestructive Evaluation (QNDE 2011), Burlington, VT.

Lin, S., and J. C. Ashlock. 2014. Comparison of MASW and MSOR for surface wave testing of pavements. *SAGEEP 2014, 27th Symposium on the Application of Geophysics to Engineering and Environmental Problems*, Boston, MA, March 16–20, 2014; extended abstract, 9 pp.

Mason, M. E., and R. C. Williams. 2009. *Investigation of Electromagnetic Gauges for Determination of In-Place Density of HMA Pavements*. Report. Ames, IA: Iowa Department of Transportation.

Mohammad, L. N., M. Y. Abu-Farsakh, Z. Wu, and C. Abadie. 2003. Louisiana experience with foamed recycled asphalt pavement base materials. *Transportation Research Record: Journal of the Transportation Research Board* 1832:17–24.

Nazarian, S. 1984. In situ determination of elastic moduli of soil deposits and pavement systems by spectral-analysis-of-surface-waves method. PhD dissertation, University of Texas at Austin.

Nazarian, S., V. Tandon, and D. Yuan. 2005. Mechanistic quality management of hot mix asphalt layers with seismic methods. *Journal of ASTM International* 2:1–12.

Nazarian, S., D. Yuan, and M. R. Baker. 1995. *Rapid Determination of Pavement Moduli with Spectral-Analysis of Surface Waves Method*. Report. El Paso, TX: Texas Department of Transportation.

Obadat, M., H. Lee, A. Bhatti, and B. Maclean. 2003. Full-scale evaluation of MEMS-based bi-axial strain transducer and its application. *Journal of Aerospace Engineering, ASCE* 2003:100–7.

Olson, L. D. 2008. *Nondestructive Evaluation of Concrete and Asphalt Pavement Thicknesses, Moduli and Subgrade Support*. Olsen Engineering.

Olson, L. D., and P. K. Miller. 2010. Multiple impact surface waves (MISW)—Improved accuracy for pavement system thicknesses and moduli vs. spectral analysis of surface waves (SASW). Paper presented at the GeoFlorida Conference.

Pagen, C. A. 1963. An analysis of the thermorheological response of bituminous concrete. Master thesis, The Ohio State University.

Park, C. B., J. Ivanov, R. D. Miller, J. Xia, and N. Ryden. 2001. Seismic investigation of pavements by MASW method—Geophone approach. Paper presented at SAGEEP 2001, Denver, CO.

Park, C. B., R. D. Miller, and J. Xia. 1999. Multichannel analysis of surface waves. *Geophysics* 64:800–8.

Park, C. B., N. Ryden, R. D. Miller, and P. Ulriksen. 2002. Time break correction in multichannel simulation with one receiver (MSOR). Paper presented at SAGEEP 2002, Las Vegas, NV.

Rix, G. J. 1988. Experimental study of factors affecting the spectral-analysis-of-surface-waves method. PhD dissertation, University of Texas at Austin, Austin, Texas.

Ryden, N. 2004. Surface wave testing of pavements. PhD dissertation, Lund University, Lund, Sweden.

Ryden, N., and C. B. Park. 2004. Surface waves in inversely dispersive media. *Near Surface Geophysics* 2:187–97.

Ryden, N., M. J. S. Lowe, P. Cawley, and C. B. Park. 2006. Evaluation of multilayered pavement structures from measurements of surface waves. Paper presented at the 32nd QNDE, Portland, OR.

Ryden, N., C. B. Park, P. Ulriksen, and R. D. Miller. 2002a. Branching of dispersion curves in surface wave testing of pavements. Paper presented at SAGEEP 2002, Las Vegas, NV.

Ryden, N., C. B. Park. P. Ulriksen, and R. D. Miller. 2004. Multimodal approach to seismic pavement testing. *Journal of Geotechnical and Geoenvironmental Engineering* 130:636–45.

Ryden, N., P. Ulriksen, C. B. Park, and R. D. Miller. 2002b. Portable seismic acquisition system (PSAS) for pavement MASW. Paper presented at SAGEEP 2002, Las Vegas, NV.

Ryden, N., P. Ulriksen, C. B. Park, R. D. Miller, J. Xia, and J. Ivanov. 2001. High frequency MASW for non-destructive testing of pavements-accelerometer approach. Paper presented at SAGEEP 2001, Denver, CO.

Saeed, A., and J. W. Hall. 2003. Comparison of non-destructive testing devices to determine in situ properties of asphalt concrete pavement layers. Paper presented at the 82nd Transportation Research Board (TRB) Annual Meeting, Washington, DC.

Stokoe, K. H. II, G. W. Wright, A. B. James, and M. R. Jose. 1994. Characterization of geotechnical sites by SASW method. In Woods R. D. (ed.). *Geophysical Characterization of Sites*. Oxford Pub, pp. 15–25.

Tertre, A., G. Cascante, and S. L. Tighe. 2010. Combining portable falling weight deflectometer and surface wave measurements for evaluation of longitudinal joints in asphalt pavements. *Transportation Research Record: Journal of the Transportation Research Board* 2152:28–36.

Van der Poel, C. 1951. Dynamic testing of road constructions. *Journal of Applied Chemistry* 1:281–90.

Vidale, R. F. 1964. The dispersion of stress waves in layered media overlaying a half space of lesser acoustic rigidity. PhD dissertation, University of Wisconsin, Madison, Wisconsin.

White, D., and D. Harrington. 2005. *Fly Ash Soil Stabilization for Non-Uniform Subgrade Soils Volume 2*. Center for Portland Cement Concrete Pavement Technology.

Williams, R. C., C. Can, T. Ahmed, and H. Lee. 2013. *Quality Control/Quality Assurance Testing for Joint Density and Segregation of Asphalt Mixtures*. Institute for Transportation, Ames, IA.

Williams, S. G. 2001. Bulk specific gravity measurements of 25.0-mm and 37.5-mm coarse-graded superpave mixes. *Transportation Research Record: Journal of the Transportation Research Board*. 2001/2007 Bituminous Paving Mixtures 2007:110–7.

Williams, S. G. 2008. *Non-Nuclear Methods for HMA Density Measurement*. Report. Fayetteville, AR: Mack-Blackwell Transportation Center and Arkansas State Highway and Transportation Department.

Yun, H. B., H. Lee, and B. Maclean. 2001. Evaluation of hybrid uni-axial strain transducer for rail infrastructure. *Transportation Research Record, TRB* 2001:78–86

APPENDIX A – FIELD TEST RESULTS

LIST OF FIGURES

LIST OF TABLES

HB1-1

HB1-3

HB1-5

Figure A.1. Results of surface wave tests on hot Boone HMA base courses several hours after paving. Left column: normalized time-domain signals, right column: frequency-domain dispersion images
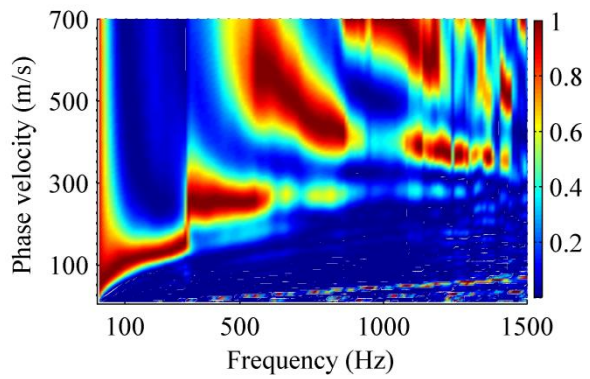
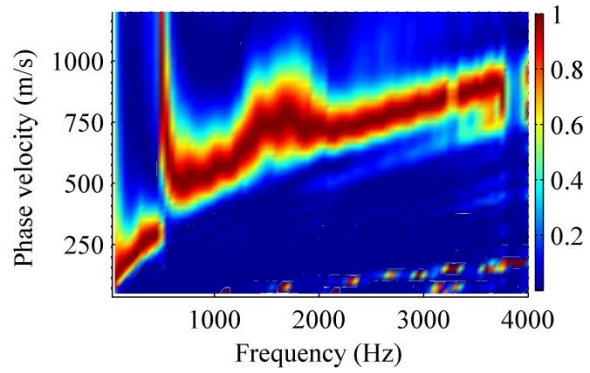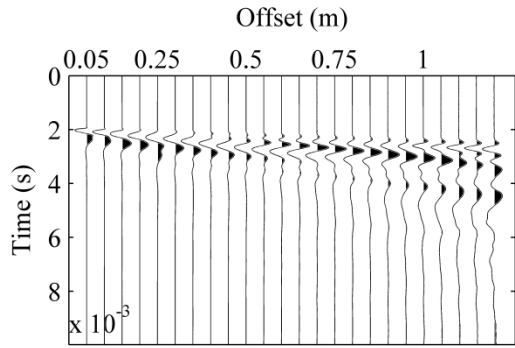86

HB1-7
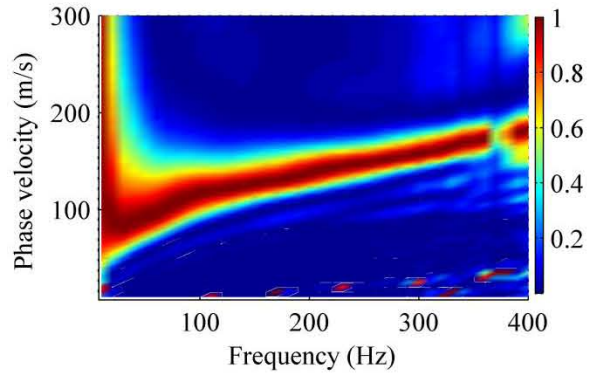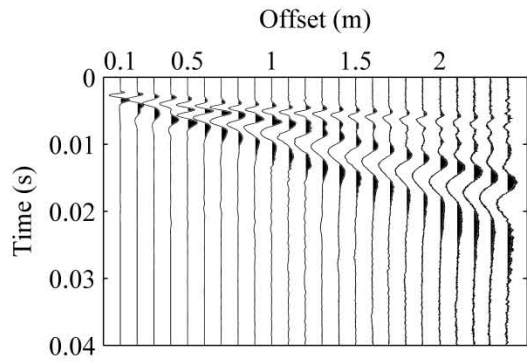
HB2-1
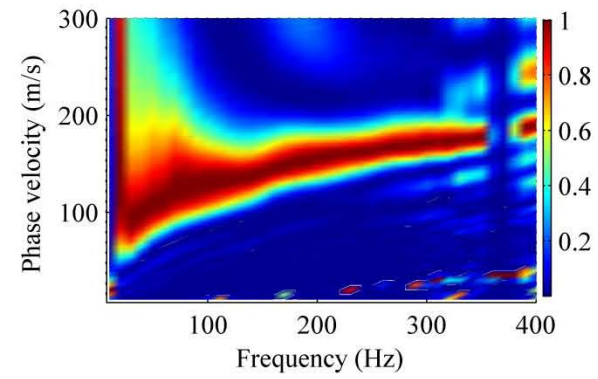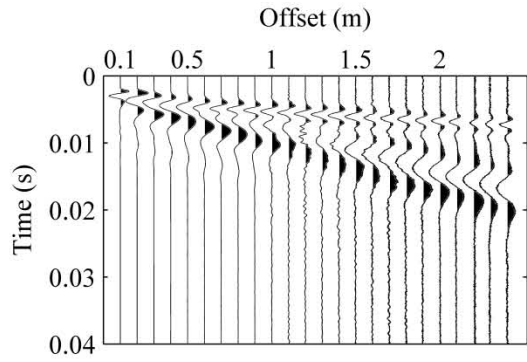
HB2-2
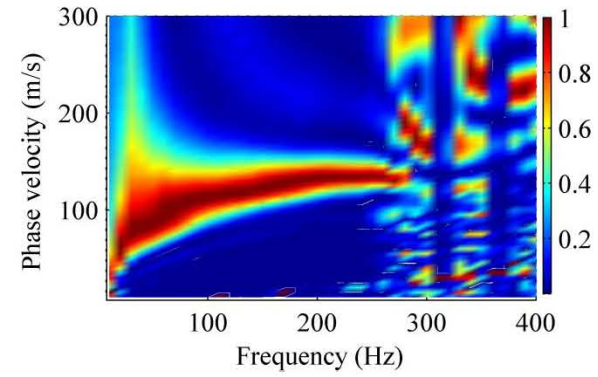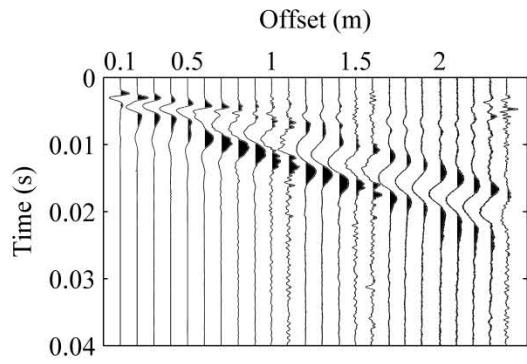
HB2-5
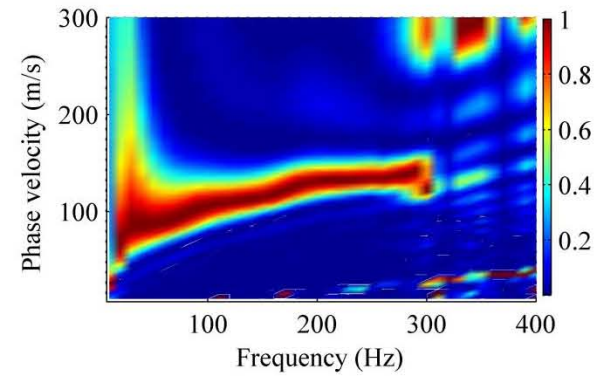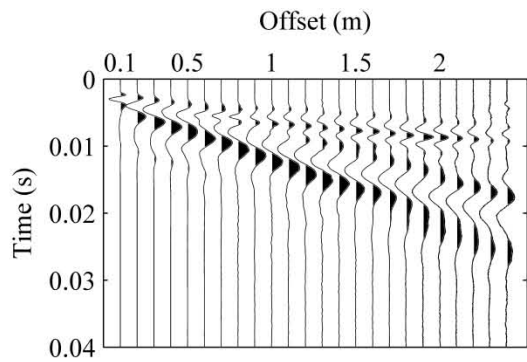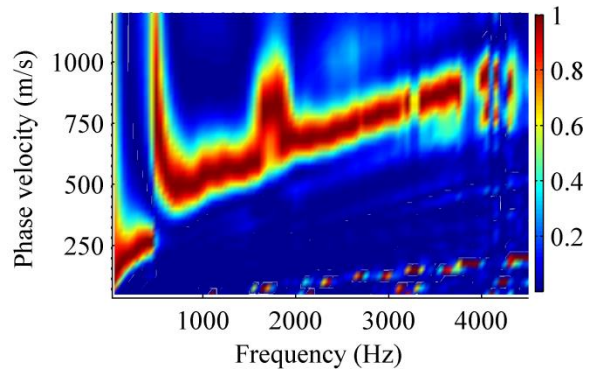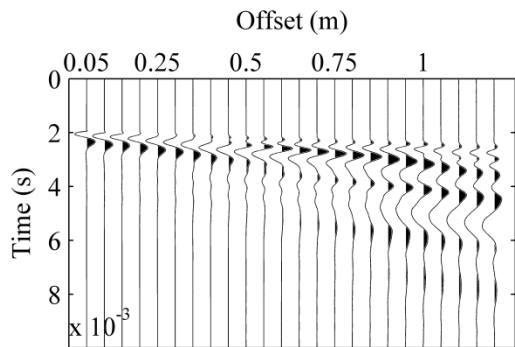

Figure A.1 (continued)

HB2-7
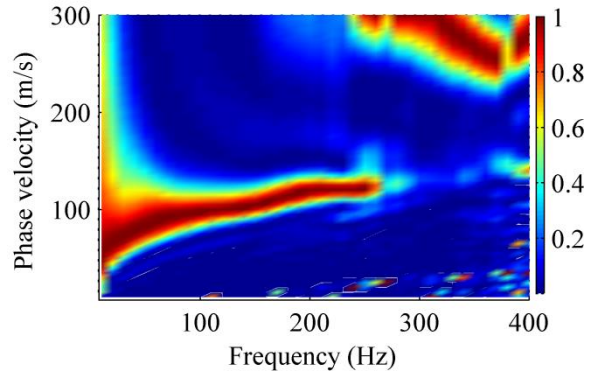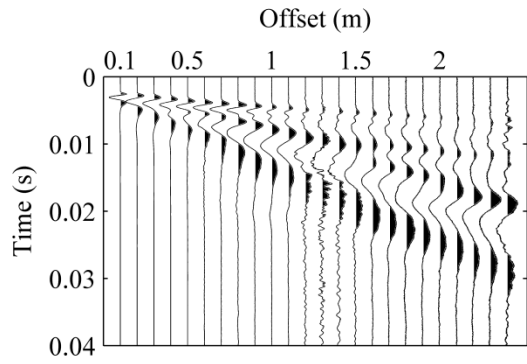
HB5-1
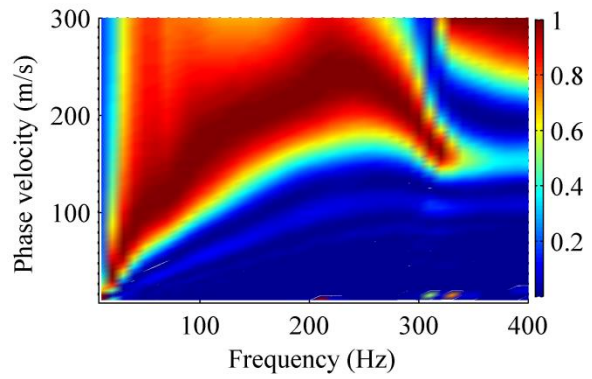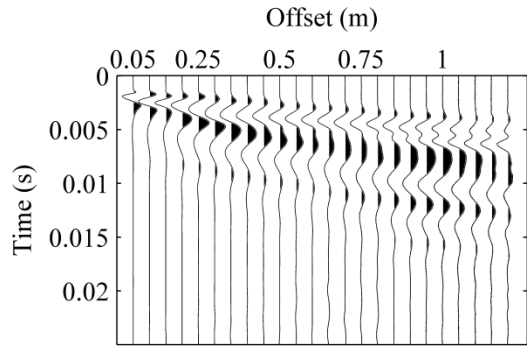
HB5-3
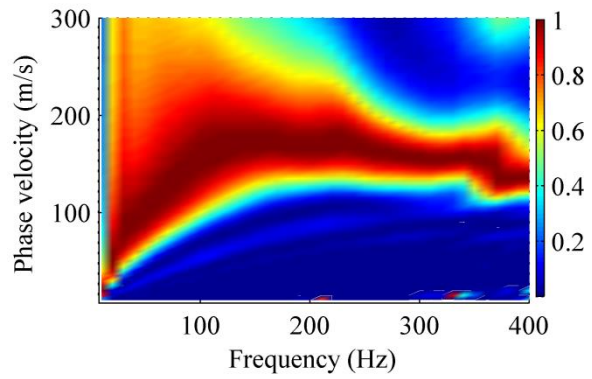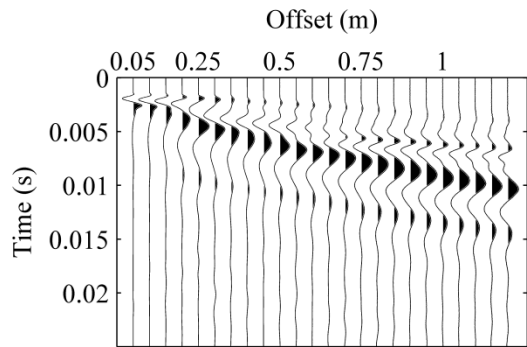
HB5-6

Figure A.1 (continued)

88
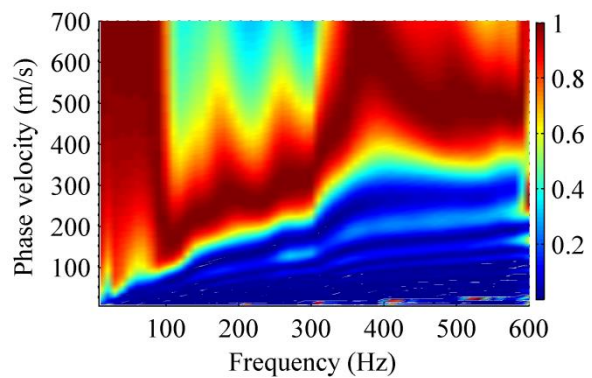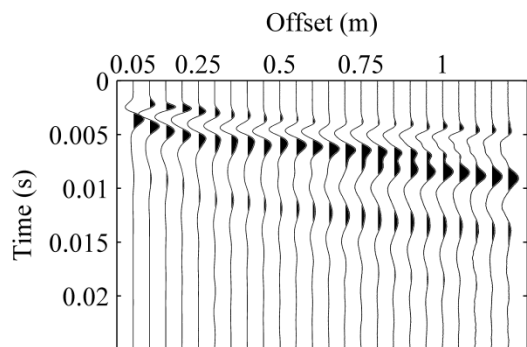
HB5-7
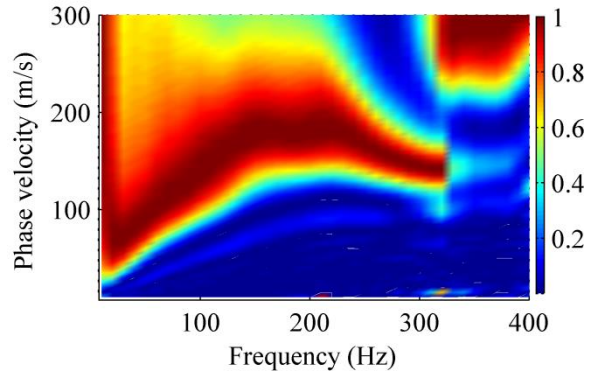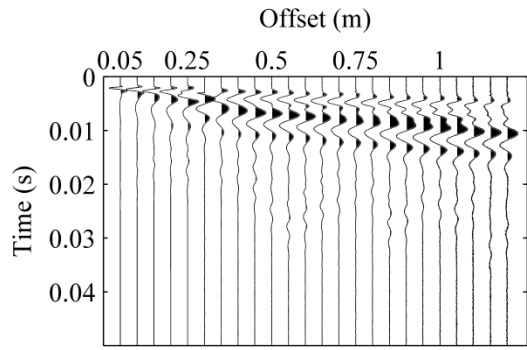
HB6-3
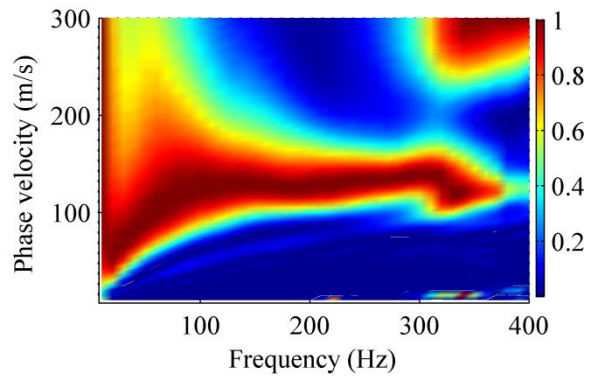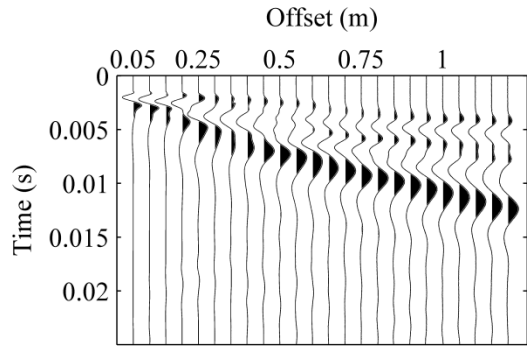
HB6-4
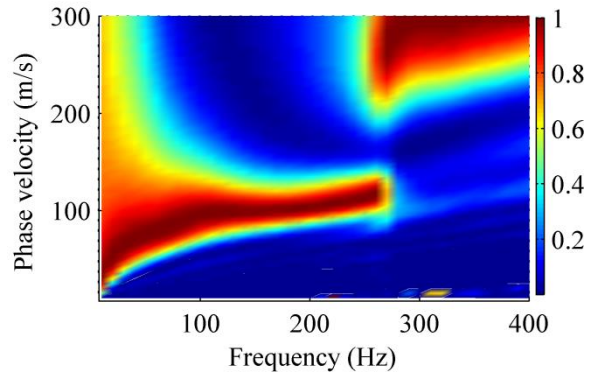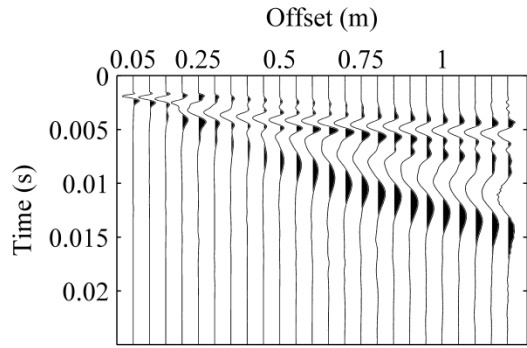
HB6-5
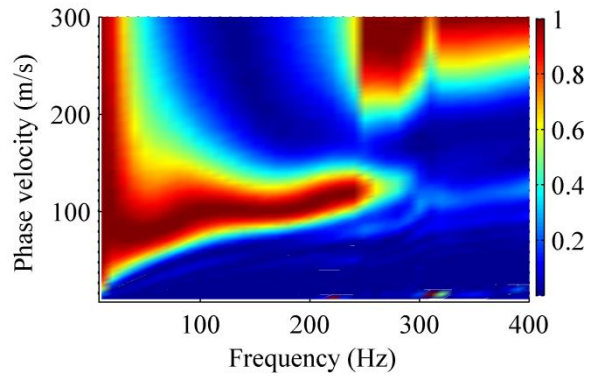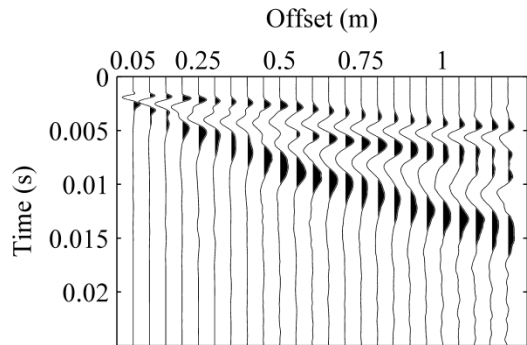
Figure A.1 (continued)

HB6-7
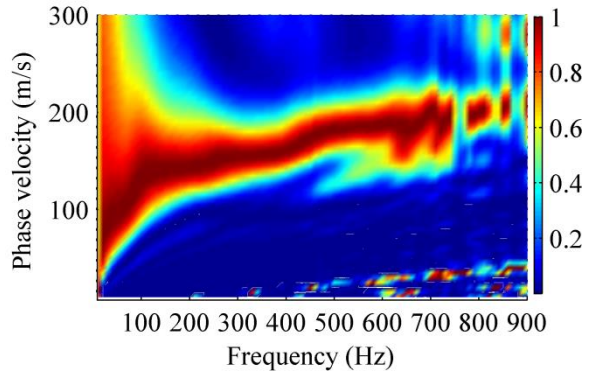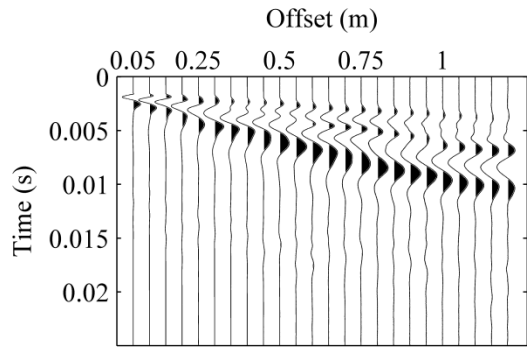
HB7-2
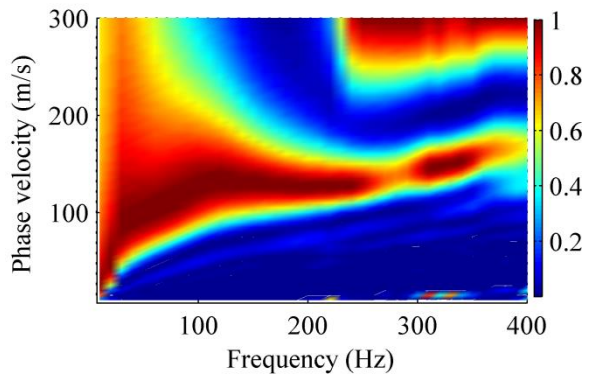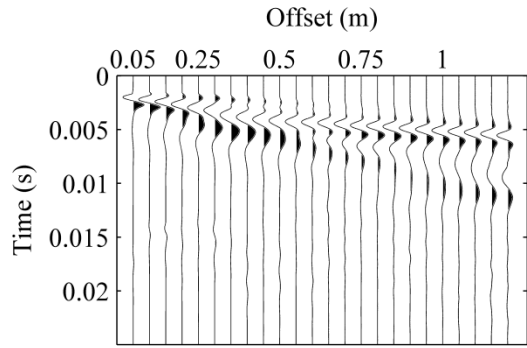
HB7-4
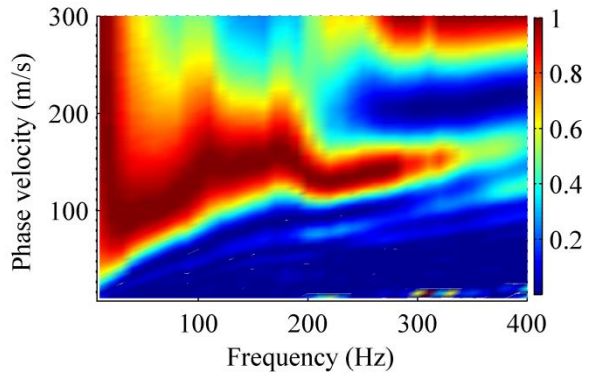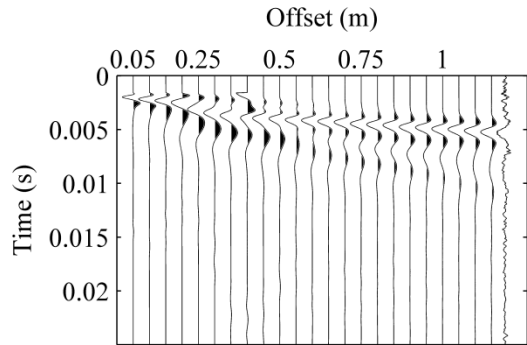
HB7-7

Figure A.1 (continued)

90

WB3-2
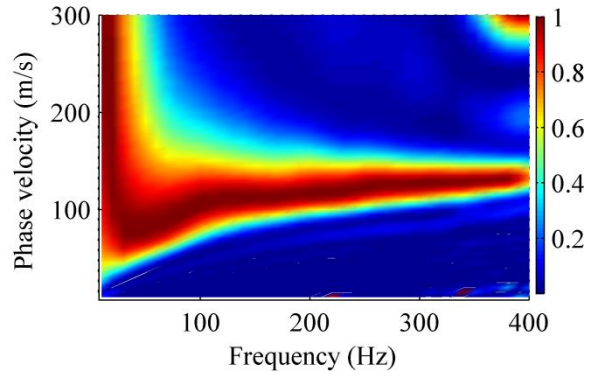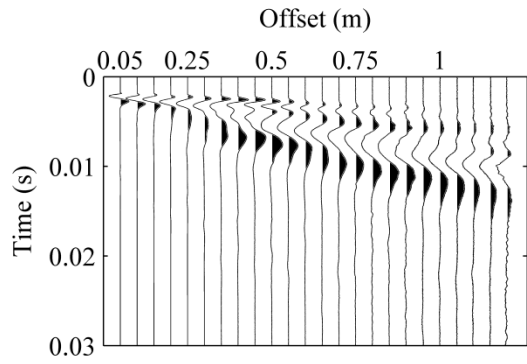
WB3-4
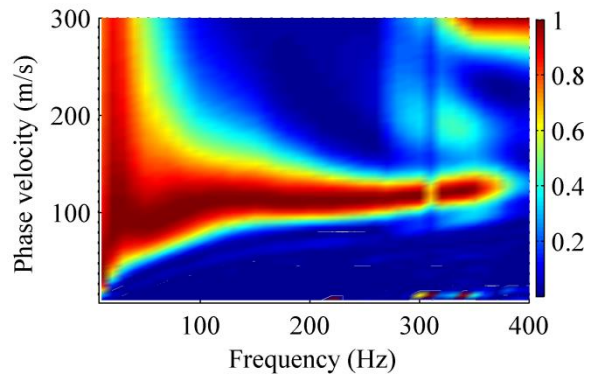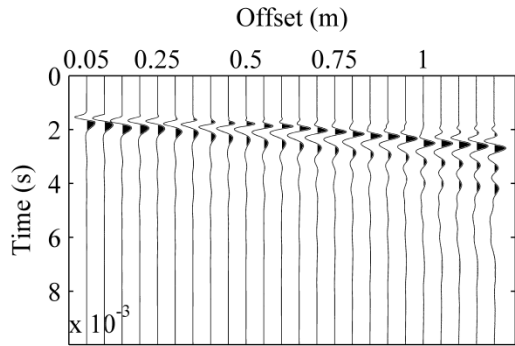
WB3-5
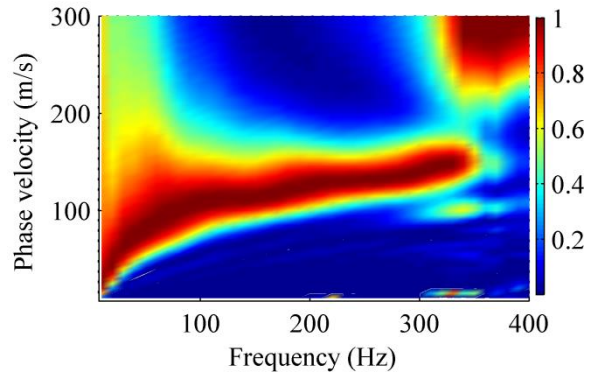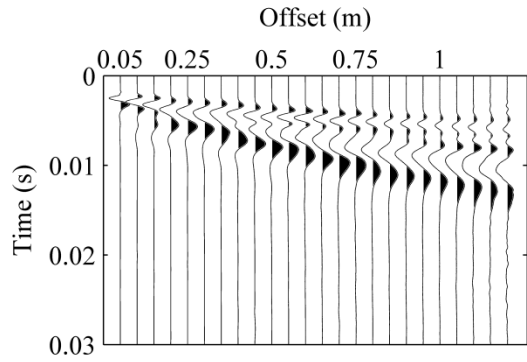
Figure A.2. Results of surface wave tests on hot Boone WMA base courses several hours after paving. Left column: normalized time-domain signals, right column: frequency-domain dispersion images

91

WB3-7

WB4-1

WB4-2

WB4-3

Figure A.2 (continued)

WB4-7
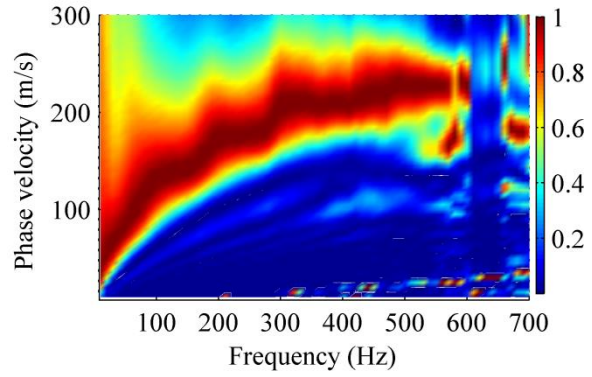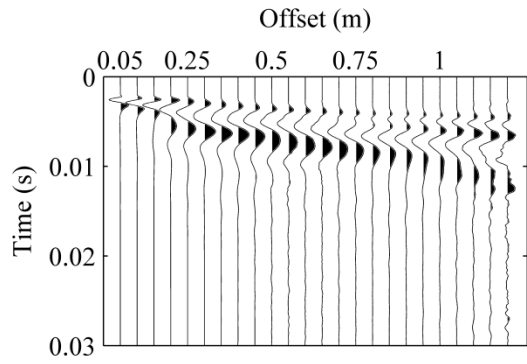
WB8-4
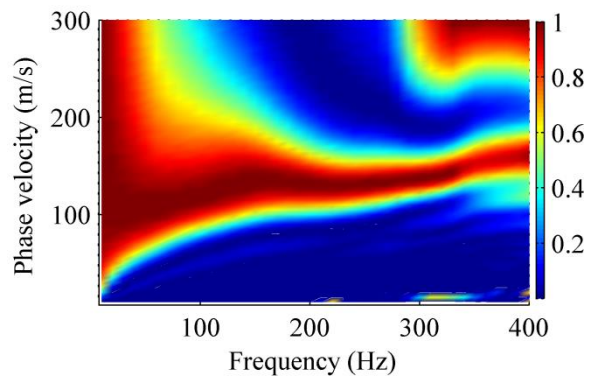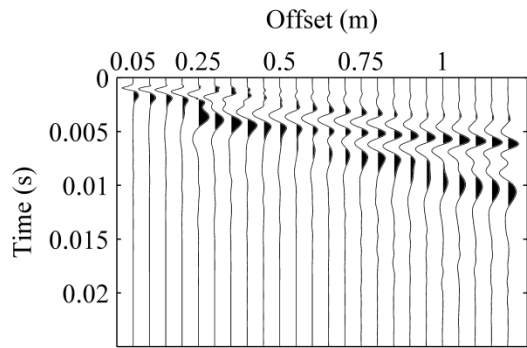
WB8-5
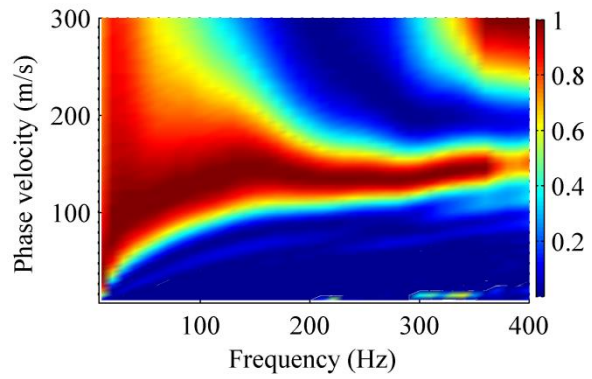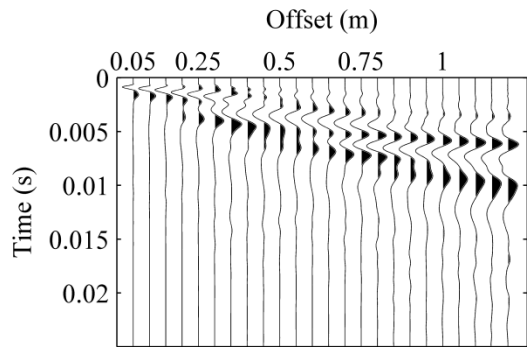
WB8-7

Figure A.2 (continued)

93
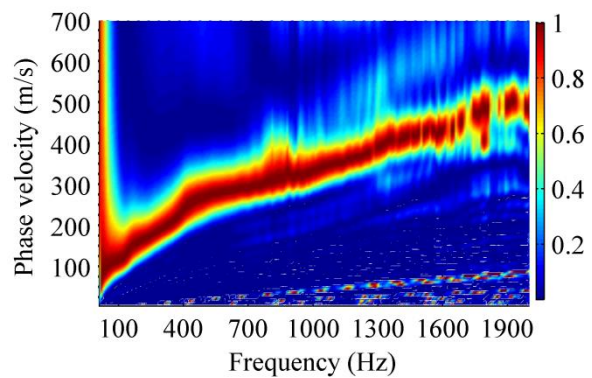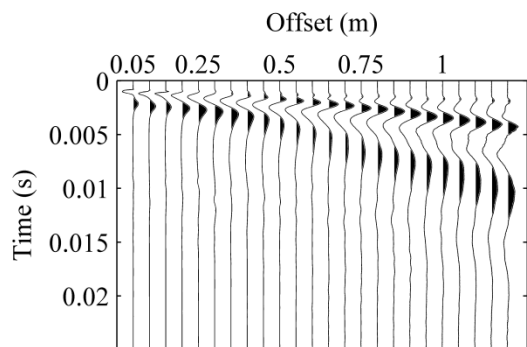
WB8-8
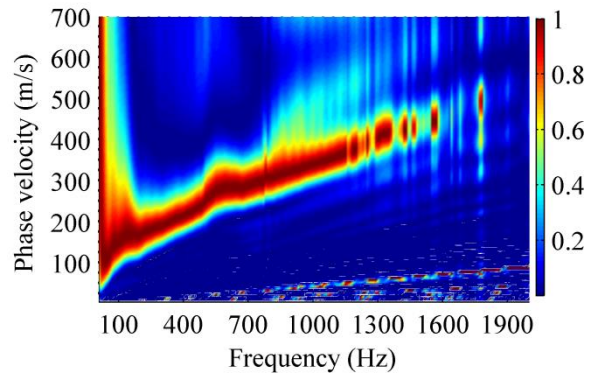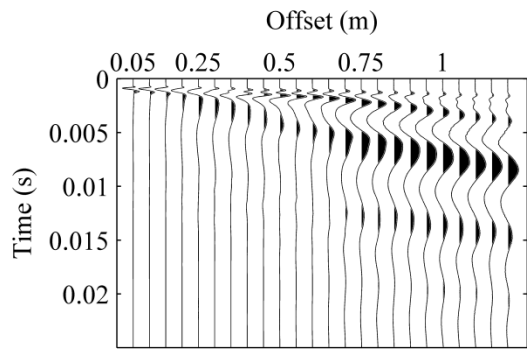
WB9-2
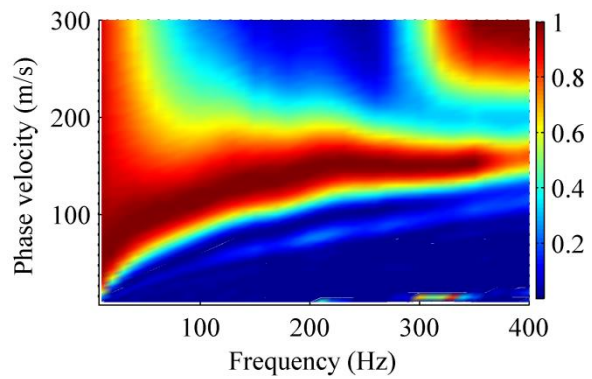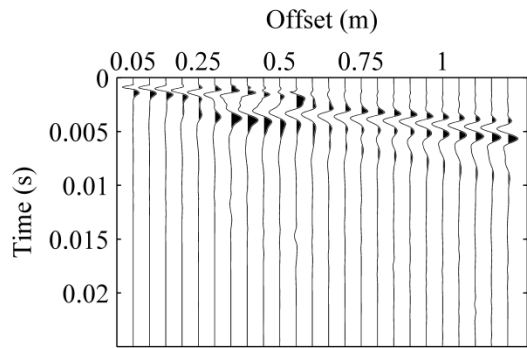
WB9-3
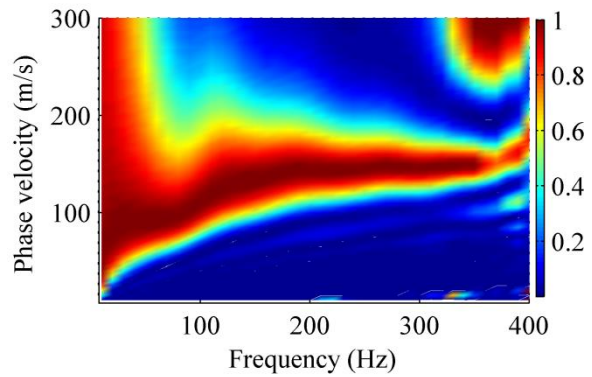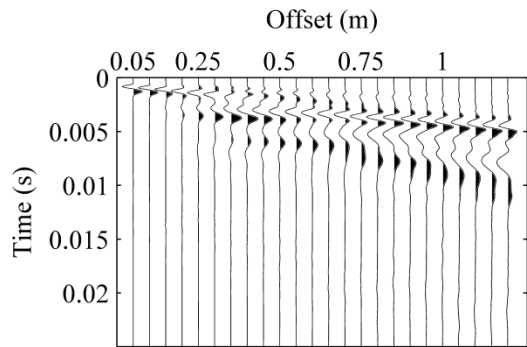
WB9-6
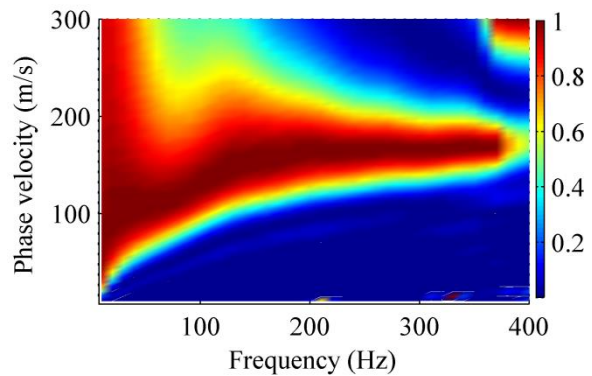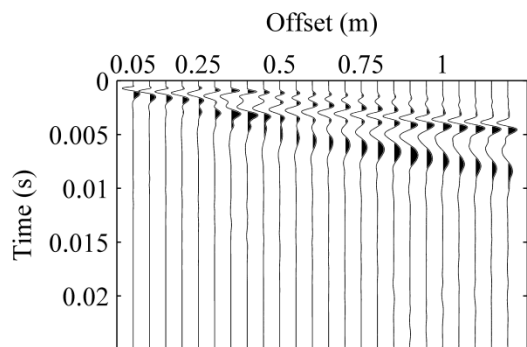
Figure A.2 (continued)

WB9-7
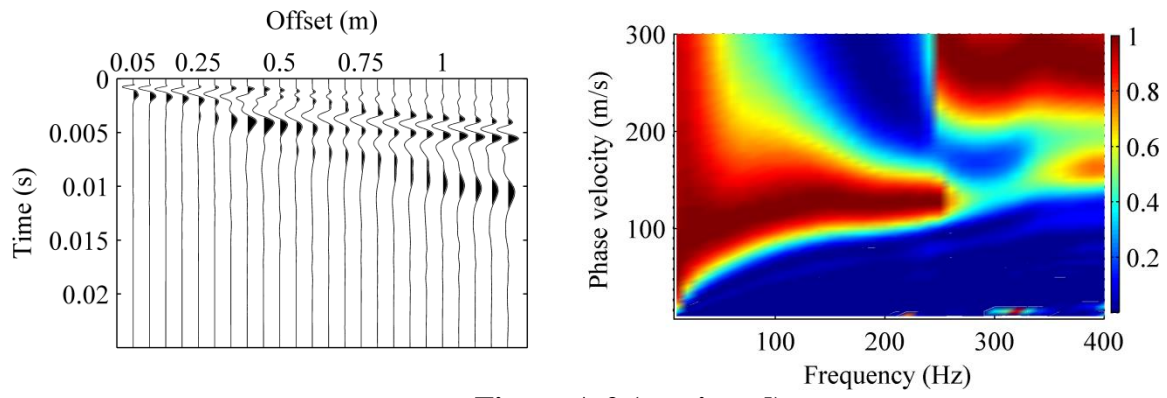
Figure A.2 (continued)

HB1-1
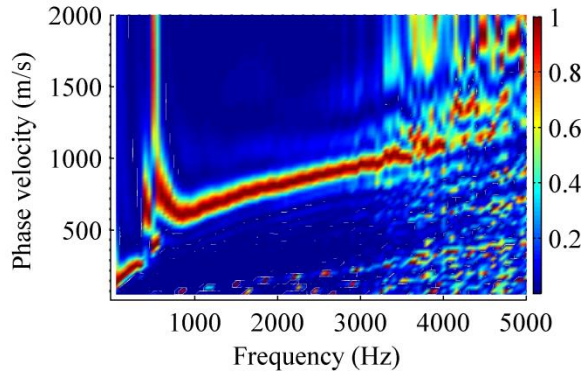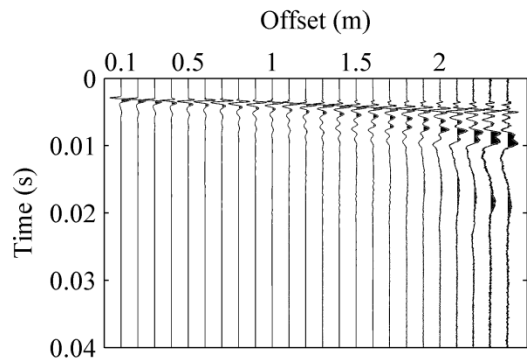
HB1-3
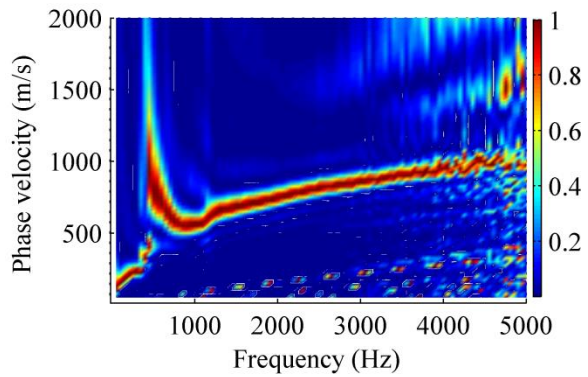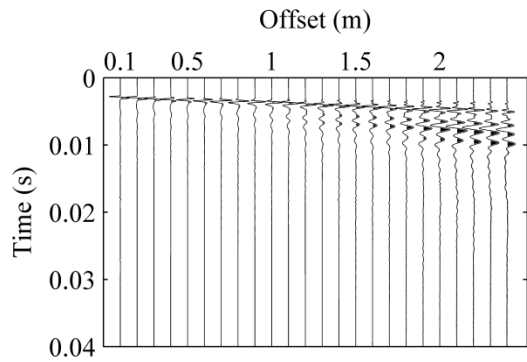
HB1-5
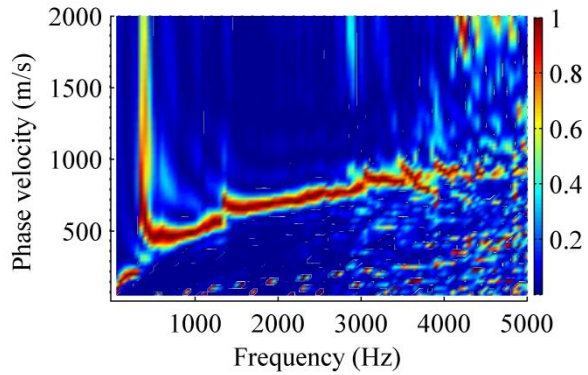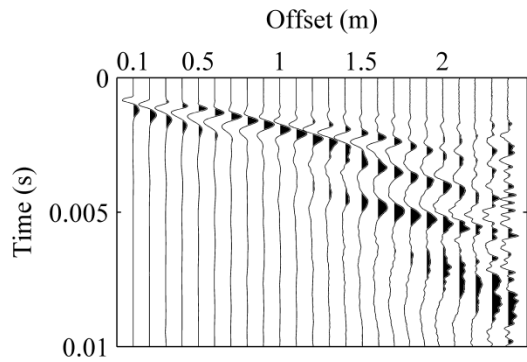
Figure A.3. Results of surface wave tests on ambient-temperature Boone HMA base courses one day after paving. Left column: normalized time-domain signals, right column: frequency-domain dispersion images

96

HB1-7

HB2-1

HB2-2

HB2-5

Figure A.3 (continued)

HB2-7
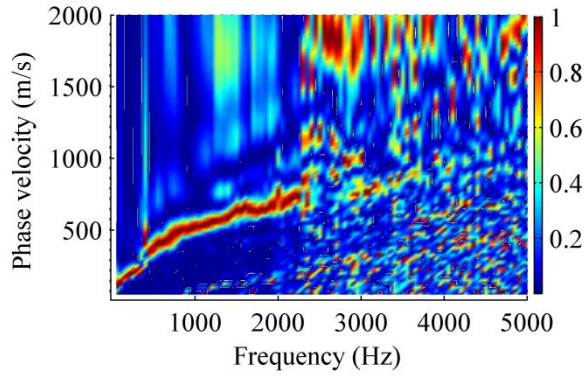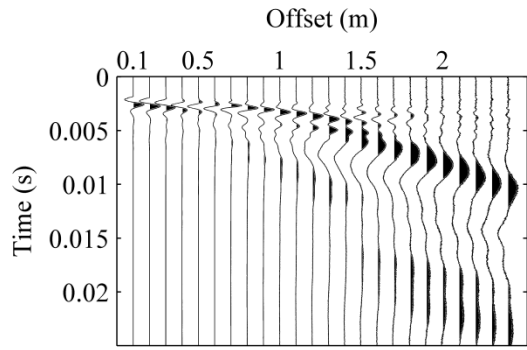
HB5-1
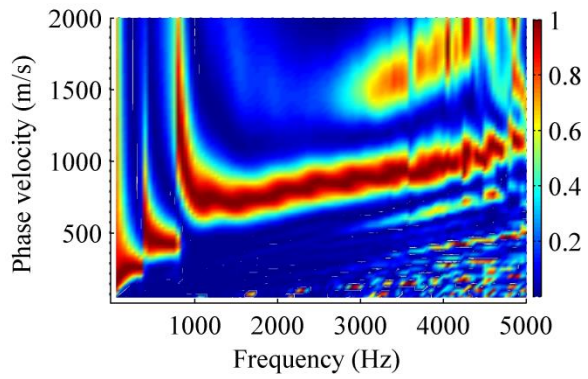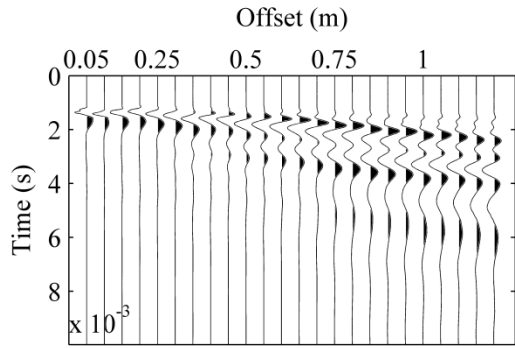
HB5-3
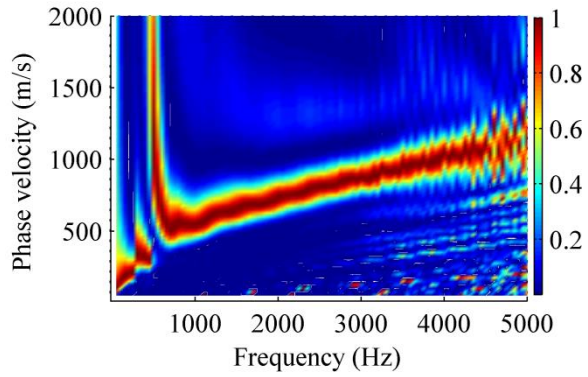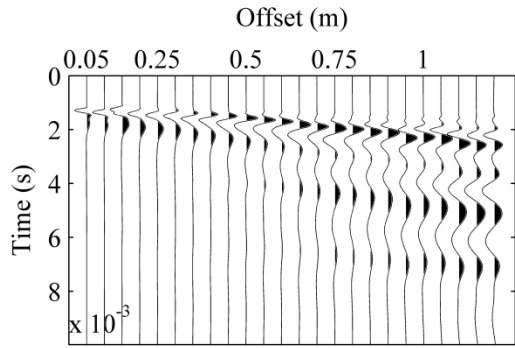
HB5-6

Figure A.3 (continued)

98
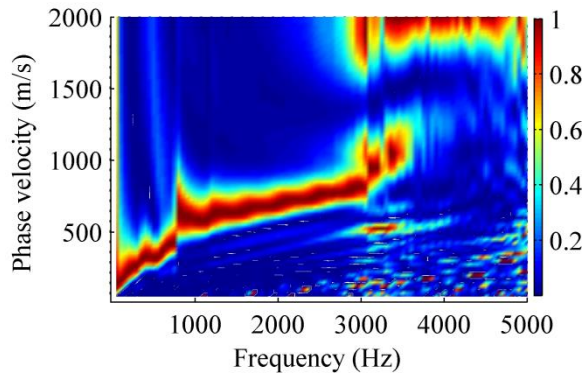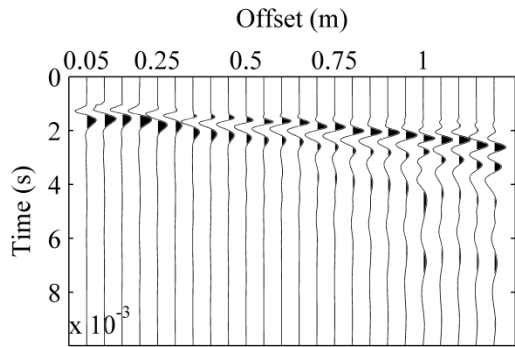
HB5-7
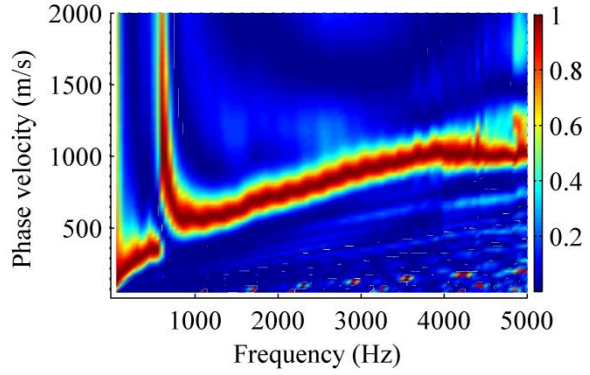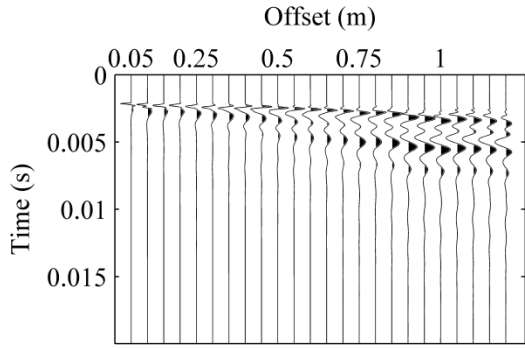
HB6-3
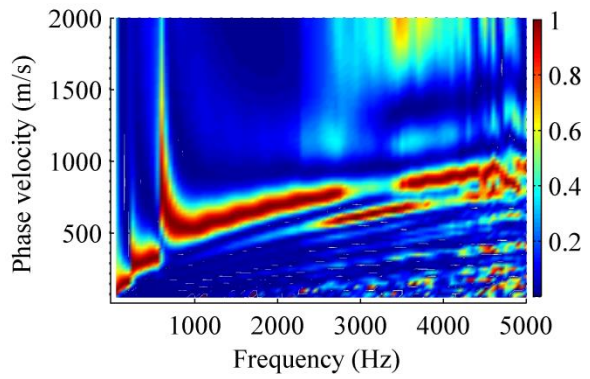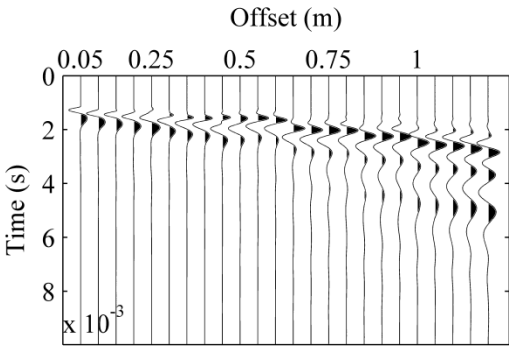
HB6-4
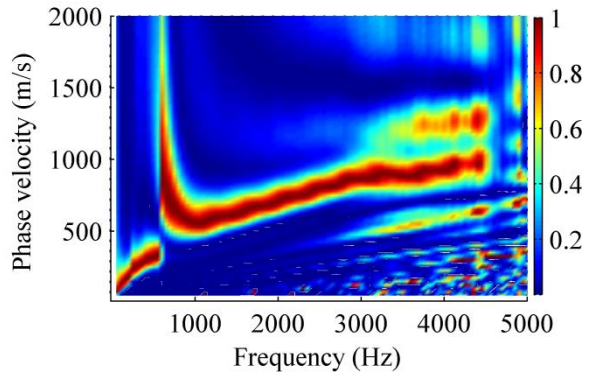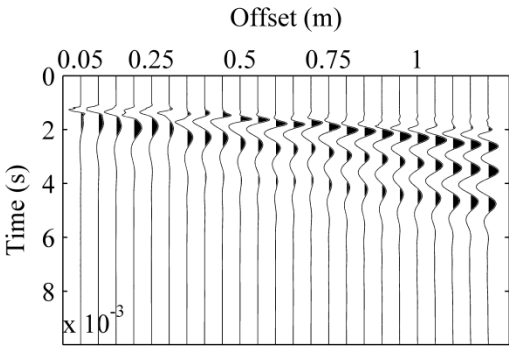
HB6-5
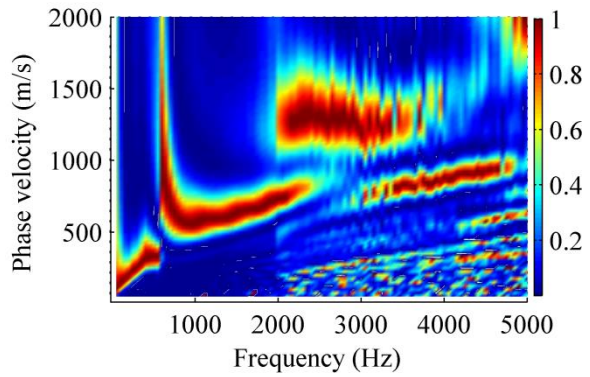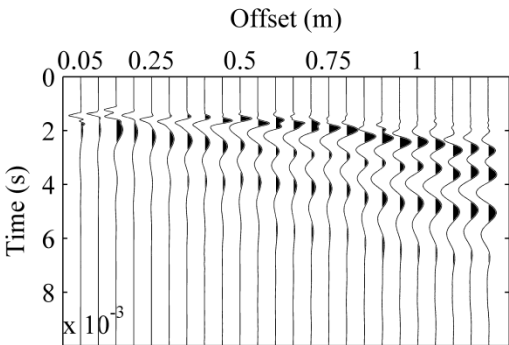
Figure A.3 (continued)

HB6-7
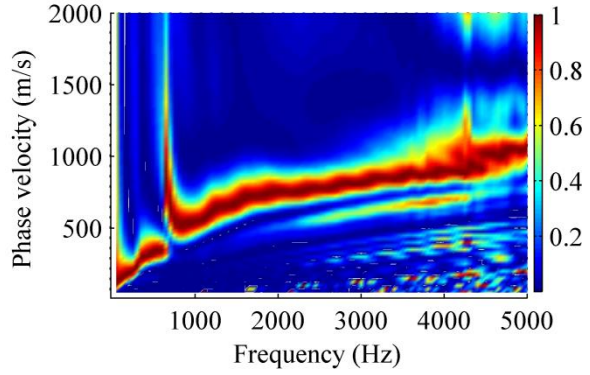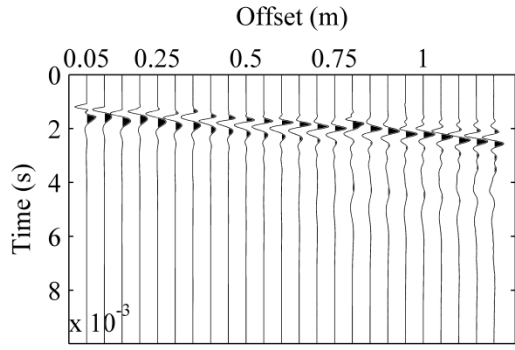
HB7-2
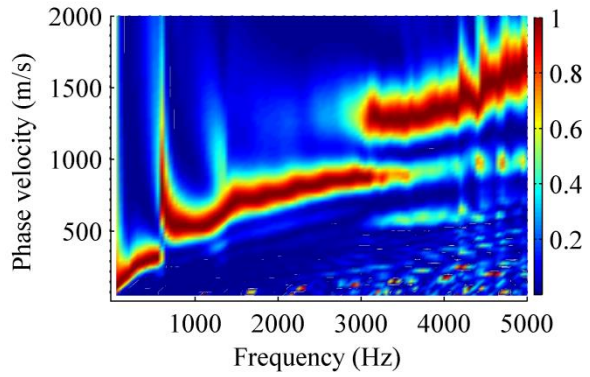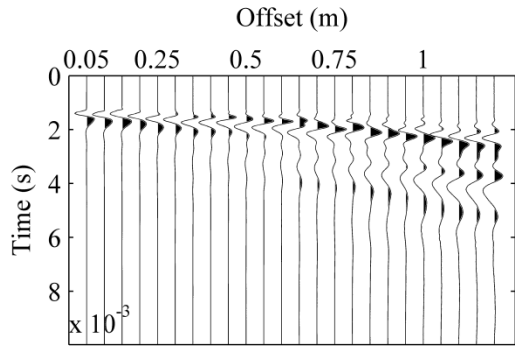
HB7-4
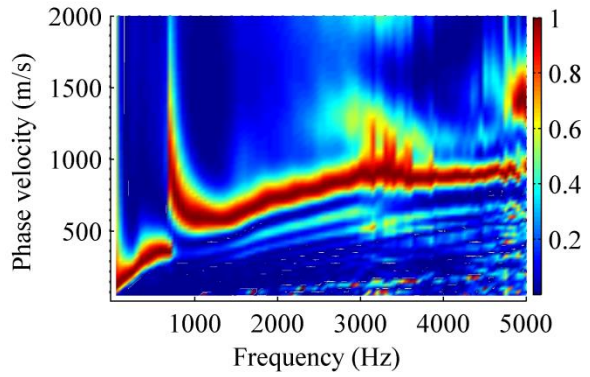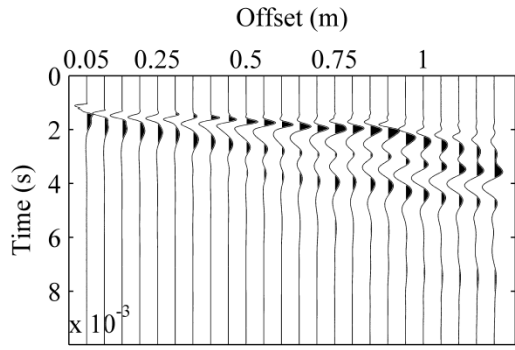
HB7-7
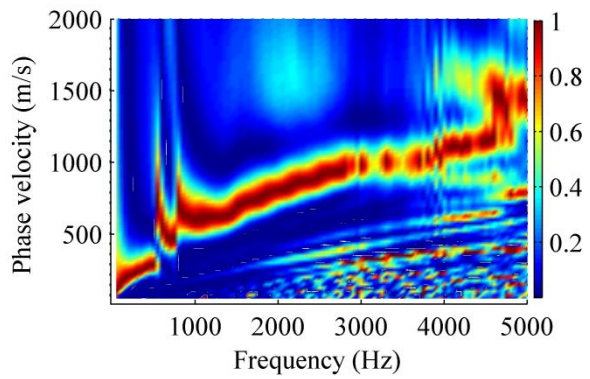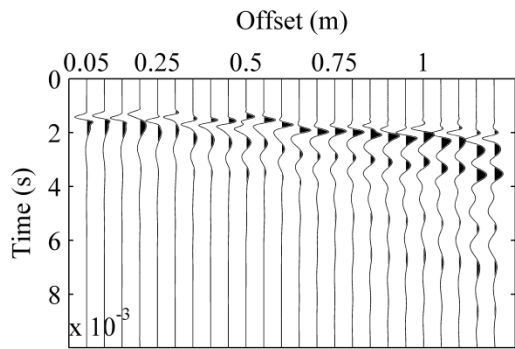
Figure A.3 (continued)

WB3-2
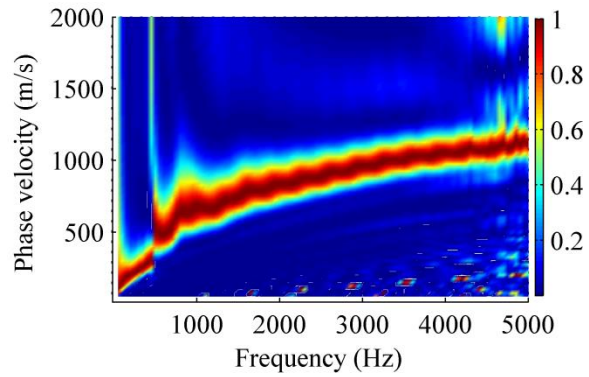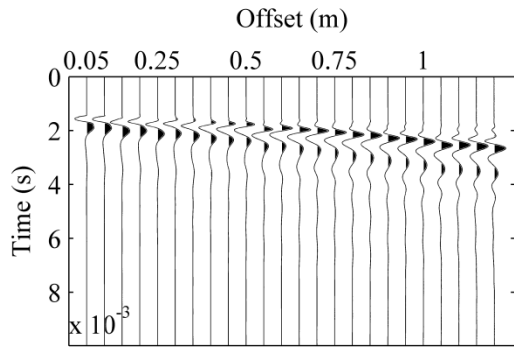
WB3-4
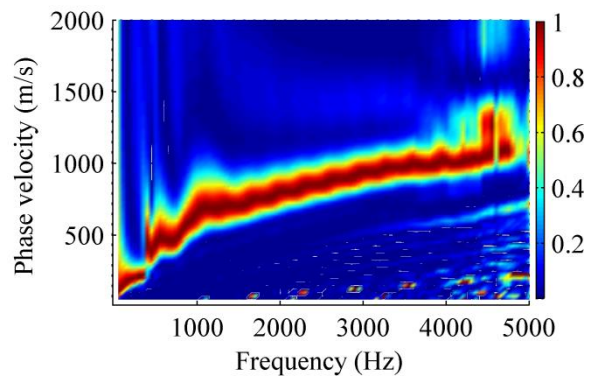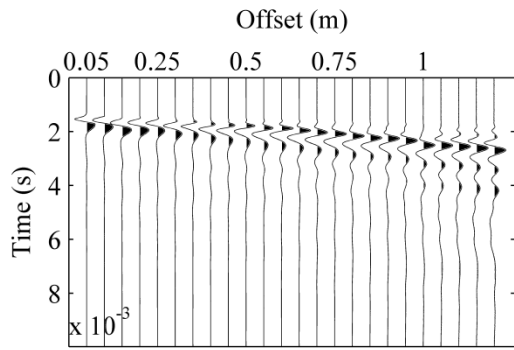
WB3-5
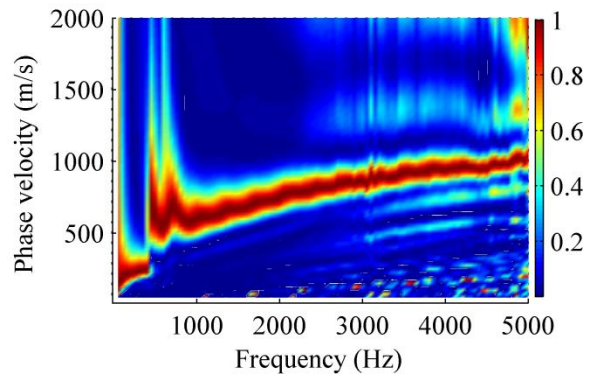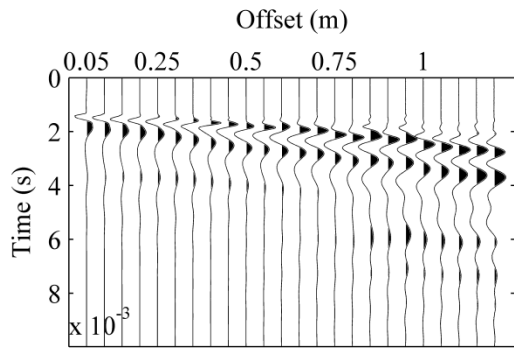
Figure A.4. Results of surface wave tests on ambient-temperature Boone WMA base courses one day after paving. Left column: normalized time-domain signals, right column: frequency-domain dispersion images

WB3-7
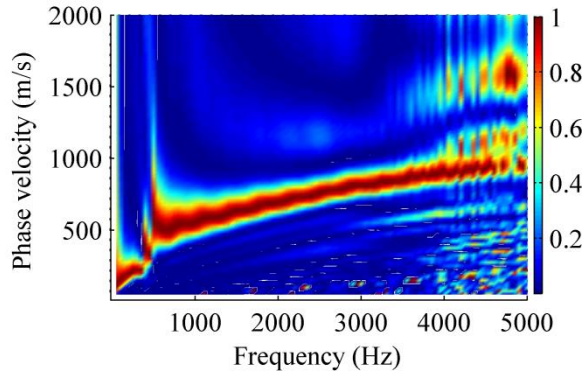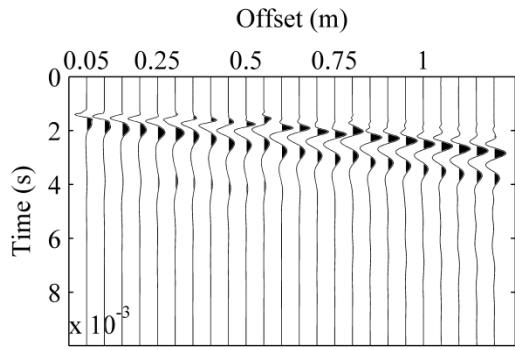
WB4-1
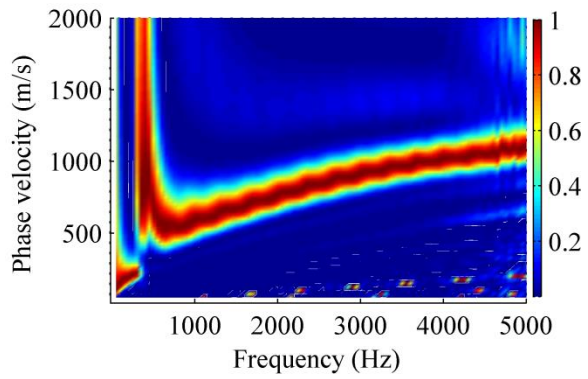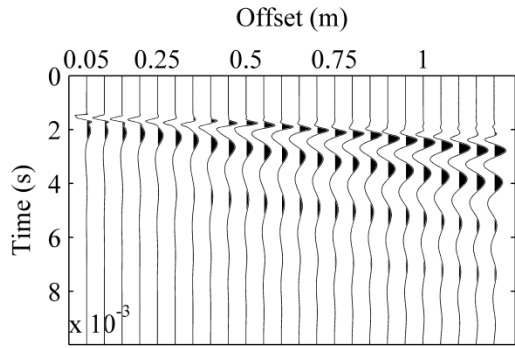
WB4-2
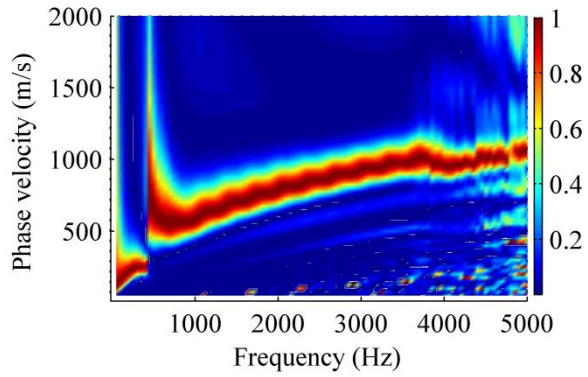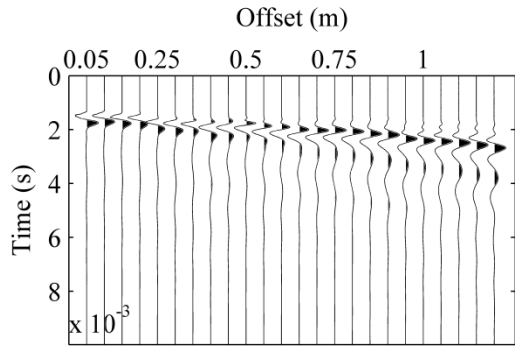
WB4-3
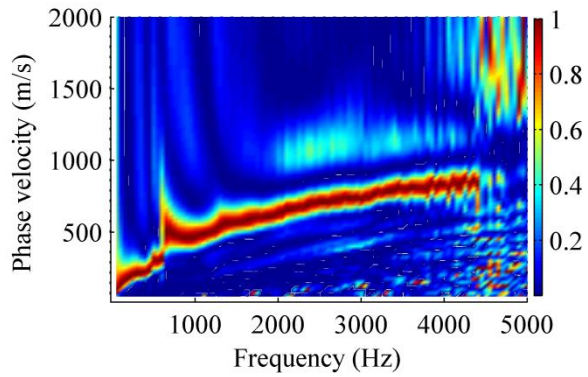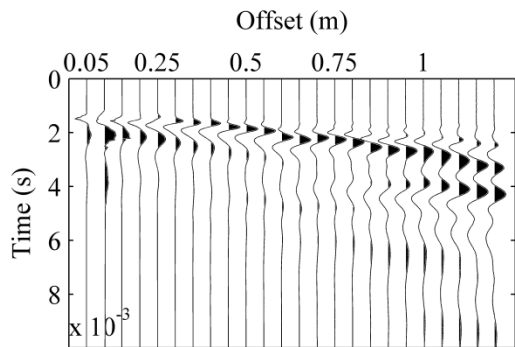
Figure A.4 (continued)

WB4-7
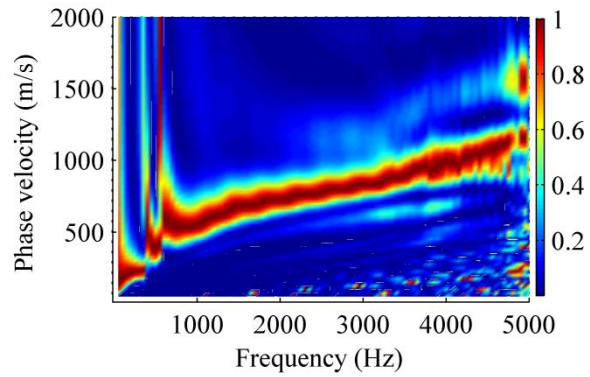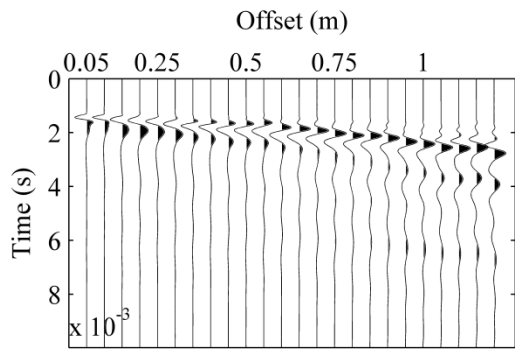
WB8-4
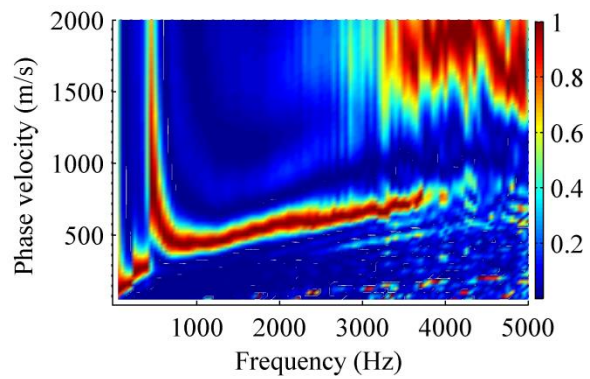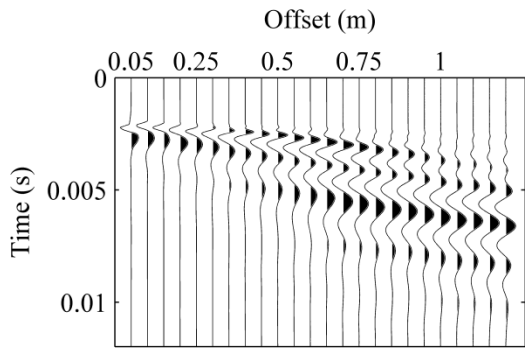
WB8-5
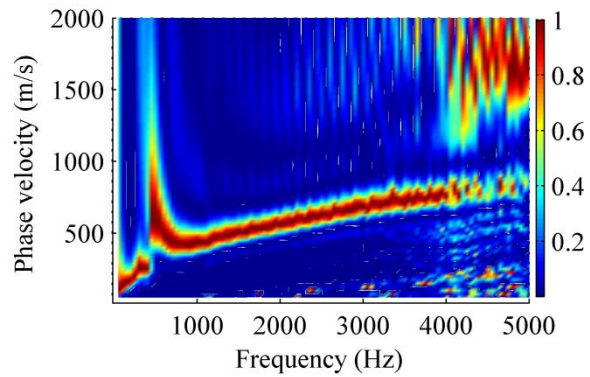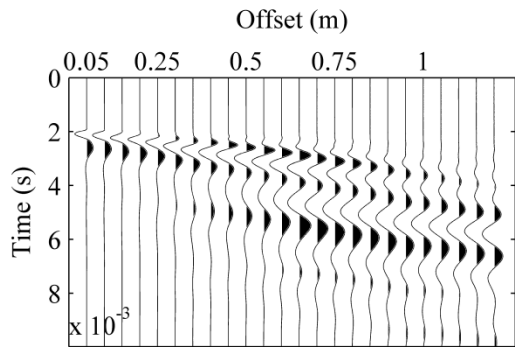
WB8-7

Figure A.4 (continued)

103
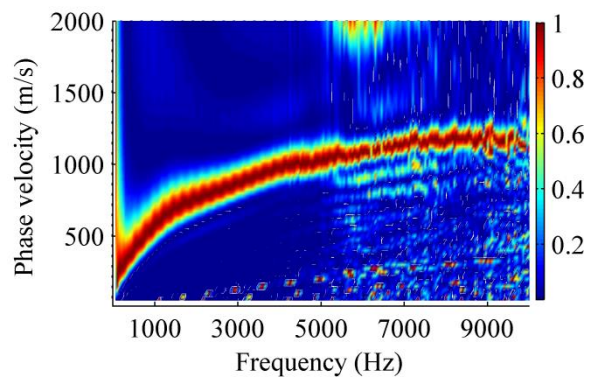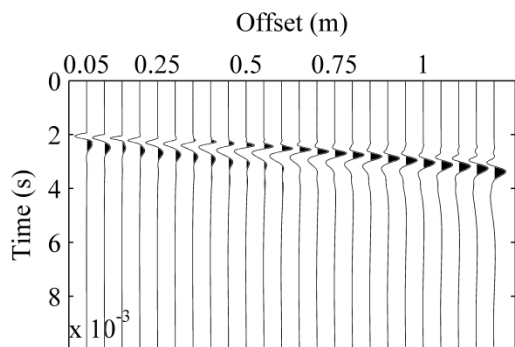
WB8-8
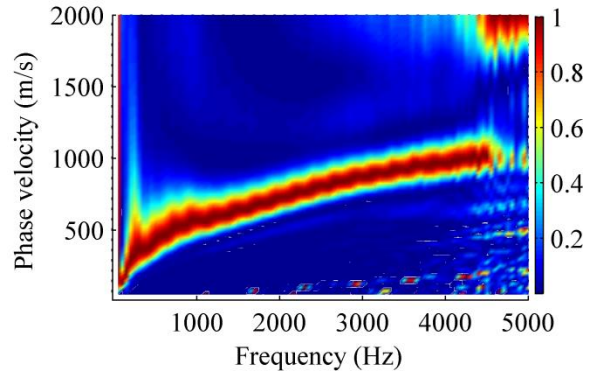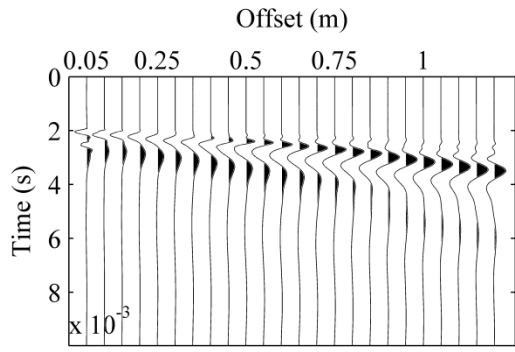
WB9-2
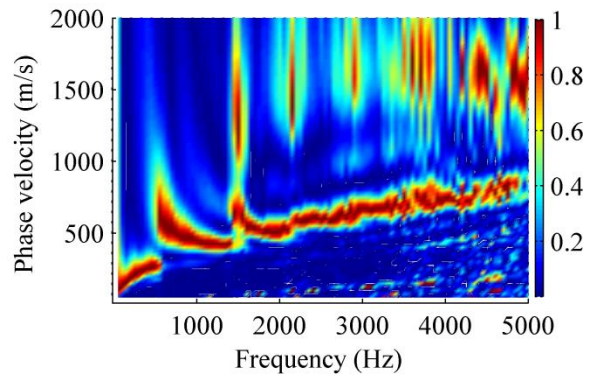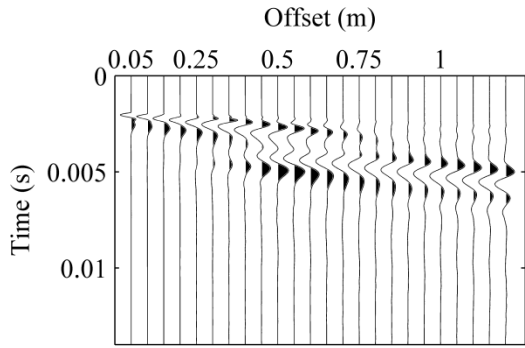
WB9-3
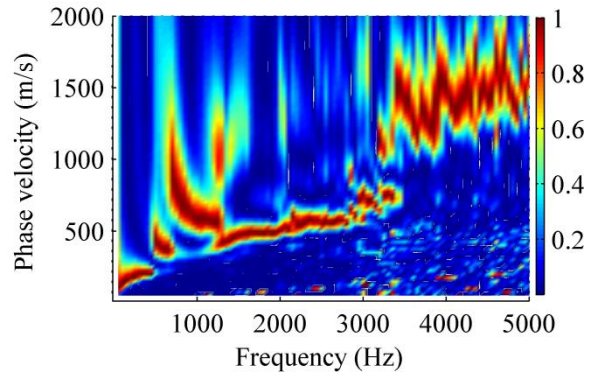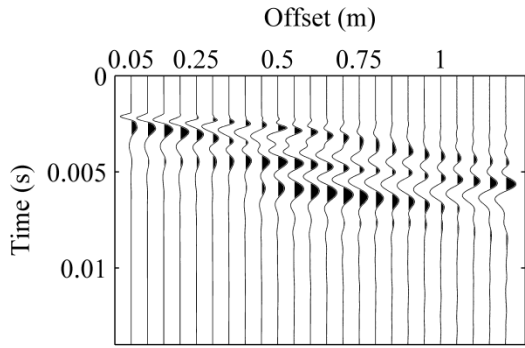
WB9-6
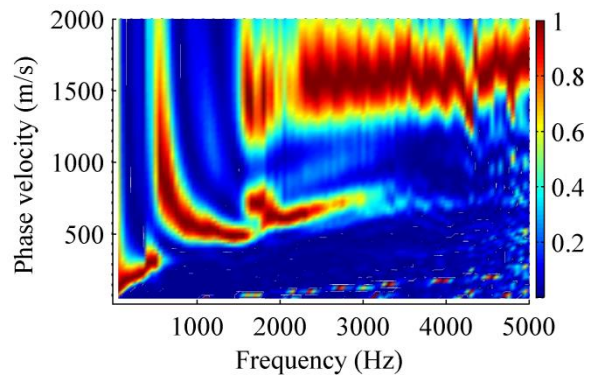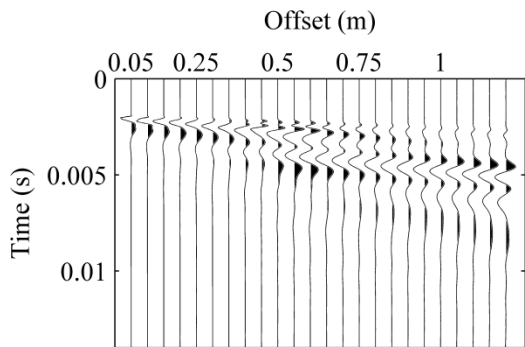
Figure A.4 (continued)

WB9-7
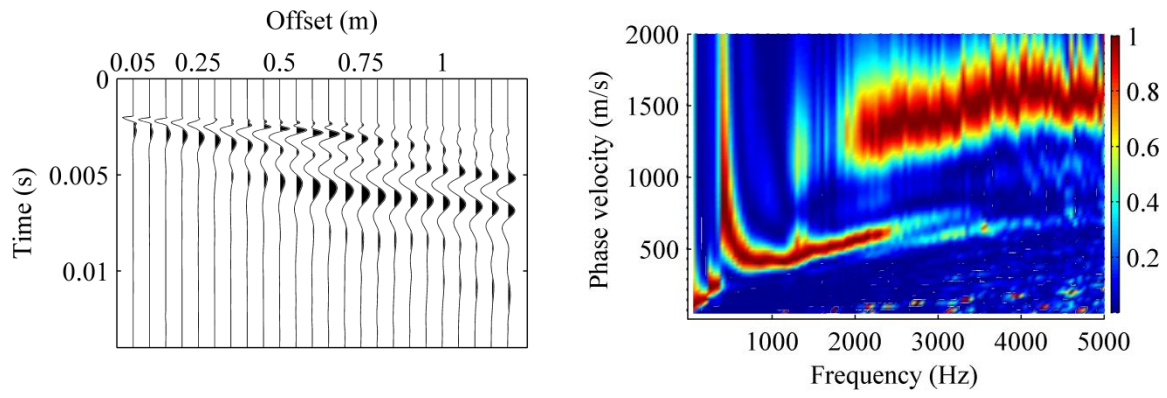
Figure A.4 (continued)

HS1-1
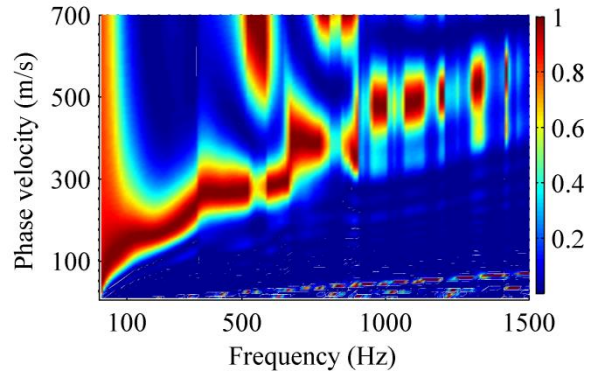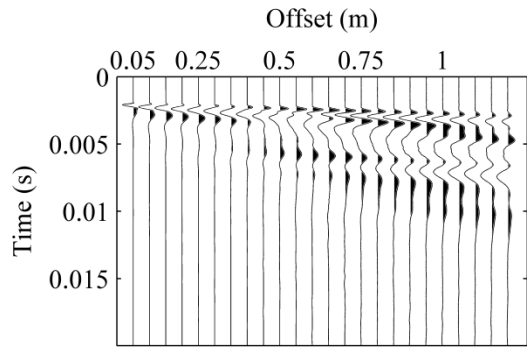
HS1-2
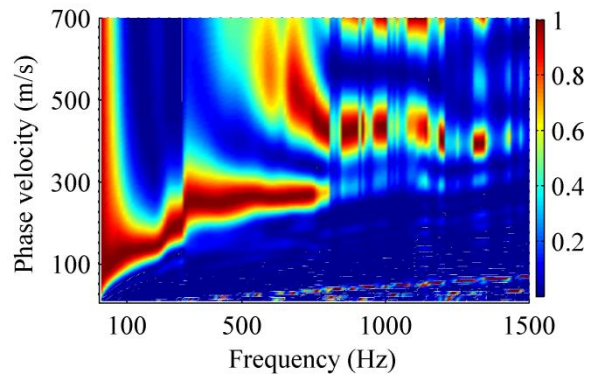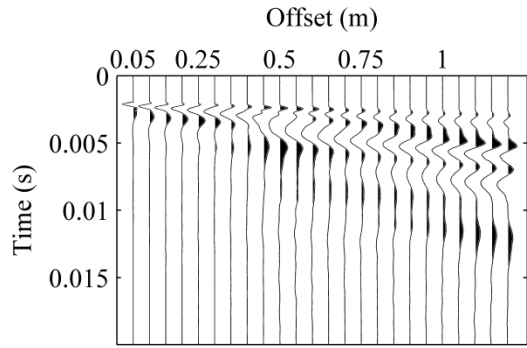
HS1-3
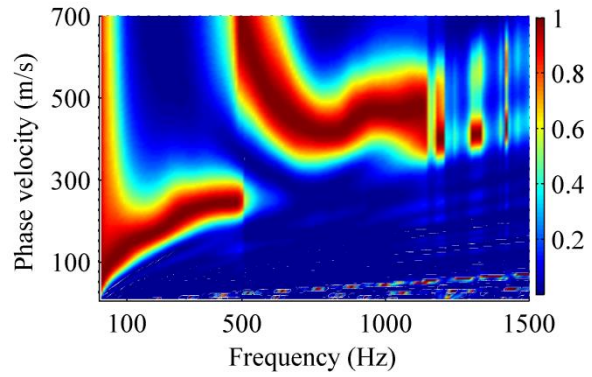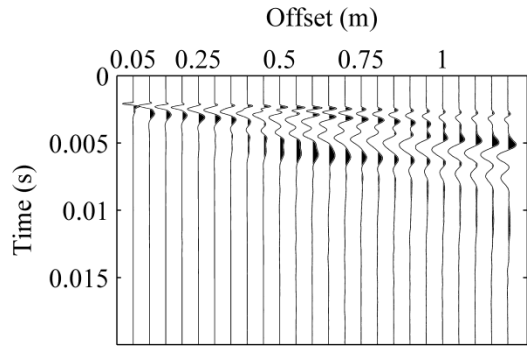
Figure A.5. Results of surface wave tests on hot Boone HMA surface courses several hours after paving. Left column: normalized time-domain signals, right column: frequency-domain dispersion images

HS1-4
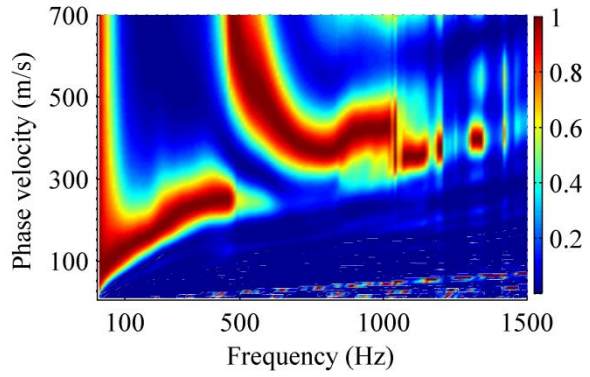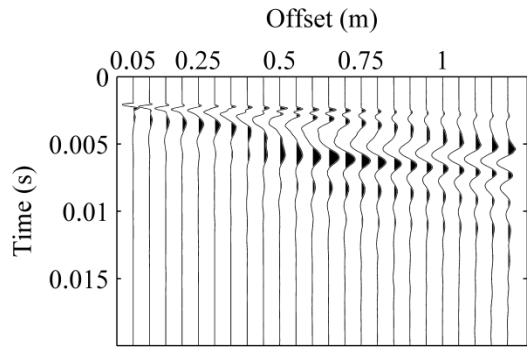
HS2-1
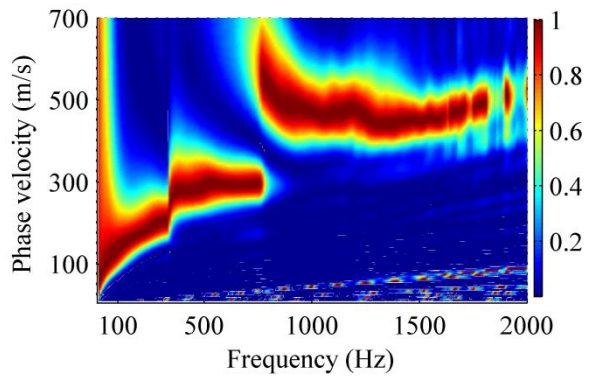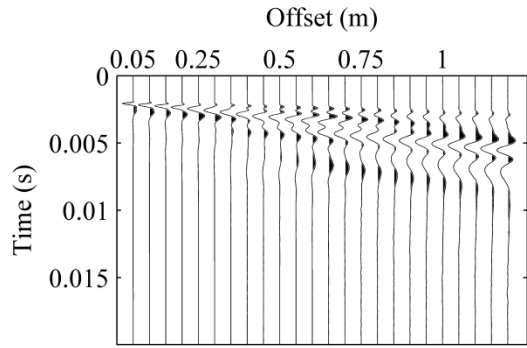
HS2-2
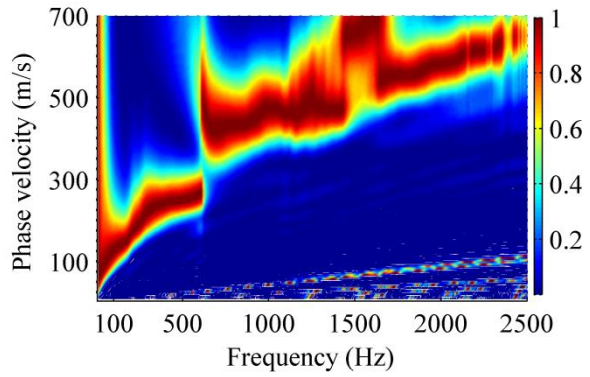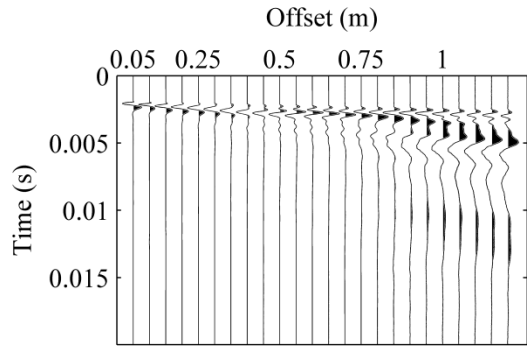
HS2-3
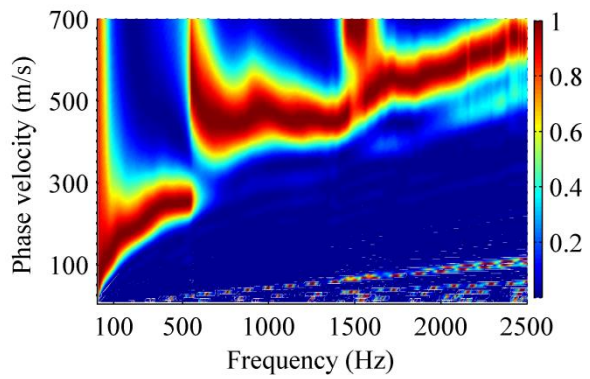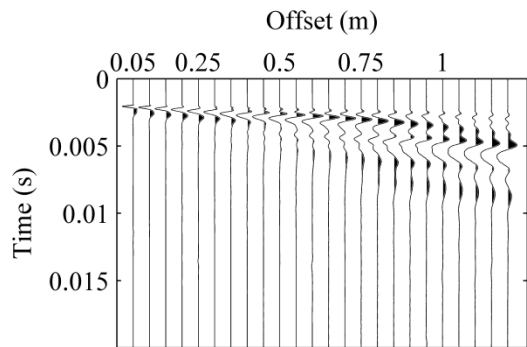
Figure A.5 (continued)

WS3-1
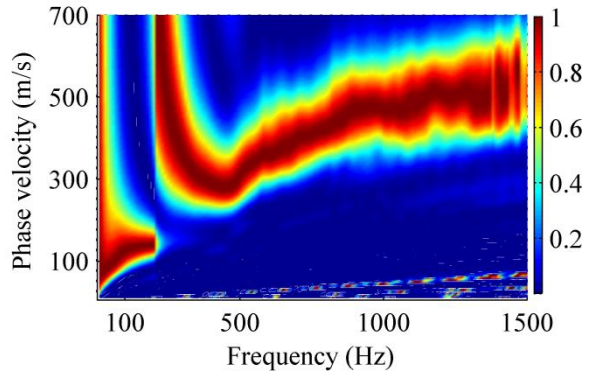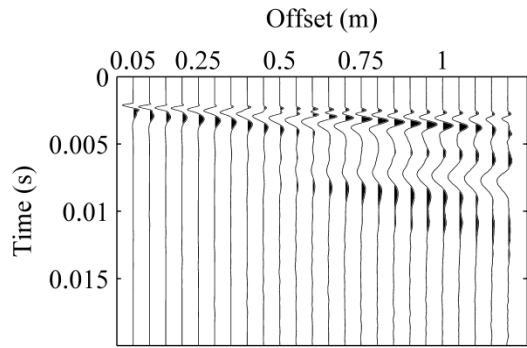
WS3-2
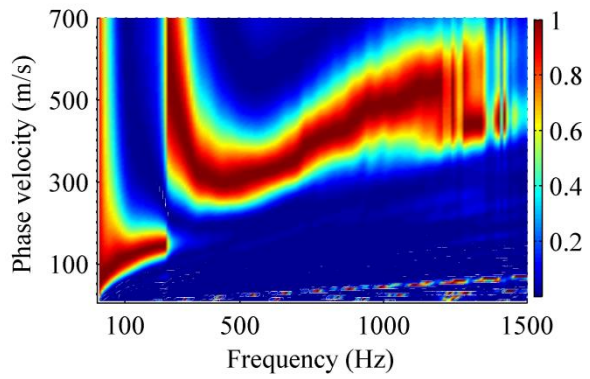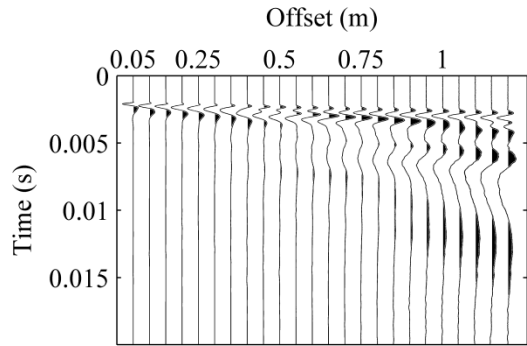
WS3-3
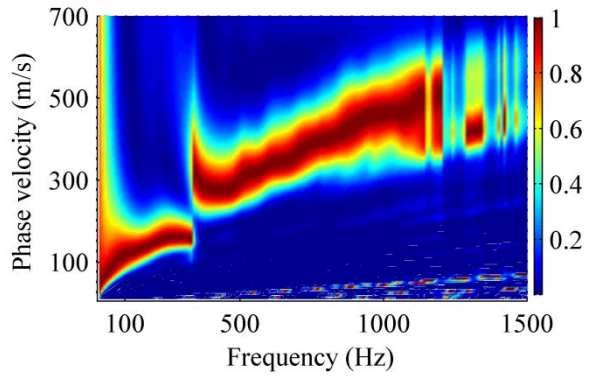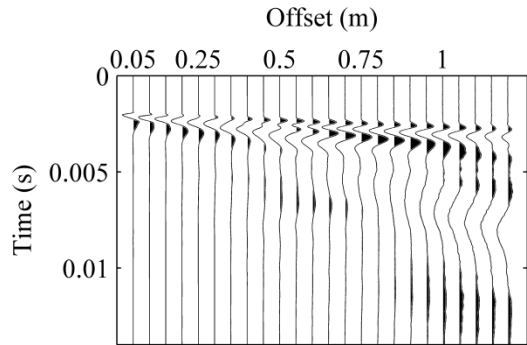
Figure A.6. Results of surface wave tests on hot Boone WMA surface courses several hours after paving. Left column: normalized time-domain signals, right column: frequency-domain dispersion images

108

WS3-4
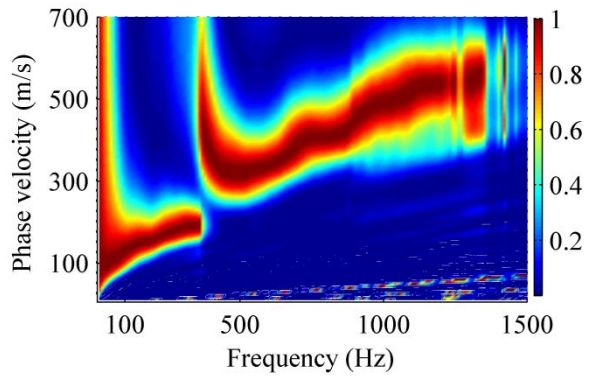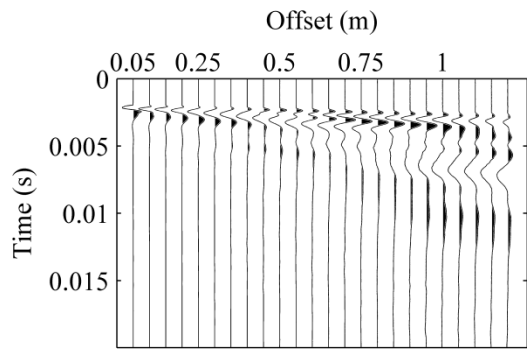
WS4-1

WS4-2

WS4-3

Figure A.6 (continued)

WS4-4
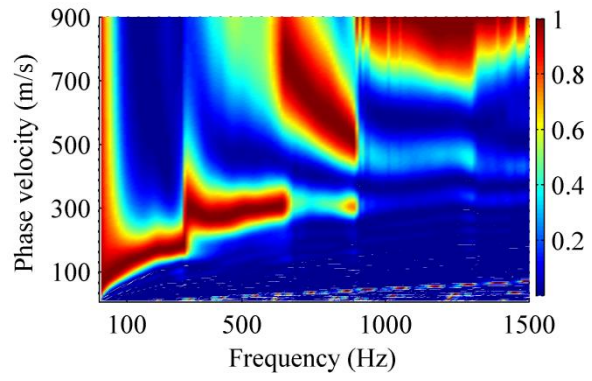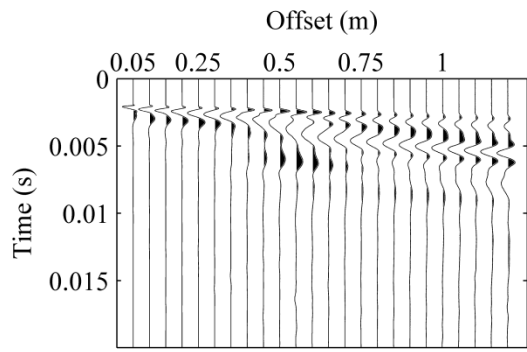
WS4-5
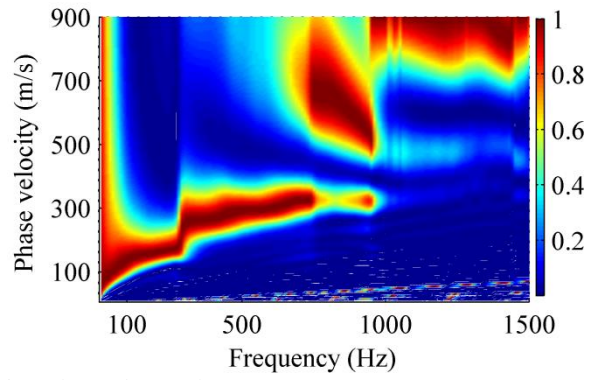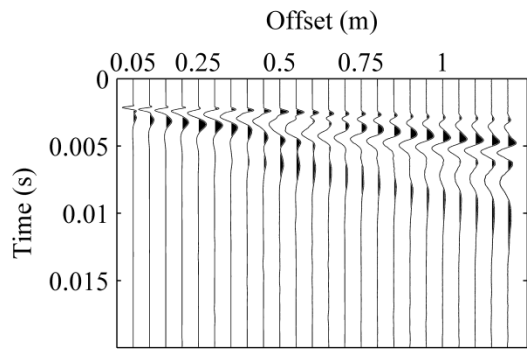
Figure A.6 (continued)

HS1-1
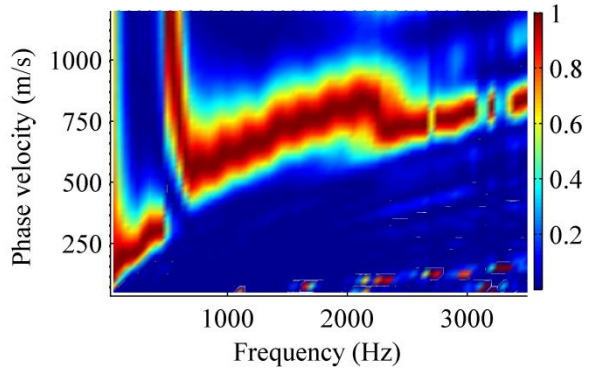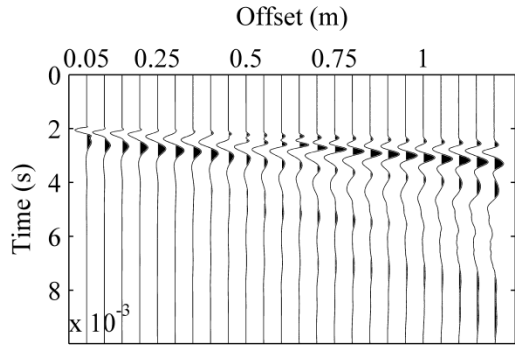
HS1-2
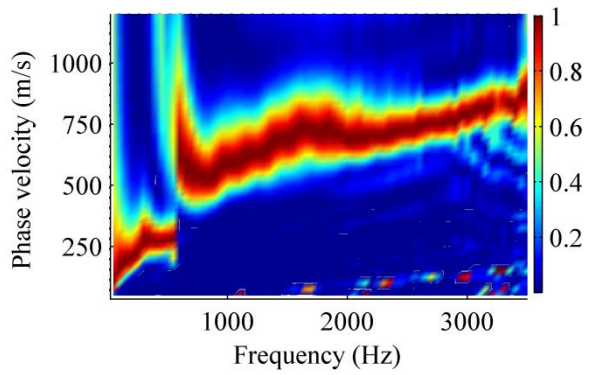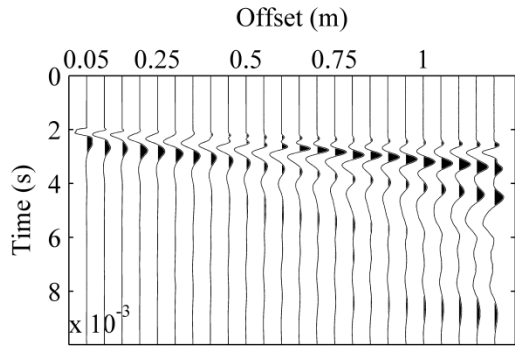
HS1-3
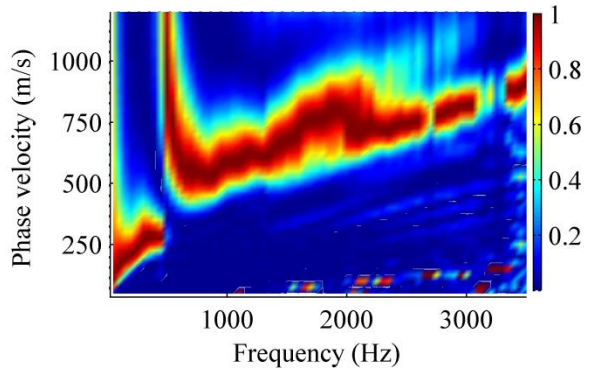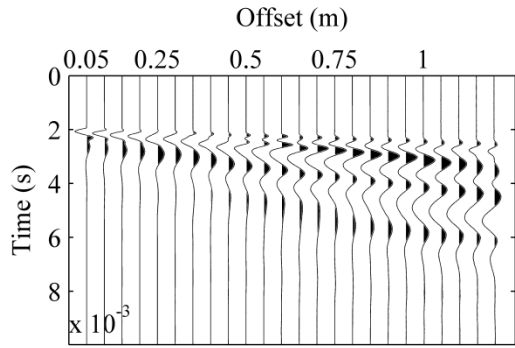
Figure A.7. Results of surface wave tests on ambient-temperature Boone HMA surface courses one day after paving. Left column: normalized time-domain signals, right column: frequency-domain dispersion images

111

HS1-4
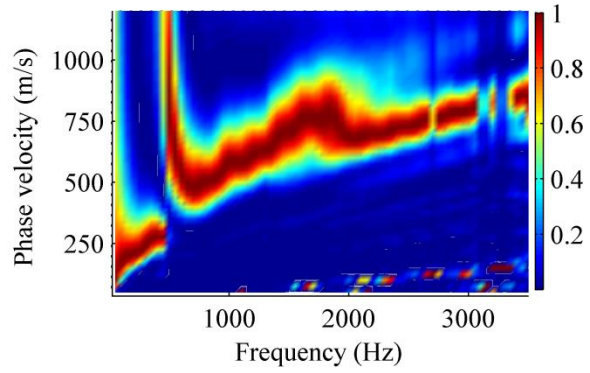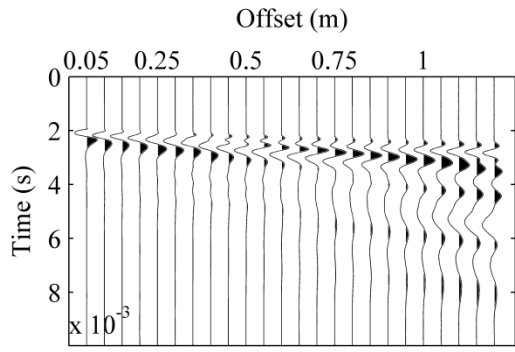
HS2-1

HS2-2

HS2-3

Figure A.7 (continued).

WS3-1
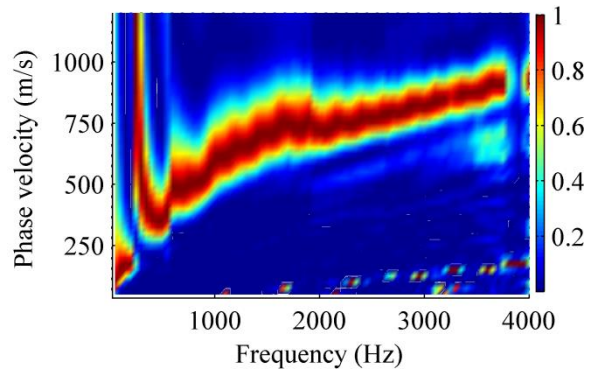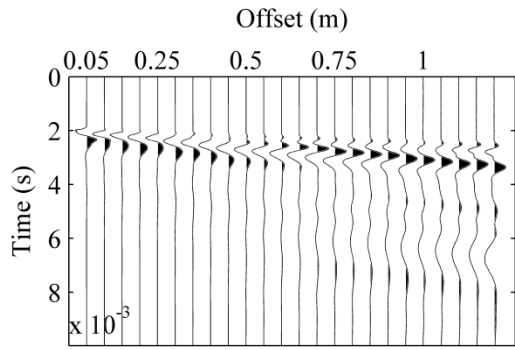
WS3-2
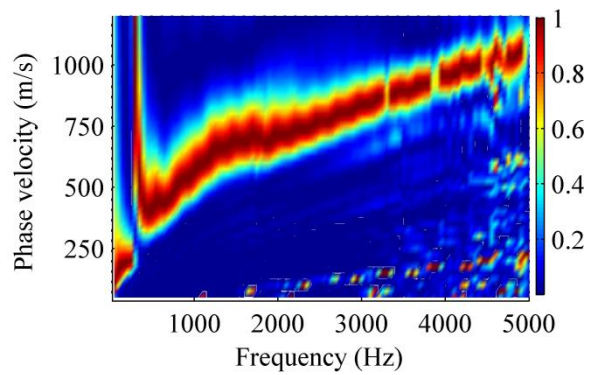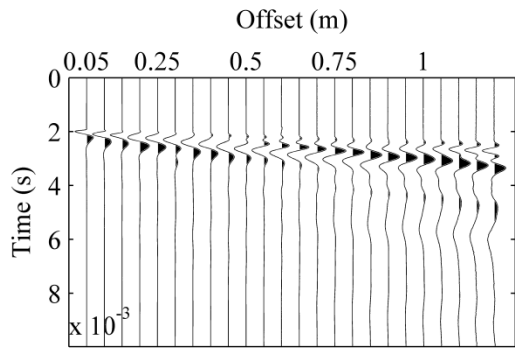
WS3-3
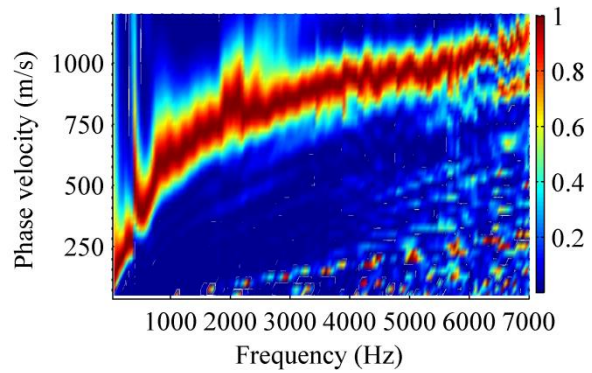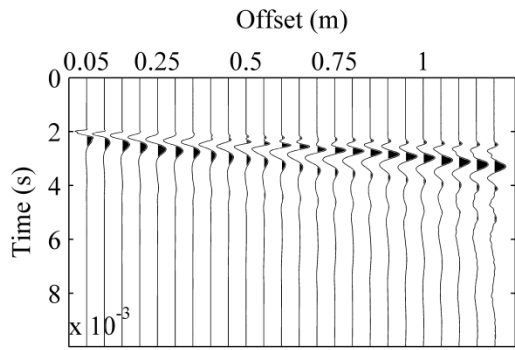
Figure A.8. Results of surface wave tests on ambient-temperature Boone WMA surface courses one day after paving. Left column: normalized time-domain signals, right column: frequency-domain dispersion images

WS3-4
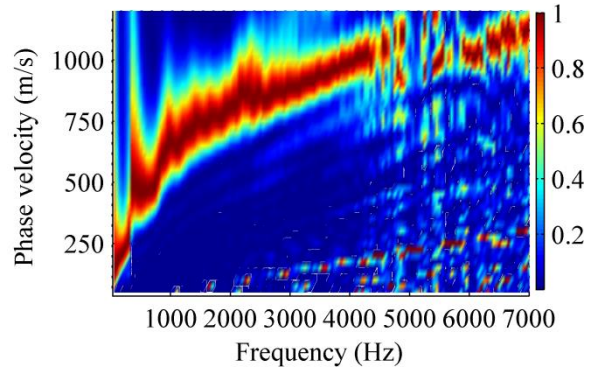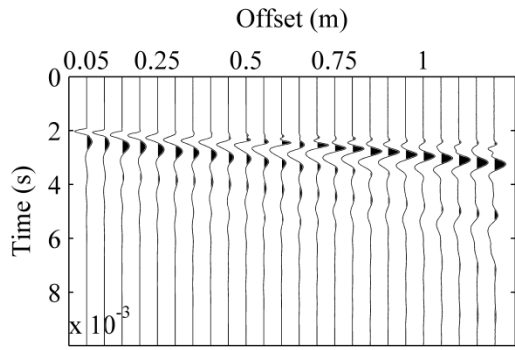
WS4-1
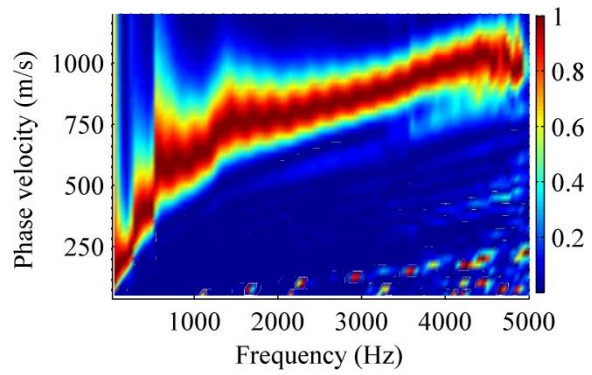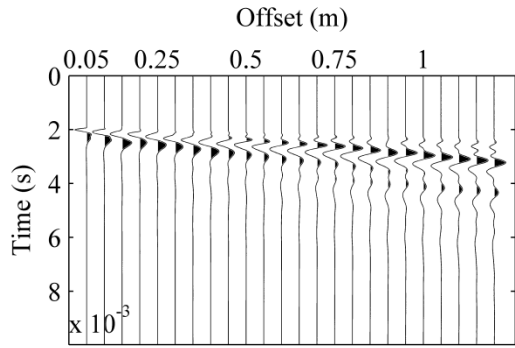
WS4-2
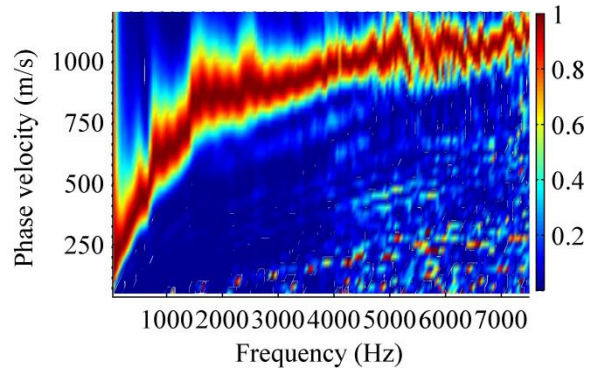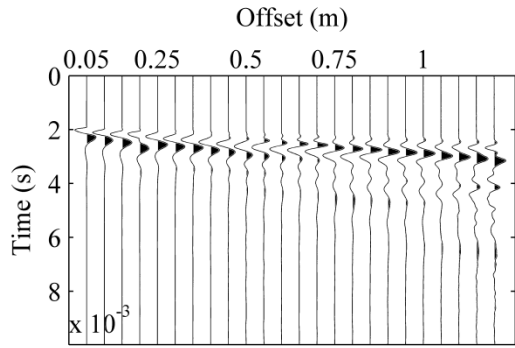
WS4-3
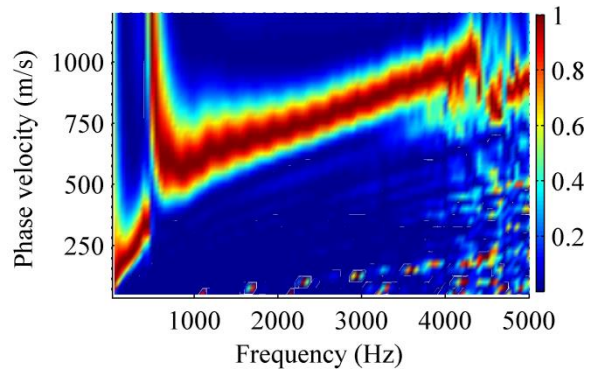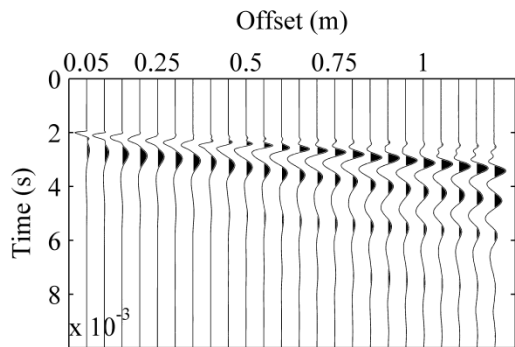
Figure A.8 (continued).

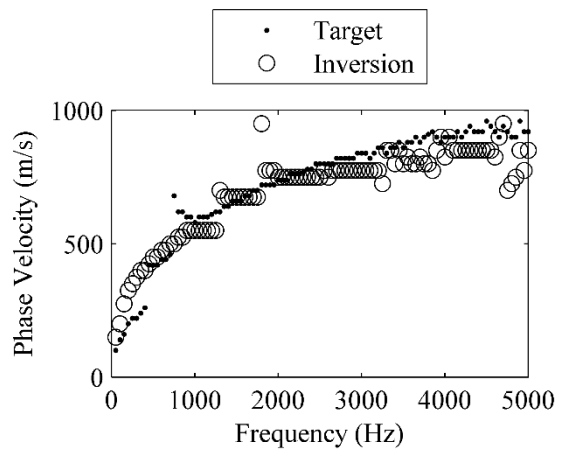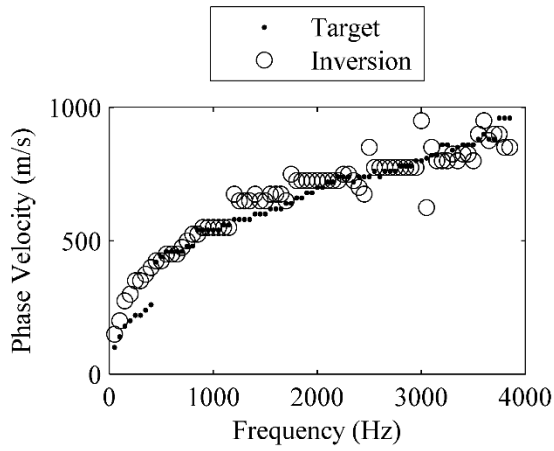WS4-4
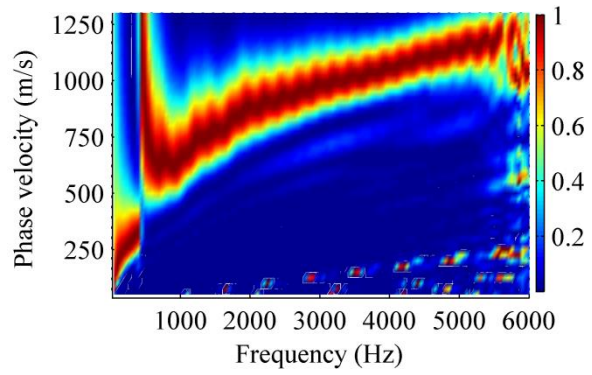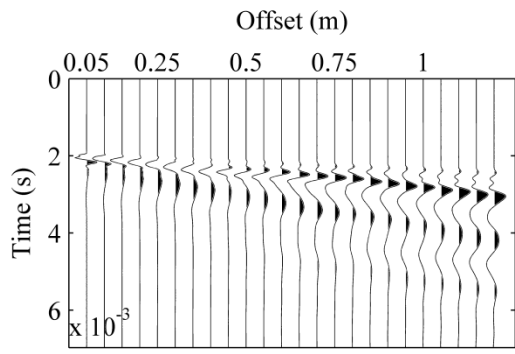
WS4-5
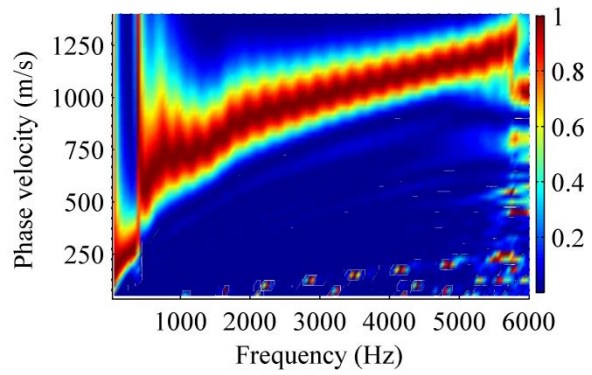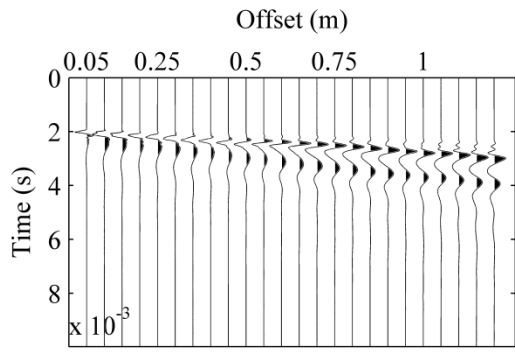
Figure A.8 (continued).

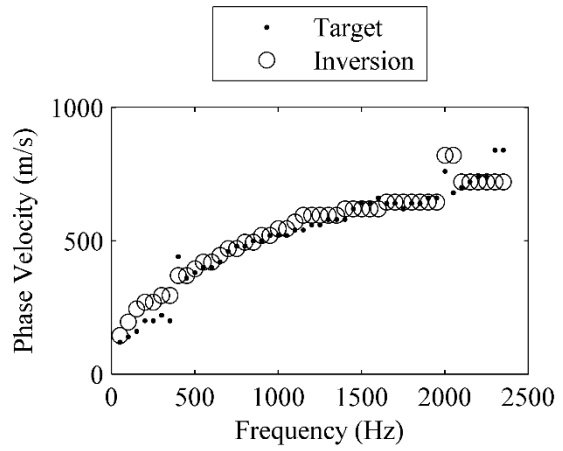HB1-1
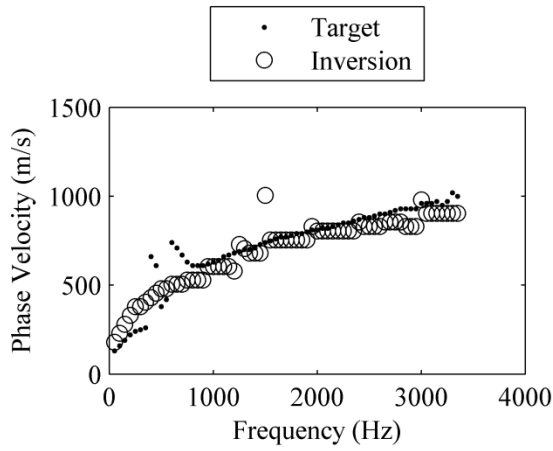
HB1-3
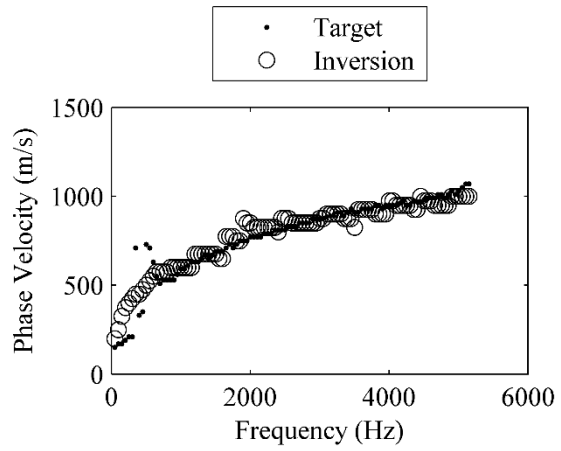
HB1-5
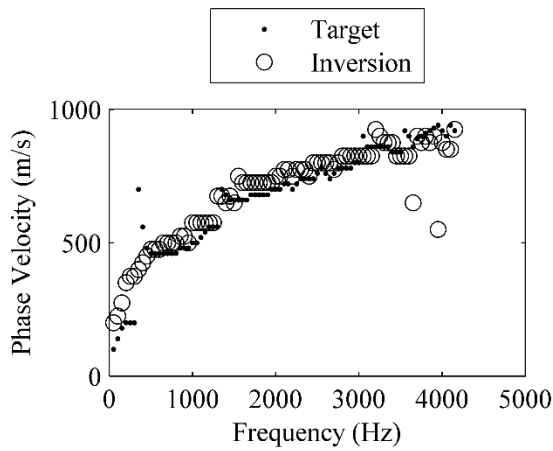
HB1-7
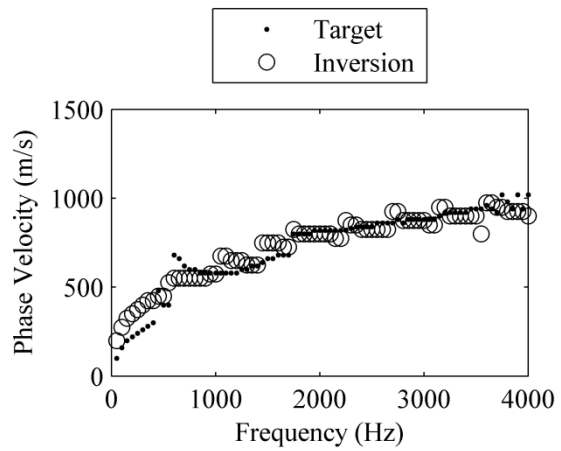
HB2-1
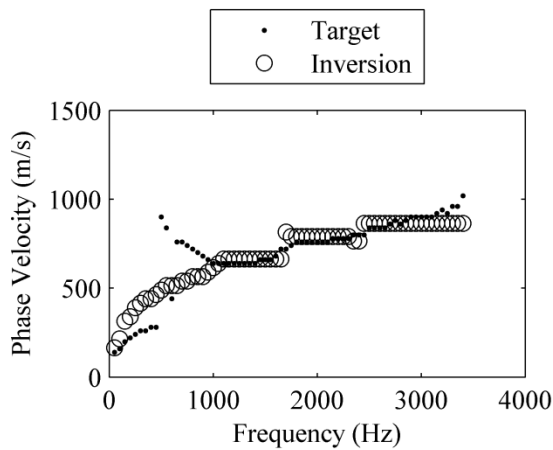
HB2-2

Figure A.9. Picked experimental dispersion curves (targets), and theoretical dispersion curves from inversion for ambient-temperature Boone HMA base courses one day after paving.
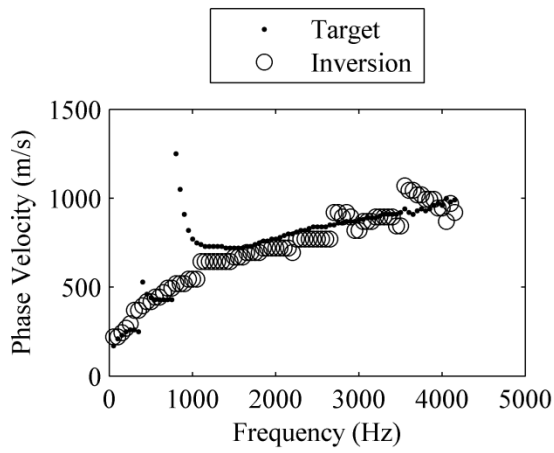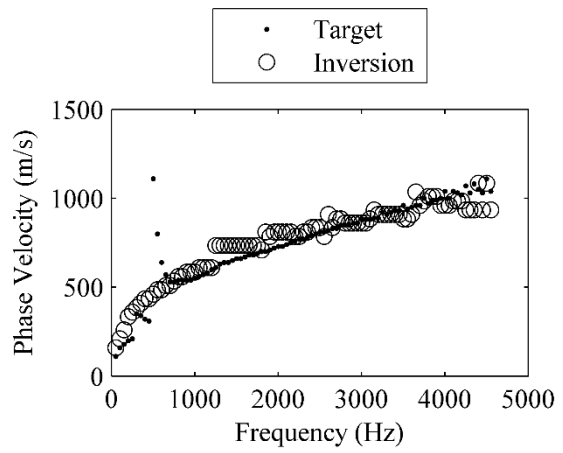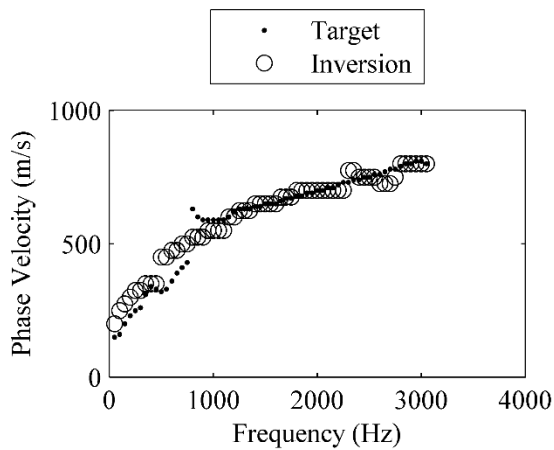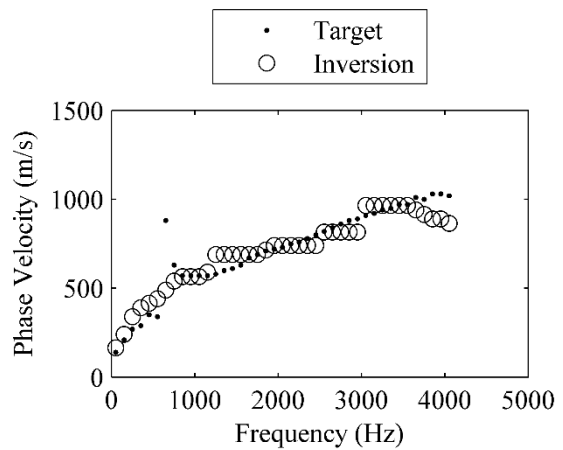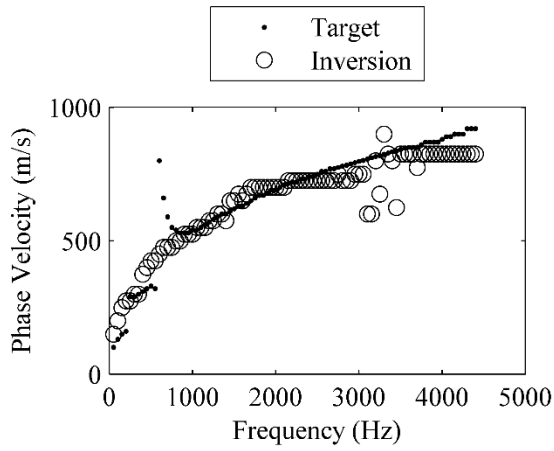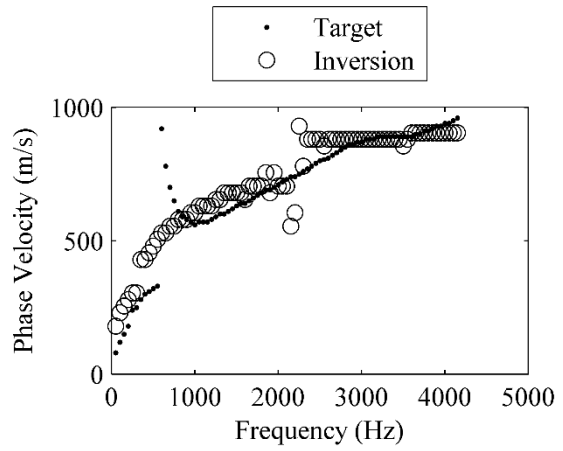
HB2-5

HB2-7

HB5-1

HB5-3

HB5-6
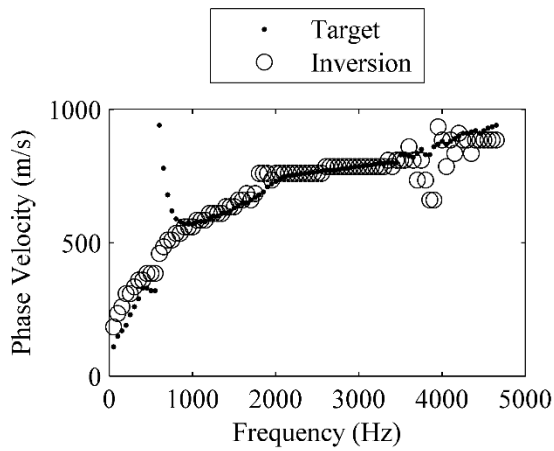

HB5-7

Figure A.9 (continued)

117

HB6-3

HB6-4

HB6-5

HB6-7
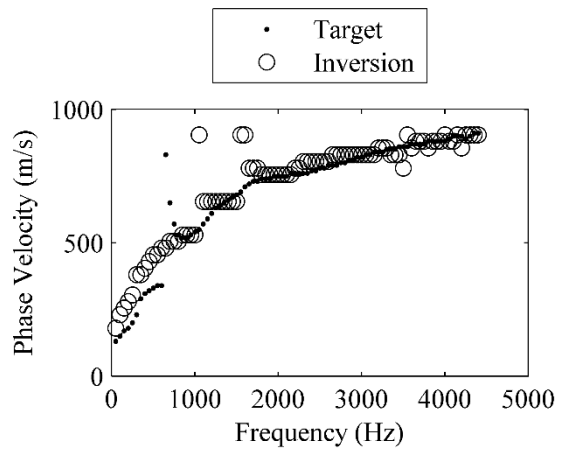
HB7-2
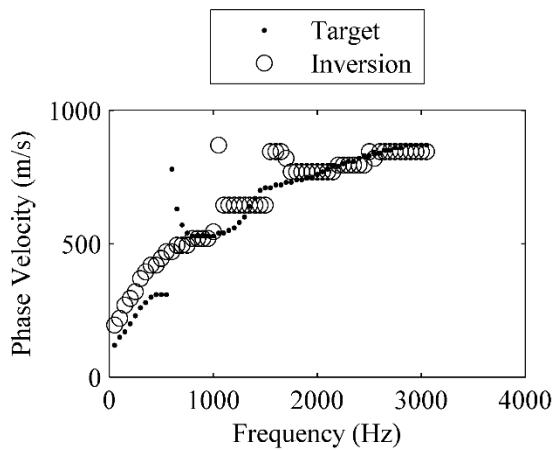
HB7-4
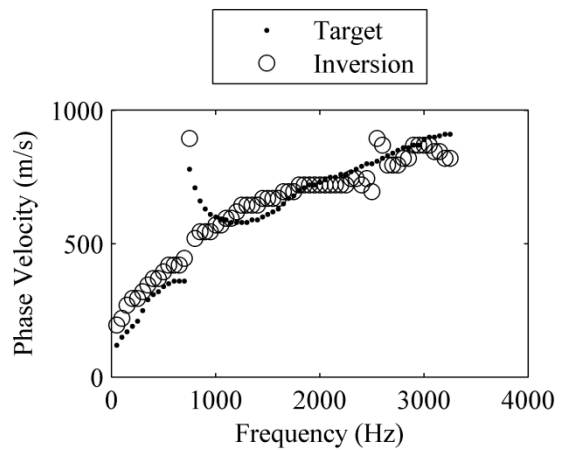
Figure A.9 (continued)

HB7-7

Figure A.9 (continued)

WB3-2
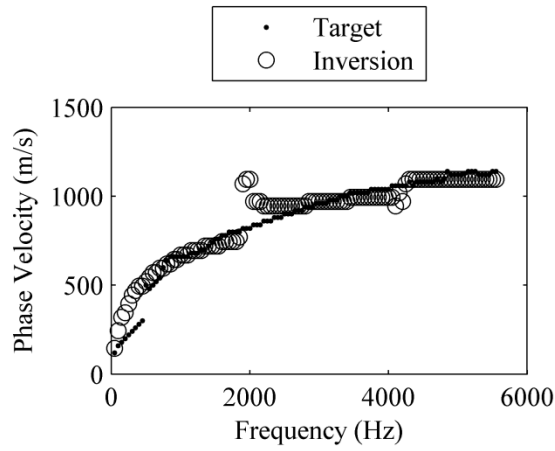
WB3-4
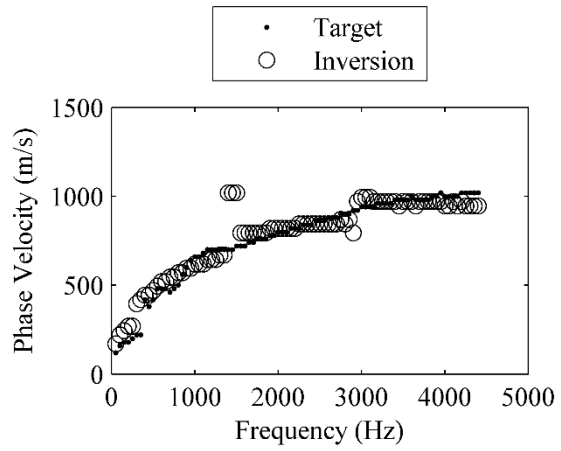
WB3-5
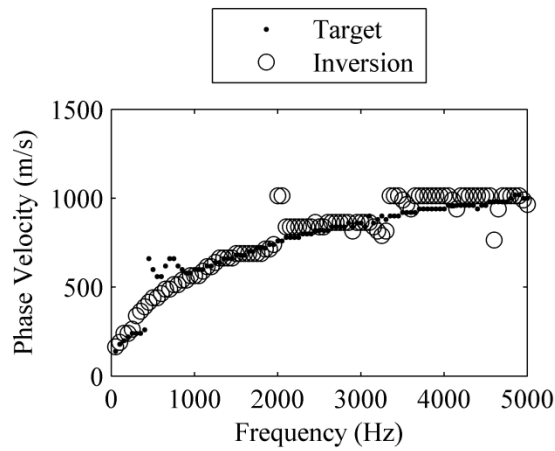
WB3-7
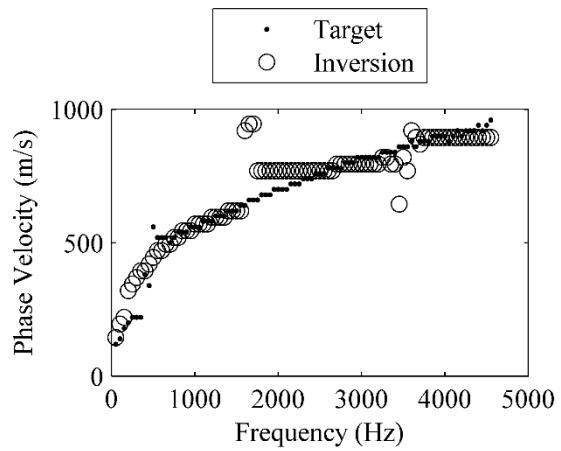
WB4-1
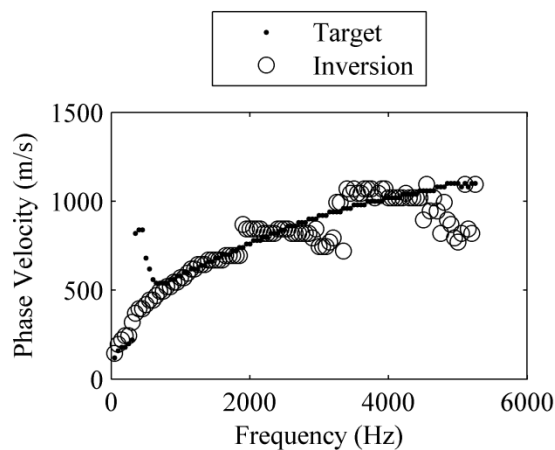
WB4-2
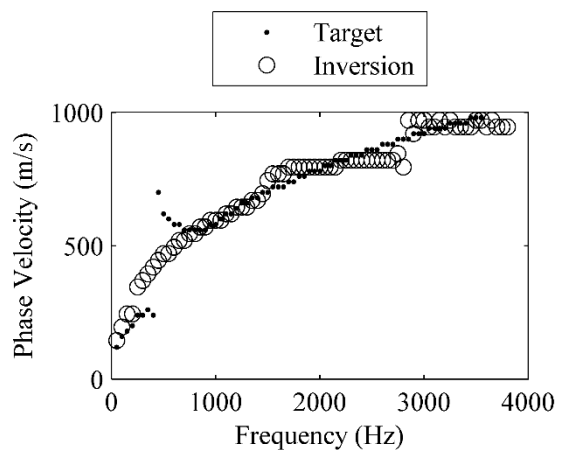
Figure A.10. Picked experimental dispersion curves (targets), and theoretical dispersion curves from inversion for ambient-temperature Boone WMA base courses one day after paving

120

WB4-3
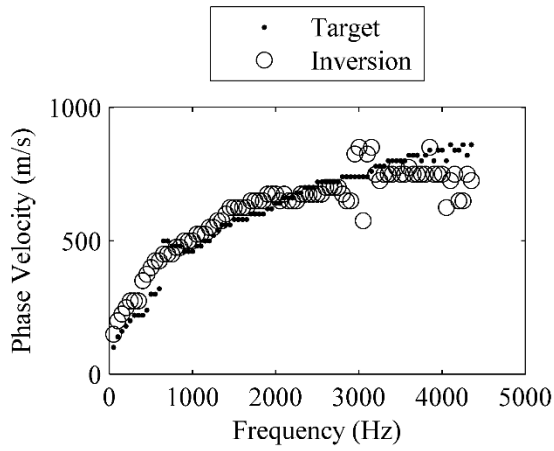
WB4-7
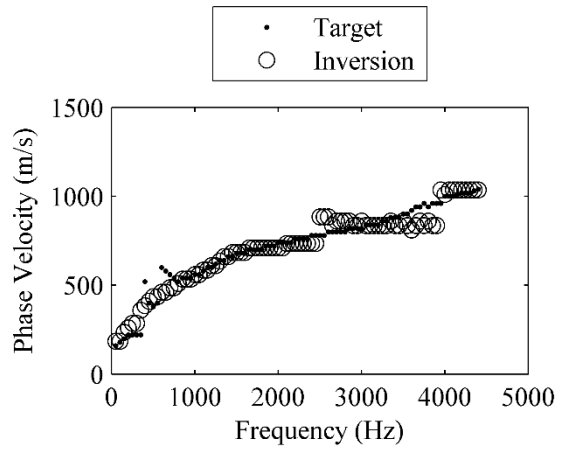
WB8-4
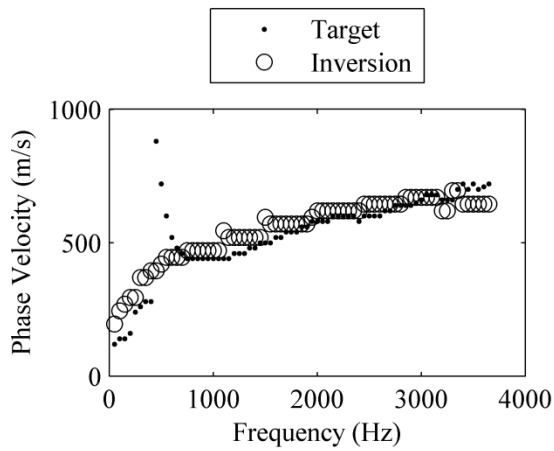
WB8-5
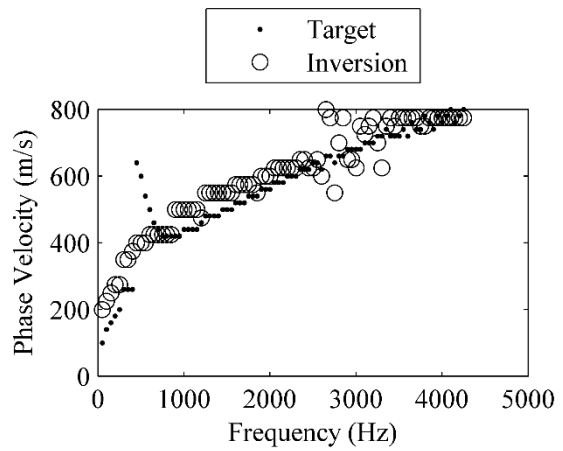
WB8-7
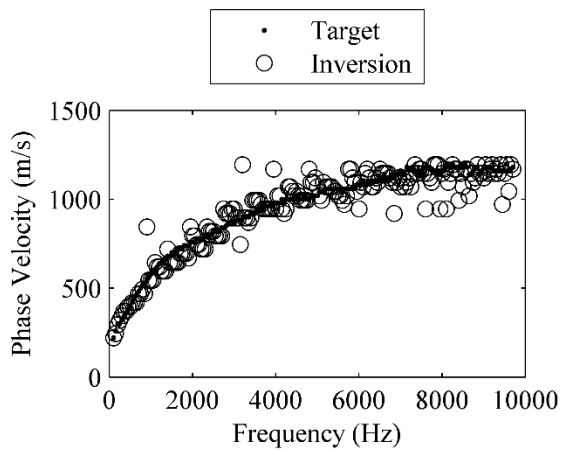
WB8-8
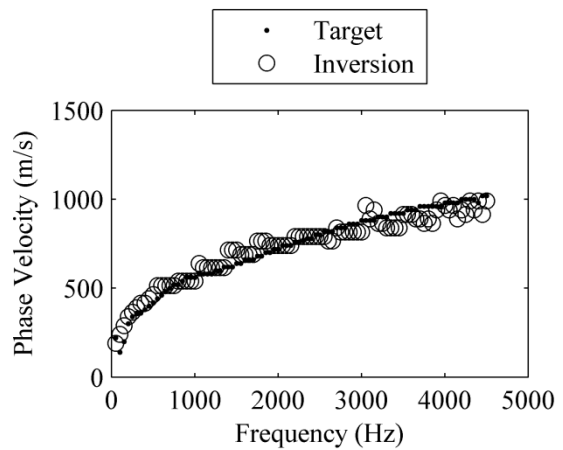
Figure A.10 (continued)

WB9-2
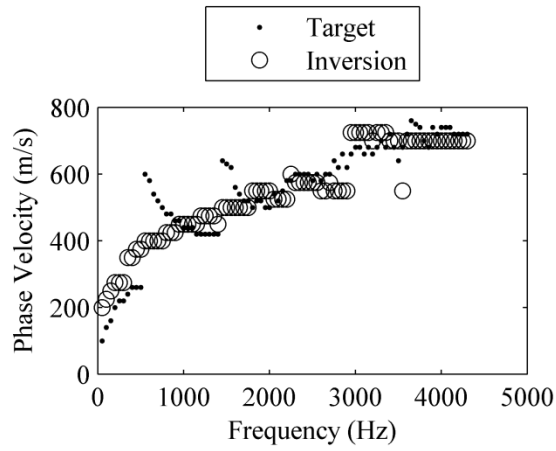
WB9-3
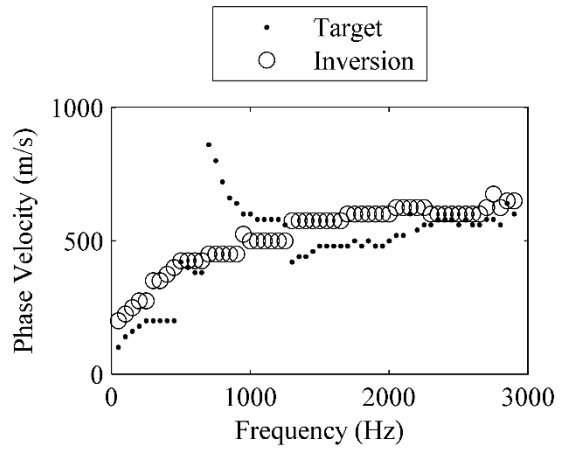
WB9-6
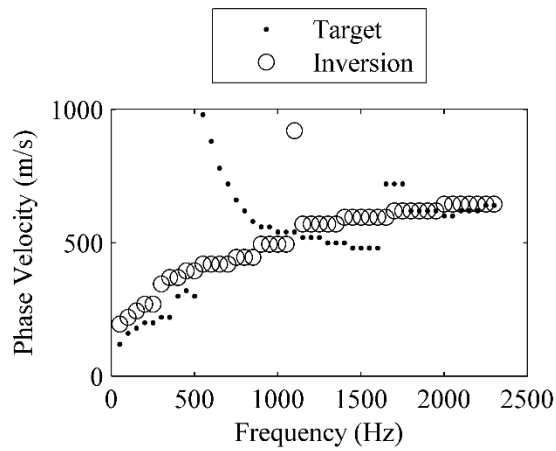
WB9-7
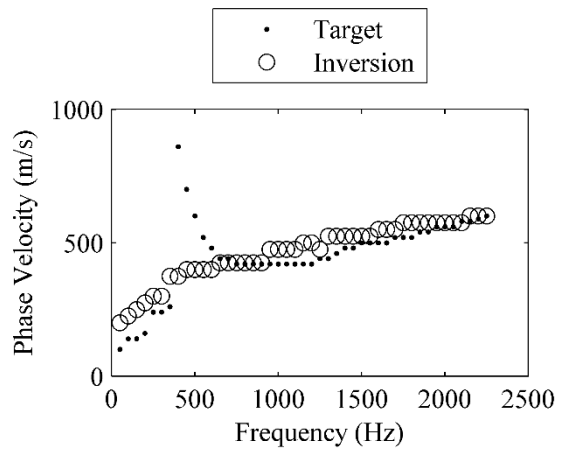
Figure A.10 (continued)

US 69-1
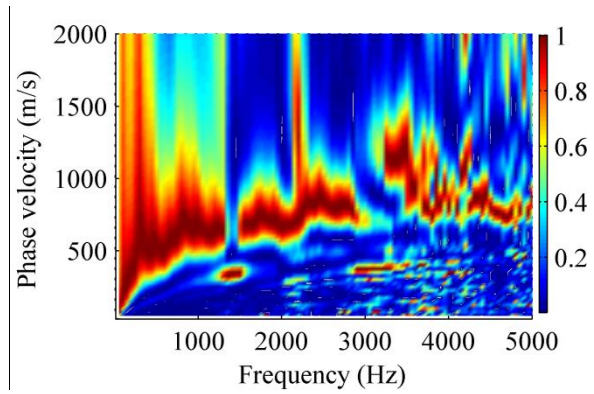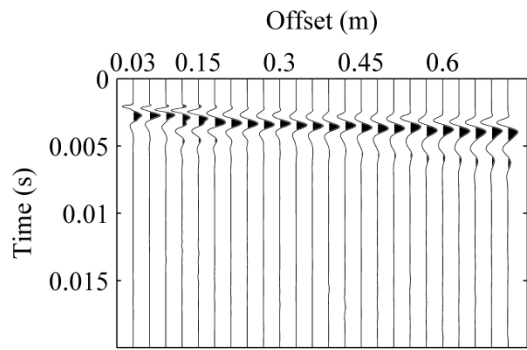
US 69-2
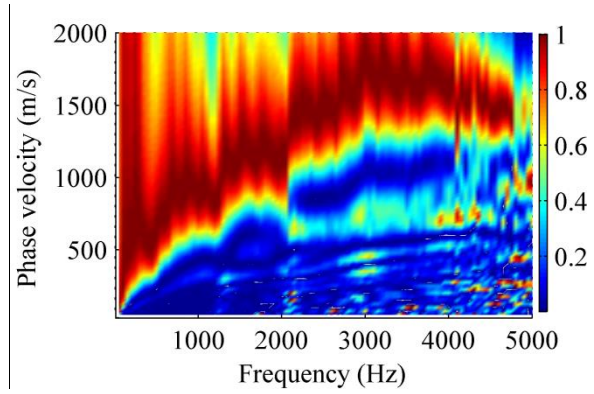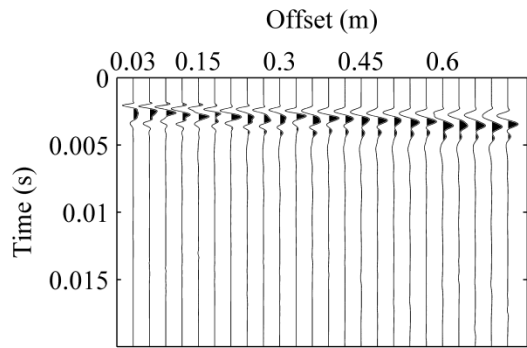
US 69-3

Figure A.11. Results of surface wave tests on hot US 69 HMA surface course several hours after paving. Left column: normalized time-domain signals, right column: frequency-domain dispersion images

US 69-9

Offset (m)
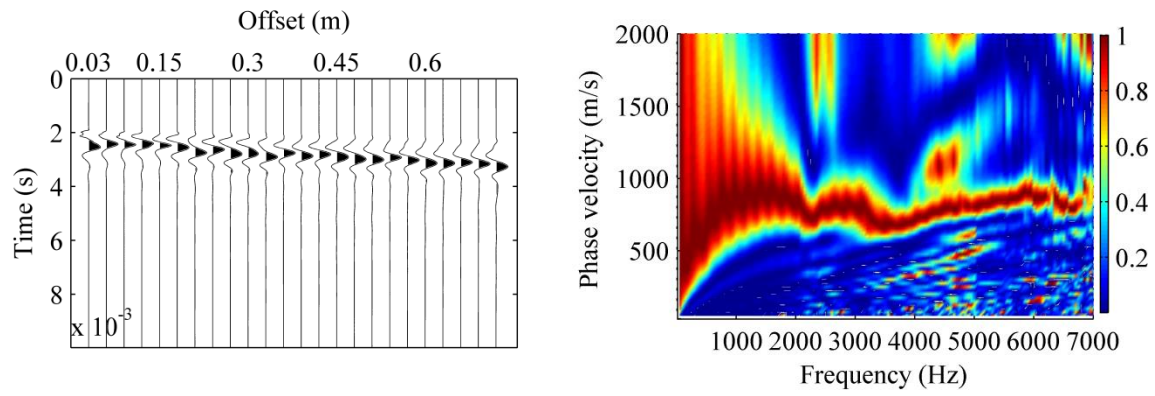
Figure A.11 (continued)

US 69-4
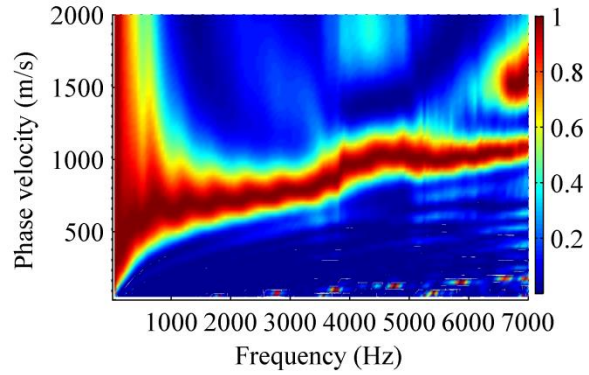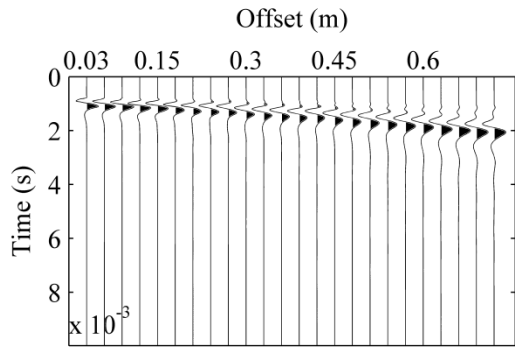
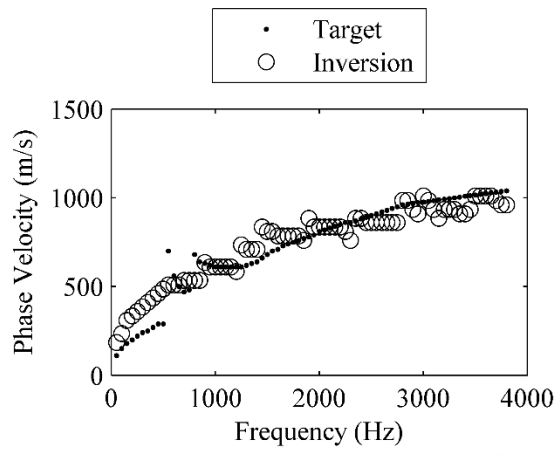
US 69-5
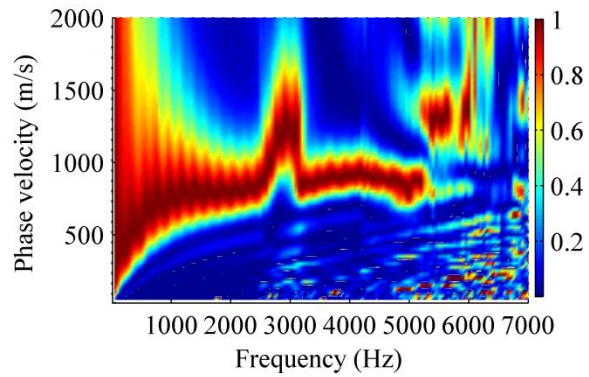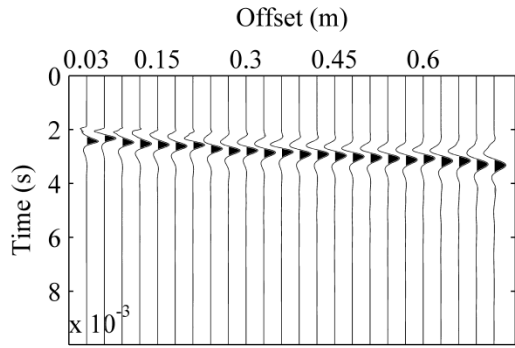
US 69-6
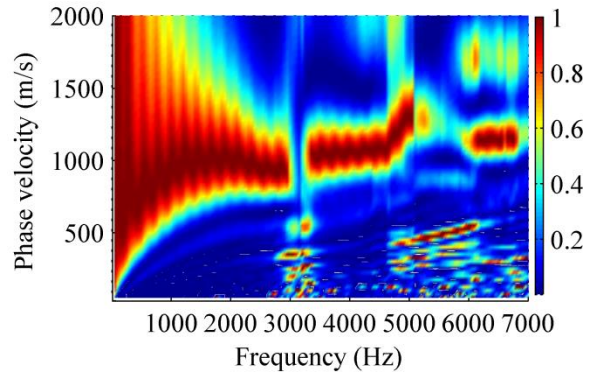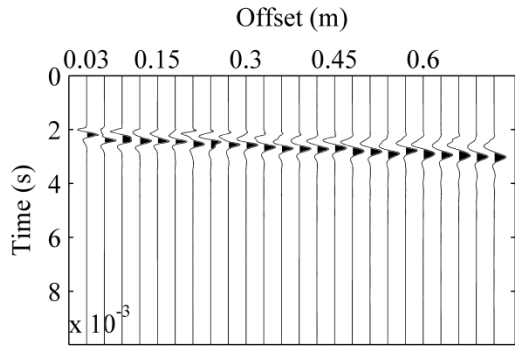
Figure A.12. Results of surface wave tests on cold US 69 HMA surface course after applying dry ice: Left column: normalized time-domain signals, right column: frequency-domain dispersion images.

125
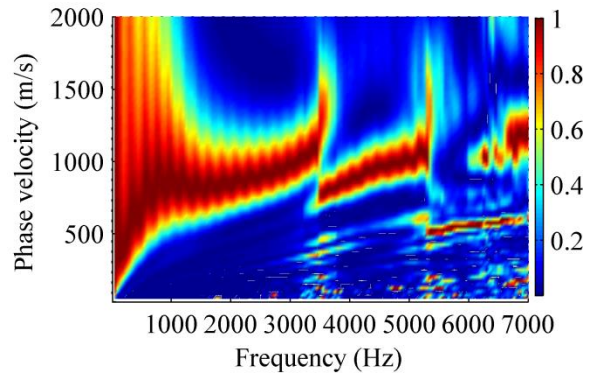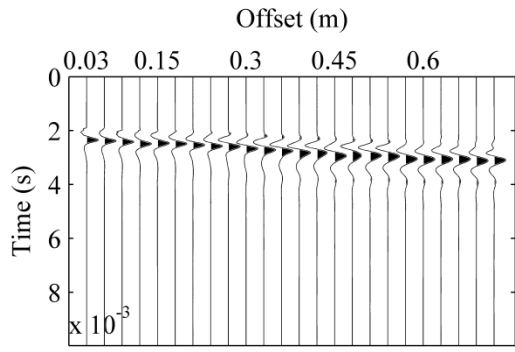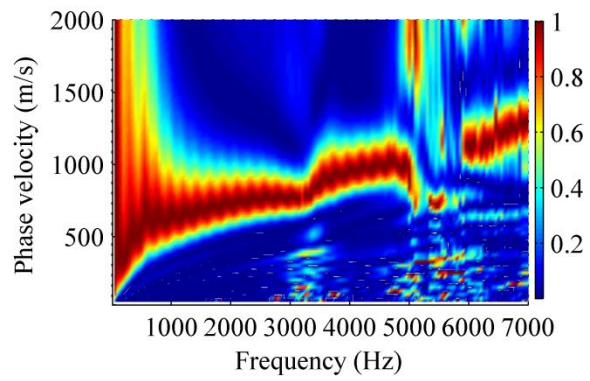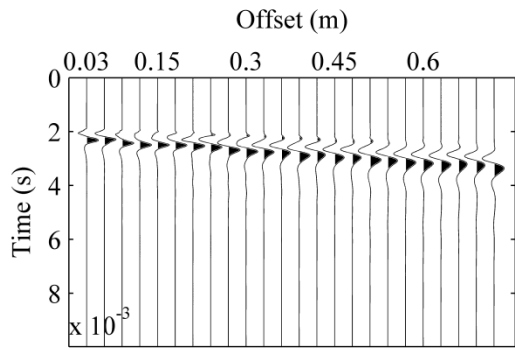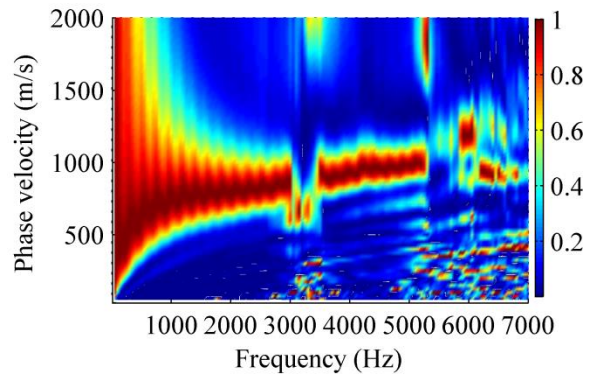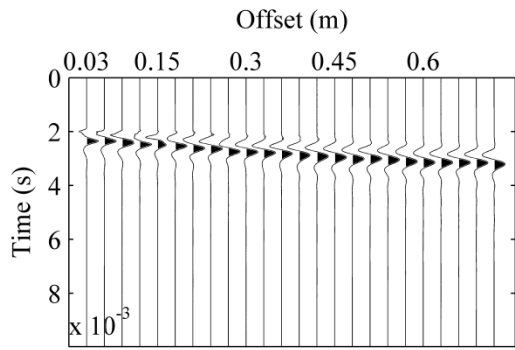
US 69-7

US 69-8

US 69-9

Figure A.12 (continued).

126

US 69-4
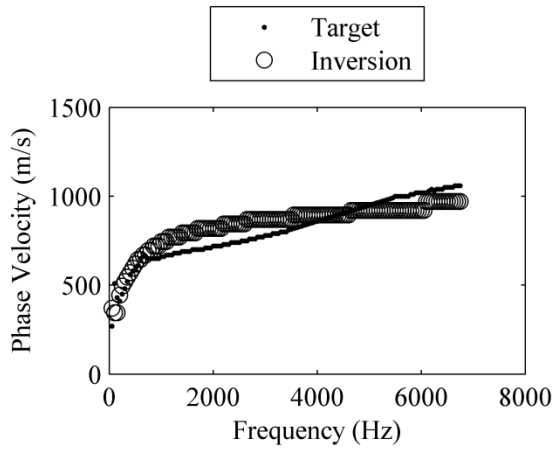
US 69-5
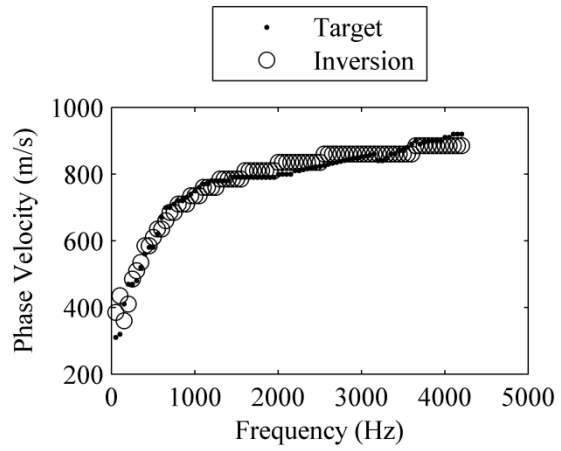
US 69-6
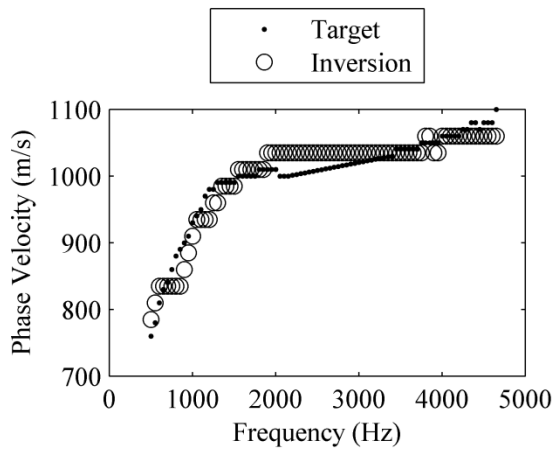
US 69-7
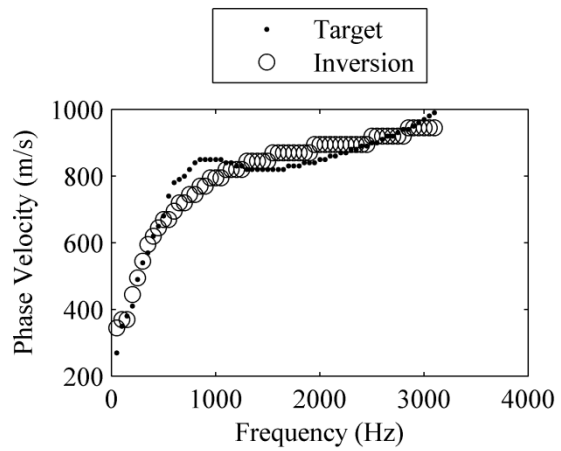
US 69-8
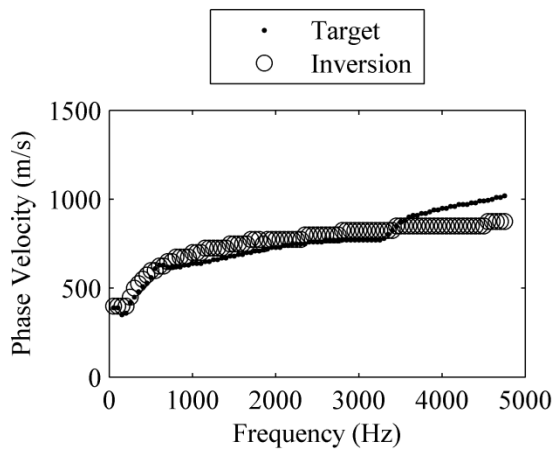
US 69-9
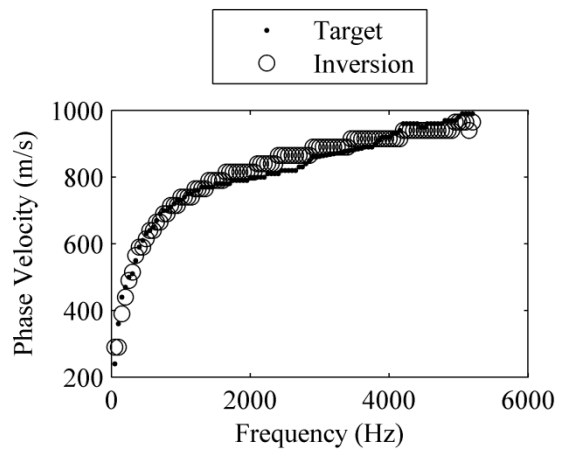
Figure A.13. Picked experimental dispersion curves (targets), and theoretical dispersion curves from inversion for cold US 69 HMA surface course tests after applying dry ice

127
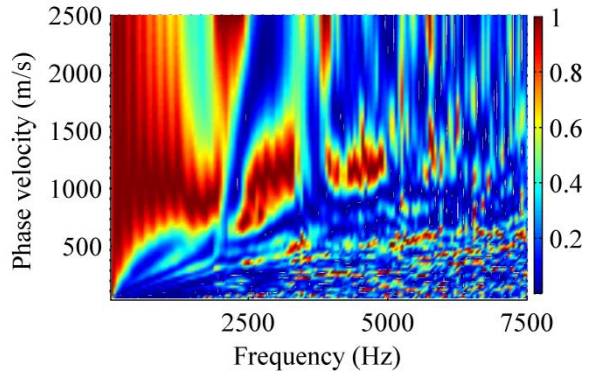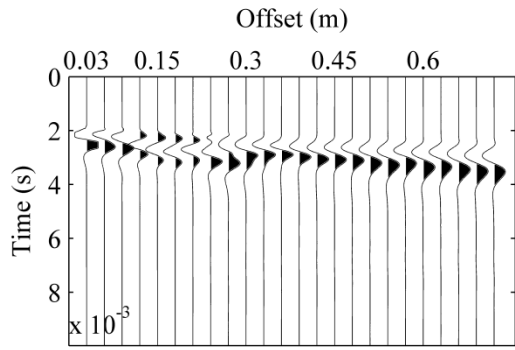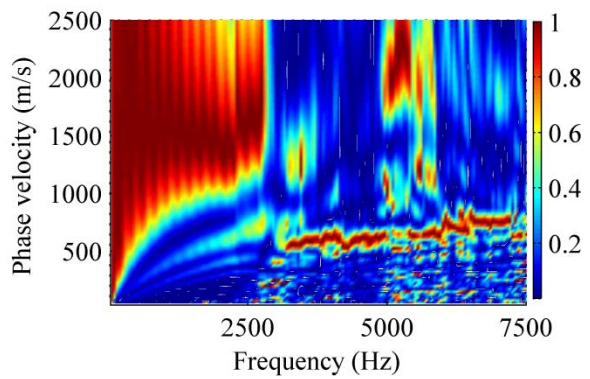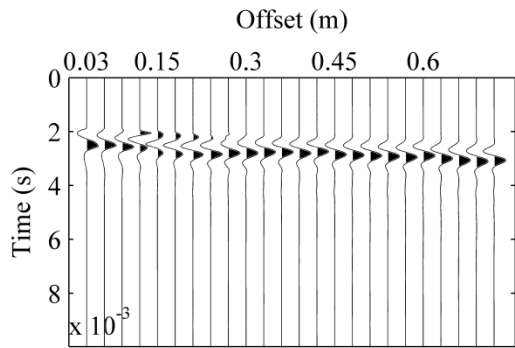
US 169-1
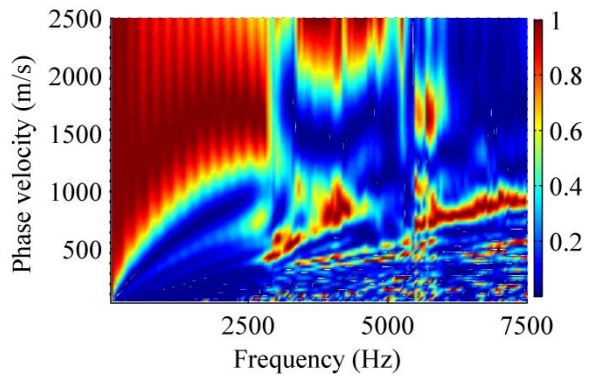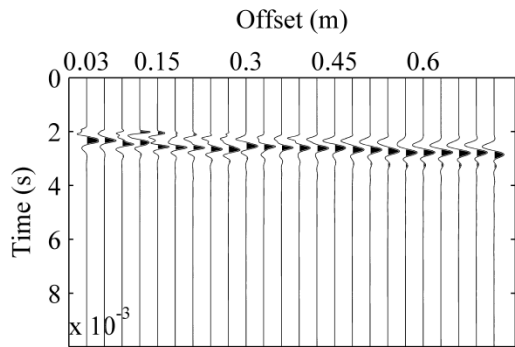
US 169-2

US 169-3

Figure A.14. Results of surface wave tests on cold US 169 HMA surface course after applying dry ice: Left column: normalized time-domain signals, right column: frequency-domain dispersion images

128
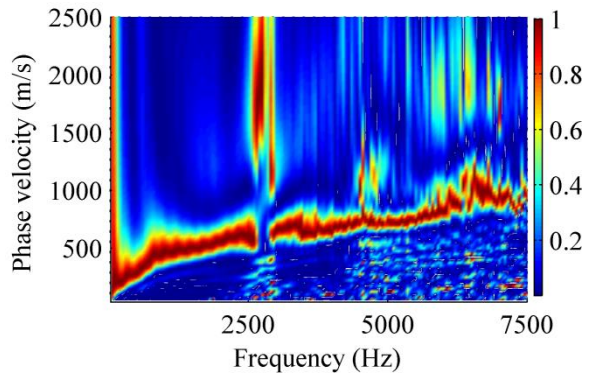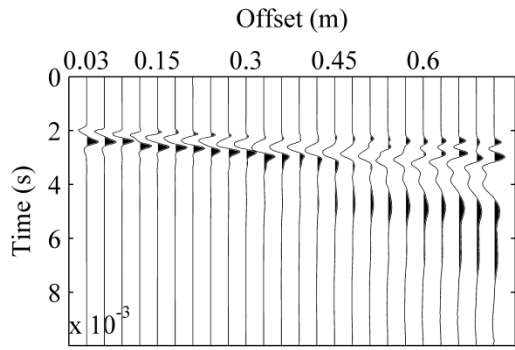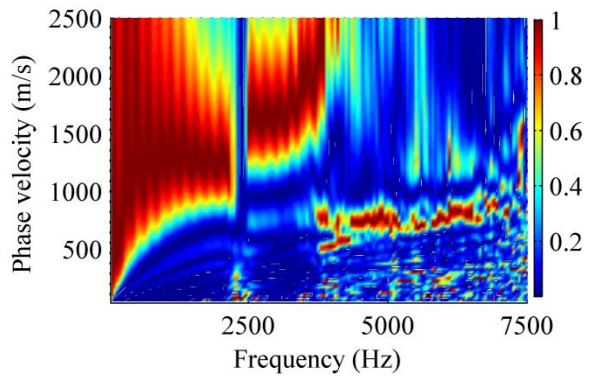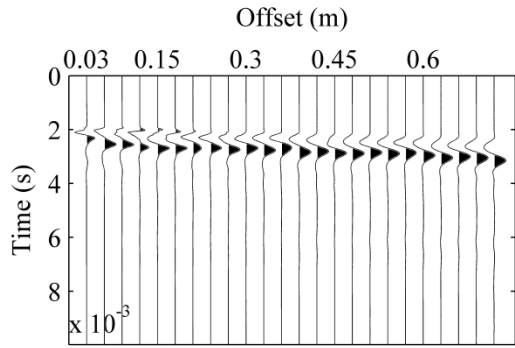
US 169-4
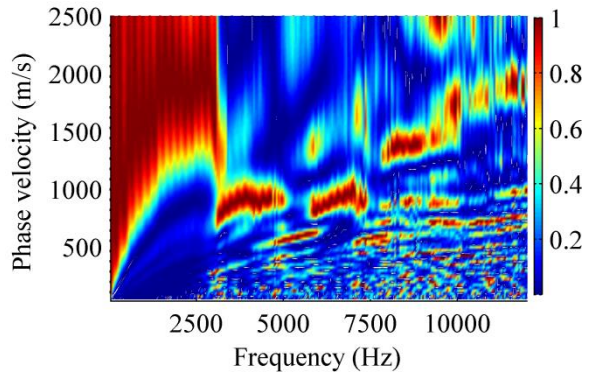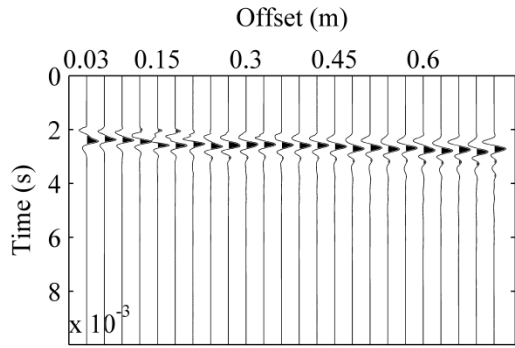
US 169-5

US 169-6

Figure A.14 (continued).

US 169-1
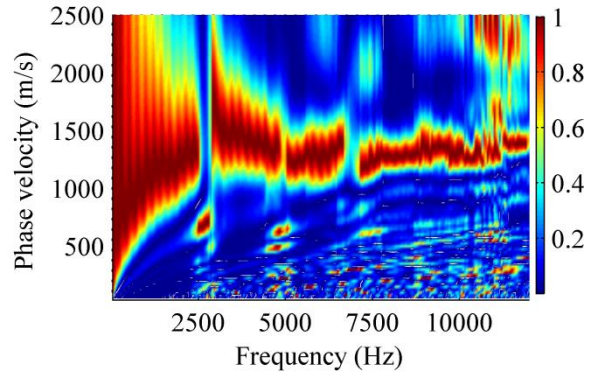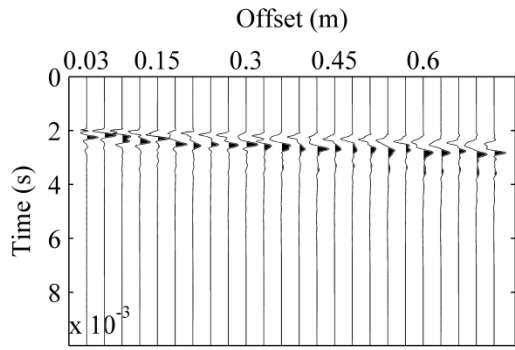
US 169-2
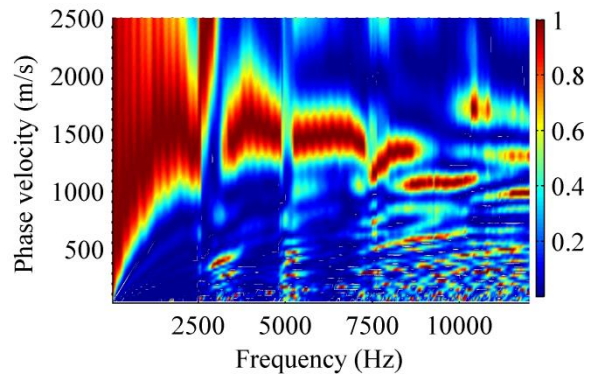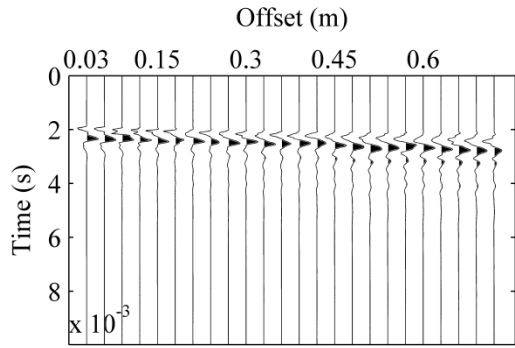
US 169-3
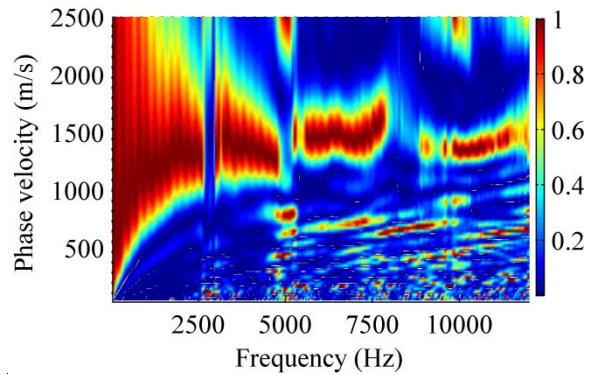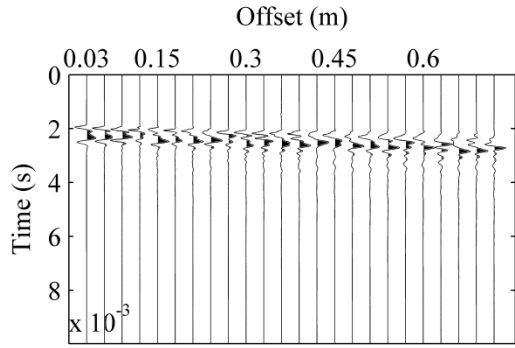
Figure A.15. Results of surface wave tests on ambient-temperature US 169 HMA surface course two days after paving. Left column: normalized time-domain signals, right column: frequency-domain dispersion images

130
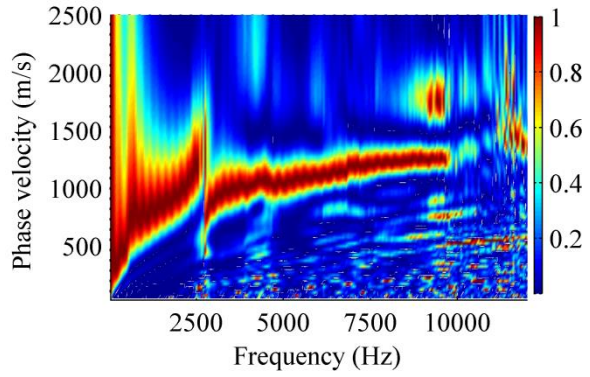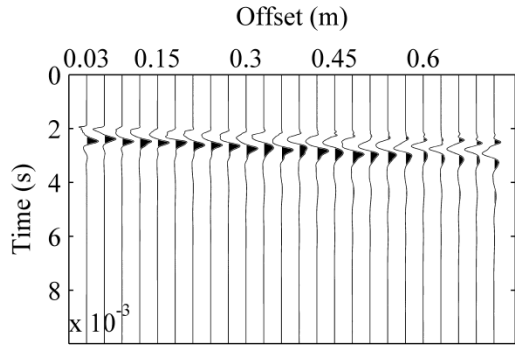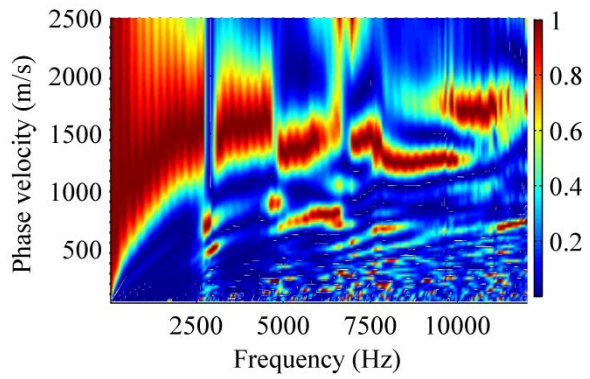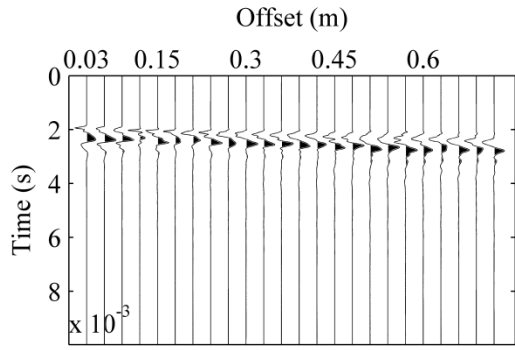
US 169-4

US 169-5

US 169-6
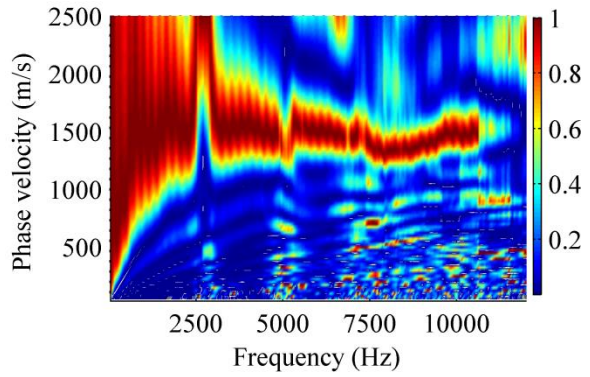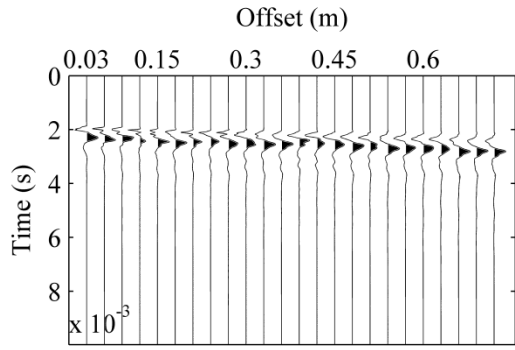
Figure A.15 (continued)

131
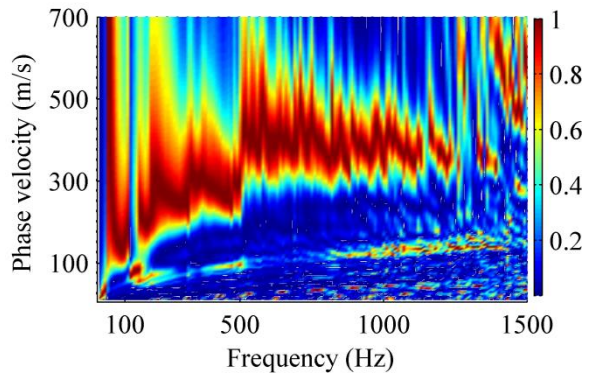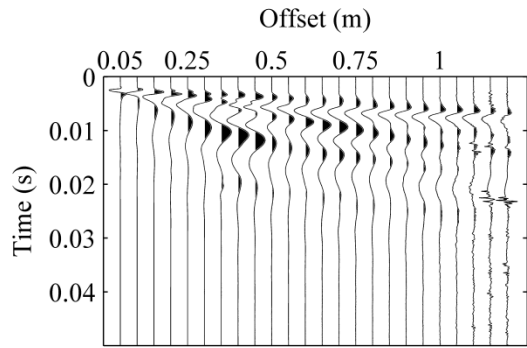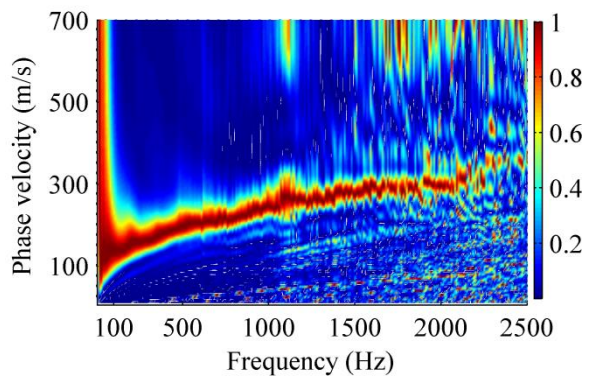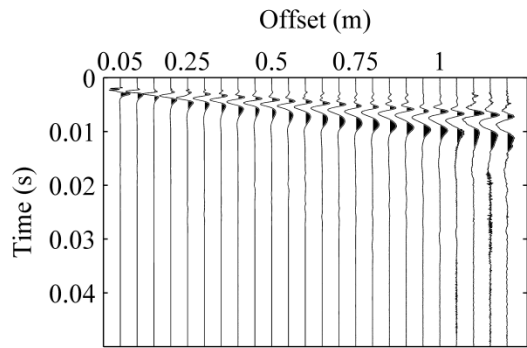
IA 93 FDR-1

IA 93 FDR-2

Figure A.16. Results of surface wave tests on hot IA 93 FDR section several hours after paving. Left column: normalized time-domain signals, right column: frequency-domain dispersion images
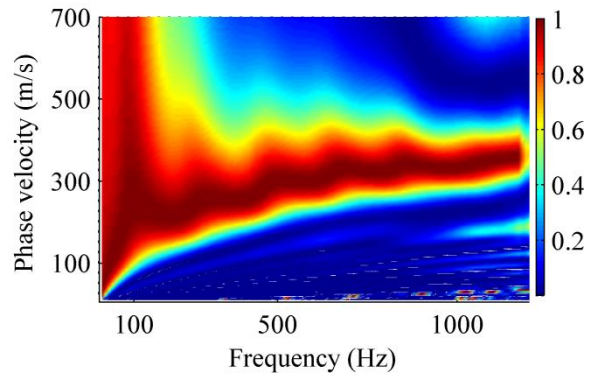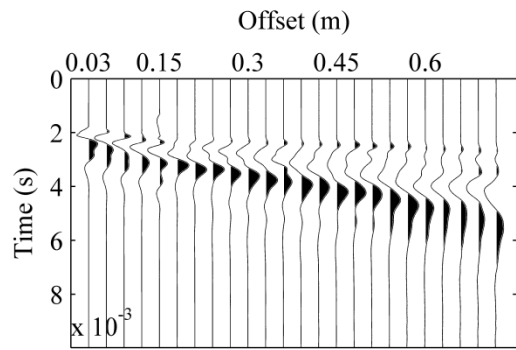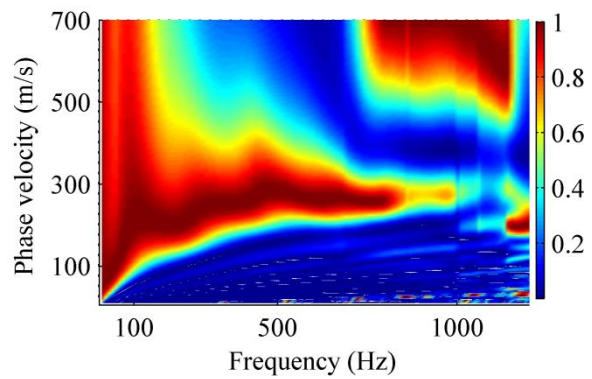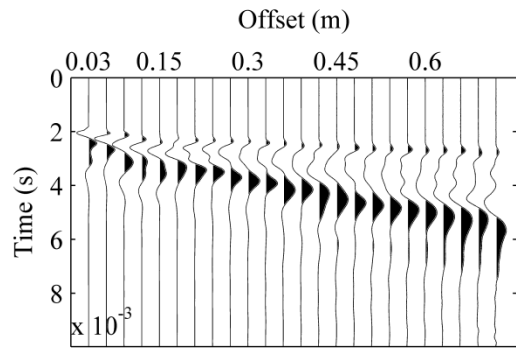
IA 93 CIP-1

IA 93 CIP-2

Figure A.17. Results of surface wave tests on hot IA 93 CIP section several hours after paving. Left column: normalized time-domain signals, right column: frequency-domain dispersion images
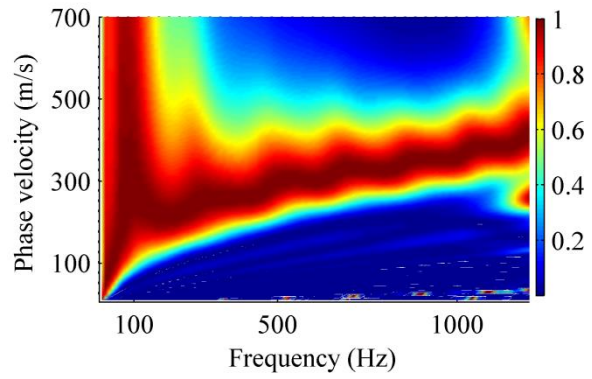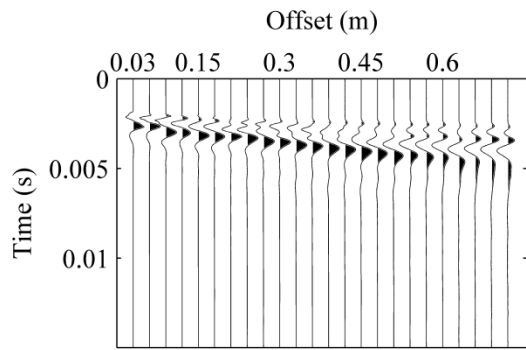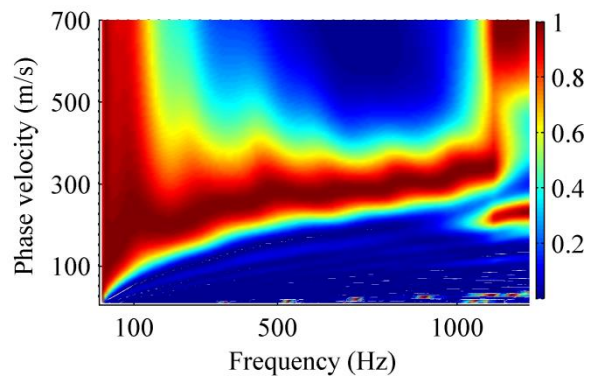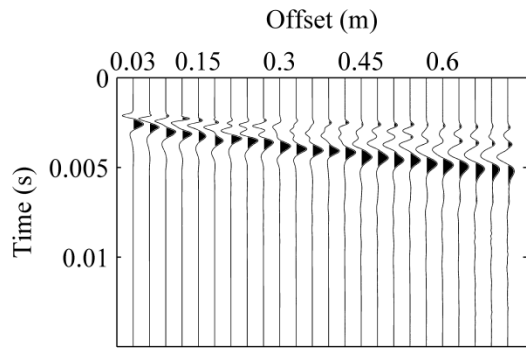
IA 93 CIP-1

IA 93 CIP-2

Figure A.18. Results of surface wave tests on cold IA 93 CIP section after using dry ice: Left column: normalized time-domain signals, right column: frequency-domain dispersion images
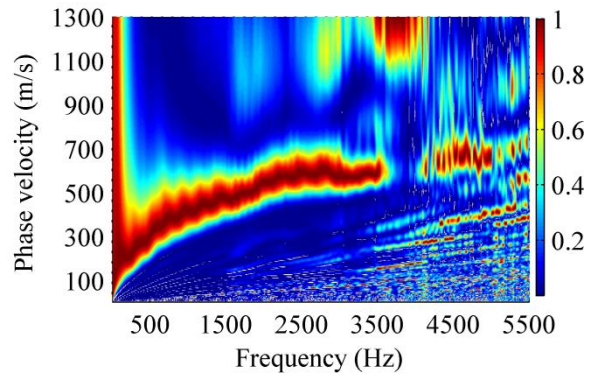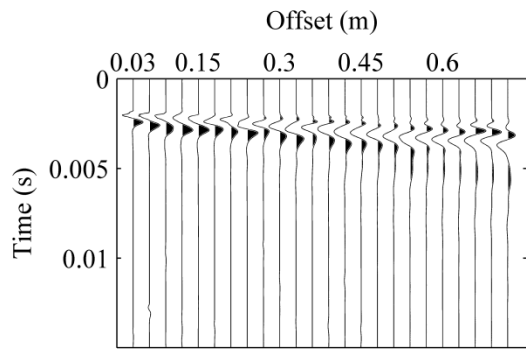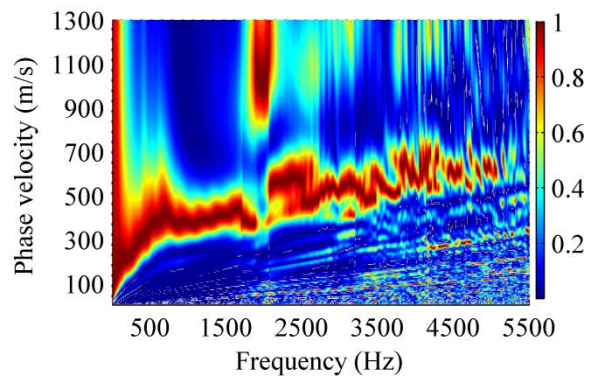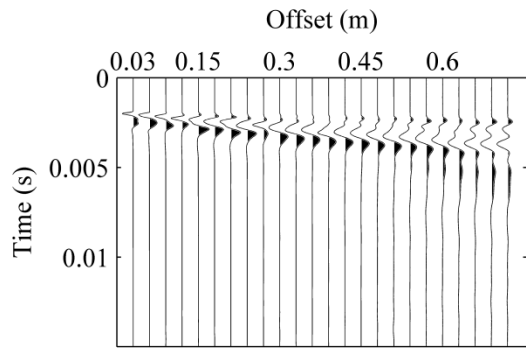
IA 93 OL-1

IA 93 OL-2

Figure A.19. Results of surface wave tests on hot IA 93 thin overlay section several hours after paving. Left column: normalized time-domain signals, right column: frequency-domain dispersion images
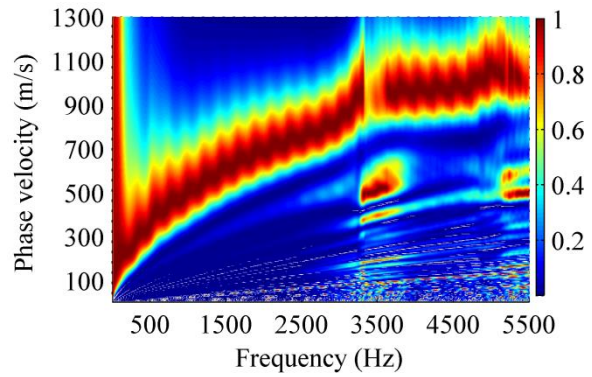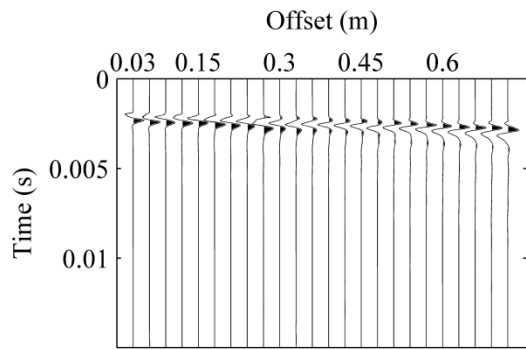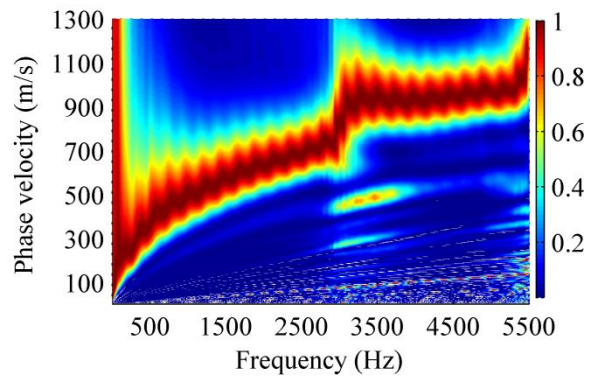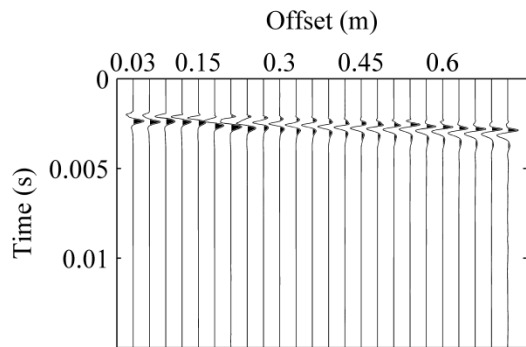
IA 93 OL-1

IA 93 OL-2

Figure A.20. Results of surface wave tests on cold IA 93 thin overlay section after using dry ice: Left column: normalized time-domain signals, right column: frequency-domain dispersion images

IA 93 FDR-1
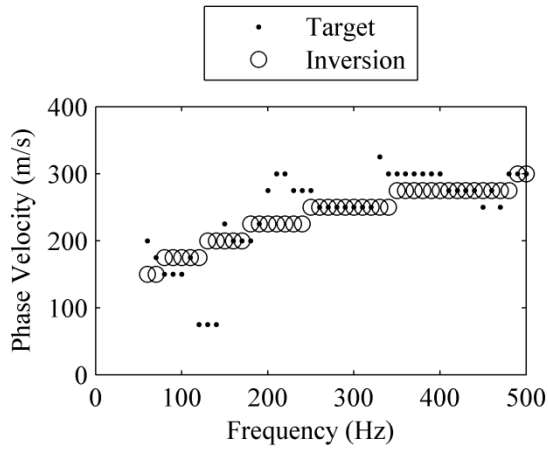
IA 93 FDR-2
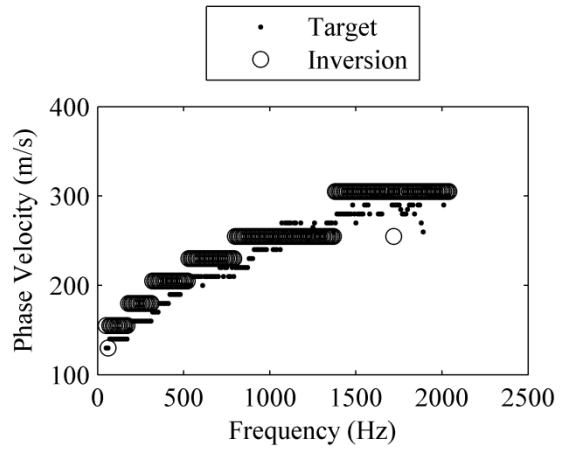
IA 93 CIP-1
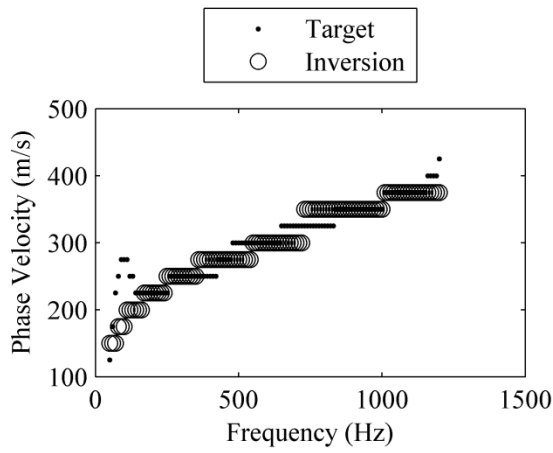
IA 93 CIP-2
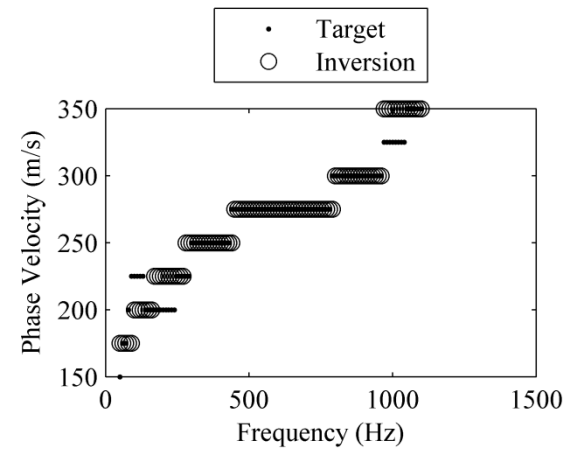
IA 93 OL-1
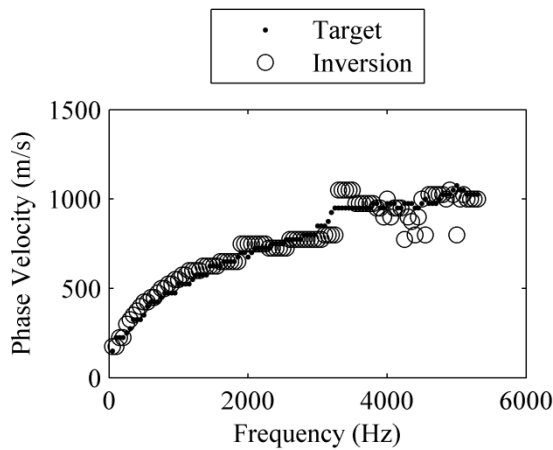
IA 93 OL-2
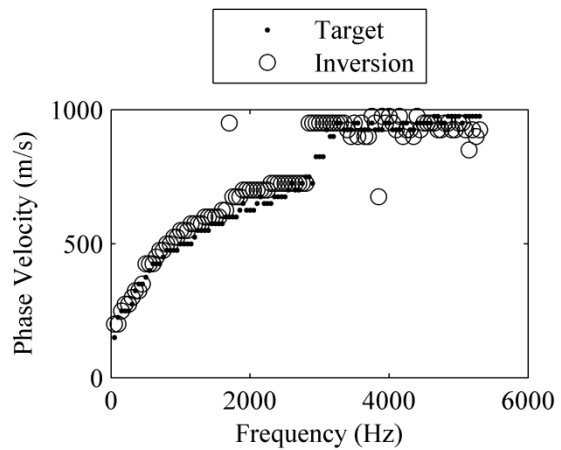
Figure A.21. Picked experimental dispersion curves (targets), and theoretical dispersion curves from inversion for cold tests on IA 93 CIP and OL sections after applying dry ice

US 6 H20-2
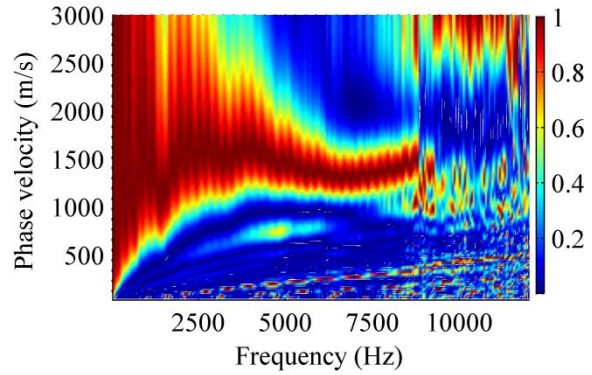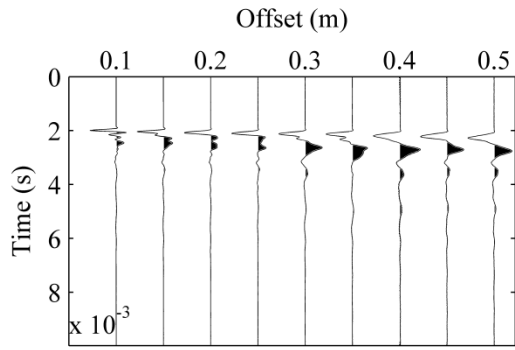
US 6 H20-3
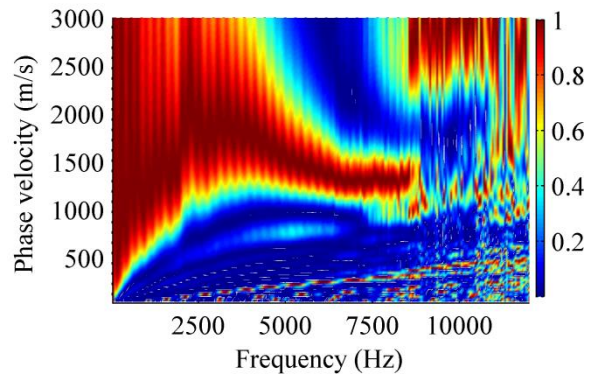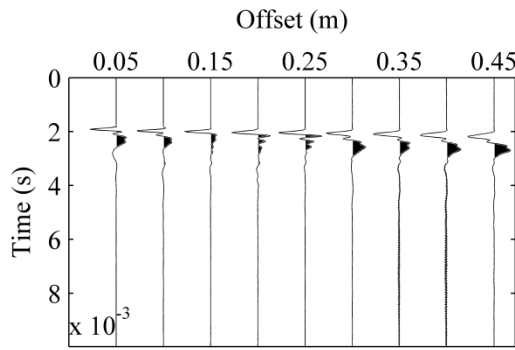
US 6 H25-1
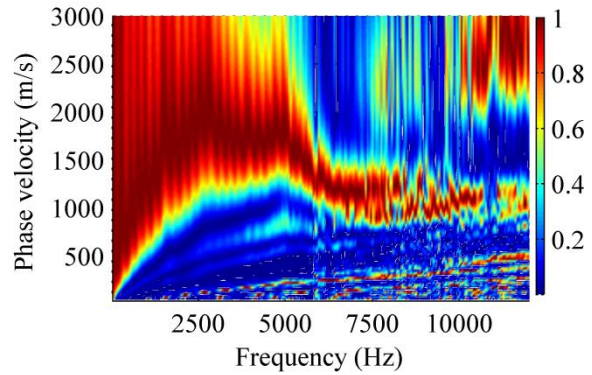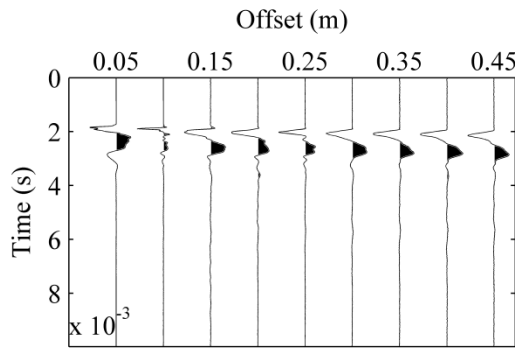
Figure A.22. Results of surface wave tests on hot US 6 HMA surface course several hours after paving. Left column: normalized time-domain signals, right column: frequency-domain dispersion images

138

US 6 H25-2
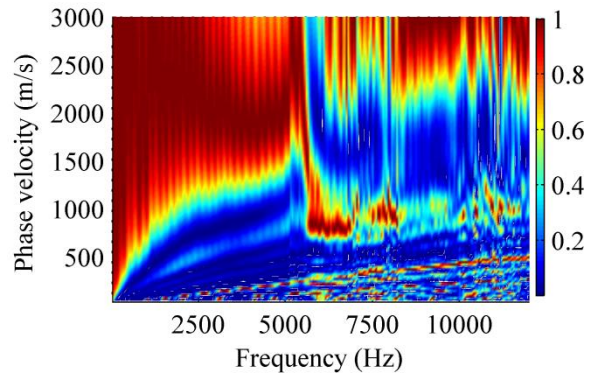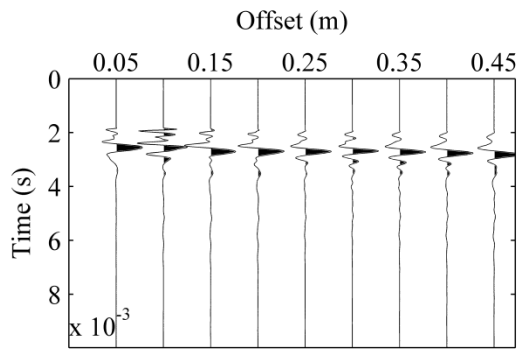
US 6 H30-2

US 6 H30-3

Figure A.22 (continued)
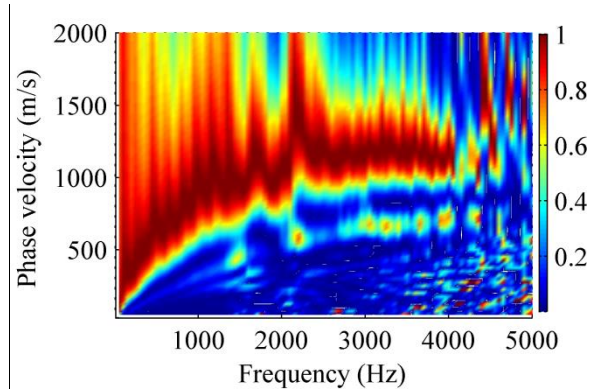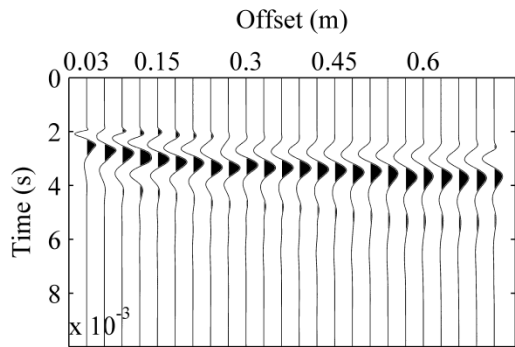
139
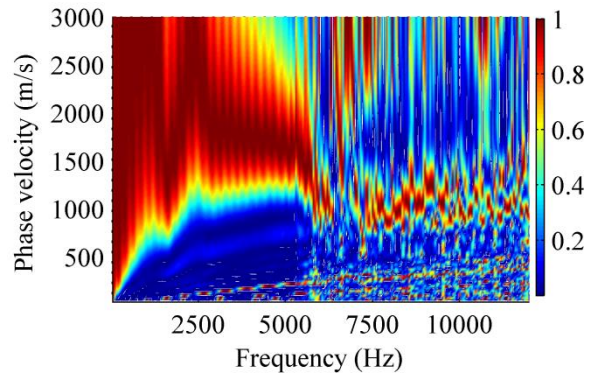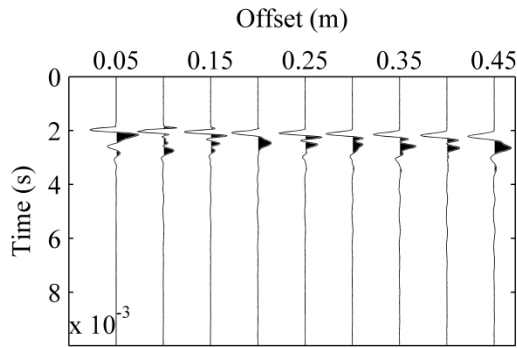
US 6 W15-1

US 6 W15-2
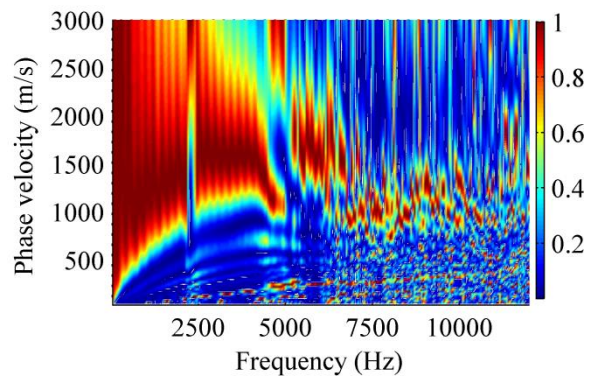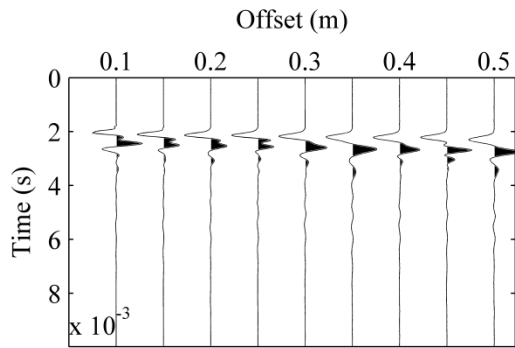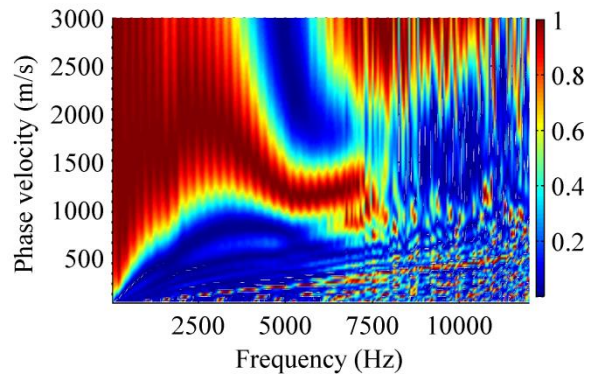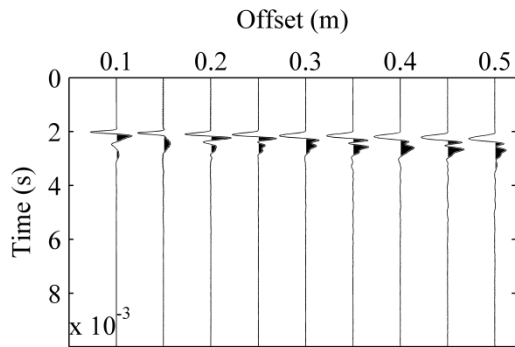
US 6 W30-2

Figure A.23. Results of surface wave tests on hot US 6 WMA surface course several hours after paving. Left column: normalized time-domain signals, right column: frequency-domain dispersion images.

US 6 W30-3
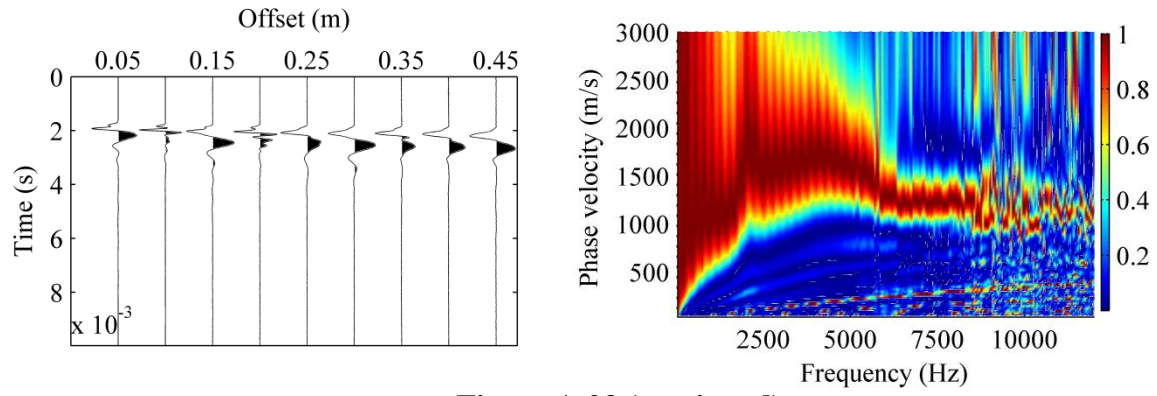
Figure A.23 (continued)

US 6 H20-2

Offset (m)

US 6 H20-3

Offset (m)

US 6 H25-1

Offset (m)
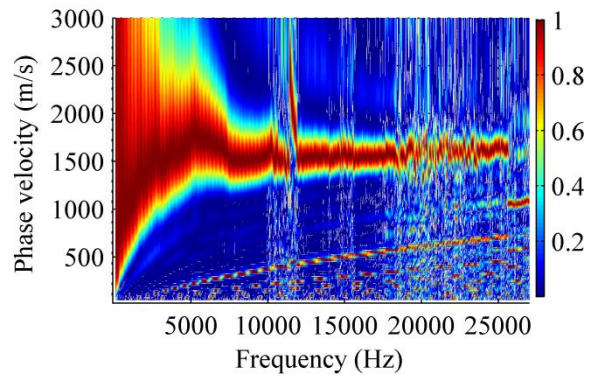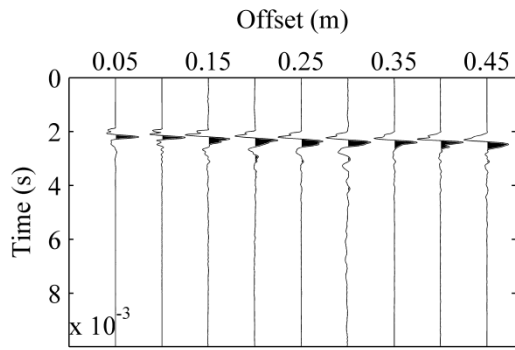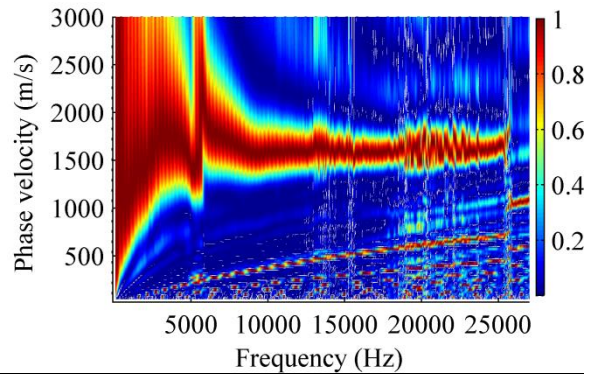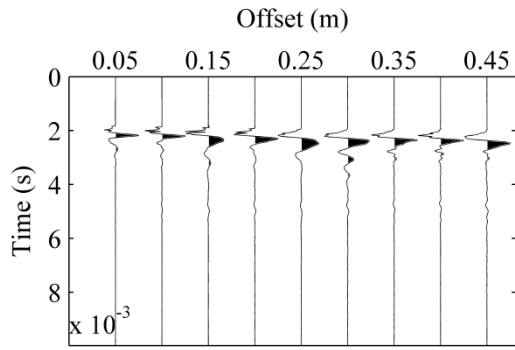
Figure A.24. Results of surface wave tests on ambient-temperature US 6 HMA surface course several days after paving. Left column: normalized time-domain signals, right column: frequency-domain dispersion images

US 6 H25-2
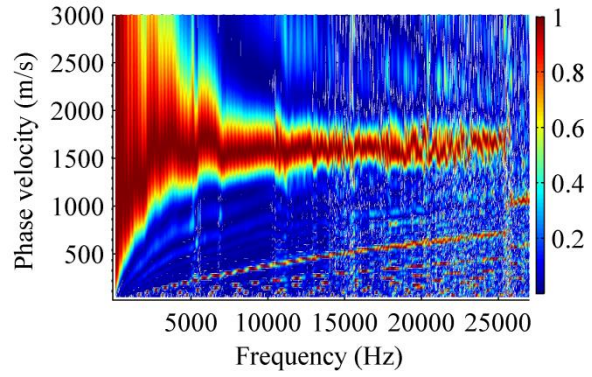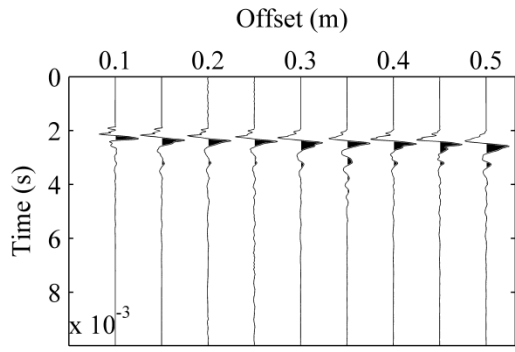
US 6 H30-2
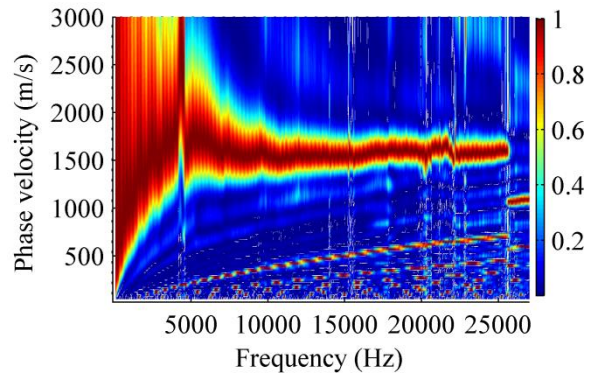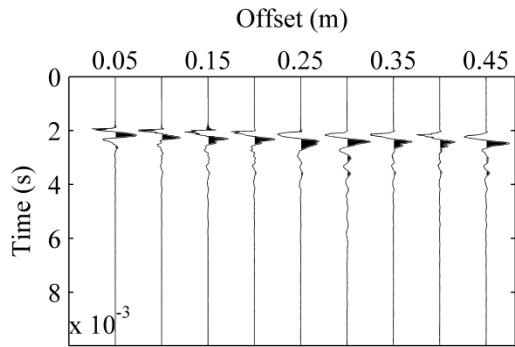
US 6 H30-3
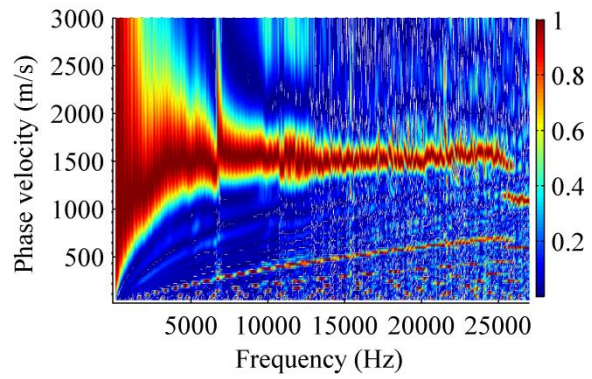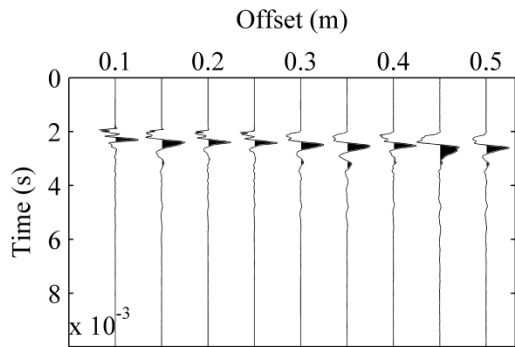
Figure A.24 (continued).

143
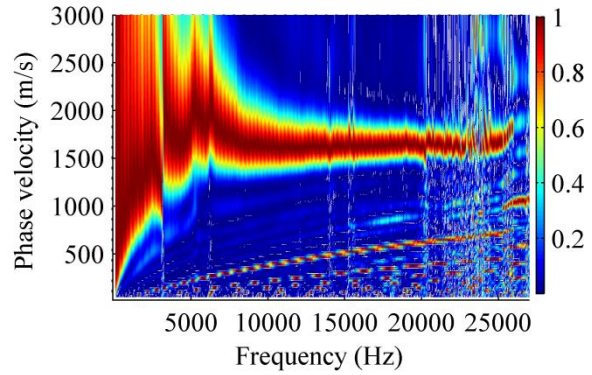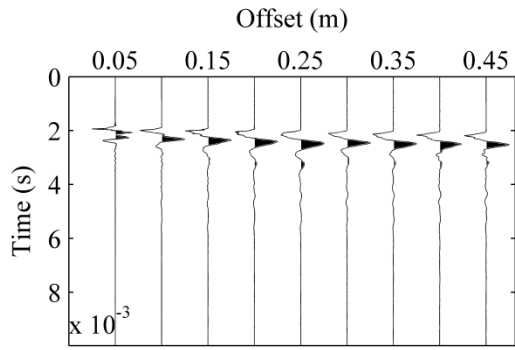
US 6 W15-1

US 6 W15-2
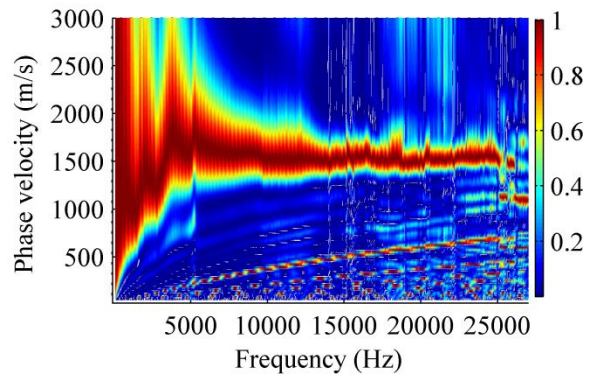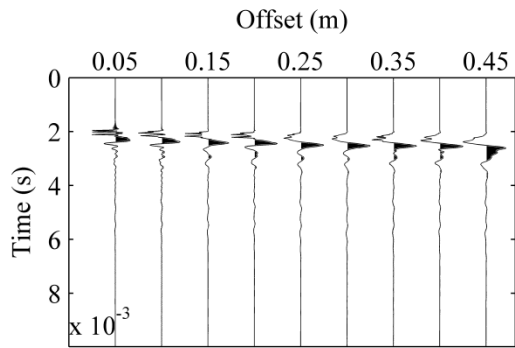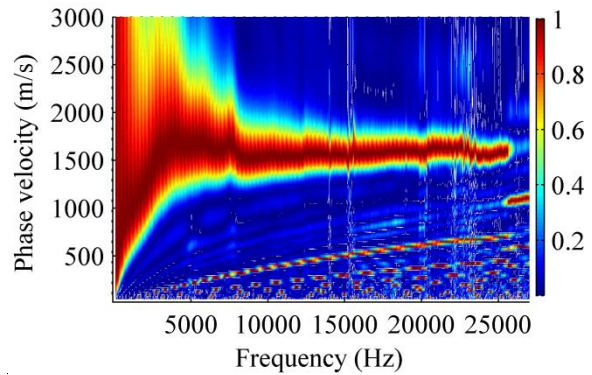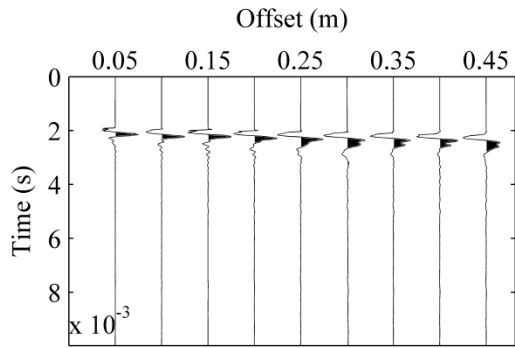
US 6 W30-2

Figure A.25. Results of surface wave tests on ambient-temperature US 6 WMA surface course several days after paving. Left column: normalized time-domain signals, right column: frequency-domain dispersion images

US 6 W30-3
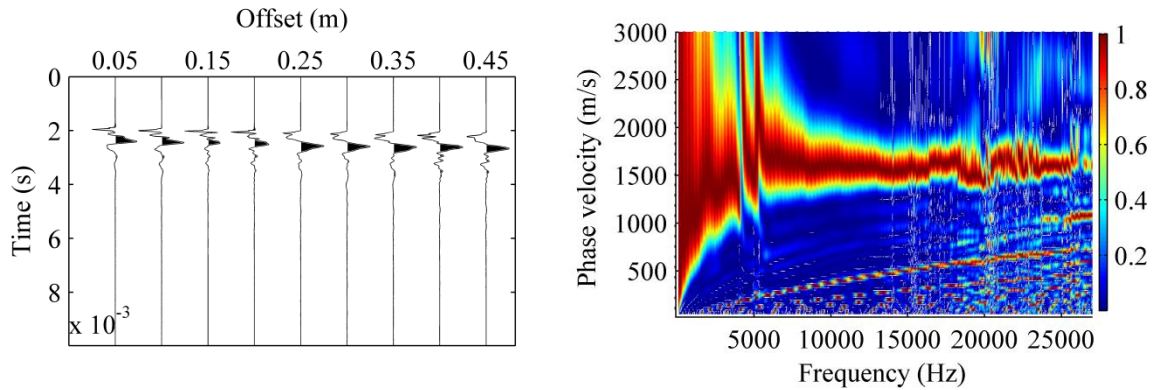
Figure A.25 (continued)

Table A.1. GeoGauge stiffness of hot Boone HMA surface courses several hours after paving

Cores	Temperature (°C)	Measurement (MN/m)				Average (MN/m)
		1	2	3	4	
HS1-1	50.4	27.46	31.00	30.08	-	29.51
HS 1-2	50.4	25.67	29.02	25.83	28.85	27.34
HS 1-3	47.7	31.70	31.32	32.60	-	31.87
HS 1-4	47	27.88	25.26	27.38	-	26.84
HS 2-1	45	31.32	27.66	31.80	-	30.26
HS 2-2	43.1	33.75	33.02	37.52	37.38	35.42
HS 2-3	39.4	36.30	33.26	36.09	32.89	34.64
Average	46.1					30.84

Table A.2. GeoGauge stiffness of ambient-temperature Boone HMA surface courses one day after paving

Cores	Temperature (°C)	Measurement (MN/m)			Average (MN/m)
		1	2	3	
HS 1-1	42.8	62.72	64.34	-	63.53
HS 1-2	45.0	50.15	51.13	-	50.64
HS 1-3	46.7	55.5	57.19	-	56.35
HS 1-4	45.5	51.21	54.55	-	52.88
HS 2-1	44.3	52.58	54.63	55.50	54.24
HS 2-2	45.7	54.84	57.74	-	56.29
HS 2-3	46.2	55.54	56.62	-	56.08
Average	45.2				55.71

Table A.3. GeoGauge stiffness of hot Boone WMA surface courses several hours after paving.

Cores	Temperature (°C)	Measurement (MN/m)			Average (MN/m)
		1	2	3	
WS3-1	48.7	27.48	25.19	25.94	26.20
WS 3-2	52.5	27.9	21.65	29.49	26.35
WS 3-3	50.8	30.23	31.79	32.15	31.39
WS 3-4	50.8	25.12	31.32	34.33	30.26
WS 4-1	56.2	22.92	25.12	25.44	24.49
WS 4-2	52.8	27.25	25.63	26.11	26.33
WS 4-3	55.4	20.56	22.41	21.47	21.48
WS 4-4	53.3	30.21	31.31	30.88	30.80
WS 4-5	51.6	30.24	29.23	29.52	29.66
Average	52.5				27.44

Table A.4. GeoGauge stiffness of ambient-temperature Boone WMA surface courses one day after paving

Cores	Temperature (°C)	Measurement (MN/m)			Average (MN/m)
		1	2	3	
WS3-1	48.2	43.92	37.86	45.99	42.59
WS3-2	49.6	49.7	51.72	52.59	51.34
WS3-3	50.8	48.11	50.88	52.83	50.61
WS3-4	47.9	52.68	53.26	52.87	52.94
WS4-1	49.1	43.47	46.71	48.61	46.26
WS4-2	47.9	54.13	55.22	56.79	55.38
WS4-3	51.8	36.07	38.61	38.04	37.57
WS4-4	52.8	51.98	53.99	57.27	54.41
WS4-5	43.8	53.77	59.81	62.65	58.74
Average	49.1				49.98

Table A.5. GeoGauge stiffness of hot US 69 HMA surface course several hours after paving

Cores	Temperature (°C)	Measurement (MN/m)				Average (MN/m)
		1	2	3	4	
US 69-1	60.8	28.22	25.92	26.32	27.37	26.96
US 69-2	56.9	28.55	35.27	45.85	40.92	37.65
US 69-3	63.9	43.34	46.53	34.98	-	41.62
Average	60.5					35.41

Table A.6. GeoGauge stiffness of cold US 69 HMA surface course after applying dry ice

Cores	Temperature (°C)	Measurement (MN/m)			Average (MN/m)
		1	2	3	
US 69-4	16	79.07	90.46	91.55	87.03
US 69-5	18.5	82.49	94.91	87.49	88.30
US 69-6	16.8	109.59	111.22	98.65	106.49
US 69-7	18	96.51	74.32	109.31	93.38
US 69-8	19.3	77.46	78.91	86.05	80.81
US 69-9	18.5	76.41	83.88	87.42	82.57
Average	17.9				89.76

Table A.7. GeoGauge stiffness of cold US 169 HMA surface course several hours after paving and applying dry ice

Cores	Temperature (°C)	Measurement (MN/m)				Average (MN/m)
		1	2	3	4	
US 169-1	20	34.42	30.3	37.37	-	34.03
US 169-2	27.9	28.92	30.6	39.49	34.52	33.38
US 169-3	33	32.67	40.37	36.63	-	36.56
US 169-4	29.6	35.33	28.98	35.91	-	33.41
US 169-5	23.5	42.22	34.14	48.22	-	41.53
US 169-6	25.4	39.25	47.89	35.59	37.87	40.15
Average	26.6					36.51

Table A.8. GeoGauge stiffness of hot IA 93 sections several hours after paving

Cores	Temperature (°C)	Measurement (MN/m)			Average (MN/m)
		1	2	3	
FDR-1	33.8	4.37	4.92	5.51	4.93
FDR-2	29.4	22.13	25.72	24.64	24.16
Average	31.6				14.55
CIP-1	42.1	26.43	28.38	31.81	28.87
CIP-2	43.3	22.93	23.76	24.62	23.77
Average	42.7				26.32
OL-1	45	35.86	32.66	36.05	34.86
OL-2	44.8	34.48	33.61	40.97	36.35
Average	44.9				35.61

Table A.9. GeoGauge stiffness of cold IA 93 sections after applying dry ice

Cores	Temperature (°C)	Measurement (MN/m)			Average (MN/m)
		1	2	3	
CIP-1	18.8	30.65	32.46	31.98	31.70
CIP-2	17.5	24.42	24.68	25.91	25.00
Average	18.2				28.35
OL-1	13.5	45.64	42.51	42.98	43.71
OL-2	12.3	46.22	42.73	41.71	43.55
Average	12.9				43.63

Table A.10. GeoGauge stiffness of hot US 6 HMA surface course several hours after paving

Cores	Temperature (°C)	Measurement (MN/m)			Average (MN/m)
		1	2	3	
US 6 H20-2	40.6	81.92	100.91	115.34	99.39
US 6 H20-3	42.3	106.21	104.00	111.49	107.23
US 6 H25-1	43.3	97.82	103.77	106.24	102.61
US 6 H25-2	45.3	43.23	41.89	45.54	43.55
US 6 H30-2	45.3	44.64	47.91	36.35	42.97
US 6 H30-3	43.8	37.66	40.54	36.24	38.15
Average	43.4				72.32

Table A.11. GeoGauge stiffness of ambient-temperature US 6 HMA surface course several days after paving

Cores	Temperature (°C)	Measurement (MN/m)			Average (MN/m)
		1	2	3	
US 6 H20-2	26.2	32.95	36.80	35.68	35.14
US 6 H20-3	25.7	35.26	38.83	34.17	36.09
US 6 H25-1	24.7	34.71	32.67	34.29	33.89
US 6 H25-2	25.9	31.45	30.82	32.50	31.59
US 6 H30-2	30.6	30.62	35.71	33.16	33.16
US 6 H30-3	26.4	29.56	29.40	29.55	29.50
Average	26.6				33.23

Table A.12. GeoGauge stiffness of hot US 6 WMA surface course several hours after paving

Cores	Temperature (°C)	Measurement (MN/m)			Average (MN/m)
		1	2	3	
US 6 W15-1	46.0	42.02	41.63	45.08	42.91
US 6 W15-2	46.0	44.68	50.00	39.60	44.76
US 6 W30-2	44.0	46.34	42.59	48.72	45.88
US 6 W30-3	40.1	40.59	45.18	54.38	46.72
Average	44.0				45.07

Table A.13. GeoGauge stiffness of ambient-temperature US 6 WMA surface course several days after paving

Cores	Temperature (°C)	Measurement (MN/m)			Average (MN/m)
		1	2	3	
US 6 W15-1	22.2	38.69	37.22	39.06	38.32
US 6 W15-2	23.0	35.59	37.32	33.88	35.60
US 6 W30-2	22.0	35.44	33.70	33.62	34.25
US 6 W30-3	22.2	36.47	38.16	39.84	38.16
Average	22.4				36.58

Table A.14. PaveTracker density of Boone HMA base courses

Cores	Several hours after paving		One day after paving	
	Temperature (°C)	Density (kg/m³)	Temperature (°C)	Density (kg/m³)
HB1-1	72.1	2,185	24.7	2,144
HB1-3	85.1	2,215	25.2	2,166
HB1-5	68.2	2,166	27.7	2,126
HB1-7	66.1	2,223	26.4	2,052
HB2-1	77.4	2,203	31.8	2,092
HB2-2	88.9	2,255	31.3	2,200
HB2-5	77.6	2,167	29.6	2,083
HB2-7	72.8	2,138	33.8	2,106
HB5-1	79.1	2,229	30.1	2,177
HB5-3	69.9	2,282	28.4	2,261
HB5-6	77.4	2,150	27.4	2,010
HB5-7	69.0	2,250	26.9	2,230
HB6-3	67.3	2,259	29.4	2,196
HB6-4	74.7	2,239	29.1	2,227
HB6-5	71.6	2,243	29.4	2,202
HB6-7	69.7	2,266	28.9	2,263
HB7-2	67.8	2,278	28.9	2,228
HB7-4	64.4	2,203	27.7	2,291
HB7-7	75.6	2,279	27.9	2,328
Average	73.4		28.7	

Table A.15. PaveTracker density of Boone WMA base courses

Cores	Several hours after paving		One day after paving	
	Temperature (°C)	Density (kg/m³)	Temperature (°C)	Density (kg/m³)
WB3-2	61.5	2,259	25.9	2,205
WB3-4	69.0	2,217	27.4	2,199
WB3-5	75.0	2,166	28.9	2,102
WB3-7	71.1	2,216	27.7	2,128
WB4-1	69.2	2,220	27.7	2,151
WB4-2	72.3	2,226	28.1	2,146
WB4-3	68.7	2,166	29.1	2,285
WB4-7	77.1	2,181	29.9	2,141
WB8-4	55.0	2,193	38.9	2,208
WB8-5	55.9	2,247	35.5	2,223
WB8-7	50.8	2,240	26.2	2,243
WB8-8	51.6	2,279	35.5	2,284
WB9-2	50.4	2,197	42.1	2,235
WB9-3	51.8	2,182	43.8	2,221
WB9-6	56.2	2,196	40.9	2,252
WB9-7	53.8	2,234	47.2	2,231
Average	61.8		33.4	

Table A.16. PaveTracker density of Boone HMA surface courses

Cores	Several hours after paving		One day after paving	
	Temperature (°C)	Density (kg/m³)	Temperature (°C)	Density (kg/m³)
HS1-1	50.4	2,229	42.8	2,235
HS1-2	50.4	2,229	45.0	2,199
HS1-3	47.7	2,238	46.7	2,234
HS1-4	47	2,248	45.5	2,249
HS2-1	45	2,225	44.3	2,209
HS2-2	43.1	2,229	45.7	2,156
HS2-3	39.4	2,259	46.2	2,247
Average	46.1		45.2	

Table A.17. PaveTracker density of Boone WMA surface courses

Cores	Several hours after paving		One day after paving	
	Temperature (°C)	Density (kg/m³)	Temperature (°C)	Density (kg/m³)
WS3-1	48.7	2,221	48.2	2,193
WS3-2	52.5	2,272	49.6	2,101
WS3-3	50.8	2,244	50.8	2,238
WS3-4	50.8	2,275	47.9	2,241
WS4-1	56.2	2,230	49.1	2,111
WS4-2	52.8	2,214	47.9	2,196
WS4-3	55.4	2,208	51.8	2,187
WS4-4	53.3	2,222	52.8	2,229
WS4-5	51.6	2,240	43.8	2,226
Average	52.5		49.1	

Table A.18. PaveTracker density of US 69 HMA surface courses

Cores	Several hours after paving		After applying dry ice	
	Temperature (°C)	Density (kg/m³)	Temperature (°C)	Density (kg/m³)
US 69-1	60.8	2,279	-	-
US 69-2	56.9	2,290	-	-
US 69-3	63.9	2,317	-	-
US 69-4	-	-	16	2,264
US 69-5	-	-	18.5	2,212
US 69-6	-	-	16.8	2,272
US 69-7	-	-	18	2,178
US 69-8	-	-	19.3	2,205
US 69-9	-	-	18.5	2,256
Average	60.5		17.9	

Table A.19. PaveTracker density of IA 93 sections

Cores	Several hours after paving		After applying dry ice	
	Temperature (°C)	Density (kg/m³)	Temperature (°C)	Density (kg/m³)
FDR-1	33.8	2,314	-	-
FDR-2	29.4	2,508	-	-
Average	31.6			
CIP-1	42.1	2,181	18.8	2,179
CIP-2	43.3	2,236	17.5	2,179
Average	42.7		18.2	
OL-1	45	2,234	13.5	2,175
OL-2	44.8	2,183	12.3	2,127
Average	44.9		12.9	

Table A.20. PaveTracker density of US 169 HMA surface course

| Cores | Several hours after paving and applying dry ice | |
	Temperature (°C)	Density (kg/m³)
US 169-1	20	2,199
US 169-2	27.9	2,345
US 169-3	33	2,321
US 169-4	29.6	2,236
US 169-5	23.5	2,300
US 169-6	25.4	2,300
Average	26.6	

Table A.21. PaveTracker density of US 6 HMA surface course

| Cores | Several hours after paving | |
	Temperature (°C)	Density (kg/m³)
US 6 H20-2	40.6	2,710
US 6 H20-3	42.3	2,577
US 6 H25-1	43.3	2,609
US 6 H25-2	45.3	2,609
US 6 H30-2	45.3	2,646
US 6 H30-3	43.8	2,683
Average	43.4	

Table A.22. PaveTracker density of US 6 WMA surface course

| Cores | Several hours after paving | |
	Temperature (°C)	Density (kg/m³)
US 6 W15-1	46.0	2,603
US 6 W15-2	46.0	2,572
US 6 W30-2	44.0	2,628
US 6 W30-3	40.1	2,582
Average	44.0	

APENDIX B – LABORATORY TEST RESULTS

LIST OF FIGURES

LIST OF TABLES

Table B.1. Laboratory density of Boone HMA base courses

Cores	SSD (kg/m^3)	CoreLock (kg/m^3)
HB1-1	2,283	2,292
HB1-3	2,283	2,275
HB1-5	2,260	2,267
HB1-7	2,303	2,311
HB2-1	2,292	2,301
HB2-2	2,303	2,284
HB2-5	2,239	2,256
HB2-7	2,284	2,301
HB5-1	2,311	2,319
HB5-3	2,305	2,314
HB5-6	2,282	2,293
HB5-7	2,317	2,328
HB6-3	2,311	2,309
HB6-4	2,305	2,313
HB6-5	2,299	2,312
HB6-7	2,328	2,342
HB7-2	2,326	2,334
HB7-4	2,291	2,299
HB7-7	2,362	2,365

Table B.2. Laboratory density of Boone WMA base courses

Cores	SSD (kg/m^3)	CoreLock (kg/m^3)
WB3-2	2,287	2,287
WB3-4	2,288	2,310
WB3-5	2,263	2,274
WB3-7	2,276	2,295
WB4-1	2,297	2,310
WB4-2	2,274	2,294
WB4-3	2,235	2,236
WB4-7	2,246	2,253
WB8-4	2,289	2,302
WB8-5	2,311	2,320
WB8-7	2,318	2,330
WB8-8	2,352	2,349
WB9-2	2,278	2,295
WB9-3	2,245	2,261
WB9-6	2,275	2,281
WB9-7	2,294	2,303

Table B.3. Laboratory density of Boone HMA surface courses

Cores	CoreLock (kg/m^3)
HS1-1	2,303
HS1-2	2,270
HS1-3	2,273
HS1-4	2,295
HS2-1	2,268
HS2-2	2,253
HS2-3	2,298

Table B.4. Laboratory density of Boone WMA surface courses

Cores	CoreLock (kg/m^3)
WS3-1	2,227
WS3-2	2,283
WS3-3	2,270
WS3-4	2,274
WS4-1	2,282
WS4-2	2,269
WS4-3	2,258
WS4-4	2,297
WS4-5	2,277

Table B.5. Laboratory density of US 69 HMA surface courses

Cores	SSD (kg/m^3)	CoreLock (kg/m^3)
US 69-1	2,241	2,262
US 69-2	2,315	2,295
US 69-3	2,293	2,275
US 69-4	2,307	2,299
US 69-5	2,298	2,290
US 69-6	2,289	2,278
US 69-7	2,319	2,289
US 69-8	2,304	2,298
US 69-9	2,290	2,286

Table B.6. Laboratory density of IA 93 sections

Cores	CoreLock (kg/m^3)
FDR-1	1,982
FDR-2	2,092
CIP-1	1,931
CIP-2	1,889
OL-1	2,077
OL-2	2,312

Table B.7. Laboratory density of US 169 HMA surface courses

Cores	CoreLock (kg/m^3)
US 169-1	2,263
US 169-2	2,335
US 169-3	2,270
US 169-4	2,242
US 169-5	2,247
US 169-6	2,299

Table B.8. Laboratory density of US 6 HMA surface courses

Cores	CoreLock (kg/m^3)
US 6 H20-2	2,482
US 6 H20-3	2,345
US 6 H25-1	2,400
US 6 H25-2	2,412
US 6 H30-2	2,469
US 6 H30-3	2,457

Table B.9. Laboratory density of US 6 WMA surface courses

Cores	CoreLock (kg/m^3)
US 6 W15-1	2,462
US 6 W15-2	2,462
US 6 W30-2	2,441
US 6 W30-3	2,398

Table B.10. Dynamic modulus of seven calibration samples measured by axial method

| Conditions | | Sample, modulus in MPa | | | | | | | Average modulus (MPa) | Modulus COV (%) |
Temp. (°C)	Freq. (Hz)	1	2	3	4	5	6	7		
4	25	9335	9532	10306	10031	10129	10261	10569	10023	4.4
	20	9036	9274	9919	9711	9782	9980	10145	9693	4.1
	10	8044	8252	8828	8683	8697	8916	9040	8637	4.2
	5	7211	7406	7868	7777	7759	7959	8010	7713	3.8
	2	6300	6462	6877	6801	6748	6814	6978	6711	3.6
	1	5634	5761	6119	6089	5997	6033	6225	5980	3.5
	0.5	4978	5082	5386	5383	5260	5296	5472	5265	3.4
	0.2	4224	4295	4537	4558	4444	4481	4600	4449	3.2
	0.1	3699	3771	3942	3966	3856	3900	4003	3877	2.8
21	25	3868	4172	4111	4350	4071	4230	4227	4147	3.7
	20	3734	3984	3921	4115	3890	4008	4053	3958	3.1
	10	3146	3361	3305	3460	3281	3395	3397	3335	3.1
	5	2631	2792	2721	2863	2729	2809	2850	2771	3.0
	2	2036	2156	2104	2198	2115	2165	2173	2135	2.6
	1	1703	1769	1739	1810	1745	1788	1811	1767	2.3
	0.5	1415	1452	1430	1478	1437	1469	1488	1453	1.9
	0.2	1130	1140	1131	1140	1126	1150	1165	1140	1.2
	0.1	935	934	922	944	942	957	956	941	1.3
37	25	1527	1515	1578	1541	1471	1448	1640	1531	4.2
	20	1411	1417	1475	1430	1361	1340	1519	1422	4.4
	10	1082	1080	1138	1106	1055	1036	1158	1094	4.0
	5	856	844	903	870	831	813	923	863	4.5
	2	619	607	663	635	607	604	670	629	4.4
	1	479	462	542	522	503	479	518	501	5.7
	0.5	406	397	478	459	442	415	440	434	6.7
	0.2	314	300	373	370	355	340	349	343	8.0
	0.1	264	254	326	319	312	293	303	296	9.3

Table B.11. Dynamic modulus of seven calibration samples measured by IDT method

Conditions			Sample, modulus in MPa							Average Modulus (MPa)	Modulus COV (%)
Temp. (°C)	Freq. (Hz)	subsample	1	2	3	4	5	6	7		
4	25	1	8255	8744	8489	8918	9106	8163	8839		
		2	8026	9280	7653	8357	9426	7543	7340	8410	8.0
		3	8577	7803	7374	8723	9537	7632	8830		
	10	1	7978	7942	7687	8258	7724	7661	8066		
		2	7012	8138	6841	7775	8379	7052	6706	7686	6.9
		3	7700	7036	7414	8182	8327	7219	8310		
	5	1	7099	6815	6693	7019	6741	6774	6861		
		2	6110	7208	5835	6539	7141	6094	5792	6713	7.2
		3	6795	6415	6611	7240	7397	6321	7466		
	1	1	5283	5004	4930	5249	4970	5006	5054		
		2	4403	5448	4147	4861	5396	4334	4157	4888	8.7
		3	4995	4603	4416	5088	5444	4492	5366		
	0.5	1	4494	4284	4184	4488	4143	4350	4353		
		2	3802	4721	3544	4181	4715	3714	3525	4184	9.4
		3	4373	3924	3630	4246	4757	3814	4625		
	0.1	1	3255	3044	2904	NA	2935	3080	3179		
		2	2580	3353	2468	2926	3322	2552	2443	2947	11.2
		3	3130	2765	2469	3038	3518	2690	3287		
21	25	1	3281	3130	3152	3080	3651	3505	3675		
		2	2830	3107	2816	2974	2935	2769	3113	3243	9.3
		3	3259	3853	3279	3240	3566	3513	3382		
	10	1	2704	2620	2494	2495	2917	2677	2653		
		2	2256	2465	2242	2355	2326	2128	2540	2582	9.5
		3	2611	3147	2582	2590	2842	2847	2725		
	5	1	2195	2088	2101	2083	2452	2290	2227		
		2	1812	2057	1816	1886	1917	1754	2041	2140	10.3
		3	2169	2587	2248	2191	2396	2350	2285		
	1	1	1373	1223	1261	1254	1496	1396	1302		
		2	1115	1286	1093	1123	1137	972	1217	1294	11.9
		3	1357	1624	1403	1294	1467	1421	1358		
	0.5	1	1041	853	960	957	1156	1066	969		
		2	847	966	819	836	857	701	900	973	13.4
		3	1039	1251	1067	934	1119	1075	1026		
	0.1	1	621	535	567	569	675	647	563		
		2	484	558	457	462	477	424	505	570	14.3
		3	601	739	619	563	660	630	619		

Table B.11 (continued)

	25	1	1148	1291	1212	1219	1419	1214	1262		
		2	963	1204	1112	995	1275	1140	966	1225	11.7
		3	1310	1449	1266	1500	1197	1247	1331		
	10	1	903	930	883	906	999	900	1035		
		2	737	874	781	704	948	806	670	887	13.0
		3	982	726	896	1101	895	1031	923		
	5	1	782	737	691	793	763	728	866		
		2	608	693	628	534	749	652	573	720	12.0
37		3	800	822	806	NA	724	723	726		
	1	1	461	402	402	432	461	424	464		
		2	336	378	353	307	400	389	340	409	11.3
		3	440	480	402	453	416	425	414		
	0.5	1	402	335	285	369	325	299	385		
		2	284	310	262	207	310	269	233	312	15.2
		3	333	349	340	312	343	303	292		
	0.1	1	207	186	165	181	191	184	224		
		2	160	179	148	124	190	156	147	179	13.5
		3	203	207	168	NA	185	183	198		

Table B.12. Dynamic modulus of six field cores from Boone HMA base courses by IDT

Conditions		Sample, modulus in MPa						Average Modulus (MPa)	Modulus COV (%)
Temp. (°C)	Freq. (Hz)	1-1	1-7	2-1	5-1	6-3	7-4		
4	25	15337	15491	13952	16111	14758	12752	14733.4	8.2
	10	14450	13889	11419	14655	13225	11430	13177.7	11.0
	5	12713	12131	11705	13285	11505	10498	11972.8	8.1
	1	9603	9390	8546	9717	8792	7678	8954.3	8.7
	0.5	8324	8181	7483	8398	7557	6521	7744.0	9.2
	0.1	5719	5641	5129	5754	4993	4107	5223.9	12.1
21	25	5274	6266	5233	5887	6102	5227	5664.6	8.4
	10	4105	4658	3818	4742	4436	3865	4271.0	9.3
	5	3261	3886	3077	3573	3669	3168	3438.8	9.3
	1	1898	2581	1856	2121	2200	1765	2070.2	14.5
	0.5	1431	1963	1383	1584	1635	1290	1547.8	15.5
	0.1	770	1098	735	883	846	674	834.2	17.9
32	25	1075	1785	1248	1920	2193	1886	1684.5	25.6
	10	723	1148	831	1405	1447	1377	1155.1	27.1
	5	515	792	623	1087	1075	1056	858.0	29.3
	1	278	338	328	525	592	505	427.8	30.1
	0.5	195	276	224	451	521	346	335.6	38.5
	0.1	115	162	122	NA	257	173	165.6	34.3

Table B.13. Dynamic modulus of six field cores from Boone WMA base courses by IDT

Conditions		Sample, modulus in MPa						Average Modulus (MPa)	Modulus COV (%)
Temp. (°C)	Freq. (Hz)	3-2	3-5	4-1	8-4	8-8	9-2		
4	25	14394	15272	11953	11036	13453	10665	12795.6	14.6
	10	13541	13756	11434	8976	12183	9491	11563.4	17.3
	5	11649	12498	NA	9755	10797	8543	10648.5	14.6
	1	8388	9296	7224	6547	7667	6424	7590.9	14.6
	0.5	7099	8011	6230	5540	6512	5515	6484.4	14.8
	0.1	4565	4989	4087	3244	4075	3750	4118.3	14.8
21	25	6695	6092	4621	6016	5059	4940	5570.3	14.6
	10	5265	4693	3403	4568	3943	3531	4234.0	17.2
	5	4178	3778	2814	3531	3267	3151	3453.1	14.0
	1	2444	2150	1648	2024	1826	1631	1953.8	16.1
	0.5	1790	1449	1219	1465	1389	1390	1450.4	13.0
	0.1	908	800	643	726	683	743	750.5	12.5
32	25	2347	2375.8	2257	2286	2269	2269	2300.8	2.1
	10	1560	1595.5	1547	1587	1438	1555	1547.2	3.7
	5	NA	1277.9	1192	1172	1116	1157	1183.0	5.1
	1	578	624.94	635	609	585	581	602.3	4.0
	0.5	559	549.99	477	443	NA	437	493.2	11.8
	0.1	275	363.77	272	242	NA	251	280.8	17.2

Table B.14. Dynamic modulus of six field cores from US 6 HMA surface courses by IDT

Conditions		Sample, modulus in MPa						Average Modulus (MPa)	Modulus COV (%)
Temp. (°C)	Freq. (Hz)	H20-2	H20-3	H25-1	H25-2	H30-2	H30-3		
4	25	17021	15967	15780	15687	16014	12742	15535.2	9.3
	10	15691	13600	14549	14594	15318	11812	14260.5	9.8
	5	14306	12309	13170	13495	14358	10304	12990.3	11.7
	1	11500	9497	10496	10771	11790	8531	10430.8	11.8
	0.5	10326	8438	9423	9603	10593	NA	9676.4	8.7
	0.1	7201	6111	6952	7217	8073	5624	6862.9	12.7
21	25	8439	8460	7063	7391	8486	9018	8142.9	9.2
	10	6870	6767	5536	6567	7022	7631	6732.3	10.2
	5	5555	5802	4682	5031	5959	NA	5405.8	9.9
	1	3670	3671	3083	3367	3425	3523	3456.6	6.4
	0.5	2844	2897	2422	2616	3174	3288	2873.4	11.4
	0.1	1612	1669	1341	1470	1852	1887	1638.6	13.0
32	25	2248	2583	2629	3208	2402	3454	2754.2	17.2
	10	1610	1735	1819	2306	1651	2440	1926.6	18.5
	5	1242	1311	1374	NA	1470	1896	1458.6	17.7
	1	654	720	701	964	739	1137	818.9	23.1
	0.5	506	529	533	688	578	812	607.8	19.6
	0.1	319	311	336	NA	371	455	358.6	16.3

Table B.15. Dynamic modulus of six field cores from US 6 WMA surface courses by IDT

Conditions		Sample, modulus in MPa				Average Modulus (MPa)	Modulus COV (%)
Temp. (°C)	Freq. (Hz)	W15-1	W15-2	W30-2	W30-3		
4	25	14842	11605	12027	12135	12652.2	11.7
	10	13801	10910	10969	11122	11700.4	12.0
	5	12598	10081	10074	10045	10699.5	11.8
	1	10041	7915	7763	7458	8294.4	14.2
	0.5	9017	7116	6826	6489	7362.0	15.4
	0.1	6987	5446	4885	4638	5489.2	19.2
21	25	7293	6712	5125	6219	6337.2	14.5
	10	6137	5737	4532	5218	5405.9	12.8
	5	4700	4524	NA	3875	4366.3	9.9
	1	3470	3263	2278	2452	2865.6	20.5
	0.5	2796	2589	1809	1844	2259.4	22.4
	0.1	1651	1544	938	1034	1291.9	27.7
32	25	2853	2921	1928	2164	2466.4	20.1
	10	2028	2165	1436	1506	1783.7	20.6
	5	1559	1577	1098	1156	1347.6	19.0
	1	947	1000	571	659	794.4	26.6
	0.5	680	733	462	483	589.5	23.3
	0.1	385	415	275	295	342.3	19.8

Table B.16. Dynamic modulus of six field cores from US 69 HMA surface courses by IDT

Conditions		Sample, modulus in MPa						Average Modulus (MPa)	Modulus COV (%)
Temp. (°C)	Freq. (Hz)	4	5	6	7	8	9		
4	25	14539	12685	13490	13968	12128	11998	13134.8	7.8
	10	12696	11360	11976	12551	10687	10543	11635.6	7.9
	5	11824	10278	10708	11218	9406	9558	10498.7	9.0
	1	9449	7927	8155	8562	7385	7296	8129.2	9.9
	0.5	8267	6768	6986	7333	6329	6261	6990.9	10.6
	0.1	5210	4674	4685	4972	NA	4180	4744.4	8.1
21	25	5964	5445	5370	5675	NA	5061	5503.1	6.2
	10	4708	3771	3932	4584	3478	3766	4039.8	12.2
	5	3884	2963	3314	3798	2880	3097	3322.9	12.9
	1	2260	1676	1796	2128	1553	1732	1857.6	14.9
	0.5	1576	1184	1308	1513	1111	1231	1320.5	14.1
	0.1	790	553	629		526	574	614.4	17.1
32	25	2581	1820	2401	3051	2158	2061	2345.3	18.6
	10	1879	1318	1698	2308	1537	1441	1696.8	21.1
	5	1497	976	1238	1647	1155	1078	1265.2	20.3
	1	722	434	671	774	625	592	636.3	18.7
	0.5	528	406	452	594	415	363	459.6	18.7
	0.1	224		240	292	238	233	245.2	10.9

Table B.17. Dynamic modulus of six field cores from US 169 HMA surface courses by IDT

| Conditions | | Sample, modulus in MPa | | | | | | Average Modulus (MPa) | Modulus COV (%) |
Temp. (°C)	Freq. (Hz)	1	2	3	4	5	6		
4	25		15274	11586	10548	10762	11403	11914.6	16.2
	10	8474	13648	12235	9151	8974	9927	10401.6	19.9
	5	7433	12309	10629	8120	7931	8646	9178.2	20.6
	1	5341	9230	7864	5913	5686	6340	6729.0	22.4
	0.5	4523	8021	6809	5040	4711	5345	5741.5	24.0
	0.1	2877	5412	4490	3271	NA	3366	3883.0	26.9
21	25	3851	5130	4415	4028	3760	4203	4231.0	11.8
	10	2832	4018	3468	3001	2786	3395	3249.9	14.5
	5	2279	3211	2790	2450	2187	2782	2616.5	14.7
	1	1216	1722	1517	1357	1169	1530	1418.5	14.8
	0.5	876	1225	1065	974	763	1097	1000.0	16.5
	0.1	423	594	506	477	424	525	491.5	13.3
32	25	1637	2513	2587	1969	1380	2002	2014.8	23.5
	10	1136	1783	1822	1411	949	1405	1417.8	24.4
	5	822	1355	1387	1106	711	1044	1070.6	25.6
	1	407	684	719	528	321	536	532.6	28.9
	0.5	268	509	492	407	255	376	384.5	28.0
	0.1	199	381	339	295	NA	275	297.8	23.1

Table B.18. Dynamic modulus of two field cores from IA 93 OL by IDT

| Conditions | | Sample, modulus in MPa | | Average Modulus (MPa) | Modulus COV (%) |
Temp. (°C)	Freq. (Hz)	OL 1	OL 2		
4	25	11905	12979	12442.2	6.1
	10	10406	11559	10982.4	7.4
	5	9211	10385	9797.6	8.5
	1	6853	7978	7415.2	10.7
	0.5	5798	6876	6336.8	12.0
	0.1	3798	4713	4255.4	15.2
21	25	4616	5151	4883.2	7.7
	10	3545	3912	3728.5	7.0
	5	2856	3128	2991.9	6.4
	1	1547	1807	1677.2	11.0
	0.5	1032	1318	1175.0	17.2
	0.1	606	714	659.9	11.6
32	25	1926	2538	2231.6	19.4
	10	1366	1674	1520.1	14.4
	5	1017	1255	1136.2	14.8
	1	559	697	627.9	15.6
	0.5	441	451	445.9	1.7
	0.1	323	NA	322.6	NA

a)

b)

100,000

10,000

|E*|, MPa

1,000

100

10

1

◆ 4°C
■ 21°C
▲ 37°C
— Fit

1.E-05   1.E-02   1.E+01   1.E+04   1.E+07

Frequency, Hz

c)

100,000

10,000

|E*|, MPa

1,000

100

10

1

◆ 4°C
■ 21°C
▲ 37°C
— Fit

1.E-05   1.E-02   1.E+01   1.E+04   1.E+07

Frequency, Hz

d)

100,000

10,000

|E*|, MPa

1,000

100

10

1

◆ 4°C
■ 21°C
▲ 32°C
— Fit

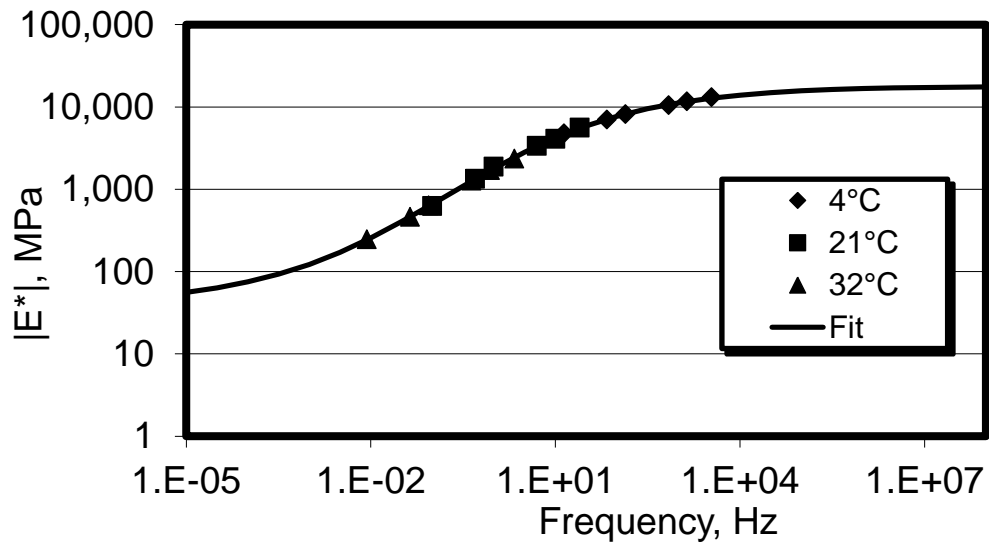1.E-05   1.E-02   1.E+01   1.E+04   1.E+07
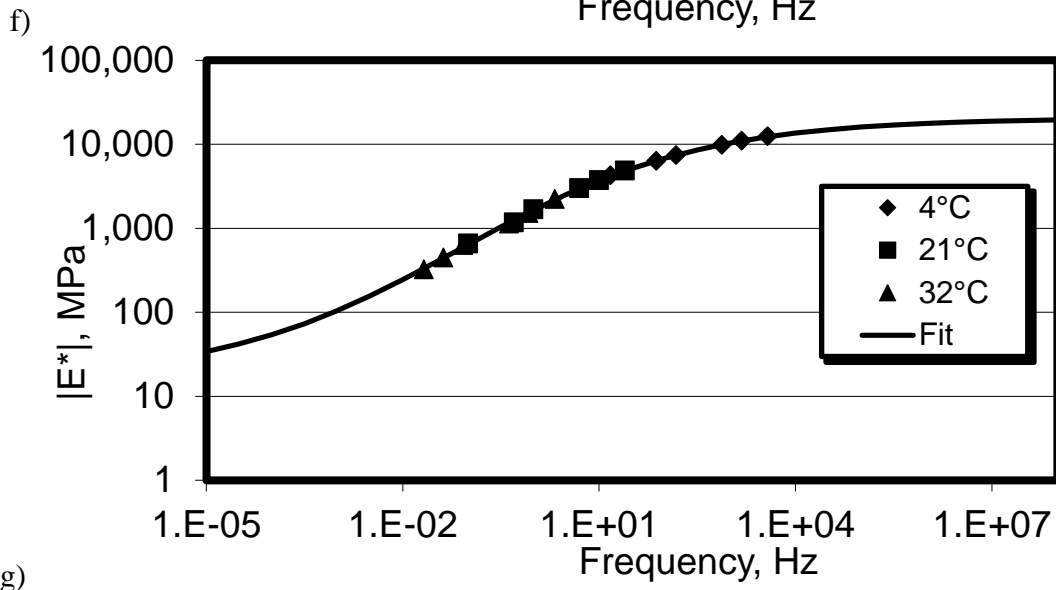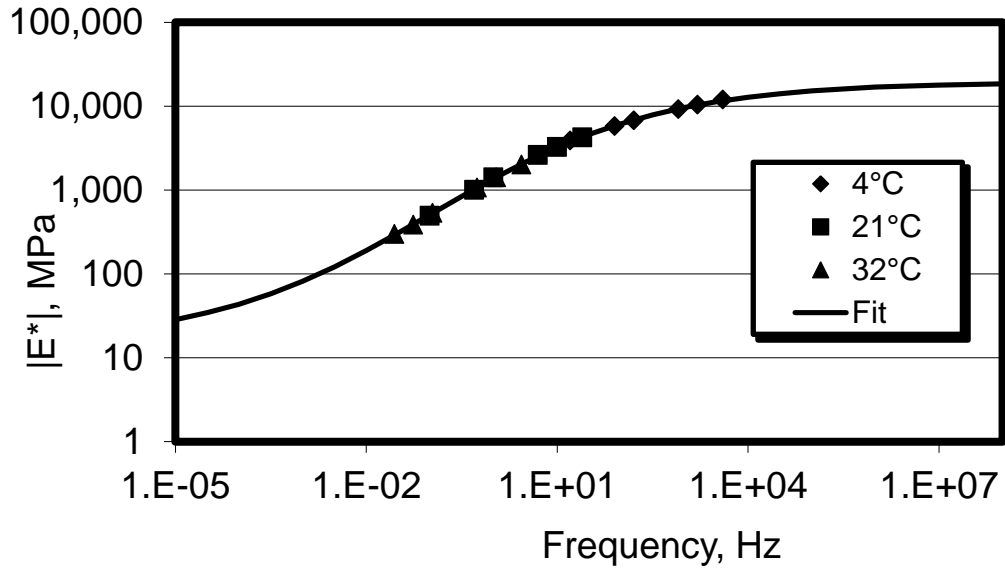
Frequency, Hz

e)

f)
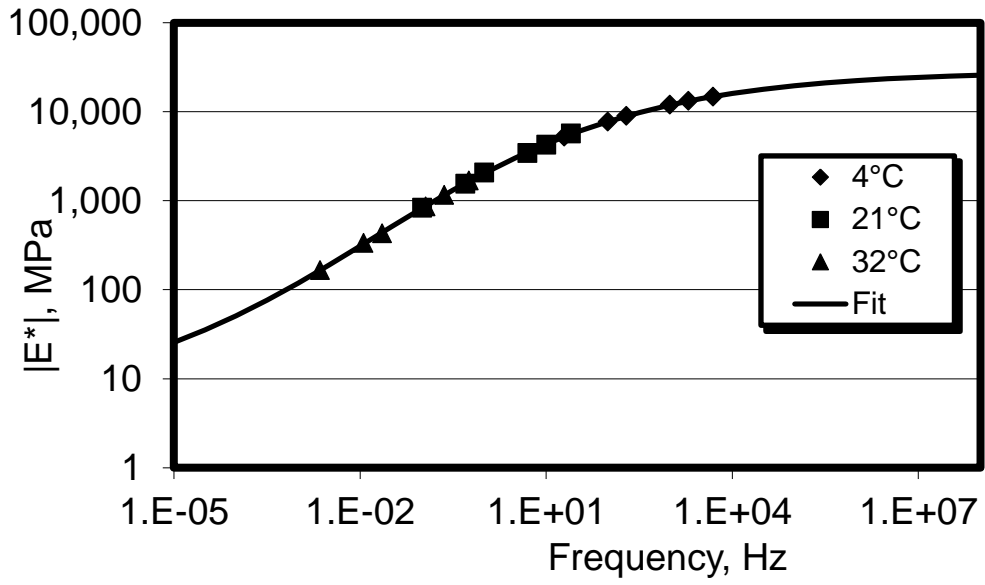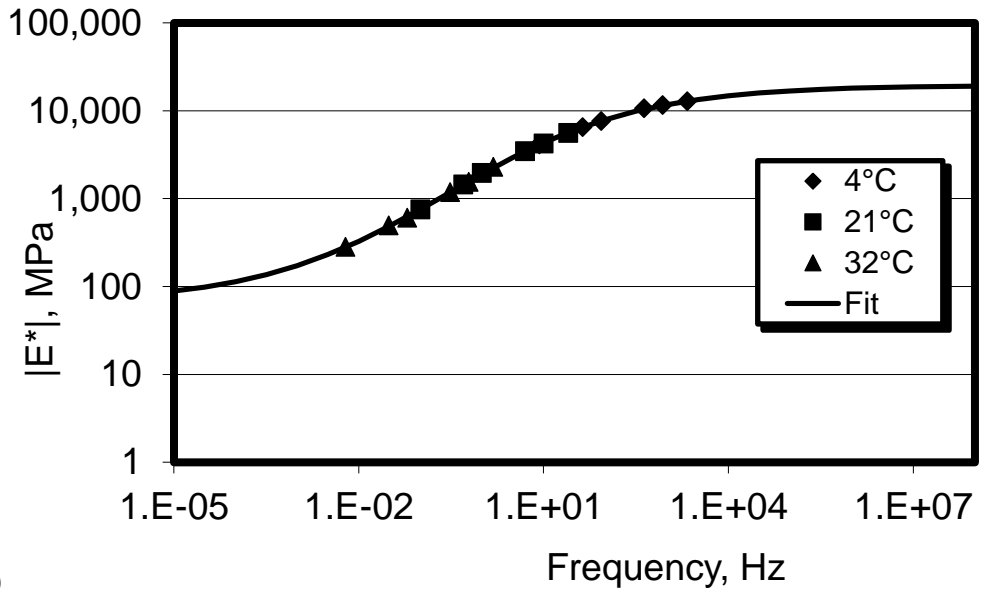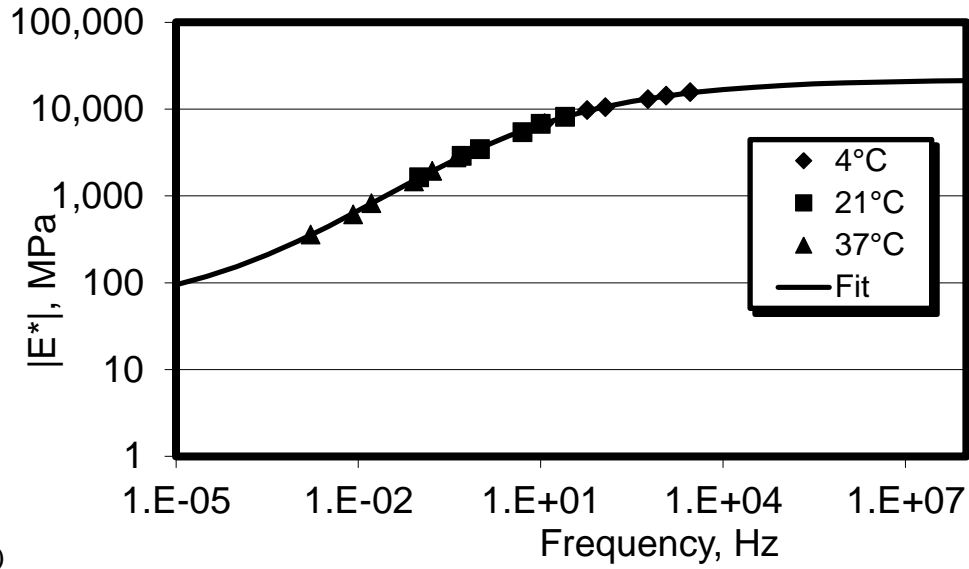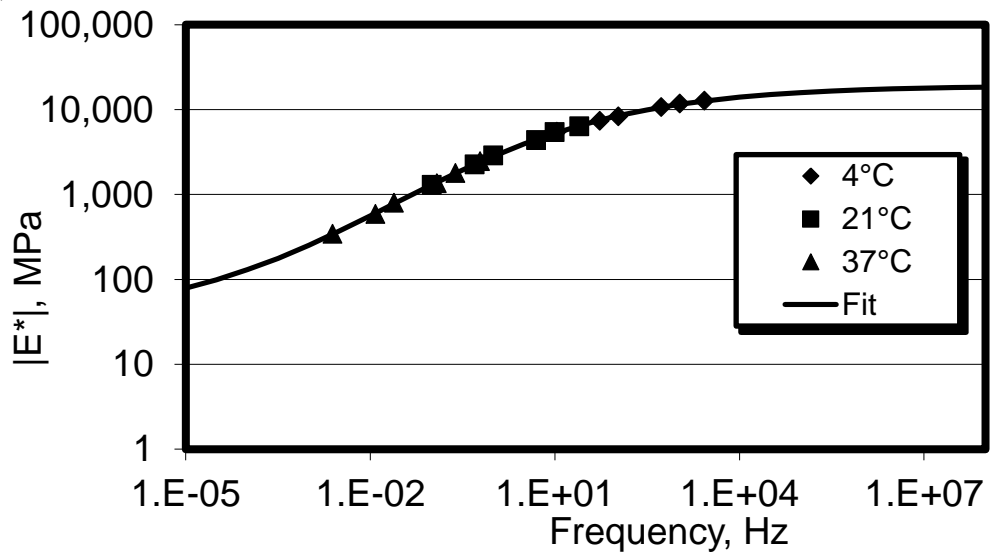
g)

Figure B.1. Dynamic modulus master curves for (a) Boone HMA base courses, (b) Boone WMA base courses, (c) US 6 HMA, (d) US 6 WMA, (e) US 69, (f) US 169, (g) IA 93 OL